The Dissertation Committee for David Sean O'Kelly
certifies that this is the approved version of the following dissertation:

Operation and Reactivity Measurements of an Accelerator Driven Subcritical TRIGA Reactor

Committee:

_____
Steven R. Biegalski, Supervisor

_____
Sheldon Landsberger

_____
Erich A. Schneider

_____
Randall J. Charbeneau

_____
Howard M. Liljestrand

Operation and Reactivity Measurements of an Accelerator Driven Subcritical TRIGA Reactor

by

David Sean O'Kelly, B.S.; M.S.

Dissertation

Presented to the Faculty of the Graduate School of
The University of Texas at Austin
in Partial Fulfillment
of the Requirements
for the Degree of

Doctor of Philosophy

The University of Texas at Austin
May 2008

Dedication

To Donna, Erin and Devin.

Acknowledgements

This project was supported by the Nuclear Engineering Teaching Laboratory (NETL) at the University of Texas at Austin, the Idaho Accelerator Center, the DOE Innovations in Nuclear Infrastructure and Education (INIE) Program and the DOE Advanced Fuel Cycle Initiative Program.

The author would like to thank the staff, students and faculty of the UT Nuclear and Radiation Engineering Program for their support in making this experiment possible. The accelerator could not have been installed or removed without their physical support and the project would not have been successful without their willingness to allow the exclusive use of the UT TRIGA reactor during the subcritical experiments. The UT linac operators, Jon Braisted, David Tillman and Brad Hurst, placed their personal projects aside during these experiments to maintain and safely operate the accelerator and their support is gratefully acknowledged. The author would like to acknowledge, in particular, Michael Krause and Larry Welch at the NETL for their technical support and personal friendship before, during and after the subcritical experiments.

The author thanks Frank Harmon, Denis Beller, Kevin Folkman and Chad O'Neill of the Idaho Accelerator Center (IAC) for their support of the UT-RACE project and use of the IAC linac. Their assistance and technical expertise was essential for the training of the UT operators and the design and fabrication of a very unique machine.

Above all others, I would like to thank my wife of twenty-four wonderful years, Donna, and my children Erin and Devin. I could not have completed this long journey without their love and support.

Abstract

Operation and Reactivity Measurements of an Accelerator Driven Subcritical TRIGA Reactor

David Sean O'Kelly, Ph.D.
The University of Texas at Austin, 2008

Supervisor: Steven R. Biegalski

Experiments were performed at the Nuclear Engineering Teaching Laboratory (NETL) in 2005 and 2006 in which a 20 MeV linear electron accelerator operating as a photoneutron source was coupled to the TRIGA (Training, Research, Isotope production, General Atomics) Mark II research reactor at the University of Texas at Austin (UT) to simulate the operation and characteristics of a full-scale accelerator driven subcritical system (ADSS)**.** The experimental program provided a relatively low-cost substitute for the higher power and complexity of internationally proposed systems utilizing proton accelerators and spallation neutron sources for an advanced ADSS that may be used for the burning of high-level radioactive waste. Various instrumentation methods that permitted ADSS neutron flux monitoring in high gamma radiation fields were successfully explored and the data was used to evaluate the Stochastic Pulsed Feynman method for reactivity monitoring.

Table of Contents

List of Tables

List of Figures

Figures

Figure

Chapter 1
Introduction

1.1 Background

It is unfortunate, but if the Yucca Mountain Repository for spent nuclear fuel and high-level radioactive waste ever gets licensed and built in Nevada, it will be essentially full on the day it opens because of the volume of materials waiting to be shipped and stored at the facility. A different problem may occur if the Repository is not built because the so-called Nuclear Renaissance of new license applications and construction is weakened, if not crippled, while the public and utilities see no progress towards a reliable final disposition path for the increased volume of spent fuel from a growth in the use of nuclear generated power. Options to reduce the volume of high-level radioactive materials must include reprocessing but that will still result in residual transuranic radioactive wastes with long-term storage problems. Research was performed for this dissertation that supported one possible pathway for a true high-level radioactive waste disposal method that could eliminate or reduce the need to store radioactive materials for hundreds or thousands of years. The experiments provided a relatively low-cost substitute for the higher power and complexity of internationally proposed systems utilizing proton accelerators and spallation neutron sources that are proposed for the burning of high-level radioactive wastes.

The experimental project was UT-RACE, for The University of Texas at Austin Reactor Accelerator Coupling Experiments[1,2]. The experiments were performed under an overall U.S. Department of Energy RACE collaborative program funded through the Idaho Accelerator Center (IAC) at Idaho State University in Pocatello, Idaho (ISU). During what became effectively a two year project, the experiment was designed, safety evaluations were prepared and submitted to the State of Texas to approve the installation and operation of the linear accelerator (linac) as a neutron source, a safety evaluation was prepared, reviewed and approved to operate the linac adjacent to the TRIGA (Training, Research, Isotopes: General Atomics) reactor core, a large experimental facility was

constructed to house the linac, difficult instrumentation problems were overcome and the electron linac was operated as a neutron source to drive a subcritical reactor to approximately 100 watts. The outcome was, to date, the highest power operational ADSS in the world but the project also provided new benchmarking of a method of subcritical reactivity determination, the pulsed Stochastic Feynman-Alpha Method, which may be used to monitor reactivity of a subcritical assembly of fissile materials interrogated by a pulsed neutron source[3].

1.2 Accelerator Transmutation of High Level Waste

Under the U.S. Department of Energy Global Nuclear Energy Program (GNEP) and the existing Advanced Fuel Cycle Initiative (AFCI), new methods and technologies are under development to reduce the total volume of high-level nuclear waste placed into the Yucca Mountain waste repository and minimize the need to expand Yucca Mountain or create several new radioactive waste repositories in the future[4]. Many of these volume reducing methods involve reprocessing of nuclear fuel to recover the useful uranium and plutonium and the separation and concentration of the long-lived radioactive wastes for a significant volume reduction. Within this concentrated, high-level waste (HLW) are two waste streams, long-lived fission products (LLFP) and minor actinides (MA), which will remain radioactive and toxic for many years due to their long half-lives. Rather than store and monitor these wastes for hundreds of years, a more active method for disposal of the LLFP and MA is needed. A disposal method that has wide international support is the concept of "burning" or transmutation by neutron capture or fission to convert the isotopes to shorter lived daughter products The HLW materials would be burned in fast neutron spectrum facilities for the most efficient conversion of the wastes without, ideally, the production of more HLW by thermal or fast fission of uranium[5].

One system currently in favor by the U.S. Department of Energy uses an Advanced Burner Reactor (ABR) with a prototype planned for construction at the Idaho National Laboratory[6,7]. Another type of transmutation facility supported by the European Union is an Accelerator Driven Subcritical System (ADSS) for the

transmutation of HLW[8-11]. The fast spectrum, sodium or lead-bismuth cooled ABR builds on technology and experience the United States already has with fast reactors but the United States currently has little experience in the safe and stable operation of an ABR loaded with large amounts of plutonium or minor actinides (MA). A critical, fast reactor core loaded with MA (*e.g.* Cm, Am, and Np) and plutonium for incineration would be characterized by a low Beta (small delayed neutron fraction), low Doppler coefficient and the positive void coefficient of the sodium coolant. For the proposed ABR system with a low (less than 0.65) conversion ratio an increase in temperature would tend to produce a positive reactivity effect because of the fast fission of the MA and the sodium void coefficient[12]. These core characteristics would make the ABR much more difficult to control and extremely difficult to license. Adding ^{238}U to the fuel would improve the reactor characteristics for operational safety but also result in the production of additional transuranic waste reducing the effectiveness of the ABR program. The operation of a transmutation reactor in a subcritical mode as proposed for an ADSS system would safely permit a wide range of fuel compositions and the accelerator-driven neutron source could provide excess fast neutrons to increase the efficiency of transmutation.

1.3 ADSS and Transmutation Research

Transmutation of elements using particle accelerators was not originally conceived to destroy long-lived radionuclides such as minor actinides and fission products (Tc, Sr, Cs, *etc.*) in high level waste but was intended to produce plutonium and tritium for the nuclear weapons effort following World War II. One of the first major projects of Livermore National Laboratory under the first Director, Ernest O. Lawrence, was to design and construct the Materials Testing Accelerator (MTA) to transmute the leftover depleted uranium from enrichment processing into plutonium because of the security concern within the government that only limited sources of uranium ore were available to the United States at that time[13]. The project was cancelled after significant domestic sources of uranium were discovered in the early 1950's and the concept of

large-scale accelerator driven transmutation was essentially shelved for the next forty years**.**

In the early 1990's, the concept of accelerator driven transmutation as a method of HLW disposal was proposed by the Los Alamos National Laboratory and research to support this program continued through the decade under the Accelerator Transmutation of Waste (ATW) program and the Department of Defense Accelerator Production of Tritium (APT) programs. These two programs were combined under the Advanced Accelerator Application (AAA) program administered by the U.S. DOE in 2001 but these programs were then moved under the overall DOE Advanced Fuel Cycle Initiative (AFCI) in 2003. As these programs evolved after 1999, the preferred method to convert or burn the HLW shifted from an emphasis on accelerator driven transmutation to fast spectrum reactor burner reactors but low level funding continued to support accelerator driven systems research in the United States[14].

All the currently proposed accelerator systems to burn HLW at reasonable transmutation rates are based on large, high energy (140 MeV-1 GeV) proton accelerators impacting on a high atomic number liquid or solid metal targets causing spallation reactions to release neutrons from the nuclei. Spallation reactions produce more neutrons per source particle so they are a more efficient accelerator-based neutron source. This is essentially the same design (proton on mercury target) as the successfully operating Spallation Neutron Source (SNS) at the Oak Ridge National Laboratory but the SNS was designed to replace nuclear reactors as neutron sources for neutron scattering science so no fissile material is used around the neutron source[15]. For the ADS burner, these spallation neutrons would be used to drive subcritical multiplication within the assembly fuel and HLW to increase the available neutrons for transmutation of the distributed waste within the assemblies.

In Europe, support remains for the disposal of HLW using accelerator driven technology and significant research has been performed in collaboration and in parallel with efforts by DOE[16]. One such effort supported by the 5th and 6th Framework Integrated Program of the European Community (EURATOM) was the successful MUSE

(MUltiplication avec Source Externe) project performed in the MASURCA critical facility at the CEA Research Center at Cadarache, France[17]. The MUSE program began in 1995 using californium neutron sources but began experiments as a true ADS in 2001 using a D-T (deuterium beam and tritium target) pulsed neutron generator (MUSE-4) designed specifically for the ADS experiments. The MASURCA facility is a an air-cooled fast critical assembly loaded with MOX fuel and uses solid sodium to maintain the fast spectrum but may safely operate up to powers of only 5 kW. The GENEPI neutron generator operated between 10 Hz and 5 kHz with either a deuterium or tritium target and produced approximately $3x10^6$ n per pulse ($1.2x10^{10}$ n s^{-1} at 4 kHz). The international MUSE program ended in 2004 providing a large amount of data on the response of the fast subcritical assembly to a high frequency pulsed neutron source.

Although the MUSE project was an important step in the development of large ADS, the neutron generator did not produce enough neutrons to raise the MASURCA assembly to the point of adding heat. It is at this point that temperature affects on reactor characteristics, such as subcritical reactivity level, may be measured and these measurements may then be used to benchmark computational methods and models that will be extended to develop higher power systems. The change in reactor or subcritical assembly power level (temperature reactivity) as reactor temperature increases may have a significant effect on the operational safety of the system. ADS designers desired a testing facility that could be driven to substantial power with an accelerator beam to evaluate temperature feedback effects as the HLW is burned in the system.

The next phase in the European ADS experimental research program to achieve temperature reactivity feedback was to couple a high energy proton accelerator and spallation target to a subcritical TRIGA reactor. The project was called TRADE (TRIGA Accelerator Driven Experiment) and occurred at the 1 MW ENEA research reactor in Casaccia, Italy[18,19]. Due to a lack of funding, the proton accelerator was never built and the TRADE experiments were performed using californium sources and a small D-T neutron generator placed in the center of the reactor fuel in the summer of 2004. In June of 2005, the AFCI RACE project joined the European project EUROTRANS (EURopean

Research Program of the TRANSmutation of High Level Nuclear Waste in an Accelerator Driven System) through a memorandum of understanding to permit the transfer of equipment and expertise between the European and U.S. collaborators. Unfortunately, the TRADE experimental program overlapped the UT-RACE project such that equipment and personnel were still being used at the Casaccia facility into 2006 while UT-RACE was in progress and very little assistance could be provided to the UT-RACE project.

Another series of experiments to model a simple ADSS with the expectation of a future coupling of a spallation neutron source to a subcritical system were performed in 2003 using the Kyoto University Critical Assembly (KUCA)[20]. Similar to previous ADS experimental facilities, the KUCA was coupled to a small D-T pulsed neutron generator to drive the subcritical assembly. The KUCA neutron generator could only pulse at three different rates (50, 100 and 1000 Hz) but these were sufficient to evaluate several recently proposed methods to monitor the reactivity of pulsed ADSS. Japan is currently constructing a large proton accelerator (FFAG) for ADSS studies and as a possible replacement for the Kyoto University research reactor[21, 22].

To fully validate models and experiments for full-scale ADSS burners a proton spallation source must drive a subcritical fast assembly to relatively high power to evaluate temperature feedback effects on performance and safety. Several systems have been proposed in Europe but only one appears to be making progress and that is the Subcritical Assembly in Dubna (SAD), Russia which will utilize a subcritical assembly driven by a 660 MeV proton beam on a lead target[23]. A recently proposed follow-up to the original MUSE project is a zero power fast assembly driven by a continuous beam neutron generator. This proposed project, now called GUINEVERE (Generator of Uninterrupted Intense Neutrons at the VEnus REactor), is expected to be on-line by 2010 and is a continuation of the ADSS experimental research under the EUROTRANS program[24, 25].

To date, no experimental ADSS programs other than the RACE projects have utilized a linear electron accelerator and target to drive subcritical multiplication of a

fueled assembly. Although the neutron production from proton induced spallation reactions is the most efficient method per source particle, the cost and complexity of the accelerator system to drive the source are very different[25]. As an example, the 1 GeV SNS system cost $1.4B to construct and, as would be expected in the first ADSS, a significant proportion of the initial costs were due to the first-of-a-kind engineering required[27]. For initial feasibility studies, the neutron energy spectrum from an electron linac bremsstrahlung source is similar to the energy spectrum from a spallation target but the average yield is much lower[28].

As a substitute for a yet-to-be-built spallation ADSS, the UT-RACE electron linac ADSS project has provided the necessary research to link the zero-power subcritical assemblies driven by low neutron flux sources to the proposed high-power fast spectrum systems driven by a high-energy proton beam and spallation target. The original goals of the research project were to:

1. Support international efforts in HLW transmutation research
2. Design, model and conduct electron linac driven subcritical multiplication experiments on a TRIGA research reactor core
3. Perform and analyze unique subcritical source-driven transients and reactivity control methods
4. Evaluate corrective methods for neutron instrumentation in high gamma-flash background
5. Evaluate asymmetric injection ADSS design and spatial response of neutron instrumentation for various reactivity measurement methods

An evaluation of the Pulsed Feynman Method of reactivity monitoring was not one of the original goals of the research project as the method was relatively unknown during the initial experiment planning. However, the method was used extensively after the completion of the UT-RACE experiments to measure the subcritical level of the TRIGA reactor as a comparison to more traditional reactivity monitoring methods.

1.4 Outline of Dissertation

This dissertation will describe the UT-RACE ADSS experimental facility, subcritical TRIGA core configuration, the basic theory and operation of the 20 MeV linac and discuss problems encountered in monitoring and controlling the accelerator for optimum beam characteristics and maximum neutron production. The experimental facilities include the nuclear monitoring and data acquisition systems and several unique instrumentation techniques that were used to overcome interference in neutron detection caused by the linac's operation will be described in Chapter 3.

The UT TRIGA core was modeled using MCNPX and MCNP5 Monte Carlo codes to more accurately determine the current core fuel depletion and buildup of fission products and benchmark the model to then have confidence in the calculated core reactivity values. These modeling and simulation results will be discussed in Chapter 4.

Chapter 5 will provide a review of traditional reactivity monitoring methods, introduce a relatively new method and show how some of these techniques were used to evaluate the subcritical level of the TRIGA core while the linac was operating. Chapter 6 will present experimental results with a focus on the Stochastic Feynman Method of reactivity determination in a pulsed ADSS and compare the reactivity measurements from a calibrated control rod to benchmark the reactivity monitoring methods.

Chapter 2

Theory

The neutron population as a function of space and time within a nuclear reactor is an entirely statistical process due to the discrete nature of neutron diffusion and the nuclear fission reactions within the constant core volume[29, 30]. This time dependence and statistical nature of the particle population may be modeled exactly using Boltzmann's equation for the general transport theory of gases modified to account for the unique nature of some neutron interactions but this neutron transport equation is difficult to solve directly and must be approximated or simplified in some manner[31].

In elementary, one-group diffusion theory, the neutron transport equation is simplified to

$$D\nabla^2\phi - \sum_a \phi + \nu\sum_f \phi + S = -\frac{1}{\nu}\frac{\partial\phi}{\partial t}. \tag{2.1}$$

Here the time behavior of the one-group neutron flux, ϕ, is dependent on the system diffusion coefficient, D, the installed or intrinsic neutron source, S, and the macroscopic cross-sections for absorption and fission (Σ_a, Σ_f) and the neutron yield per fission, ν. For a critical reactor at some relatively high fission rate level, the source, S, may be assumed to be zero and the neutron population constant (these assumptions do not generally hold for an ADSS or a zero-power subcritical system but the result here at criticality is important). The parameter, 1/k, is inserted into the equation to provide a balancing, multiplication factor that maintains the fission production term ($\nu\Sigma_f\phi$) equal to the loss terms of the fission neutron life cycle resulting in the solution at steady-state (*i.e.* critical) of

$$1 = \frac{\nu\Sigma_f}{DB^2 + \Sigma_a} = \frac{\nu\Sigma_f / \Sigma_a}{L^2B^2 + 1} = \frac{k_\infty}{L^2B^2 + 1} = k_\infty P_{NL} \tag{2.2}$$

where k_∞ is defined as an infinite multiplication factor (assuming a reactor of infinite volume), B^2 is the configuration buckling, L is the diffusion length and P_{NL} is the nonleakage probability. The outcome from this diffusion approximation is that the reactor is exactly critical when the multiplication factor, k, is equal to one and has some time dependence when k is not equal to one. Another useful derived term based on 'k' is the core 'reactivity' (ρ) or the departure from the critical condition and defined as

$$\frac{k-1}{k} = \rho \tag{2.3}$$

Equation 2.1 has significance for ADSS because the condition of $k < 1.0$ or $\rho < 0.0$ implies the neutron population will decrease unless forced to remain at some measurable level by an external or internal non-fission source and that the arbitrary multiplication factor or eigenvalue, k, is only a valid solution to the state of the reactor when the reactor is critical or slightly perturbed from critical. The difficulty in using the definitions of "critical" and "reactivity" for subcritical source-driven systems has led to some reconsideration of these definitions when applied to ADSS; however, in many cases with the system near critical the in-hour equations and the definition of k-eigenvalue criticality are sufficiently accurate[32-37]. The units of reactivity used in this dissertation are in "dollars" and "cents" where

$$\$ = \frac{\rho}{\beta} \tag{2.4}$$

The parameter β is the effective delayed neutron fraction and is fully defined below. Another result of this simple analysis is that every nuclear reactor with an installed neutron source or significant intrinsic spontaneous fission sources is in itself a source-driven subcritical reactor with the losses in the fission and delayed neutron life cycle made up by the production of neutrons from the source.

The strength of the external neutron source in relation to the fission rate will determine whether a nuclear reactor or subcritical system is *source-dominated* or *core-dominated* and has a significant effect on the reactor dynamics and neutron flux distribution. Calculations for the TRADE project with a central spallation source have shown the TRIGA reactor transitions from source to core-dominated behavior around a k of 0.97 at which point the neutron flux radial profile changes from an exponential form with the source location the highest magnitude to an approximate cosine shape as the reactor neutron flux achieves a stable fundamental harmonic[38].

As was already noted, when the reactor is not exactly critical there is a time dependency in the neutron population and reactor power is increasing without bound if supercritical or decreasing to a state of statistical randomness if the reactor is subcritical. This leads to the α-eigenvalue solution of the time-dependent form of the diffusion equation

$$n(\vec{r},t) = A_1\psi_1(\vec{r})e^{-\nu[\Sigma_a-(1-\beta)\nu\Sigma_f+DB^2]t} \tag{2.5}$$

or

$$n(t) = e^{-\left[\frac{\rho-\beta}{\Lambda}\right]t} = e^{-\alpha t}. \tag{2.6}$$

This solution, Equation 2.5, assumes the geometry dependent shape factor ($A_1\psi_1$) is in the constant fundamental mode and only considers the prompt neutrons (1-β) from fission. The parameter, Λ, is the neutron generation time or the time for a neutron born from fission to reproduce itself by a subsequent absorption and fission and is fully defined as

$$\Lambda = \frac{1}{\bar{\nu}\nu\Sigma_f} \tag{2.7}$$

The quantity $1/\Sigma_f$ is the mean-free path for birth to subsequent fission and average speed of the neutron determines the time it takes to get there to produce υ neutrons. Although Λ has been termed "generation time" for many years (since 1960),

the individual who introduced the above equation has recently requested the term's name be changed to "prompt neutron reproduction time" as it better reflects the process[39].

The use of Λ simplifies the reactor kinetics equation to the common form

$$\frac{d\phi}{dt} = \frac{\rho - \beta}{\Lambda}\phi + \frac{1}{\Lambda \nu \Sigma_f}\sum_6 \lambda_i C_i \tag{2.8}$$

The first term in Equation 2.7, (ρ-β/Λ), considers only those neutrons produced in very short time periods directly from fission while the second term considers delayed fission rate controlled by neutron production that is a function of the radioactive decay of neutron-rich fission fragments. The delayed fission rate is therefore additionally defined by the balance equation for the concentration of delayed-neutron precursors in the core, or

$$\frac{dC_k}{dt} = -\lambda_k C_k + \nu_d \Sigma_f \phi, \quad \text{k = 1,..., 6.} \tag{2.9}$$

The production of delayed neutrons (C_k is the concentration of delayed neutron precursors) is a function of the population or yield of delayed neutron parent isotopes directly from fission ($\nu_d \Sigma_f \phi$) while the loss of these parent isotopes (producing the neutron during the decay) is controlled by the individual decay. Each of the over 271 known parent isotopes or *delayed neutron precursors* (DNP) has a characteristic decay constant. The DNP time constants have been traditionally lumped into six empirically determined groups to simplify calculations[40]. There has been recent interest in defining a larger number of delayed neutron groups to more accurately model fast reactor transients and to change the weighting of the groups for mixed fissile material cores such as MOX (mixed oxide fuel) reactors[41].

The effective delayed neutron fraction, β, is the ratio of the delayed neutrons to all neutrons produced in the core and because the delayed neutrons are born at an average

lower energy than those neutrons directly from fission, the delayed neutrons are more likely to remain in the reactor and travel shorter distances with a high probability of capture producing a subsequent fission. Equation 2.7 shows the importance of the delayed neutron induced fission contribution to the rate of neutron flux change because the rapid change caused by the prompt fission term is offset by the much longer times associated with the production of the delayed neutrons. Thus, when a thermal reactor is critical by the combination of prompt and delayed neutron fission contribution (*delayed critical*), the rate of change in reactor power is limited. When a reactor is *prompt critical* (or the value of β is small as for the proposed ABR), reactor power may change very quickly and would be difficult to safely control.

For very rapid reactor transients that occur in time spans shorter than the time to produce the first delayed neutrons, equation 2.7 is simplified by the *prompt jump approximation* and written as

$$\frac{d\phi}{dt} = \frac{\rho - \beta}{\Lambda}\phi . \tag{2.10}$$

This form of the reactor kinetics equation is useful for approximating the change in fission neutron flux induced by the rapid injection of neutrons due to the operation of a accelerator driven pulsed neutron source, as well as changes to the core neutron population from large changes in control rod position or rapid removal of the installed or driving neutron source (source jerk).

The reactivity of the reactor or subcritical assembly may be easily derived if the ratio β/Λ is known. The ratio may be determined by a measurement at critical conditions when the reactivity is zero by using dynamic methods such as a source jerk or pulsed experiment[42, 43]. The value was recently (2004) measured using reactor transfer functions on a TRIGA Mark II and was found to be 132 $\pm$ 2 s^{-1} at exactly critical[44]. The accepted value of β provided by General Atomics for the TRIGA reactors is 0.0070 with the resulting neutron generation time of 53μs[45]**.** This compares well with a value of 60.1$\pm$ 3 μs measured in 1966 for a TRIGA reactor with an assumed β of 0.073 (α=121.4 s^{-1})[45].

The value of 132 s^{-1} may be assumed to be more accurate for UT-RACE based on the improvements in measurement electronics over forty years and the higher burn fuel used in the recent measurement being more representative of the NETL TRIGA. These values were used as fixed benchmarks for the UT-RACE reactivity analysis but these should not necessarily be assumed constant for systems that are far from critical as β and Λ are both functions of the neutron energy spectrum, geometry and fissile material densities.

Chapter 3
Experimental Facility and Instrumentation

3.1 NETL TRIGA Reactor

The UT-TRIGA Mark-II research reactor is licensed to operate at a nominal full power of 1.0 MW with natural circulation cooling. The fully operational reactor core consists of up to 116 reactor fuel elements and four control rods for a total of 120 grid locations. The hexagonal-spaced grid plates are surrounded by an aluminum-canned graphite reflector assembly with an effective inside diameter of 54.93 cm and a radial thickness of 25.91 cm. The graphite acts as a neutron reflector to the reactor core and couples the reactor neutrons to the various beam-type experiments. One beam-port (BP) experiment in particular, is the BP1 and BP5 single port that passes through the reflector graphite directly adjacent to the reactor core area. The entire reactor assembly is located near the bottom of an eight-meter deep tank of demineralized water for cooling and radiation shielding. The average uranium depletion of each of the 78 fuel elements in the UT-RACE experimental core was approximately 1.7 MW-days. The core load configuration and fuel element placement were not optimized in any way from the critical core due to time constraints and subcritical configuration was created by removing just enough fuel elements to make the reactor core subcritical by a small amount (this amount was found to be approximately \$0.181 as determined during later measurements and calculations).

The TRIGA reactor fuel consists of individual fuel elements with an active fuel region 38.1 cm in length and with a diameter of 3.63 cm. The fuel is a solid alloy of uranium-zirconium-hydride containing 8.5% by weight uranium and a ratio (for most fuel elements) of hydrogen to zirconium atoms of 1.6. A small diameter (0.25 cm) solid zirconium rod is inserted into the center of the fuel following the hydriding process during fuel fabrication. A graphite slug, approximately 8.7 cm long, is located at each end of the fuel region to serve as a neutron reflector. The entire fuel-reflector section is

clad in 0.508 mm of alloy 304 stainless steel. Fittings welded on the top and bottom of the element make the overall length 73.2 cm.

Graphite dummy elements are often used in the reactor grid plate in grid locations not filled with a fuel element to displace the reactor coolant. These dummy elements are entirely filled with solid graphite and clad in aluminum. There are four control rods in the core, three are identical designed fuel-followed control rods (Shim-Safety 1, Shim-Safety 2 and Regulating Rod) and one is a void-followed pulsing rod (Transient Rod). The fuel-followed control rods consist of an upper region with 38.1 cm of boron-carbide (B_4C) as a neutron absorber and a lower region composed of Zr-U fuel and graphite essentially in the same dimensions as the standard fuel elements. The purpose of the fuel-follower is to increase the reactivity worth of the control rod by inserting or removing fuel from the core as the poison (neutron absorber) of the control rod is withdrawn or inserted respectively.

3.2 UT-RACE Core Configuration

Ideally, for the purposes of the ADSS experiments, the linac target would have been placed in the center of the TRIGA core to provide maximum coupling of the isotropic neutrons from the source into the surrounding reactor fuel[47, 48]. This configuration was not possible with the limited resources available to conduct the experiment and the significant facility reconfiguration required. Without placing the linac at the pool surface, the closest location for the target was within the watertight, tangential beam port (BP1 and BP5) shown in Figure 3.1 and Figure 3.2.

Fig. 3.1. UT-RACE accelerator and core locations.

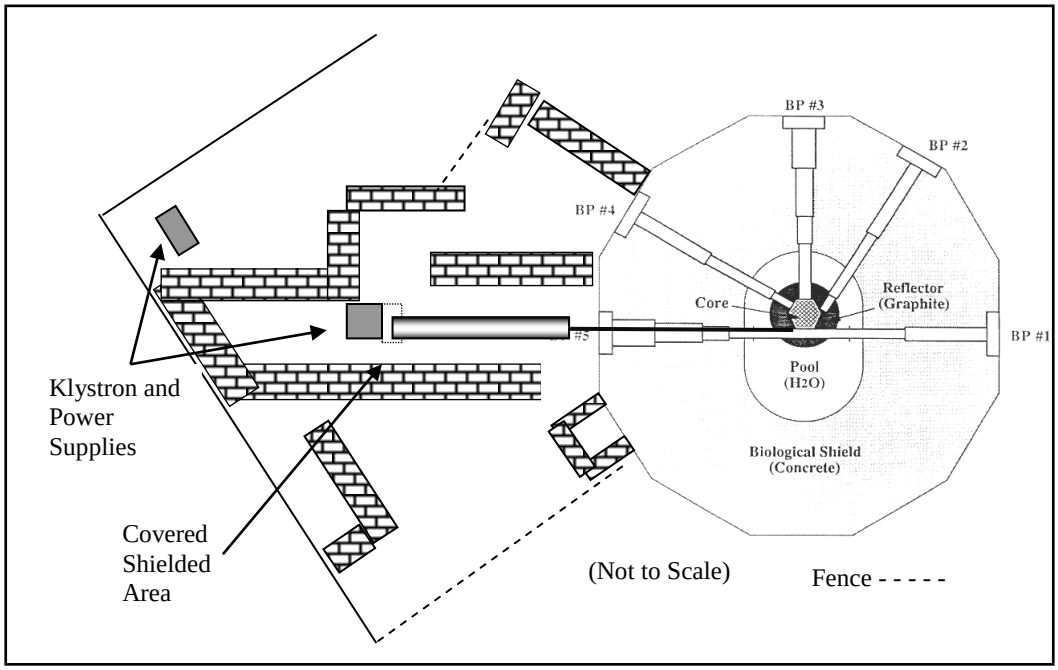

Fig. 3.2. UT-RACE accelerator in cave (roof removed).

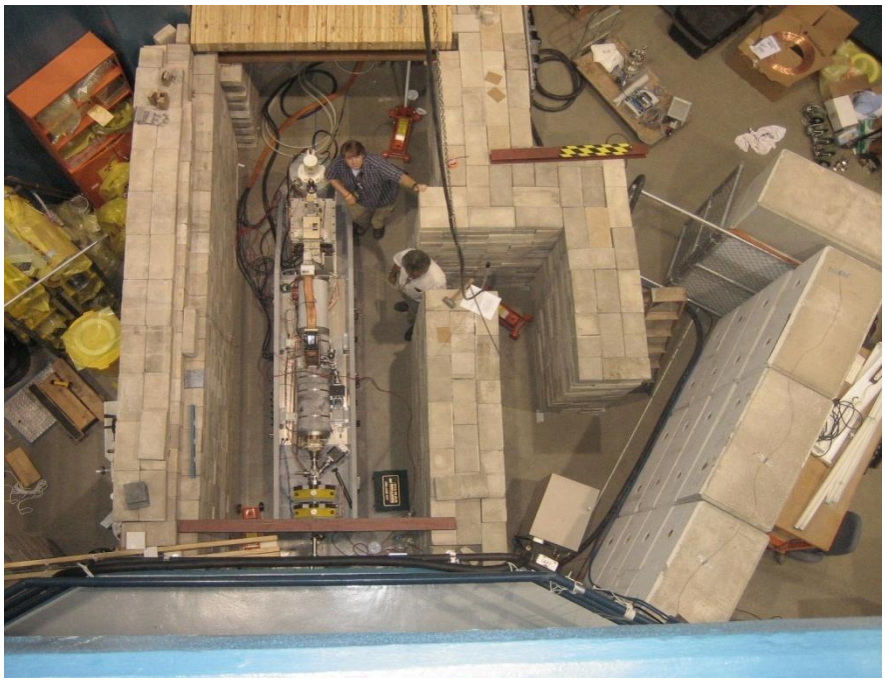

Operating the linac with the target in Beam Port 5 placed the neutron source within ten centimeters of the reactor fuel as shown in Figure 3.3 but the source was now primarily surrounded with the graphite of the TRIGA reflector reducing the effective importance of the linac source as many of the neutrons produced by the bremsstrahlung-photoneutron source entered the graphite and then diffused into the reactor or leaked out of the system altogether. Figure 3.4 is an MCNPX mesh tally showing the neutron flux around the linac neutron source in the beam port and indicates the extent that the source neutrons are "lost" and not available for subcritical multiplication.

Fig. 3.3. MCNPX model of UT-RACE configuration.

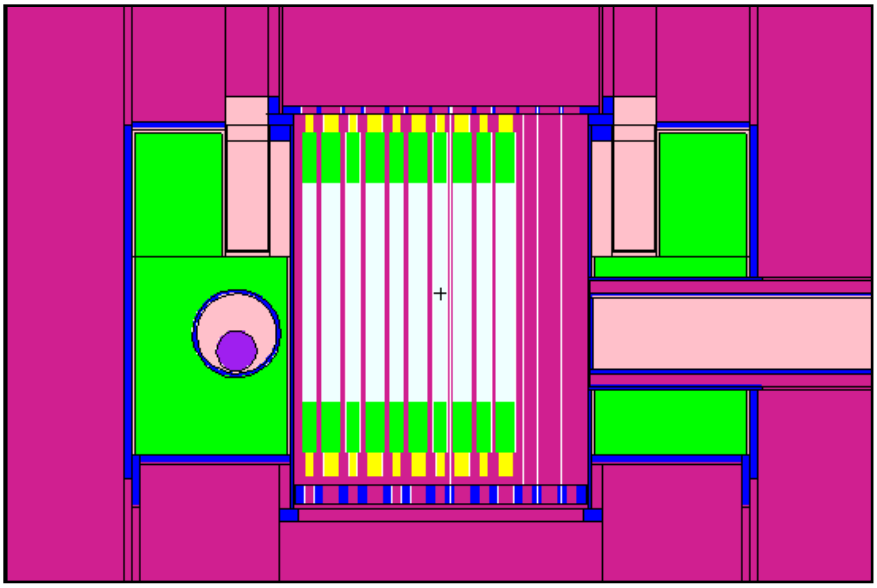

Fig. 3.4. MCNPX mesh tally of neutron transport from linac target.

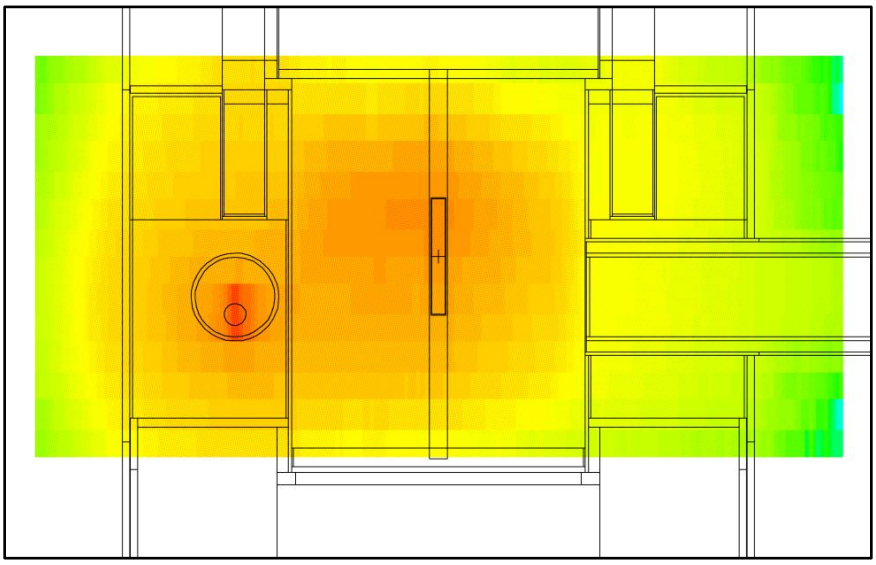

Full scale ADSS are expected to operate with all control rods (very few are needed) fully withdrawn with power controlled by the external accelerator beam[49, 50]. The UT-RACE subcritical configuration was adjusted based on recommendations from the EUROTRANS collaborators to operate with all four control rods fully withdrawn to avoid rod-shadowing of detectors and to simplify the modeling and analysis of data. Maintaining the reactor subcritical with all rods withdrawn also prevented inadvertent criticality as this was prohibited under the authorization to operate the electron linac within the neutron beam port. This configuration required unloading 25 fuel elements from the reactor core prior to each experiment phase but the core was unloaded asymmetrically to maintain the most efficient coupling of the reactor fuel to the linac target as shown in Figure 3.5 and a core grid location map in Figure 3.6.

Fig. 3.5. MCNPX model of UT-RACE core configuration with linac target.

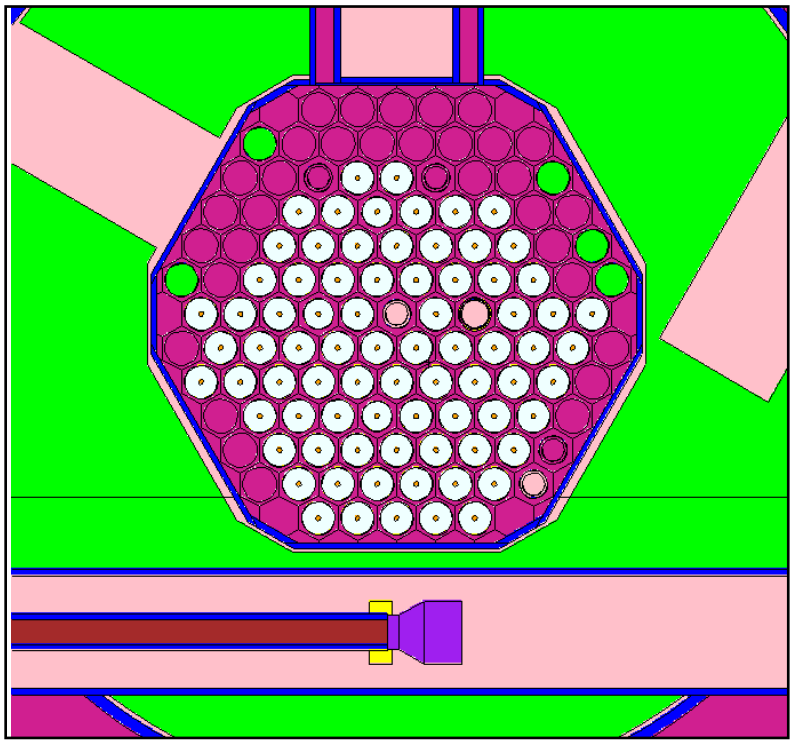

Fig. 3.6. Core location map.

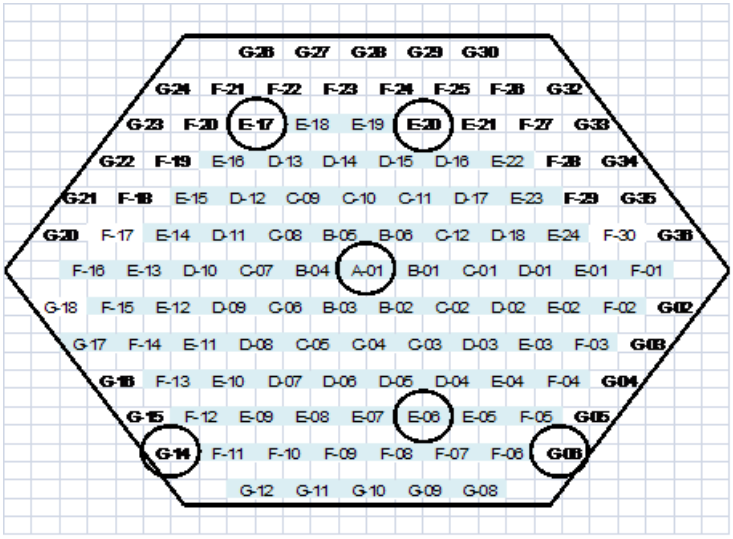

3.3 Linear Electron Accelerator (Linac) Installation

The electron linear accelerator used in the UT-RACE project was a modified Varian Clinac 20 system originally used for medical radiation therapy and irradiation of mail. The typical medical oncology linac is vertically aligned to conserve floor space but for the UT-RACE project the accelerator was configured to be horizontal and relatively easy to move by installing it on a wheeled, steel carriage. The installation of the linac began with the nearly complete tear down of the existing Beam Port 5 neutron radiography shield area. At a minimum, the roof of the "cave" had to be removed to install the linac but additional space was needed within the cave to permit movement of the linac for temporary removal and storage during alternate critical reactor operations. The length of the cave was increased to permit the linac carriage to roll back approximately 2 meters into a storage position while other experiments were performed using the facility.

The power requirements of the linac power supplies and cooling system were calculated to be 150 Amps but with an expected peak current of 175 Amps during linac startup. Permanent local power was avoided in order to reduce costs for the temporary installation of the linac and a single 3-inch diameter, 3-phase, 200 Amp power cable was installed with a large power disconnect mating to the linac systems.

3.4 Operation of an Electron Linac

The fundamental operation and the operational characteristics of the small electron linear accelerator used in the RACE project is important as it played such a significant role in the overall neutron production and experiment success. The Clinac 20 electron accelerator system consists of an RF (radio frequency) driver, modulator, pulse transformer tank, klystron RF amplifier, circulator, and accelerator guide[51]. These components are shown in Figure 3.7. The klystron is shown in blue, the accelerator guide is magenta and the quadrupole magnet is red. Additional high voltage power supplies, pulse forming network (PFN) and cooling systems were maintained outside of the shielded cave area.

Fig. 3.7. 3-D view of UT-RACE linac.

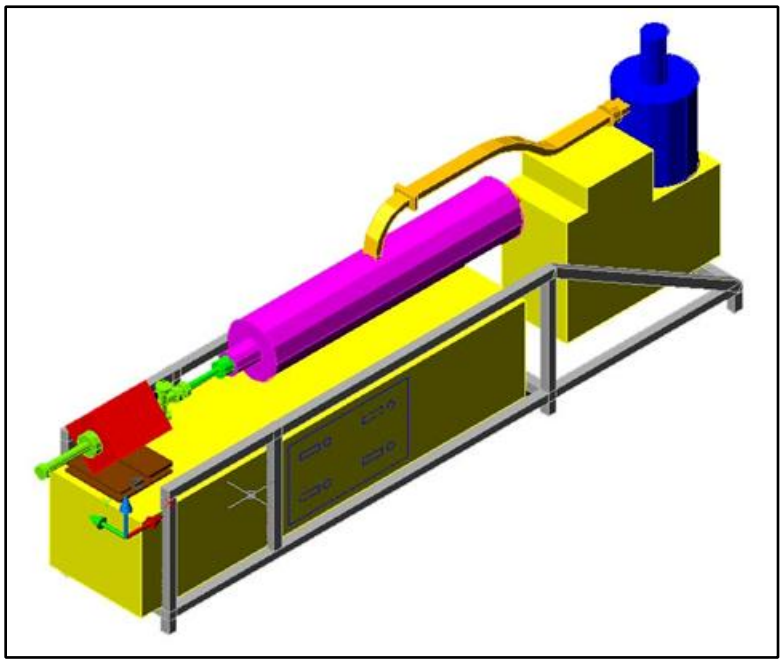

The initial electron pulse from the linac is formed from a cloud of electrons produced within the linac electron gun assembly. The electron cloud is formed around a heated thermoionic filament and held in location around the cathode by a slight (-110 VDC) negative bias on a control grid. When the linac is pulsed, this grid is rapidly switched to a positive potential and the electrons are forced into the entrance to the accelerator guide as diffuse pulse. The copper accelerator guide consists of an initial buncher cavity followed by a series of resonant accelerating cavities designed to operate at 2856 MHz. This frequency is in the so-called "S-band" between 2.0 and 4.0 GHz that lies technically between Ultra and Super High Frequency (UHF and SHF). The buncher cavity forms the initial 5 μsec electron pulse with RF energy from the klystron amplifier and the subsequent resonant cavities accelerate the electron pulse to nearly the speed of light with an energy output somewhat dependent on the tuning of the system and the total energy available from the RF system.

The RF system consists of the RF driver, klystron, circulator and wave guide although the accelerator guide is usually considered a part of the RF system. The RF driver produces approximately 400 W of instantaneous RF power which is then amplified by the klystron. The klystron operates in similar fashion to the accelerator cavities but uses a very high negative voltage (125 kV) pulse from the pulse transformer to drive the electron pulse past the resonant cavities in the klystron which the transfer power to the electrons traveling through the klystron. This high voltage pulse comes from the pulse forming network (PFN) which is charged by the 21kV produced by a Lambda 1202 capacitor charging power supply. The electrons do not leave the klystron but will transfer the remaining power (approximately 50%) to the anode which must be constantly cooled to prevent damage and maintain the internal vacuum. The instantaneous RF power of the klystron used in RACE was 5.5 MW.

Unfortunately, linacs such as the UT-RACE machine do not have infinite power available to accelerate electrons. The energy transfer from the RF field to the electron cloud has limitations and the linac operators had to carefully observe and adjust the linac parameters for the highest neutron yield. The linac operation may be best characterized by the accelerator dependent load-line which has the equation

$$E = A(P)^2 - BI \tag{3.1}$$

Where: E is beam energy in MeV;

P is the RF power in MW;

I is the instantaneous beam current through the guide in Amps;

A and B are linac dependent (number of cavities, frequency, *etc.*) constants.

Figure 3.8 shows that the average energy of the electrons within the pulse goes down as more beam current is extracted from the linac and the stored RF energy is used.

Fig. 3.8. Typical load-line for electron linac.

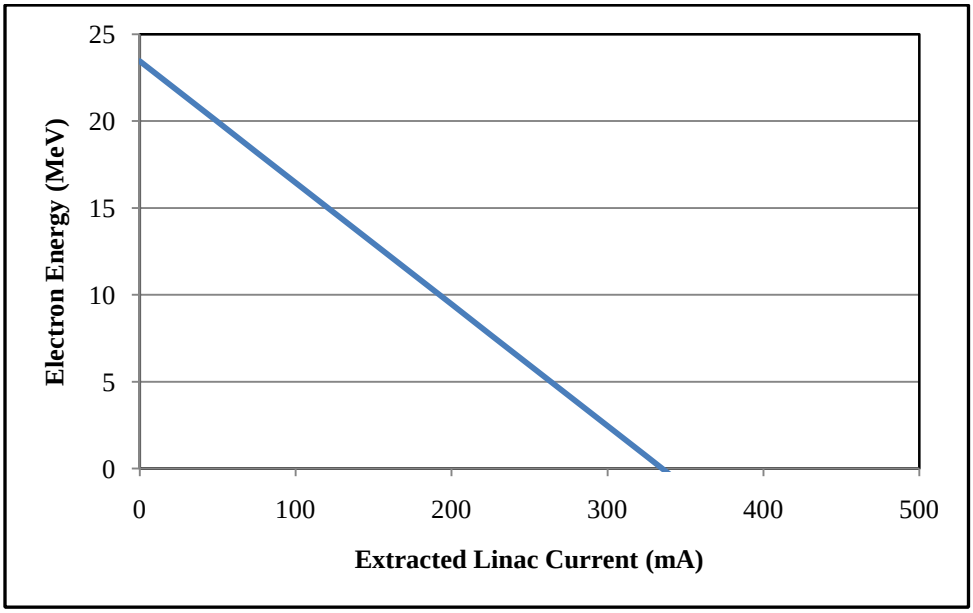

During the initial test phases of the project, the linac operators attempted to maintain an electron current of 300 mA to produce as many electron interactions as possible but this proved counterproductive and the current was reduced to 200 mA as balanced point of operation[52]. The neutron production rate with the W-Cu target was dependent on electron energy and small deviations in average beam energy had significant effects on the total neutron production in the target because the threshold point for photoneutron production in these materials was greater than 12 MeV[53-60]. For a heavily loaded linac (high extracted current) the average electron energy of the pulse could fall below the threshold energy for photonuclear neutron production and significantly reduce the neutron production in the target.

Another limitation of the RACE accelerator was the overall duty cycle of machine. The duty cycle is simply the ratio of the linac pulse width and the time between

pulses in which the PFN recharges and sufficient RF power is produced for another accelerated electron pulse. The Varian Clinac 20 was designed for high duty cycles and a typical value for the machines is 0.01. At too high an operating frequency (low pulse repetition rates), the linac RF system could not sufficiently recover between pulses to fire and produce additional high energy pulses and the beam power will drop off.

The UT-RACE project was also intended to demonstrate the feasibility of accelerating electrons and then allowing the electron pulse to travel or drift for significant distances (as much as 4 m for UT-RACE) before impacting the target. A concern was that the limited space in a reactor beam port or pool would inhibit the use of quadrupole focusing magnets to keep the beam well focused within the vacuum tube. The mutual repulsion of the electrons (space charge effects) and stray magnetic fields could induce a beam spreading or defocusing that could result in no usable beam interacting with the target. Minor beam divergence was not expected to affect neutron production within the W-Cu target because there was no need for a small, focused beam. A defocused (but small diameter) beam improved the safety of the experiment because a small spread in the beam reduced the local heating and likelihood of damage to the W-Cu target. However, there was no experience base on how far the beam could drift after acceleration before diverging and impacting the walls of the beam tube. The beam optics and electronic transport of the UT-RACE project were modeled using the code COSY INFINIT and it was shown that a 25 MeV unfocused but parallel 1 cm diameter electron beam could be transported up to 9.71 m in vacuum and maintain beam structure with an approximate 10% beam loss from off-energy electrons[61].

3.5 Linac and Target Instrumentation

There were three experimental phases of the UT-RACE project from August 2005 to March 2006. Phase One consisted of the installation, initial testing and first experiments with the linac installed at the NETL. Phase Two was performed for two weeks in October 2005 to fully characterize the linac and shield structure, evaluate the IAC instrumentation system and perform neutron flux measurements to evaluate the neutron

production of the linac and target system. Each phase required at least a week before beginning experiments to allow time for conversion of the TRIGA core and the installation of the linac and target. An additional week was required following experiments to convert the reactor back to an operational status and allow the radioactivity of the W-Cu target to decay for safe handling and removal.

Table 3.1. Operational schedule for UT-RACE experiments.

UT-RACE Linac Operational Period	Dates of Performance
Phase 1	August 10 - August 20, 2005
Phase 2	October 10 - October 20, 2005
Phase 3	January 17 - March 8, 2006

3.6 Performance of UT-RACE Linac

The linac was fabricated and briefly tested by the IAC prior to shipping the machine to Texas in late July 2005. The installation was completed and the first operational tests began in the first week of August 2005. Radiation dose rates outside the BP5 cave were far higher than expected from leakage electrons as the primary target stopping the electrons was within the reactor pool adjacent to the reactor and heavily shielded[62]. These high doses required the addition of more shielding to cave and linac to reduce the dose rate outside the NETL building to less than 2 mR hr^{-1} as required by Federal regulations[63].

During the linac testing and operation, it was difficult to determine exact beam position and focus because of the lack of beam diagnostic equipment. In other circumstances, particle beam energy and quality may be determined by an analyzing magnet which will bend the charged beam in a curved path and the amount of magnetic field required to turn the beam is a function of the particle energy. An analyzing magnet system was not used during the UT-RACE project due to the limited space available in

the BP5 cave and beam pipe to the reactor. Initial beam focus was determined by the amount of energy deposited onto the target as shown by the change in thermocouple temperatures. The linac operator adjusted the focus to achieve a maximum temperature and the beam energy was correlated very roughly to the neutron count rate on the reactor instrumentation. This crude instrumentation was felt to be sufficient at the time because, as was noted previously, tight beam focus was not a requirement to the photoneutron production within the target. There was concern that the electron beam energy or current from the target was low because the temperature of the W-Cu monitored by thermocouples did not rise above approximately 40C which was far lower than the 300C calculated for a 1.6 kW electron beam using the program heat transfer code FLUENT[64]. Figure 3.9 below is a compressed data stream of target temperature as a function of linac power and time. The periodic oscillations in front and back target temperatures (RTD-f and RTD-b, respectively) were caused by the cycling of the target chiller that cooled circulated cooling water. The linac power and neutron production were monitored using the TRIGA reactor console NM-1000 wide-range neutron instrument. The left-hand chart scale is not directly correlated to the data plot due to the auto-scaling of the NM-1000 Wide Range neutron monitor.

Fig. 3.9. Linac target temperature and reactor console neutron instrument response.

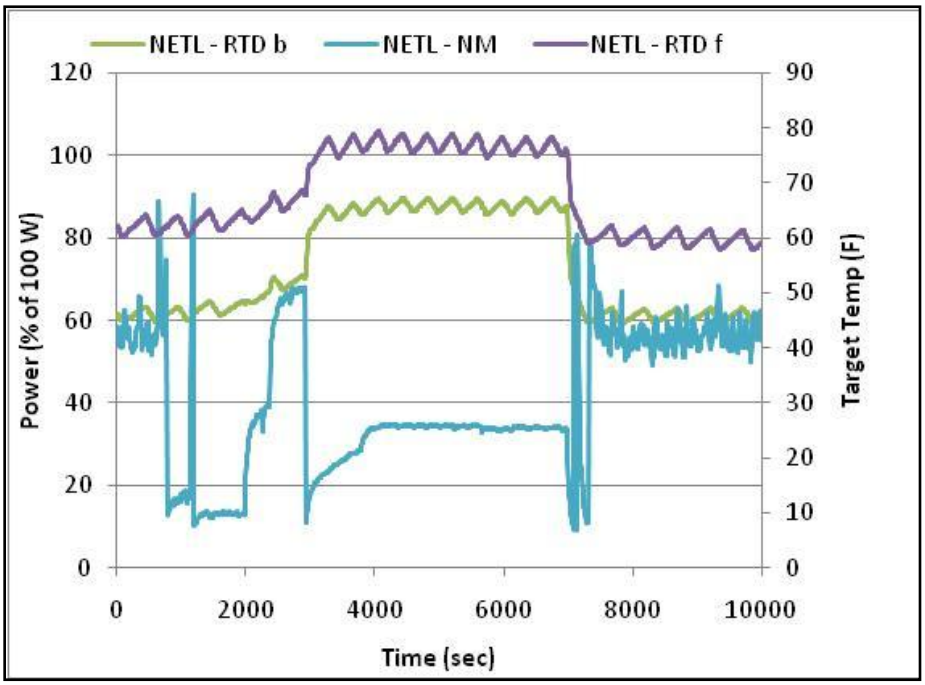

Lower than expected target temperatures, lower than expected neutron production and high external radiation levels produced from the operating linac during the initial testing phase of linac operations were evidence that insufficient electrons were emerging from the linac or impacting the W-Cu target. During the preparations for Phase II, the linac quadrupole magnet on the front of the machine was found to have moved out of alignment slightly but enough that the centerline of the accelerator cavity was not aligned with the vacuum pipe passing through the quadrupole. This clearly would interfere with the electron beam travel through the focusing magnets and would result in a significant beam fraction impacting the stainless-steel walls of the beam tube. The location of this misalignment was in the approximate position within the cave in which unusually high radiation levels were found during Phase One testing. The quadrupole magnet was realigned prior to Phase Two linac operations but the current output of the linac still needed to be measured to address the low neutron production from the target. To

measure the electron current exiting the linac and entering the vacuum drift tube to the target, a round pickup-coil was installed around the beam pipe prior to installation of the linac vacuum pipe and target in the beam port. This pickup-coil worked on the same principle as a clamp-on ammeter to measure current in electrical cables and had been previously calibrated at ISU. The electron current leaving the accelerator was measured during the second phase of the UT-RACE project and was found to be approximately 100 mA which was the expected current output put from the linac. The realignment of the quadrupole magnet allowed more of the electron beam to travel to the target but there did not appear to be any increase in the target neutron production or target temperature from previous testing.

During Phase Three, the linac target was modified to act as a current sink or Faraday cup so the actual electron beam current impacting the target could be measured. The current flowing into the target was found to be only 50 mA indicating that half the electron beam leaving the accelerator was lost prior to reaching the target[65, 66, and 67]. It is suspected that the lost electron current was low-energy particles that were easily swept from the primary beam by space charge interactions and local magnetic fields but this could only be evaluated with more sophisticated beam quality indicators and analyzing magnets .

The electron accelerator performance from day to day was another uncontrolled experimental variable because the neutron production from what appeared to be consistent and identical linac control setting would drift for no apparent reason. This random variable made comparison between individual data sets difficult as there was no pattern to the variations. Table 3.2 gives examples of essentially constant electron beam current and frequency resulting in large changes in the indicated power as read on the NM-1000 neutron monitor which was proportional to the neutron production in the linac target.

Table 3.2. Daily variation of linac neutron production.

Date (2006)	Target Current (mA)	Linac Frequency (Hz)	Indicated Reactor Power (watts)
Feb 14	38	170	70
Feb 15	34	170	35
Feb 16	39	170	51
Feb 17	38	170	37
Feb 27	39	180	40
Feb 28	38	150	20

3.7 Neutron Monitoring Instrumentation

To evaluate the neutron production of the target and the multiplication in the UT-TRIGA core, some method of real-time neutron flux measurement was required for UT-RACE. Traditional pulse-counting nuclear detection systems were difficult to use because the so-called gamma flash of bremsstrahlung radiation when the linac electron pulse hits the W-Cu target[68]. A typical neutron counting experiment using neutron sensitive boron-trifloride (BF_3), Fission Chambers or ^{3}He detectors is shown here:

Fig. 310. Typical neutron pulse counting electronics.

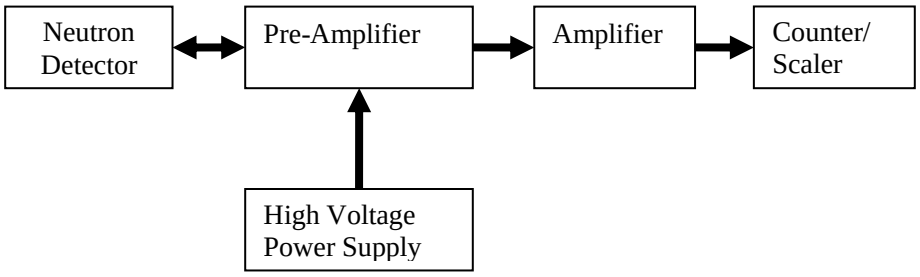

The preamplifier has three functions: it must provide impedance matching to the detector and cabling to avoid reflected pulses and loss of signal, it must block the high DC voltage (300-2000VDC) that powers the radiation detector from damaging the circuits following the preamplifier and it must provide a high gain amplification (typically >30,000) of the detector pulses to improve the signal to noise ratio[69, 70]. The preamplifier is generally placed as close as possible to the detector so the pulses are amplified before travelling a possible large distance to the remaining electronic systems. The high voltage powering the detectors is blocked by a capacitor circuit which passes the varying pulses with a frequency response that is a function of the circuit time-constants.

The neutron detectors are sensitive to neutrons and gamma-rays so each type of radiation will produce an electric pulse but the neutron will produce a slightly higher magnitude pulse because the daughter particles from neutron absorption are more ionizing than photons. Gamma-ray background and electrical noise is removed by the adjustment of the lower level of the discriminator to filter out low intensity pulses. However, in a high gamma-ray background or with electrically noisy systems, the non-neutron pulses may pileup and become much larger than the neutron pulse giving a false neutron count.

Because the radiation environment near the UT-RACE core had a very high gamma to neutron ratio, fission chambers were selected for neutron detection. The UT-RACE radiation environment was not typical of the radiation field around a nuclear reactor and the very high bremsstrahlung burst when the linac fired produced a gamma

pulse in the FC that was many times higher than the neutron pulses produced from the photonuclear produced neutrons. Although the linac pulse width was only 3-5 microseconds, the large spike on the sensitive electronics caused an over-range condition that required 5 to 10 msec for the system to recover sufficiently for individual pulses to be counted. Thus normal gamma and noise discrimination was found to not be possible using pulse counting electronics to monitor the UT-RACE experiments.

No matter what the upper frequency of detector saturation, eventually the pulses will no longer be separable and the detector signal will appear as a continuous current (DC, direct-current) with a varying signal (AC, alternating-current) around the average current. Information about the overall reactor environment is contained within this detector current. The DC portion of the signal is blocked in the preamplifier but the AC signal is used in so-called Campbelling-mode or Mean Square Voltage circuits in wide-range reactor nuclear instrumentation (such as the UT-TRIGA NM-1000) by rectifying this varying signal and producing a voltage proportional to the square of the charge deposited in the detector volume. This function weights the instrument response towards the radiation producing the greatest charge deposition (*i.e.* fission fragments from neutron reactions). This mode of detector operation still requires a preamplifier circuit but the response of the NM-1000 during the first phase of linac testing indicated the reactor control system was insensitive to the gamma-flash saturation.

During the initial testing of the linac with the target adjacent to the reactor, the only neutron detector signal that was found reliable at the time was the installed Reuter-Stokes RS-314 wide range fission chamber used in the TRIGA console NM-1000 Wide Range Instrument. The indicated power on the NM-1000 during all three phases of the UT-RACE project was never greater than 100 watts, which is below the range of Campbelling operation (cross-over is adjusted to occur around 1 kW), but the instrument operated reliably throughout the range of the UT-RACE experiment and was expected to be a primary safety channel during proposed high-power linac operations.. This fission chamber is located approximately 15 centimeters above the top of the reflector in a detector support tube attached to the outer wall of the reflector assembly immediately

outboard of position G-33 of the reactor grid plate. This places the FC approximately 1.2 meters from the target on the other side of the reactor and reflector. It is theorized that the distance from the linac target and the shielding of core materials reduced the gamma flash sufficiently for the NM-1000 to provide useful information on the neutron multiplication while the linac operated at various frequencies. A plot of a typical NM-1000 output is shown in Figure 3.11. It is noted that the signal is very smooth as would be expected with the relatively long time-constants of the NM-1000 and the diffusion of the initial neutron pulse through the reactor core. Figure 3.10 shows the typical response of the TRIGA reactor while operating as an ADSS over long periods including a step response to the linac operating at 180 Hz at approximately the 25 s point. The linac frequency was dropped momentarily near 300 seconds and finally the linac was tripped fully off at approximately 425 s.

Fig. 3.11. TRIGA console data log of linac transients and ADSS response.

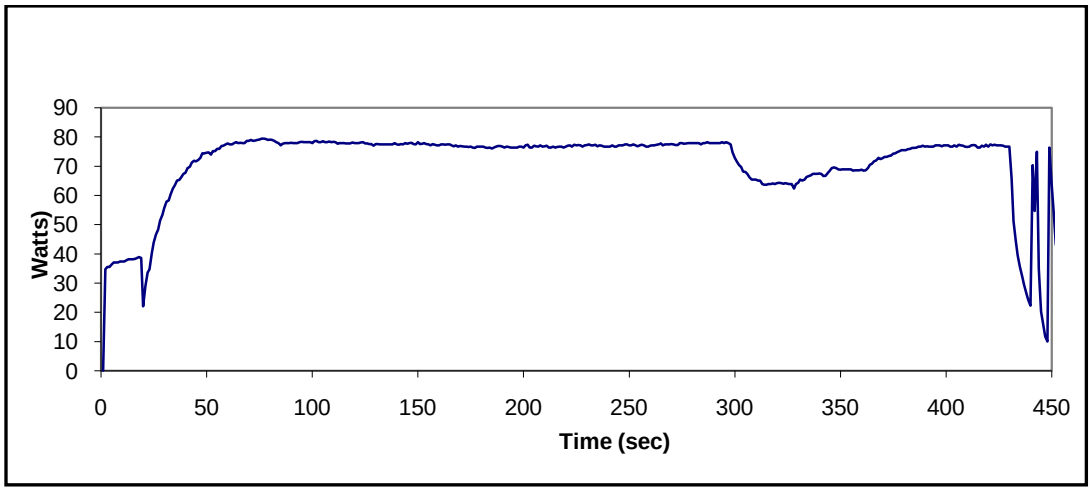

The RF and gamma-flash when the linac fired and the electron pulse hit the W-Cu target saturated the input capacitor circuit of the preamplifier for a short period (~ 5-20 msec) due to the large detector pulse but this signal time was important for the

experiment to have a full evaluation of the reactor response to the initial neutron pulse. Additionally, the relatively large signal produced by the electron linac on the detector cables due to the operation of the radio-frequency components of the accelerator power supplies produced a very high background level on the cables and no linac pulses could be discerned from the background.

Significant effort during the UT-RACE project went towards providing usable detector signals. The first new method investigated for gamma-flash discrimination was to try and suppress the short but large magnitude pulse saturating the amplifier in order to use the available pulse counting equipment for data acquisition. One option considered but eliminated was to electronically suppress the amplifier while the linac pulsed (5 microsecond pulse width) by using a gating signal to effectively turn off the amplifier for a short period initialized by the same signal that caused the linac to fire. The gating of the amplifier was effective but the preamplifier was still recovering from the detector pulse after the gating signal was removed. This indicated the primary cause of the system deadtime during and following the pulse was the saturation of the preamplifier (ORTEC 142PC) which did not have a gating capability.

As was noted before, the preamplifier blocks the high voltage that is used within the FC from entering the low voltage pulse amplification electronics by shunting the voltage to ground via an RC coupling circuit. The large capacitors used in the UT-RACE charge-sensitive preamplifiers slowed the time response of the preamplifier but must be larger than the total capacitance of the detector and coaxial cables to avoid pulse reflections. The feedback capacitor in one 142PC preamplifier was temporarily replaced with a smaller capacitor to reduce the RC time constant and the time the circuit was saturated but an improvement could not be determined because the system continued to saturate while the linac was operating.

A common method of gamma-ray compensation in nuclear instrumentation for control and monitoring of larger nuclear research and power generation reactors may use the technique of gamma-compensated ion chambers to reduce the magnitude of the gamma-induced currents at low reactor power levels when the gamma background is

proportionally higher than the neutron level. This technique was extended by Koehler to monitor (n, p) and (n,α) reactions but included a gamma background reduction using uranium as a shielding material[71]. Space limitations in the TRIGA grid plate prevented the use of gamma-ray shielding around the detectors during the UT-RACE experiments although experiments performed at IAC indicated an improvement of approximately 5 msec in the recovery time of the detection electronics using lead shielding around the neutron detectors. A variation of the lead and uranium gamma shielding method was evaluated during the UT-RACE project by placing the monitoring neutron detectors on the opposite side of the TRIGA core from the linac target. Unfortunately, the gamma-ray and radio-frequency noise from the linac operation continued to saturate the detector electronics and no usable neutron signal was produced.

An extension of the compensated ion-chamber technique is currently utilized to monitor the Los Alamos Neutron Science Center (LANSCE) lead slowing-down spectrometer (LSDS) near the 800 MeV proton beam spallation source by using photovoltaic cells coated with ^{235}U or ^{239}Pu[72]. These detectors significantly reduced the gamma-flash induced signal before preamplification allowing measurements with time resolutions of nearly 1.5 μs following the pulse of the accelerator but the specialized detectors and electronics were beyond the budgetary constraints of the UT-RACE program.

3.8 Gamma Flash Compensation in Pulse Mode

Although there was insufficient linac operation time to fully test it, a unique method of gamma-flash suppression and high voltage blocking was devised and tested for the UT-RACE project using a three-winding isolation transformer. The system developed is shown here in Figure 3.12 where the "dot" convention for transformers indicates if the current flow in the primary windings are in phase or opposite phase of the secondary winding.

Fig. 3.12. Pulse transformer coupling and gamma compensation circuit.

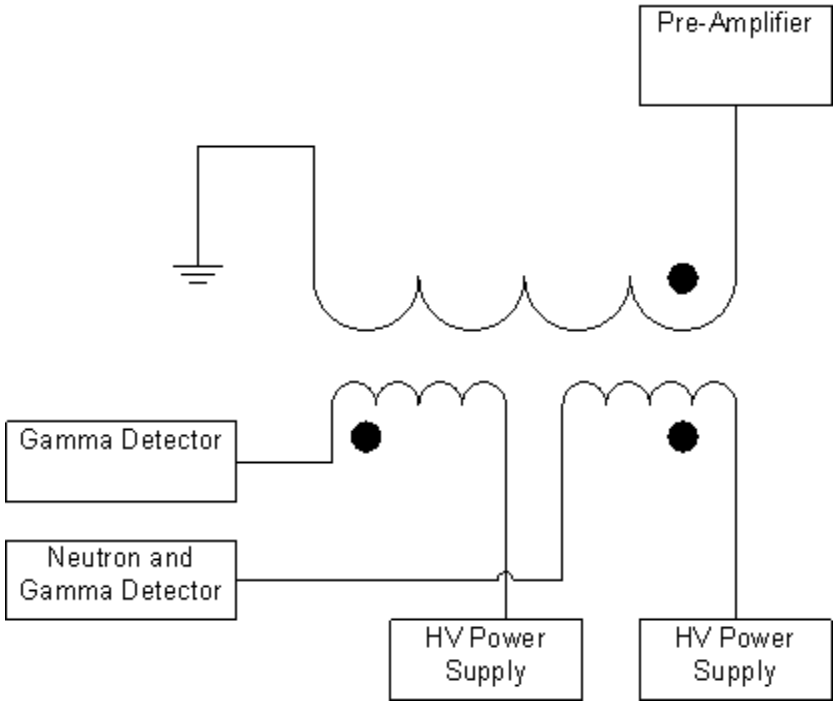

The compact pulse transformer selected (C&D Technologies 1002) had a 1:1:1 turns ratio, was rated at 2000 V_{RMS} and was wired such that the DC voltage used to bias a detector passed through the primary (one of two) of the transformer and was not placed directly on the preamplifier input eliminating the DC-blocking capacitor saturation. A separate gamma sensitive (not neutron) detector signal passed through the other primary winding but counter-flow to the neutron-gamma current from the other detector. The magnetic fields produced from the neutron detector and the gamma detector would cancel each other within the secondary winding but because the neutron pulses would be a higher magnitude than the gamma pulses, the net effect would cancel only the gamma pulses (including the gamma-flash pulse) and the common-mode electrical noise from the detector cables. The output of the secondary winding would output to the preamplifier and carry the signal without the high voltage or the gamma flash. In order to operate correctly, the magnitude of the signals coming from the two detectors would need to be

approximately equal and the cable lengths from the detectors would need to be equal to assure the pulses would arrive at the transformer at the same time.

This transformer filtering system was built for in-core detector testing but the only gamma sensitive detector that was available and could be used during the initial tests was a Geiger-Mueller detector that was operated at lower voltages in an attempt to use it as an ionization chamber. Unfortunately, the detector tube was very radiation sensitive and would stay fully ionized at low voltage when the linac was operating. A set of small (0.635 cm OD, 2.54 cm length), matched fission chambers and gamma ionization chambers (LND-30753 and LND-50111) had been ordered from LND in June 2005 for delivery before the second phase of the RACE project scheduled for October 2005. The four chambers arrived in the first week of January 2006. It was determined after testing the new fission chambers and gamma detectors with various neutron and gamma sources that the detectors were not operating and they were returned to the factory for repair. The four detectors did not arrive again until the first week of March 2006 at which time other neutron detection systems were utilized and there was no time to test the chambers with the available time remaining to complete the UT-RACE experiments.

To show the circuit performed as designed, the circuit was bench-tested using a separate pulse and square-wave generator to simulate detector pulses. A square wave input was generated to simulate a periodic neutron pulse train from the fission chamber with a frequency of 50 kHz and an amplitude of 1 volt. To simulate the periodic pulse of the linac firing, a 20 Hz series of pulses with an amplitude of 7.5 V (the maximum output of the pulse generator) and width of 3 μs was used for an interference signal.

Fig. 3.13. Transformer pulse in and pulse out.

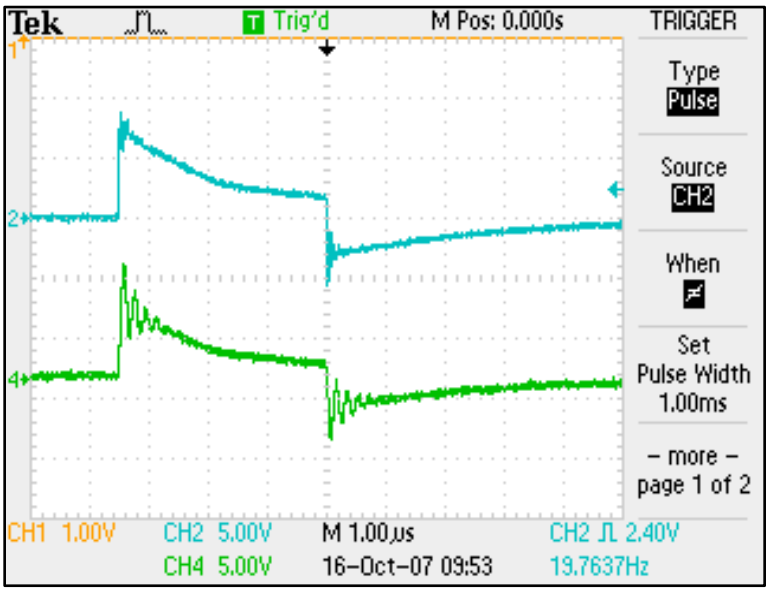

In Figure 3.13 above, the 20 Hz pulse is monitored with a Tektronix 2150 four-channel oscilloscope at the input of the winding #1 and again after it has been passed to winding #2 with no change in amplitude. A rapidly changing signal passing through a circuit with reactive (capacitance and inductance) components may induce a "ringing" that is at a frequency determined by the installed and stray capacitances and inductances and this ringing may be seen on the leading and trailing edge of the pulse at the output. The input pulse was then split between the two primary windings with current flow through the windings in opposite directions to show the cancellation of the pulse on the secondary winding (Figure 3.14).

Fig. 3.14. Pulse subtraction in transformer.

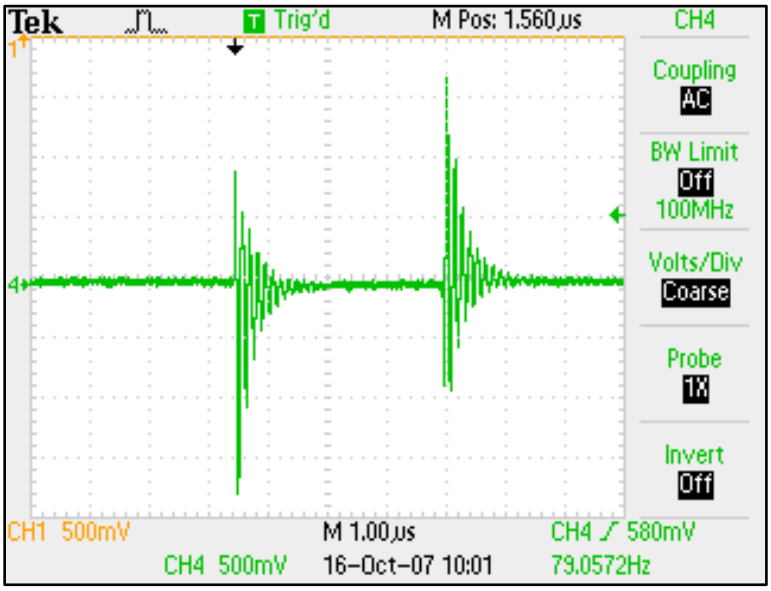

Figure 3.14 shows the input pulse was completely cancelled with only the smaller magnitude ringing remaining on the output. This ringing is at a frequency of 80-90 Hz but appears at the lower pulse frequency of 20 Hz.

Figure 3.15 shows the reference relationship between the input pulses and the high frequency square wave. The combined waveforms are shown in Figure 3.16 and indicate the interfering pulse has modulated the carrier square wave to produce a 15.3V peak to peak signal at the 20 Hz frequency.

Fig. 3.15. Square wave and pulse waveforms.

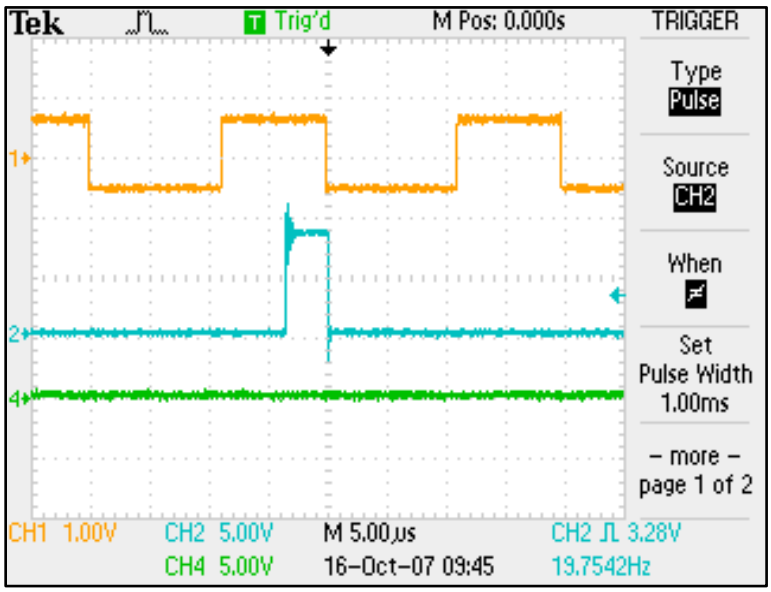

Fig. 3.16. Two signals added at input of transformer.

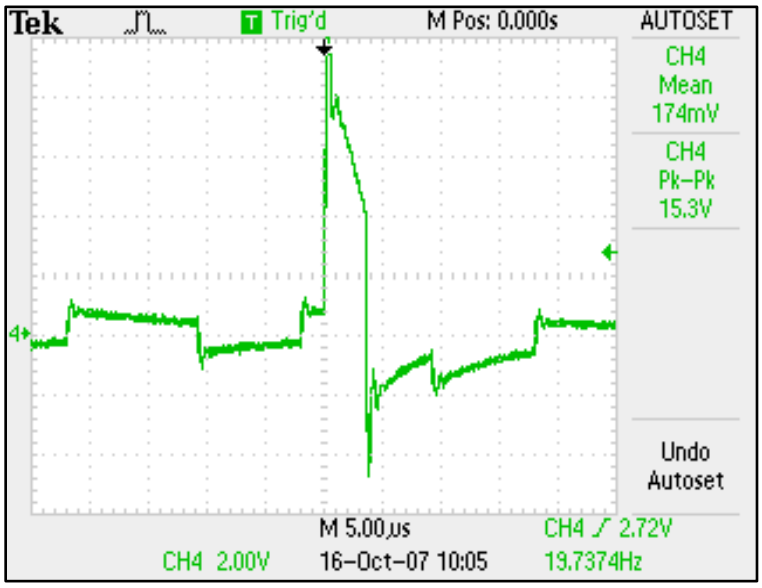

Fig. 3.17. "Linac" pulse cancelled at output to pre-amplifier.

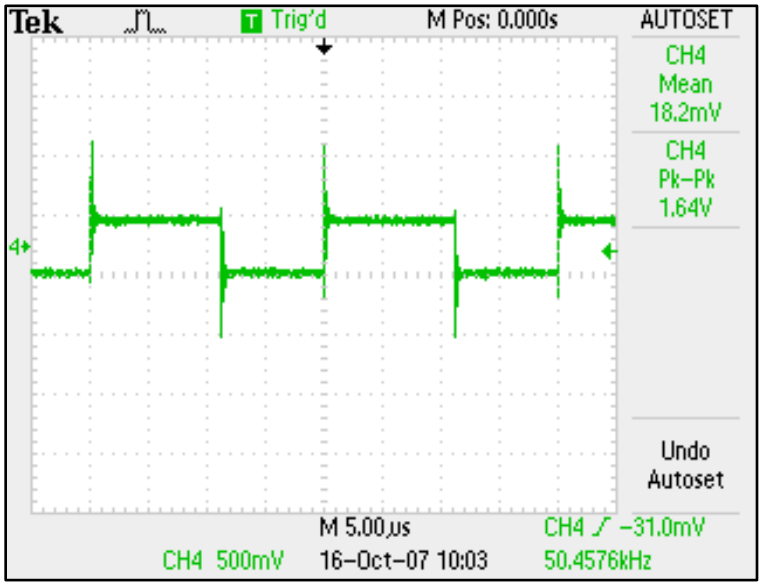

Finally, the isolated and inverted pulse signal is applied to the other primary winding resulting in an interference-free signal as shown in Figure 3.17. The normal ringing of the transformer is seen at the leading and trailing edge of the square wave but

this would not be a problem for the remaining pulse amplification and processing electronics.

3.9 Current Mode of Operation for Neutron Detectors

In January 2006, as preparations to start the final experimental phase were beginning, no reliable method of localized core neutron detection based on pulse counting technology had been developed that would not be saturated by the gamma flash. The decision was made to operate and monitor the fission chambers in current mode as pulse monitoring techniques had been unsuccessful. It had been noted that the current reading on the detector bias power supply (ORTEC 710 Quad 1-kV) would change with linac operation but when the current converted to a voltage signal was monitored with an oscilloscope it was found to be extremely noisy and the radiofrequency from the linac pulse forming network and other sources picked up on the long coaxial cables to the detectors made the signal unusable for pulse detection. Two Keithley 6485 Picoammeters were purchased to monitor the current from two available fission chambers. The Keithley 6485 (K-6485) is a digital picoammeter that may be programmed and monitored remotely via RS-232 or IEEE-488[73].

3.10 Frequency Response of Instrumentation

In order to use the FC in current mode is was necessary to provide bias voltage to the detector but not allow this voltage (+300 to 500 VDC) at the input of the Keithley 6485 as this would damage the picoammeter. To keep the electric field in the same direction within the detector and thus produce pulses with the same polarity, the bias voltage on the outer detector can was set at negative 300 VDC. The voltage configuration, shown in Figure 3.18, electrically raised the center FC anode to a positive 300 VDC relative to the cathode while maintaining the anode at ground potential relative to the input of the K-6485. The detectors and all connectors were electrically insulated for personnel safety and to prevent grounding the power supply to the aluminum pipe surrounding the detector by heat shrinking insulating sleeving around the detectors. The

high voltage supply and the low voltage signal return were provided by two separate coaxial cables to reduce electrical noise pickup on the long detector cables. The outer shield braids of the two coaxial cables were shorted together and connected to the chassis ground of a separate electronic system to prevent ground loops.

Fig. 3.18. Reverse biasing of fission chamber.

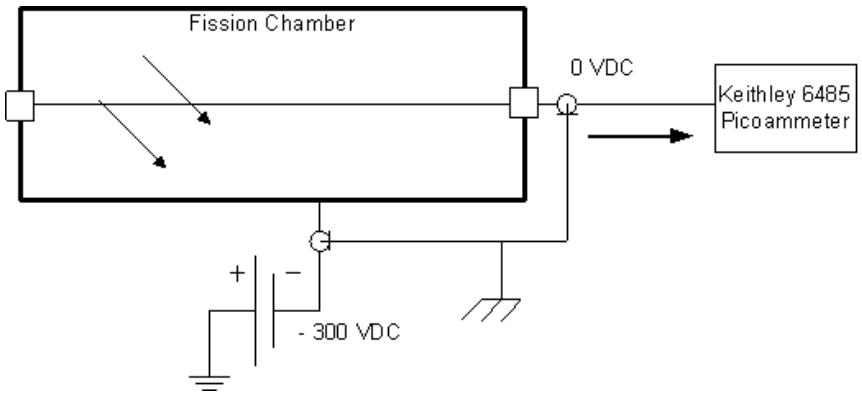

The K-6485 is a low-cost, high-resolution programmable digital picoammeter but was not designed to be a high speed data acquisition system front-end. The inherent system limitations were due to the relatively slow analog to digital (A/D) conversion but also to the slow rise time caused by the high (1 μF) input capacitance of the instrument. The K-6485 front panel RATE selection changed the integration time of the internal A/D converter which was the sampling time as a function of the power line frequency or cycles (*i.e.* 1 PLC is a16.67 ms sample rate) and allowed the operator to selectively filter the input by taking an average measurement over a longer time period. The measurements for UT-RACE were initially taken on the FAST setting which gave a sampling time of 0.1 PLC or 1.667 ms. This sampling frequency (600 samples s^{-1}) was adequate to avoid signal aliasing because the highest expected linac frequency was 200 Hz which was below the Nyquist frequency of 300 Hz[74]. However this sampling rate was not adequate to measure the higher frequencies of the neutron counting rate and the rapid signal level changes as the linac pulsed. Rather than use the K-6485 A/D circuitry to acquire and process the detector signal at a relatively low sample rate with a limited

storage buffer size, the decision was made to use the analog output of the K-6485 for a faster and more reliable time and sampling response. The K-6485 analog output has a 500 μsec rise time response to a step input signal and provided an inverted and scaled ±2 V output without losing information by digitizing the signal. The 500 μs rise time of the K-6485 is equivalent to a 700 Hz bandwidth which is a slightly improved frequency response but still significantly slower than the 200 ns rise time of the pulses and pulse frequency coming from the fission chamber[75].

This limited frequency response of the system was found to not be a significant problem because the detector current measured was the total charge deposited within the chamber per unit time or the neutron count rate. Operating the detector system in current mode integrated the charge deposited per unit time which was provided an average count rate and the desired parameter necessary for later analysis. The slower rise time of the K-6485 provided a secondary but significant system benefit by acting as a high frequency filter and limiting the measured peak current from each 5 μs linac pulse. The slower response time of the K-6485 meant that the transient was over before the picoammeter responded more than 3% of the full pulse magnitude and prevented overdriving subsequent circuits in the acquisition system.

The 500 μs rise time (or fall time for a step-down signal) is equivalent to a 0.227 ms RC time constant and limited how quickly the K-6485 would respond and reproduce a pulse or step change[76]. Several important methods of subcritical reactivity measurement use the decay of the prompt neutron level with time to determine system reactivity so a very long time constant could obscure the neutron level decay. This was found to not be a problem for the UT-RACE data because the time constants of the critical thermal reactor system are at least 20 times longer than the K-6485 input time constant.

The output of the K-6485 was directed to a 4-channel, Tektronix oscilloscope to visually monitor the detector outputs during the experiment and, in parallel, to a DAQLab-2005 bench-top data acquisition system[77]. The DAQLab-2005 is a very versatile Ethernet-based PC-interfaced system with a 16-bit, 200 kHz A/D converter. The DAQLab-2005 will interface with several common acquisition programs (*e.g.* Lab

VIEW) but the system was delivered with a simple data logging program (DAQView) which proved more than adequate and was used for the UT-RACE project to save time. When monitoring the two fission chamber currents, the DAQView data logger could only acquire and store the two detector signals at the reduced sampling rate of 80 kHz because the sampling time was shared (multiplexed) between the two input channels. This time sharing reduced the effective sampling rate and this provided time bins of 13 to 20 μs. The time bins sampled were fixed at 20μs during the majority of the experiments because this resulted in cumulative time gates that were an integer multiple of the linac repetition rate. The final data acquisition system is shown in Figure 3.19.

Fig. 3.19. UT-RACE data acquisition system.

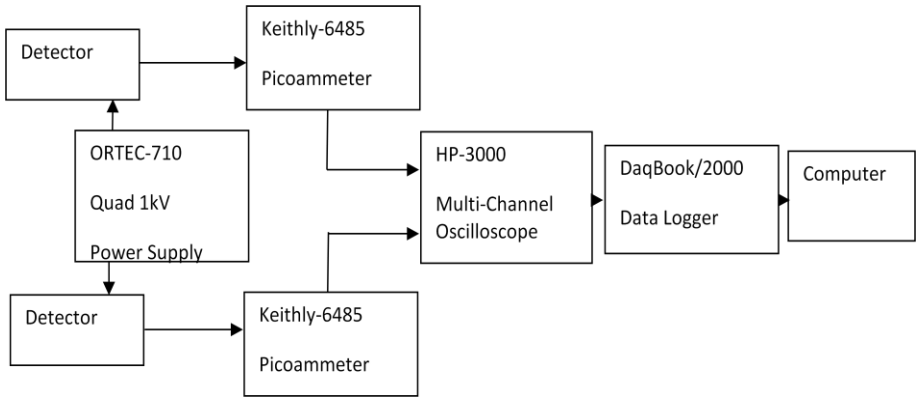

3.11 Neutron Detector Sensitivity

Due to procurement problems, a matched set of fission chambers was not available during the UT-RACE experiments to test and use the RACE transformer coupling method. Radiation detectors for neutron monitoring needed to have a diameter of less than one inch to fit down the 3.175 cm OD temporary aluminum detector tubes installed in the reactor grid plate. The only cylindrical detectors fission chambers at the NETL were two inches in diameter so one chamber was borrowed from Texas A&M University Nuclear Science Center and another was obtained from project collaborators at the Idaho Accelerator Center. The detector data is given here in Table 3.3.

Table 3.3. Fission chamber specifications for UT-RACE.

Detector Type	**Mass ^{235}U (mg) (93% enriched)**	**Efficiency (count per neutron)**	**Volume (cm^3)**	**Charge/pulse (C)**
LND-30773	120	0.001	83.66	$1.\ 0x10^{-12}$
RS-P6-0805-134	12	0.00016	83.66	$1.0x10^{-12}$

The efficiency (or sensitivity) value above is a function of the total mass (reaction cross section) of uranium although there are other efficiencies of detection based on detector geometry, physical location of the detector relative to the source and the energy of neutrons that one is attempting measure (the cross section efficiency above assumes the energy of the neutrons to be 0.025 eV).

When operating in current-mode to monitor neutrons around a nuclear reactor, the total number of fission events or pulses in the chamber per unit time are summed to create a continuous but alternating current of some root-mean-square (RMS) value that is a function of the neutron reaction rate in the chamber[78]. Each ^{235}U fission releases two fission fragments with an approximate total kinetic energy of 165 MeV. To conserve momentum, the fission fragments will travel in essentially opposite directions with one impacting the anode wall and the other entering the gas-filled chamber for ionization. The accepted value for the ionization of argon gas by a fission fragment is $2x10^8$ ion pairs $bar^{-1}m^{-1}$. Thus there were $2.54x10^6$ initial ion pairs produced by one fission event for the one-inch diameter fission chambers used in the UT-RACE experiments. Each ion pair produces $4.07x10^{-13}$ C of electric charge in the pulse by direct ionization but there will be some increase in the number of ion pairs from secondary ionization or gas amplification and contamination of the argon gas with fission product gases[79]. The manufacturer of one FC, LND, quotes a value of 1E-12 C/pulse as the measured value of the detectors but this value is quoted for all chambers purchased from the manufacturer so it is likely an

average value. It is noted that operating fission chambers in pulse mode has inherent limitations related to the fission rate in the chamber. The detectors used in the UT-RACE experiments were not qualified above a neutron flux of $1x10^6$ to $1x10^7$ n cm^{-2}-s^{-1} due to pulse pileup and a higher recombination rate so it is quite likely the linearity of the detectors would have been poor at the levels required for the experiments.

There were no data from the manufacturers, LND and Reuter-Stokes (now GE-Nuclear), providing a correlation between the current output of the detectors and the neutron flux measured. However, the following equation for fission chamber sensitivity relating current to neutron flux may be used to find this relationship if the parameters of the fission chamber are known[80].

$$S = \frac{I_{SAT}}{\phi_{th}} = \frac{\pi^2}{2} LeI_0^c P \frac{\mu_s}{M_U} N_A \sigma_{th} (r_c^2 - r_a^2) \tag{3.2}$$

Where:

I_{SAT} = Saturated detector current

ϕ_{th} = Thermal neutron flux

e = Single unit of charge

I_0^c = Number of ion pairs produced by one fission fragment

P = Pressure of gas filling chamber

$\frac{\mu_s}{M_U} N_A \sigma_{th}$ = Macroscopic cross section of U

$(r_c^2 - r_a^2)$ = Distance between anode and cathode

L = Active detector length

This equation has been shown to be accurate and benchmarked against several detectors with known parameters in Poujade and Lebrun[80]. The sensitivity of a FC may be increased by adding more uranium but this has an upper limit because the uranium coating on the anode becomes too thick and the fission fragments cannot escape to ionize the argon gas filling the detector volume or simply lose significant energy traveling

through the uranium coating[82]. Another problem discovered during ADS research requiring high-sensitivity FC is the double counting of neutrons within a FC with high uranium loading because the actual fission event in the chamber releases neutrons and the high efficiency fission chambers will detect the neutrons produced within the volume of the detector[83, 84].

The only information about the fission chambers used in the UT-RACE project not directly available from the product information sheet was the electrode gap distance so this was calculated from fundamentals based on the detector capacitance of 40 pf and the results used to compute the individual detector sensitivities here in Table 3.4[85]. As expected, the difference between the current outputs is a direct function of the mass of the uranium coating. The calculated fission chamber sensitivities are given in Table 3.4.

Table 3.4. Calculated fission chamber sensitivities.

Detector Type	**Calculated Sensitivity ($\mu A\ nv^{-1}$)**
LND-30773	5.82×10^{-8}
RS-P6-0805-134	5.82×10^{-9}

Integrated neutron flux measurements were performed using foils and wires several locations within the subcritical core while operating the linac at 180 Hz over two days in an early test phase of the UT-RACE project[86]. Gold and Indium foils were irradiated in the Rotary Specimen Rack (RSR) 18.2 cm above the linac target with 6.3 cm of graphite in the intervening space. These flux wires were placed in the five locations noted in Green[86] and Figure 3.5. Unfortunately, a direct comparison of the foil measurements to the detector currents cannot be performed as there were several physical and operational changes to the linac to increase the linac power and the number of neutrons produced for a given linac frequency between the two experimental phases. The

final data acquisition system was not available during the flux foil experiment so the only neutron level monitor available was the TRIGA reactor console NM-1000 wide range neutron monitor. Although recorded reactor power levels as read on the reactor console NM-1000 on the separate dates with nearly equivalent linac powers indicate that the neutron level was effectively the same, the daily fluctuations of the linac power for identical settings make a one-to-one correlation unreliable. Table 3.5 compares the one-group foil measurements to the calculated neutron flux values from measured detector currents obtained during later operations.

Table 3.5. Fission chamber fluxes compared to foil measurements.

Method and Location	**Neutron Flux (n cm^{-2} s^{-1})**
LND FC in G5 (Linac at 200Hz)	3.81×10^{8}
RS FC in A1 (LINAC at 200Hz)	9.40×10^{8}
RSR (18 cm above target)	3.63×10^{8}
Position A (11 cm from target)	5.89×10^{8}
Position B (22 cm from target)	1.27×10^{9}
Position C (29 cm from target)	1.26×10^{9}
Position D (34 cm from target)	1.28×10^{9}
Position E (41.5 cm from target)	8.55×10^{8}

*Foil data from Green[86].

The detectors and foils closest in physical location were the RS-P6-134 detector and the flux wire in position D near the A1 central core location. Besides the linac fluctuations, several reasons may contribute to the 30.6% difference in the two measurements. First, during the subcritical tests, the FC was within a dry, aluminum tube that displaced the reactor coolant from the A1 location changing the neutron flux and spectrum from operation with the flux wire in place. Second, the samples in the lettered positions were only two-inches long versus the six-inch effective height of the fission

chamber and in somewhat unknown axial locations producing different capture efficiencies within the non-uniform neutron flux profile. During the flux measurement experiments, the wire and foils samples were counted on a gamma detector position with a calculated efficiency and all isotopes were averaged to produce a one-group flux possibly introducing some calculation errors. Finally, the ^{235}U FC are considered thermal neutron detectors so only the thermal cross section for fission was utilized in the sensitivity calculation. The measured neutron flux values in the table account for total neutron flux of all energies and this would cause the largest difference in the measured values.

Data was compiled to verify the linearity of the FC with linac power in Figure 3.19. The detector currents exhibit some non-linearity at low pulse repetition rates but this is to be expected with low frequency oscillations because the average current has a high variability. There was no indication of detector saturation or non-linearity at higher linac frequencies giving confidence that the detectors provided a useful flux measurement.

Fig. 3.20. Fission chamber response to linac frequency.

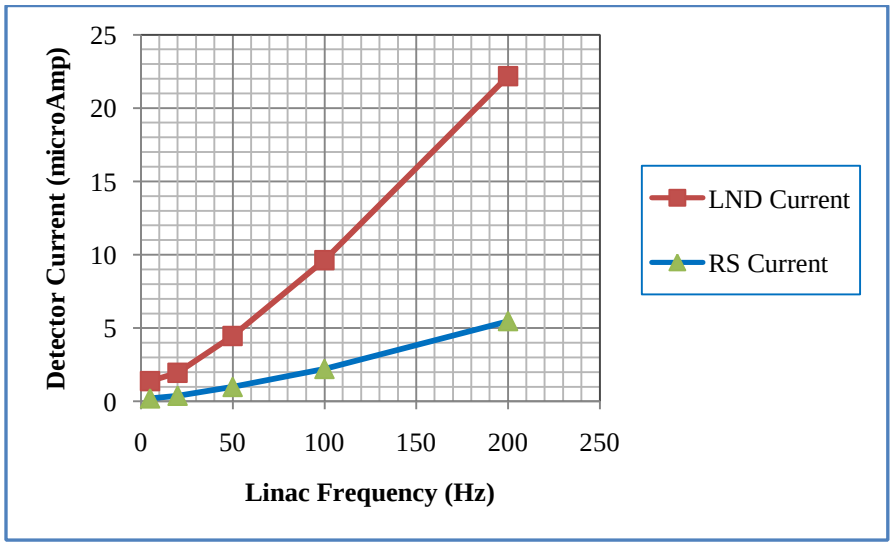

Chapter 4
Modeling Core Depletion and Reactivity

4.1 Non-Uniform Depletion of NETL TRIGA Fuel

For each full day of reactor operation, a ^{235}U fueled thermal reactors burns 1.05 gm of ^{235}U for each equivalent 1 MW-day and most of this mass is converted into fission products within the fuel[87]. Fission product production and concentrations essentially scale with reactor power but the change in core parameters such as average neutron energy, power history and the change in material cross section over core life require more facility-specific models. To complicate the modeling of the burnup and depletion of the reactor fuel, the power production and therefore the burn rate, is not uniform across the reactor core. A steady-state, homogeneous reactor core has an approximate cosine-shaped neutron flux profile across the core with the resulting higher neutron density (and burn rate) in the center of the core. This non-uniform flux profile of the heterogeneous TRIGA reactor effects this cosine-shape and, in particular, for the UT-RACE project, the reduction of the effective core height by the insertion of the control rods. The four control rods of the UT-TRIGA cause a large perturbation and reduction in the neutron density around the rods. In general, the TRIGA core has enough excess fuel loaded at all times so the control rods will remain in a region of 40 to 60 percent withdrawn during normal operations to maintain criticality. To add to this already complicated core depletion map, the NETL TRIGA, as do most reactors, shuffles high burn fuel out of the central core towards the edge over time and replaces the fuel with less burned reactor fuel elements from the core periphery.

This power shape may be measured using flux mapping techniques such as wires or movable detectors to evaluate local perturbations or local power density for short periods. Longer term depletion measurements on several TRIGA fuel elements were performed by Wang and Peir using gamma spectroscopy and these data show the non-uniform depletion for eight TRIGA elements that had been burned in the core for 3 and 19 years (Figure 4.1)[88]**.** The fuel elements in the 10000 series (lower graphs) were

removed after 3 years and the 8000 series remained in the core for 19 years but all eight elements were removed within one month of each other for measurement.

Fig. 4.1. TRIGA element depletion measurements by gamma scanning.

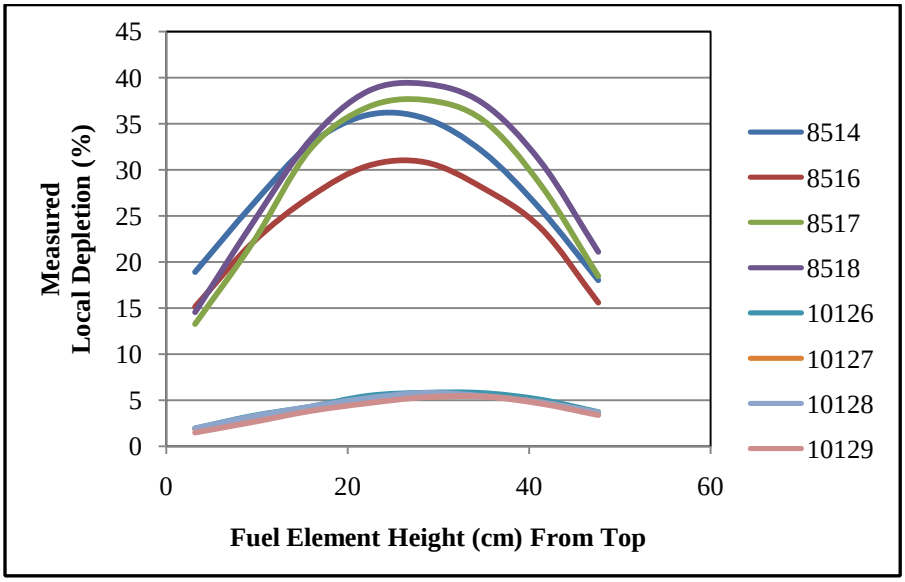

Ref: Data from Wand and Pier[88].

The non-symmetric depletion has significance for the modeling of the UT-RACE project for two reasons: first, because the majority of the core burnup and fission product inventory can be assumed to be in the lower half of each fuel pin, the UT-RACE configuration resulted in two reactor fuel zones (more burned and less burned) with the control rods fully withdrawn. Secondly, the complete withdrawal of the three fuel-followed control rods brought fuel elements with an inverse depletion profile into the core because the *lower* fuel-follower is usually down below the core out of the direct reactor neutron flux.

In 2003, fourteen TRIGA fuel elements with between 6 and 15% depletion were measured at the NETL using a nondestructive assay technique and were found to have an average 6% greater ^{235}U than had been calculated by the power history approximation[89].

Fuel use (in core and in storage) is tracked at the NETL research reactor using burn approximations that average the total power produced per day in the core and divide this power evenly across all fuel elements in the core. This value is then multiplied by constants that convert the time at full power to effective uranium lost (fission and neutron capture) to produce the power (*e.g.* gm/MW-day). This approximation has been used for at least 15 years for the NETL data, but for better tracking of element by element burn, the fuel element depletion may be corrected for power generated in each core location by multiplying the average core burn by a reactor power weighting factor for each ring of fuel. Based on reviews of the NETL fuel history documents, this has not occurred (at least post-1992) for the NETL TRIGA fuel.

Values for these power factors by TRIGA ring location are found in the NETL fuel burn-up calculation documents provided previously by General Atomics[90]. These values were thought by operators to have been applied by the spreadsheet calculations but, after detailed review of the equations, this was found to be not true. These ring-factors were applied to the existing fuel use data to provide a rough correction for core location during each period of time the element was in the reactor core since 1992 (initial startup of the reactor).

This comparison data is shown in Figure 4.2 with an overall increase in the total core burnup by 23.9% by using the correction factors. The actual power history for the element in B-2 (Serial Number 5198) was divided by two to reduce the graph height. The data showed that the correction may be significant for most of the fuel elements with the largest change in the Ring E elements because these elements were moved in 2004 from the inner Ring D where they had received more burn-up. These higher calculated burn-up values of the UT-TRIGA core did not explain the lower than expected burn found in the 2003 gamma and neutron scan of the fourteen elements but it is hypothesized that their previous unknown core locations and actual power history (the fuel had never been used in the NETL TRIGA Mark II) may have been in low flux/low power regions or the recorded data simply overestimated the number of full power hours the fuel was operated.

Fig. 4.2. Corrected and uncorrected NETL TRIGA core depletion data.

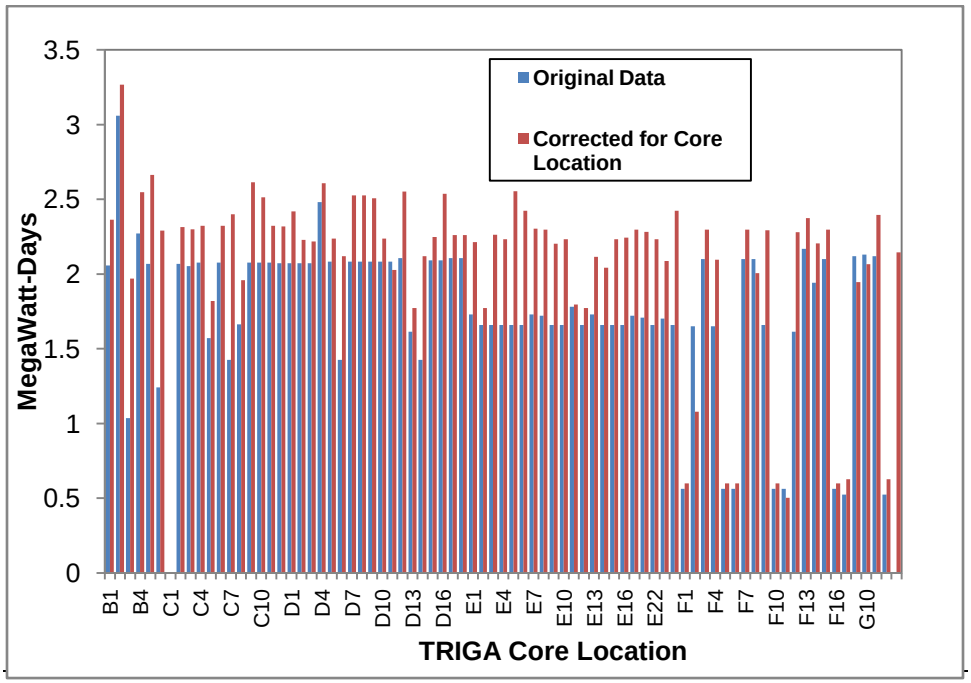

4.2 Modeling Reactor Fuel Depletion and Fission Product Inventory

For over 25 years, the ORIGEN (Oak Ridge Isotope Generation) code and its most recent version ORIGEN2.2 has been used for calculating reactor fuel burnup, time dependent fission product concentrations and output from reprocessing activities[91, 92]. To perform these operations, ORIGEN2.2 requires an initial, homogenized bulk composition of each material in a single volume, the one-group microscopic cross-section for each isotope, the length of irradiation time, the reactor power or neutron flux during the irradiation and the material feed or removal rate (if reprocessing or performing isotope production continuously). ORIGEN2.2 is a useful and very fast code but its ease of use also limits the effectiveness of the results. ORIGEN2.2 uses a fixed set of nuclear databases (cross sections, fission yields, *etc.*) based upon a small group of nuclear reactors that are most typically simulated (*e.g.* BWR and PWR). The fixed set of nuclear

parameters and the one-group neutron cross section library in ORIGEN2.2 do not fully reflect actual conditions in facilities or reactors not included in the limited ORIGEN2.2 reactor database and do not sufficiently compensate for the change in these parameters over core lifetime. Over the past ten years, several intermediate codes or scripts have been written to link various Monte Carlo reactor modeling codes with deterministic point-depletion codes such as ORIGEN2.2 to achieve this goal[93-97]. MONTEBURNS was significant because it coupled MCNP with ORIGEN2.2 or CINDER90 using the Perl scripting language as a fully automated linking script[98]. CINDER90 is a 63-neutron energy group depletion code refined from the original CINDER code by LANL for depletion and accelerator-driven transmutation research but its wide-spread use is impaired by poor documentation and small user experience base.

The next evolution in the coupling of stochastic radiation transport and deterministic depletion may be modeling codes such as MCNPX (version 2.6D+). MCNPX (Monte Carlo N-Particle Extended) is an enhanced version of MCNP4C3 that includes high-energy physics capability supporting accelerator–driven transmutation research[100]. The burnup capability of the MCNPX code is still in beta-testing but may be used in the performance of fully automatic coupled monte-carlo transport and depletion calculations in a manner similar to the MONTEBURNS process. The burnup/depletion calculation in MCNPX uses the CINDER90 implementation and data libraries but the capability is transparent to the user and fully integrated in the MCNPX executable. The performance of a material burn calculation in MCNPX is step-wise process and follows the essential logic of the MONTEBURNS code. MCNPX (2.6D) will first perform a criticality calculation (KCODE) on the defined system to determine the system multiplication, reaction rates and collapsed 63-group neutron fluxes. This information is then passed to the CINDER90 routine that performs a depletion calculation to generate new material densities for the time step simulated. These atom densities are then passed back to MCNPX as new materials for a subsequent transport calculation for new fluxes and reaction rates generation. The depletion process implemented in MONTEBURNS and MCNPX2.6+ (Beta) uses the predictor-corrector technique to account for changes in

neutron flux caused by varying localized material depletion rates occurring during the time period of interest. This is performed by averaging the changes over the burn period using a half-time corrective calculation to model the fluxes and materials densities at the half-way point in the time period. These fluxes and reaction rates are then returned to the beginning of the selected time period and used for the full burn calculation.

The first version of MCNPX that included the CINDER90 burnup and depletion capability was version 2.6, a beta-test version, with 2.6C released to registered beta-testers in December 2006[101]. A copy of this code that had been compiled for multiprocessing on the Windows XP operating system was obtained from LANL in January 2007. For the BURN subroutine, MCNPX must perform the initial criticality calculation to develop a steady-state neutron flux and generate the collision densities that are stored for the subsequent CINDER90 depletion calculation. MCNPX will only track and report those isotopes listed on the MCNPX material cards, isotopes produced by the CINDER90 isotope generator algorithm or those isotope groups selected from a three-tier schedule. However, the CINDER90 algorithms will track reaction rates and changes in concentrations for over 3000 fission product isotopes for an accurate depletion calculation. The isotope generator algorithm only produces daughter products of those isotopes listed on the material card for tracking and not the entire decay chain so it is necessary to list several isotopes in a decay chain of interest by including them with very low atom densities (such as 1E-36) in the MCNPX input deck. As a necessary step towards the accurate depletion/burn calculation, MCNPX generates collision densities normalized per source neutron but CINDER90 requires the system total flux. Total flux for CINDER90 is determined from

$$\phi_{Total} = \left(\phi_{MCNPX}\right)\left(\frac{PowerLevel \cdot \nu}{Q_{prompt} \cdot (\text{Normalization Factor})}\right) \tag{4.1}$$

where the Power Level is selected to be 1.0 MW at full power for the UT-TRIGA but may be a value less than full power if a more dynamic power history were to be modeled.

The Q-value is the prompt recoverable energy per fission (~200 MeV for ^{235}U) and ν is the average number of neutrons emitted by each fission. The constant normalization factor of 1.111 accounts for the additional energy added to the system by delayed fission and capture gamma reactions. The normalization constant is system geometry dependent and may not result in a corrected Q that reflects the true reactor power but it accounts for extra heat input in a reactor that would not be accounted for by a simple fission model and prompt energy deposition.

In order to burn materials properly, MCNPX requires that each cell to be burned have a unique material number. This assures the burn rate is distributed according to the ratio of power generated in each cell to the total of all other cells. For correct flux normalization, every cell that contributes to the reactor power must have a corresponding unique material and all fission and activation products in that cell will be tracked. Significant errors in flux and burnup rates were noted while attempting to use MCNPX version 2.6C with the NETL TRIGA reactor model in early 2007. These errors were later attributed by LANL to a program error in the MCNPX code in which the volumes of repeated structures, as would be found in the lattice arrangement of the TRIGA core, would result in incorrect material volume calculations. This problem was corrected in the June, 2007 Beta test release of version 2.6D by adding the MATVOL card to manually calculate the total cell volume of repeated structures.

An additional problem with the performance of fuel depletion calculation using the UT-TRIGA model in MCNPX2.6C was the memory limitations of the compiled versions for Windows XP and Linux operation systems. The large arrays containing cross-section data and material neutron density for tracking of nuclides during the depletion runs for each material monitored in the TRIGA core would exceed allocated dynamic (stack) memory in Windows XP (32-bit version) and cause segment memory faults on the Linux systems that were available to run the program. Several methods of changing the system parameters were attempted, including reallocating the stack memory in the compiled version by performing a binary edit of the executable file, increasing the message size (MPI) for parallel execution on the Linux cluster and greatly simplifying

the UT-TRIGA model so as to have only two fuel materials in the core[102]. The maximum message size limit in the parallel execution was addressed in MCNPX version 2.6D by breaking these large arrays into smaller segments when passing the array within a parallel cluster**.** A beta-test version 2.6D of MCNPX compiled for parallel execution on the 32-bit Windows XP operating system was obtained in August, 2007 but there was not a version compiled for a Linux cluster available. The UT-TRIGA core model running on MCNPv2.6D, and later MCNPXv2.6E, continued to exceed the stack memory on several available multi-processor Windows XP machines so the model was simplified to a single fuel element for the burn calculations.

4.3 Depletion Calculations with MCNPX-CINDER90

Several MCNPX-Burn calculations were performed using a single-pin approximation for burns of 0.5, 1.5 and 2.0 MWD (Figure 4.3). In order to simulate a power shift in the reactor due to the perturbing affects of the control rods, an additional two depletion calculations were performed with 0.15 wt/% ^{10}B added to the upper fuel zone to depress the flux and the upper graphite slug replaced with control-rod equivalent boron-carbide. This resulted in 97% of the pin power and depletion occurring in the lower fuel pin. This was an over-estimation of the actual axial power-shift but this was performed to develop two clear high and low burn zones within the fuel element.

Fig. 4.3. Single TRIGA fuel element model burned with MCNPX2.6D.

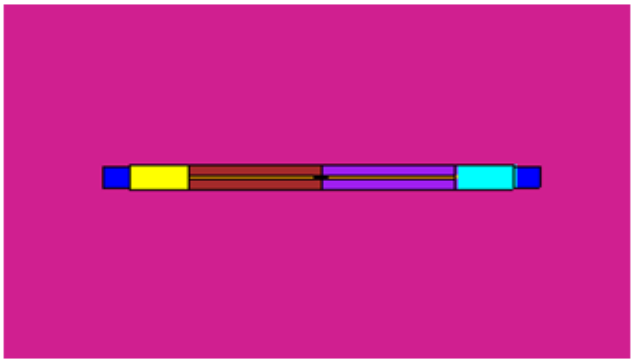

The depletion runs using MCNPX were performed in a continuous fashion. For lower, more realistic neutron densities an irradiation was scaled to a fractional power over many days by location rather than a single 1 MW irradiation for a few days. This cycle did not reflect actual core power history where a typical operational week consisted of four to five normal work days of 6-8 hours and thus many short-lived materials in the output inventory were in a saturated condition in far higher concentrations than would be expected in a NETL TRIGA pin. Some of these isotopes (*e.g.* ^{135}Xe) would have significant reactivity affects over a lengthy burn cycle but the majority would not due to their relatively low macroscopic cross-sections. The final isotope inventory produced by MCNPXv2.6D was reduced manually by removing all high activity (specific activity greater than 1 Ci gm^{-1}) materials as these typically had short-half-lives and would have decayed in the one to four week shutdown period prior to each phase of the UT-RACE project. The next step to eliminate the tracking of isotopes with low concentrations was to remove isotopes with weight fraction of less than $1x10^{-9}$. Although this was an arbitrary selection, it was based on including even the trace concentrations of the samarium isotopes and some transuranics for their important reactivity affects.

The irradiations performed with a single fuel pin resulted in high calculated neutron fluxes to produce the given power in the small, unrealistic volume of a fuel element. For example, a single fuel element producing one MW for one day required a neutron flux of approximately $9.95x10^{15}$ n cm^{-2}-sec^{-1}. This high neutron density increased the probability of double neutron captures and unrealistic neutron capture rates of fission products which would be important and retained in the lower power TRIGA cores. Reducing the simulated power generated and burning for longer periods on the single pins was more realistic but the model still lacked interactions with other core components and fuel elements and did not represent an improvement in depletion modeling of fuel materials in a TRIGA reactor core.

4.4 Depletion Calculations of the NETL TRIGA Using MONTEBURNS

Because of the difficulties using the Beta version of MCNPX (2.6C+) it was necessary to return to the use of separate codes in order to calculate the three-dimensional depletion of the TRIGA fuel using an MCNP model and the depletion code ORIGEN2.2. To perform this coupled calculation, the code MONTEBURNS 2.0 was obtained from the Radiation Safety Information Computational Center (RSICC) at Oak Ridge National Laboratory to link MCNP5 and ORIGEN2.2[103]. MCNP5 was selected because the initial tests of the Beta versions of MCNPX with MONTEBURNS yielded output file conversion errors resulting in output files containing no burn information. Both the ORIGEN2.2 and MCNP5 codes had been successfully used on a 64-bit computer with a Windows XP64 operating system but these two codes would not successfully operate under the MONTEBURNS program due to file access and read errors. Finally, the source code for the executable, *MONTEB.EXE*, was recompiled using Intel FORTRAN Version 9.0 on a Windows XP-64 machine and passed all test benchmarks under that operating system.

The MCNP model of the TRIGA core was divided into material zones to evaluate the local change in fuel and fission product density over the core lifetime. Each ring of the core (B through F) was modeled with each fuel rod in a ring divided into and upper and lower fuel zone (Figure 4.4 and Figure 4.5). Ring G only contained graphite in the simulation because the majority of the UT-TRIGA operations since initial criticality occurred with only partial fuel loadings in this area.

Fig. 4.4. TRIGA model for MCNP5/MONTEBURNS depletion calculation.

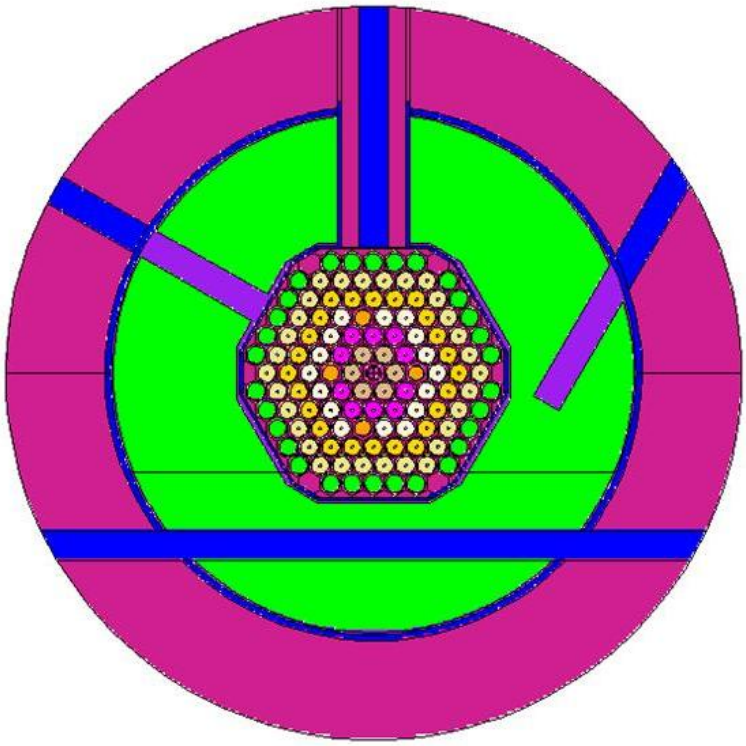

Fig. 4.5. Split core TRIGA model for depletion calculations.

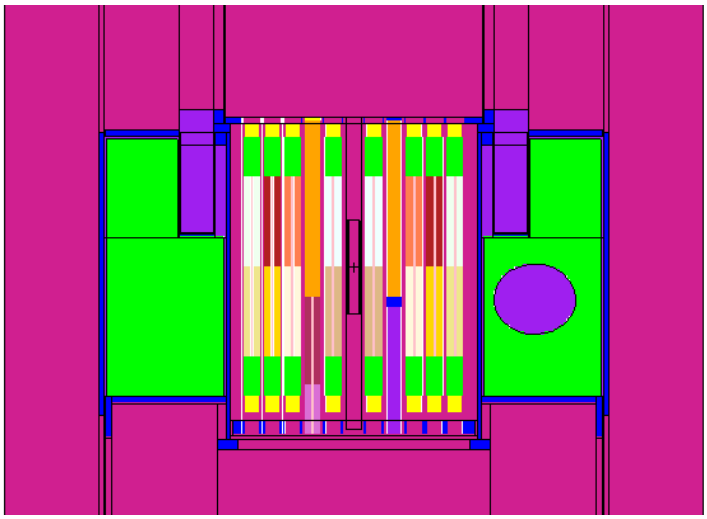

The MONTEBURNS input job file provides several options for the program including power produced from each fission (typically 200 MeV contributing to the total reactor power). This value was multiplied in the UT-TRIGA simulations by 1.11 as is performed in MCNPXv2.6 to account for the additional system heat input from decay heat and delayed neutrons. The initial simulation burned the TRIGA core for the effective core lifetime of the NETL TRIGA of 130 MW-days but this resulted in MONTEBURNS calculating lower MW-days of burn for individual fuel pins than required for actual fuel element power history.

To produce the depletion necessary, the burn time was doubled to 260 MW-days with 8 cycles to permit flexible fuel element burn selection from the output files. As an additional process, MONTEBURNS tallies the power generated (and the change over burn cycle) in each material burned which provided information on the axial burn profile of the fuel and control rods as shown in Figure 4.6. The MCNP materials were located in five concentric rings of the TRIGA core so the power generated per Ring was used to calculate core-specific Ring Power Factors and compare them to values provided previously by General Atomics (GA) in Table 4.1. The MONTEBURNS input files are given in Appendix A.2.

Fig. 4.6. Power in TRIGA fuel zones using MONTEBURNS.

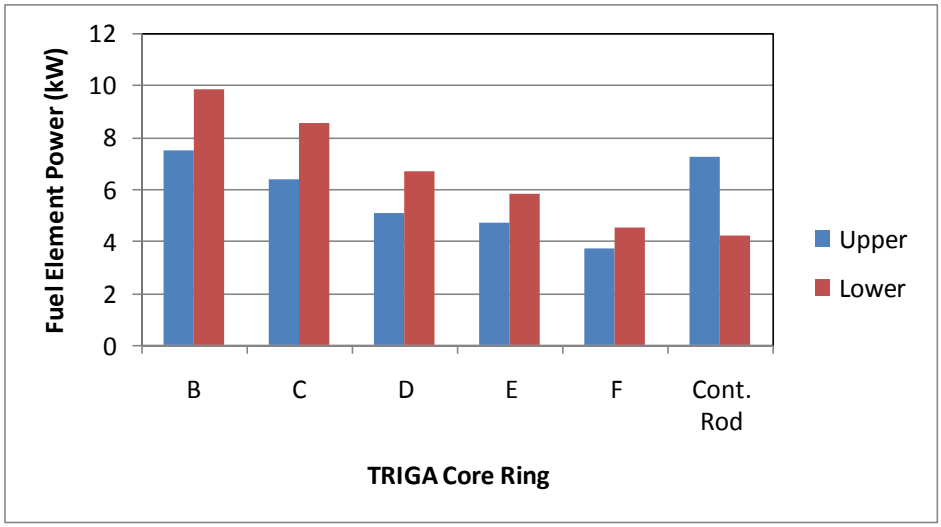

Table 4.1. TRIGA Ring Factors.

Location	GA Ring Factors	MCNP Ring Power to Average Ratio
Ring B	1.57	1.37
Ring C	1.46	1.18
Ring D	1.29	1.04
Ring E	1.07	0.85
Ring F	0.81	0.67
Ring G	0.66	----
Control Rods	----	0.90

Following each cycle in which ORIGEN2.2 performs a depletion and burn operation on the selected core materials, MONTEBURNS evaluates the output isotopes for their "importance." The importance is evaluated using several parameters (concentrations, reactivity *etc.*) but whether an isotope is ultimately considered important is determined by MONTEBURNS testing against a user determined setting of a fractional level in the input job file. Based on work by Jeraj, Zagar and Ravnik supporting TRIGA II criticality benchmarking, several isotopes were selected to have automatic importance because they were shown to contribute over 90% to the total reactivity changes from fuel burn[104, 105]. ^{135}Xe is an isotope with a very large neutron capture cross section and high importance but its half-life (9.10 hr) is short enough that it would normally not be in the fuel after a lengthy shutdown. For the MONTEBURNS depletion, the ^{135}Xe density in the fuel was allowed to build to saturation rather than perform numerous cycles of buildup and decay but this large negative reactivity served as an approximate substitute for the inherent temperature reactivity of the TRIGA reactor operating at 1 MW. It should also be noted that the typical maximum power during operation of the NETL reactor is 950 kW due to frequent spurious shutdowns at 1 MW but the simulation was performed at 1 MW for direct scaling to other reactor data. The following table list the

nuclides produced in a fuel element with 1.5233 MW-days burn as determined by MONTEBURNS.

Table 4.2. MONTEBURNS calculated fission product inventory for 1.5233 MWD.

Nuclide	**Grams**	**Mass-Fraction**
^{149}Sm	0.000857	7.17×10^{-07}
^{151}Sm	0.00215	1.80×10^{-06}
^{239}Pu	0.132	1.10×10^{-04}
^{143}Nd	0.0443	3.71×10^{-05}
^{236}U	0.262	2.19×10^{-04}
^{103}Rh	0.141	1.18×10^{-05}
^{131}Xe	0.0212	1.77×10^{-05}
^{147}Pr	0.017	1.41×10^{-05}

The burn calculations using a single pin TRIGA element in MCNPXv2.6D (CINDER90) performed at 16.5 kW over 120 days were compared to an equivalent calculated depletion (2.0 MW-days) using MONTEBURNS (ORIGEN2.2)[106,107]. Only the isotopes with the most significant reactivity effect as previously determined were compared in Figure 4.7.

Fig. 4.7. MCNPX2.6D v MONTEBURNS.

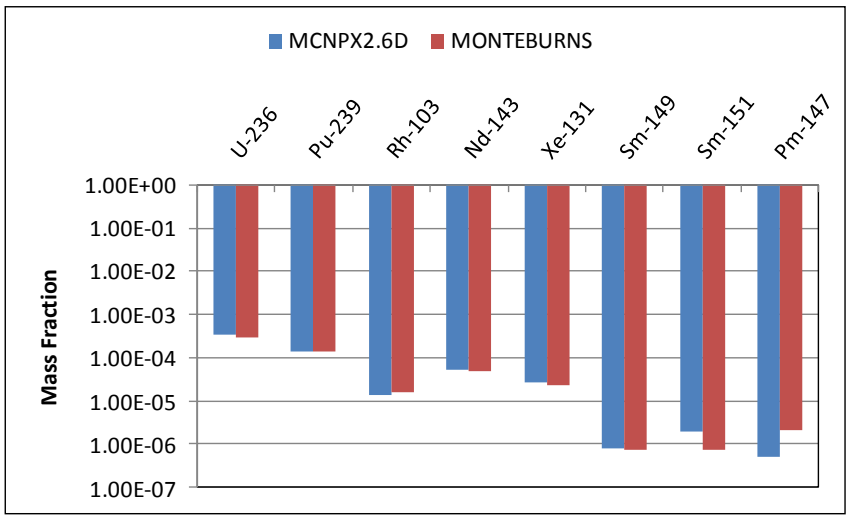

There is very good agreement between the burn calculations using both codes. The ease of use in a single program such as MCNPX version 2.6+ is preferred but at this date the program is still in Beta testing and some functions have not been benchmarked or validated.

4.5 Benchmarking of MCNPX Models

The loading patterns used in two critical benchmark TRIGA cores performed for the International Criticality Safety Benchmark Evaluation in 1991 placed the elements into as compact a configuration as possible[108]. These benchmark loadings (Core 132 and 133) were modeled with MCNP4B in 1997 and the calculated K_{eff} for each core were 0.9994 ± 0.0002 and 1.0042 ± 0.0002 respectively. These results are significant for the UT-RACE modeling because they show the computation errors using a Monte Carlo code such as MCNP under ideal critical conditions may still result in an overestimation of the reactivity by as much as \$0.60[109].

An opportunity to benchmark the UT-TRIGA MCNPX core model became available in August 2007 with the initial startup of the CNESTEN (National Center for

Nuclear Science and Technology) 2 MW TRIGA Mark II reactor near Rabat, Morocco[110]. The design of the CNESTEN TRIGA reactor is essentially identical to the UT-TRIGA with the exception of five versus four fuel-followed control rods and the location of the experimental beam ports. The CNESTEN TRIGA was the first TRIGA reactor with a hexagonal grid plate in the world started up with fresh fuel since 1988 providing a true benchmarking of the UT-TRIGA criticality MCNPX model. The UT-TRIGA MCNPX model was modified to reflect the minor design differences between the two reactors and a criticality calculation was performed using the previous ENDF/B-VI and the new ENDF/B-VII cross-section library with the initial startup core configurations obtained from the CNESTEN facility[111]. The CNESTEN core modeled using the NETL TRIGA MCNPX input deck with assumed fresh fuel loaded and with control rods heights measured at cold, xenon-free low power critical rod heights overestimated the core reactivity by $1.26 and $2.25 for ENDF/B-VI and ENDF/B-VII libraries respectively. The MCNP calculated values are given in Table 4.3 for comparison. These results indicate there is a bias in criticality results obtained using the NETL MCNP model but additional benchmarking should be performed with the CNESTEN facility to validate models for both reactor cores.

Table 4.3. MCNPX benchmarks for CNESTEN core using ENDF/B-VI and ENDF/B-VII.

CNESTEN Core Configuration	**Critical Control Rod Heights (5 Fuel-Followed Rods)**	**MCNPX calculated K_{eff}**
101 fuel elements	325, 325, 326, 328, 324 units	1.00887 +/- 0.00063 (ENDF/B-VI)
101 fuel elements	325, 325, 326, 328, 324 units	1.01582 +/- 0.00064 (ENDF/B-VII)

4.6 UT-RACE Subcriticality Determination Using MCNPX

The NETL core configured for UT-RACE was very near critical but by an unknown amount because of the limitations in the MCNPX criticality calculations. The loading of the core in January 2006, included several reflector or dummy graphite elements with the neutron source removed by procedure. When the final fuel element (78 total) was placed into core location G17, the reactor operator noted that the neutron level monitored by the NM-1000 began to increase indicating criticality (or, more correctly, super-criticality as the power was increasing). A graphite reflector element was removed from G6 and the reactor was again subcritical as indicated on the NM-1000. This indicated the reactor reactivity level during the accelerator driven experiments was the difference between the reactivity added by a fuel element and a graphite element in Ring-G locations around the modified core.

During the final days of the UT-RACE project in late March, 2006, the core was brought to a slightly supercritical condition by the addition of two graphite elements and removal of the startup source. The graphite elements were placed in the G18 and G6 locations and the neutron level was monitored by the NM-1000 console instrument. Reactor power as monitored on the NM-1000, increased from 2 W to 9 W in 227.31 seconds. This increase correlates to a positive reactor period of 341.89 seconds. Using inverse kinetics and the in-hour formula as programmed into a computer, this reactor period is equivalent to a positive reactivity of $0.037. Later, the UT-RACE core was brought to an exact critical condition by insertion of only the Shim Safety 2 rod from 960 to 825 units. A critical control rod worth measurement performed later (with nine additional fuel elements added) indicated that this amount of rod movement was approximately $0.032 worth of reactivity confirming the initial measurement.

Performing a MCNPX criticality calculation with and without the graphite elements would provide a differential reactivity value that could be compared to the +3.7 cents known reactivity value. It was expected that the replacement of a single graphite element with water in the model would introduce far less error in an MCNPX calculation

than swapping burned fuel elements. To provide some confidence that this statement is true, the measured control rod worths of two rods were compared to the MCNPX evaluation of the rod worths in the UT-RACE 87 element critical configuration. The comparison is provided in TABLE 4.4.

Table 4.4. Measured versus Calculated Control Rod Worth for UT-RACE.

Control Rod	Measured Total Worth ($)	MCNPX Total Worth ($)	% Error
Shim Safety 2 (FFCR)	1.232	1.517 ± 0.102	23.133
Transient Rod (VFCR)	2.647	2.670 ± 0.113	0.869

FFCR=Fuel Followed Control Rod
VFCR=Void (Air) Followed Control Rod

Although both MCNPX calculations are in good agreement, the larger difference in the values for Shim Safety 2 can be attributed to the approximate 1.5 MW-day burnup of the fuel and fission products within the control rod fuel follower whereas the Transient Rod does not contain any reactor fuel. The difference between the two calculated multiplication factors for the 78 and 87 element cores was subtracted from the known supercritical condition to arrive at the final multiplication factor value for the 78 element UT-RACE configuration. The MCNPX results and the corrected reactivities are shown in Table 4.5.

Table 4.5. Calculated and corrected reactivity for UT-RACE.

Core Configuration	Calculated K_{eff}	Calculated Difference	Corrected K_{eff}
Subcritical UT-RACE	0.99360 ± 0.00050	0.00151 ± 0.00069	0.99873± 0.00069
Supercritical UT-RACE	0.99511 ± 0.00048		1.00026*

*Experimentally determined value (error unknown).

The corrected value for the subcritical configuration (0.998733 ± 0.00069) was the benchmark used for determining the effectiveness of reactivity monitoring methods. Any new MCNPX calculation used the corrected multiplication factor as the reference value to determine a differential reactivity worth. For example, in order to evaluate the reactivity monitoring methods further from criticality without a significant perturbation, as was caused by control rod insertions, a single fuel element was removed from the E-6 location. This location was selected to be closer to the center of the off-set RACE core configuration and still fairly accessible for neutron detector installation. The calculated and corrected multiplication factor for the core without the E6 fuel element was 0.99269± 0.00100 and a reactivity worth for the fuel element of $0.863 ± 0.104.

Chapter 5
Subcritical Reactivity Measurement

5.1 Subcriticality Monitoring

Nuclear engineers and scientists have been attempting to determine the subcriticality condition of a fissile material without inadvertently reaching the critical chain reaction from the early years of the Manhattan Project. Louis Slotin, a scientist at Los Alamos and the individual who defined the dollar unit of reactivity, died in 1946 from high exposures to radiation brought about while performing an approach to criticality experiment that had become known as “tickling the dragon’s tail” because of the high risk involved in the procedure[112]. Fortunately, other methods have been developed to evaluate the subcritical level of a nuclear assembly[113, 114,115].

5.2 Rod Drop Method

The control rod drop experiment is a frequent method of control rod calibration but may also provide reactivity calibration of a subcritical core[116]. Even though it provides reasonable results, the method has inherent errors because the act of dropping a strong neutron absorber into a steady-state critical or near-critical reactor causes a significant perturbation of the neutron flux within the reactor core. This may also cause "shadowing" if the rod is near a monitoring neutron detector by intercepting neutrons that would have been absorbed and detected in the detector. Point-reactor kinetics assumes the neutron flux profile across the core is essentially constant during the transient so this large perturbation from the neutron absorbing control rod may produce errors greater than 10%[117,118].

The essential technique in a critical and subcritical reactor is to monitor the change in reactor neutron level before and after the transient and approximate the change in neutron population as a rapid, prompt-drop by assuming the delayed neutron level is constant during the drop. For a subcritical reactor, three neutron levels are measured to determine the core reactivity before the rod drop: N_0, the initial neutron level, N_p, the

neutron population measured immediately after the prompt-drop and N_1, the asymptotic neutron level several seconds after the initial rod-drop. These values are then used in a formula called the "three point formula" for the initial subcriticality:

$$\frac{\rho_0}{\beta} = \frac{\left(\frac{1}{N_0} - \frac{1}{N_p}\right)}{\left(\frac{1}{N_1} - \frac{1}{N_p}\right)}, \tag{5.1}$$

where ρ_0 is the initial core reactivity and β is the delayed neutron fraction. Substituting this into

$$\frac{\rho_1}{\beta} = \frac{N_0}{N_1}\frac{\rho_0}{\beta} \tag{5.2}$$

yields the system subcriticality (ρ_1 is the final reactivity level) in dollar units. Figure 5.1 is a plot of reactor power before and after a drop of the Regulating Rod during operation of the linac at 150Hz. The TRIGA control system NM-1000 wide range neutron monitor was used during initial accelerator testing before a secondary, dedicated neutron detector and data acquisition system was in operation because the system proved stable and was not susceptible to gamma-flash saturation.

Fig. 5.1. NM-1000 response to RR drop.

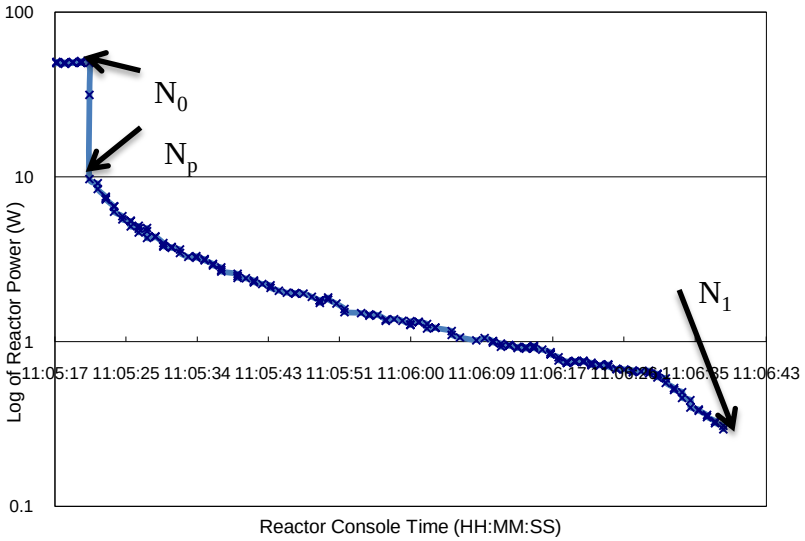

The TRIGA console system outputs in parallel to a Honeywell electronic chart and data logger but this system is used for process monitoring and was only configured to acquire a data point three times per second. The subcritical rod drop method using the Regulating Rod yields a value for the initial core reactivity in the RACE configuration of -2.45 cents or a multiplication factor of 0.9998 which overestimates the subcritical level by 0.11%. Subtraction of the final and initial reactivity values gave the approximate worth of the Regulating Rod in the UT-RACE configuration of $3.61. Unfortunately, this rod was not calibrated in the UT-RACE critical configuration so the accuracy of this value is unknown, however; the value may be compared to an MCNPX calculation for the rod worth which was found to be $3.206 $\pm$ 0.105 or an 11.9% difference between the two values. The critical calibration for the RR worth in July 2006 was $ 3.092 but the operational NETL core has a flatter flux profile due to the 104 fuel elements in the full core versus the 78 for the RACE configuration and with a neutron flux depressing water-hole (3-L) near the RR so it is expected that the RACE configuration would have higher RR rod worth.

5.3 Source Jerk (Linac Trip) Method

The Source Jerk method is similar to the rod drop methods in that the reactor begins in some subcritical condition with a steady or stationary neutron level and the driving neutron source is removed quickly to cause a rapid, prompt jump change in neutron level[119]. This method is a contender for on-line subcriticality measurement of an operational fast-spectrum ADSS because the accelerator driving the source may be programmed to switch on and off for short durations without causing a large thermal transient[120]. This method is not likely to be used routinely for thermal ADSS because the necessary beam interruption would be longer due the longer neutron generation time but it may be used for occasional calibration of other methods. Although the near constant flux shape following a linac trip has been shown to allow the point-kinetic approximations for low subcriticality there are still detector location effects that reduce its accuracy[121,122].

For the source jerk method, the response of the subcritical system may be evaluated at two states, n_0 and n_1:

$$\frac{\rho_0}{\beta} = \frac{n_1 - n_0}{n_1} = 1 - \frac{n_0}{n_1} \tag{5.3}$$

Where

$\frac{\rho_0}{\beta}$ is the core reactivity in dollar ($) units

n_1 is the final neutron count rate

n_0 is the initial neutron count rate

An early evaluation of subcriticality monitoring in the UT-RACE project utilized the installed TRIGA instrumentation. In order to perform the test, the accelerator was

deliberately tripped following a sustained (> 3 hours), full power linac run at 180 Hz to determine if the NETL reactor console NM-1000 wide-range fission chamber neutron monitor could provide reactivity data to the ADSS operators. A plot of the instrument response is given in Figure 5.2. The calculated value for initial core reactivity using this method and data obtained at one-second intervals from the control room data logger was negative $ 0.517 or an initial multiplication factor of 0.99639.

Fig. 5.2. NM-1000 response to linac trip from 180 Hz.

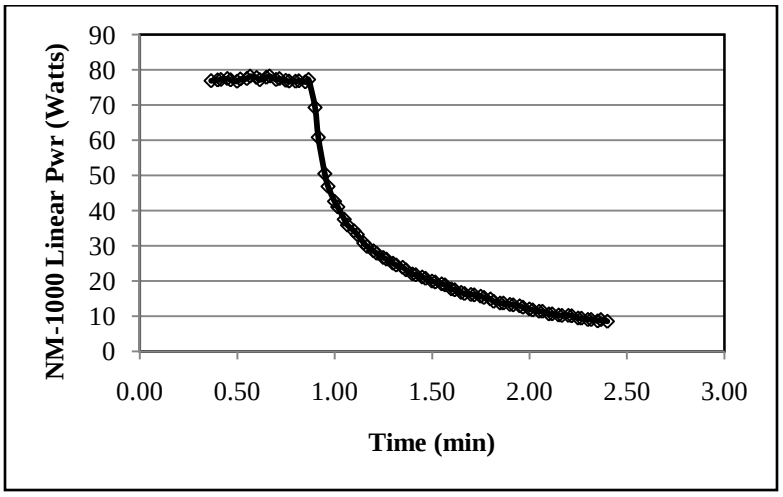

This value of K_{eff} is 0.2% from the benchmark value providing confidence in the ability of the reactor operators to evaluate subcritical levels with the available console instrumentation. To the reactor console instruments, the linac trip was an essentially instantaneous source jerk but the neutron level of the subcritical core responded at the prompt and delayed neutron time constants. More information and better precision could be obtained from a linac trip with a faster acquisition system and this was evaluated under different core conditions (fuel element E6 was removed) and the linac operating at 200 Hz (Figure 5.3). The additional signal detail provided by the enhanced acquisition system permitted reactivity determination by the "source-jerk" approximation and by the prompt decay constant of the system following the final linac pulse (Figure 5.4).

Fig. 5.3. ADSS response to linac trip from 200 Hz.

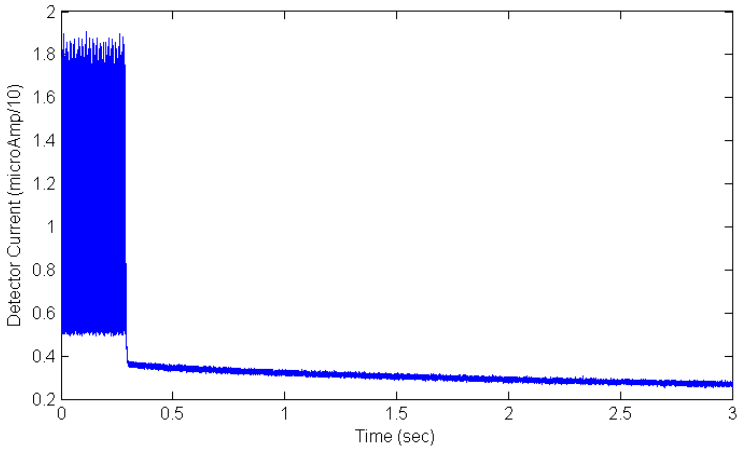

Fig. 5.4. ADSS decay following linac trip.

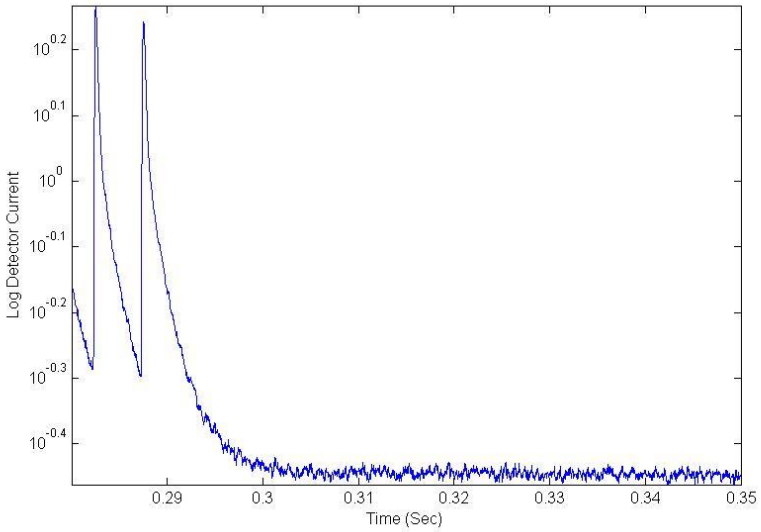

The detector current before and after the linac trip was calculated by taking an average value of the detector signal data before and after the linac trip. The reactivity of the core by the source-jerk ratio was -$1.272 or a multiplication factor of 0.99117. This represents a 20.9% error from the benchmark calculation with E6 removed from the core (-$1.052). Performance of a curve fit to the decaying detector signal following the linac trip gave the values in Table 5.1. The large errors are expected when using the pulsed neutron source method with low repetition rates because the subcritical system does not reach equilibrium between pulses.

Table 5.1. Reactivity values determined by decay of neutron population after linac trip.

Detector Location	Curve Fit Alpha	Multiplication Factor	Alpha Error (%)
A1	168.4 ± 4.6	0.99807	37.8
E6	134.9 ± 3.1	0.99985	50.2

5.4 Pulsed Neutron Source Method

The response of a subcritical assembly to an initial burst of neutrons is the basis for the Pulsed Neutron Source (PNS) method of reactivity measurement[123-128]. In the PNS method, an accelerator is used (typically through a Deuterium-Tritium reaction) to produce a burst of neutrons within a subcritical or critical assembly. The exponential decay of the neutron flux following the initial neutron pulse but before significant delayed neutrons are produced will provide a measure of the system reactivity by a determination of the prompt neutron decay constant, α. Many variations of this fundamental experiment have been developed to reduce the effect of prompt neutron harmonics and the time-decay of delayed neutrons following the brief increase in the assembly fission rate. One method used frequently in recent ADSS experiments is called the Sjöstrand-Gozani or Area method and uses the ratio of the area of the prompt detector

response and the area of the delayed neutron signal after the prompt response has decayed away**.** This method has been shown to provide accurate reactivity measurements with good precision in controlled environments but requires a low accelerator pulse rate ($R>>1/\alpha$) for the delayed neutron background to fully stabilize. This may require the accelerator to pulse at frequencies less than 10 Hz for a thermal subcritical assembly. A low pulse rate to measure the subcritical level is a disadvantage for an operational ADSS because these systems are expected to operate at higher accelerator frequencies to maintain high transmutation rates. The highest sustained frequency used while attempting to reach a maximum indicated power in the UT-RACE project was 200 Hz but a plot of the neutron detector current while operating at 200 Hz is shown in Figure 5.5 and indicates the pulse train does not permit a separation of the delayed neutron and prompt neutron contributions.

Fig. 5.5 Linac waveform operating at 200 Hz.

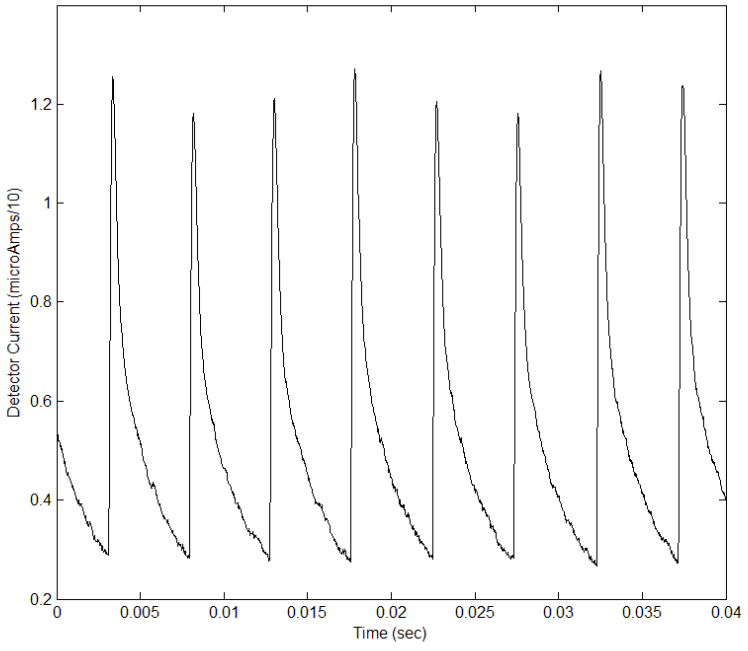

The exponential decay of the neutron population shown in Figure 5.5 may provide an alpha measurement at lower frequencies by a curve fit to the data but the choice of where to start and stop the curve fit to avoid harmonic and delayed neutron effects is subjective and may be difficult to automate for an ADSS monitoring and safety system. The electronics systems available for the UT-RACE did not permit the time analyzer to reset after each linac pulse but individual pulses could be used to determine the alpha by curve fitting to the exponential data. As an example, the height of control rod Shim Safety 2 was varied and single linac pulses were introduced into the system by "one-shot" firing of the linac. The individual data sets were manually overlaid in Figure 5.6 and show the expected change in the prompt neutron decay constant as the control rod is inserted. The MATLAB curve fitting package was used for each pulse to produce decay constants representing the reactivity inserted by the control rod. The results of the curve fits will be compared to calibrated reactivities in Chapter 6.

Fig. 5.6. Single linac pulse on ADSS with different subcriticalities.

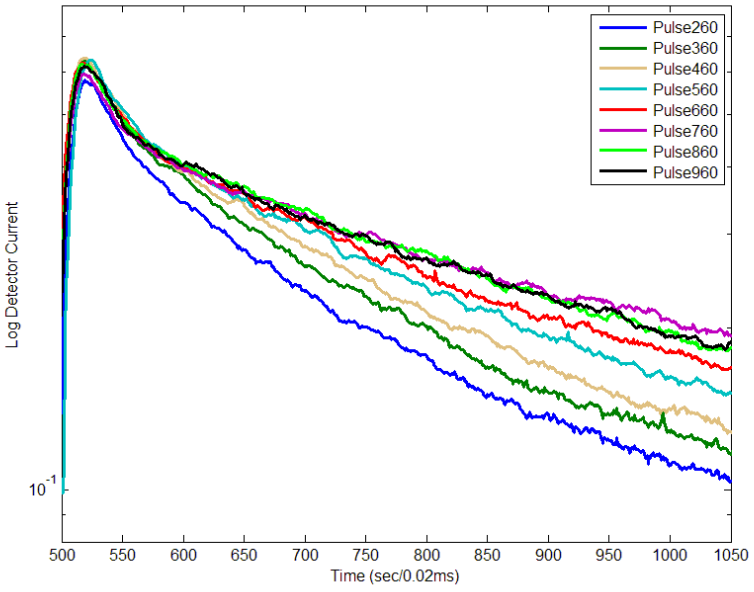

5.5 Statistical Reactivity Determination Methods

The mean behavior of the neutron population in a nuclear assembly has been successfully approximated with theories, such as diffusion and point-kinetics, that model the macroscopic behavior with continuous distributions and deterministic equations but the actual population in a steady-state reactor will vary locally due to the inherent random (or stochastic) processes of the neutron life-cycle with some average or mean value and statistical variance around that mean. These fluctuations or reactor "noise" may be monitored using internal or external neutron detectors to evaluate the average behavior of the overall reactor system by assuming the neutrons detected are a representative sample from the large population in the core. The use of the term "noise" is appropriate because many of the reactor stochastic phenomenon (*e.g.* random power and temperature variations) have been modeled using theories of random noise in electronic systems and integrated circuits[130-136].

5.6 Rossi-Alpha Method

Bruno Rossi proposed during the Manhattan Project that the observation of the time distribution of neutrons from a single chain could provide a means to measure the prompt neutron average lifetime [137]. Feynman, de Hoffmann and Serber fully developed the theory where the change in the prompt neutron population with time is equal to the ratio of the neutron multiplication per generation divided by the neutron generation time or

$$\frac{dN}{dt} = \frac{(1-K_p)N}{\Lambda} \quad . \tag{5.4}$$

Integrating this equation will give

$$N = N_0 e^{\left[\frac{1-K_p}{\Lambda}\right]t} = N_0 e^{\alpha t} \tag{5.5}$$

where K_p is the prompt reactivity and α is defined here as the Rossi-alpha[138]. Setting a time analyzing multi-scaling neutron detection system to trigger on the first neutron

detected from a subcritical assembly with a weak neutron source and count subsequent neutrons for a short period of time (the gate period) will provide the time distribution of the neutrons from a single fission chain and a value for the Rossi-alpha. Essentially, each fission chain starts with a single neutron from an intrinsic or external source and the chain population exponentially decays if the reactor is subcritical. The low count rate requires long count periods and neutron detectors with high efficiency to produce a value of alpha with good precision. Experience has shown that the time gates must not too wide or overlapping neutron fission chains will be detected and result in an alpha measurement that is too large.

5.7 Variance to Mean Ratio (Feynman-Alpha) Method

From fundamental statistics, the average number of events recorded in a particular time interval may be represented by the average count rate, $\bar{C}$, and the fluctuations around this value or the sample variance by $(\overline{C^2} - (\bar{C})^2)$. For a sample from the Normal distribution, the ratio of the sample variance (σ^2) to the mean (x) is called the relative variance but Wilhelm Lexis formulated the ratio, now called the Lexis' ratio or the Divergence Coefficient,

$$Q^2 = \frac{n-1}{n}\frac{(\overline{C^2} - (\bar{C})^2)}{\bar{C}} = \frac{n-1}{n}\frac{\sigma^2}{\bar{x}} \tag{5.6}$$

which determines if a data set follows the Poisson distribution because the ratio in that case is equal to unity[139]. Nuclear fission is a non-Poisson process in that the number of neutrons produced per fission (ignoring delayed neutrons) is not constant value and each event does not have a fixed expected outcome. The average number of neutrons released from fission $\bar{\nu}$ for ^{235}U is 2.43 but this value varies for each fissile isotope and is a function of the energy of the incoming neutron as shown in Table 5.2.

Table 5.2. Average number of neutrons produced from fission for several isotopes.

Isotope	^{233}**U**	^{235}**U**	^{238}**U**	^{239}**Pu**	^{232}**Th**
E_n (MeV)	0.0	0.0	1.50	0.0	1.50
$\bar{\nu}$	2.50 ± 0.02	2.43 ± 0.02	2.60±0.09	2.89±0.03	2.6±0.20

The variance and mean of the Poisson distribution are equal but the neutron yield probability distribution relative width is characterized by the Diven parameter or

$$D_\nu = \frac{\overline{\nu_p^2} - \bar{\nu}_p^2}{\bar{\nu}_p^2} \tag{5.7}$$

which is approximately 0.795 for $^{235}U^{141}$. The deviation of the reactor neutron population statistics from Poisson as the reactor approaches criticality is the basis of the Feynman-alpha method for reactivity determination.

In 1944, Feynman et al. extended the use of the Lexis ratio and derived a formula for the excess above Poisson ($Q^2 > 1$) that occurs in fission chain reactors due to the non-Poisson nature of the neutrons from fission, $Q^2 = 1 + Y$, when neutron count data, C, is taken during a time interval, T

$$\frac{(\overline{C^2} - (\bar{C})^2)}{\bar{C}} = 1 + Y(T) = 1 + \sum_1^7 \frac{\varepsilon D_\nu}{\alpha_i^{\,2}\Lambda^2}\left[1 - \frac{1 - e^{-\alpha_i T}}{\alpha_i T}\right] \tag{5.8}$$

ε is the detection efficiency,

Λ is the neutron generation time,

D_ν is the dispersion of the number of neutrons or the Diven factor,

α_i is the neutron population decay eigenvalues

(i=1 is prompt decay and i=2,3...7 are delayed groups),

Y(T) may be defined as the Feynman Y-function and is the asymptotic value of the relative variance for each neutron group.

Typically, Equation 5.8 is rewritten to isolate the Y-parameter such that it represents the difference between the reduced variance of the fission multiplicity and the Poisson random variable. Eigenvalues less than α_1 are usually ignored because the decay constant for the prompt neutrons is much larger than the decay constant for the first group of delay neutrons but for Equation 1.2 to remain valid the data acquisition must assure the longest time gates are much less than $1/\alpha_2$ (~0.25 s) to ignore delayed neutrons. To determine the prompt neutron decay constant, the ratio of data variance to the mean is plotted against the increasing time intervals or gates in which the neutrons detections from a subcritical reactor are recorded. The data is then fitted to the Y-parameter to determine the value of the "Feynman-alpha." Figure 5.7 shows three Y-Function curves evaluated at different subcriticality levels.

Fig. 5.7. Continuous Feynman-alpha method curves.

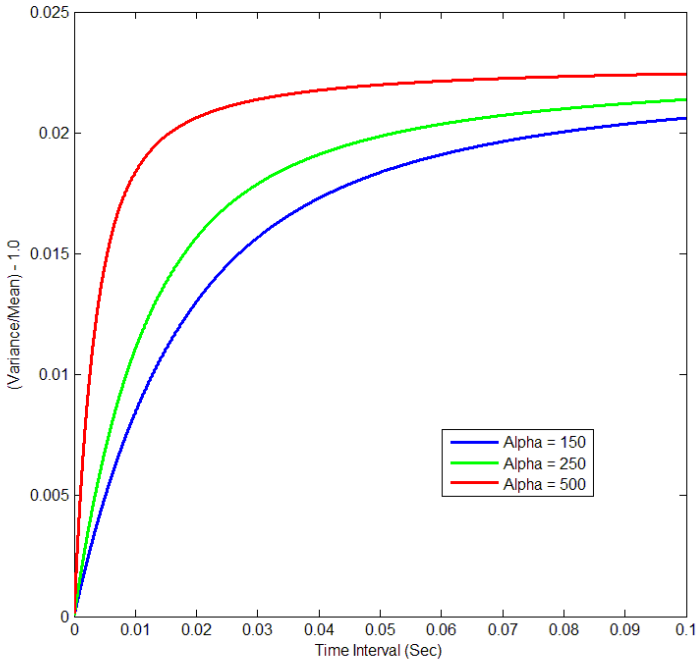

The Y-function eventually reaches a saturation point as the time gates get larger due to more uncorrelated neutron chains overlapping in each time bin. The value of Y is highly dependent on the system α when the time gate is less than $1/\alpha$ but this also requires high detection efficiency and long counting times to acquire sufficient neutron counts in small time gates for good precision. A stronger neutron source may reduce the counting period but with a possible negative effect of detector and system dead-times on the overall statistics that requires subsequent correction[142].

Ideally, a subcritical system could be driven by a continuous beam neutron source such that the large neutron multiplicity would be a function of beam strength and the target/source emission would then be a Poisson process. Some recent ADSS research has involved continuous beam systems and the next project proposed under the European EUROTRANS program (VENUS-Guinevere) will couple a continuous beam D-T neutron generator to a subcritical multiplying assembly. It is not clear if this research will extend to full scale ADS burners as current technology for high power proton and electron accelerators is limited to pulsed power systems.

The traditional Feynman-Alpha method requires a subcritical system in a stationary state with the neutron source governed by Poisson statistics (*i.e.* random single event decay mode). The periodic accelerator pulses driving the UT-RACE project or the operation of a proton-driven ADSS inject high-energy particles into a dense target and produce a cascade of neutrons from a single accelerator pulse. Because the neutron intensity in pulsed ADSS is not invariant to an arbitrary time shift, the systems are not in a stationary condition making the analysis more difficult.

The ADSS may be viewed as pseudo-stationary by randomizing the detection process with time by randomly sampling the interval between accelerator pulses or randomly starting the data acquisition without attempting to synchronize with the linac period[143-148]**.** This method has been called the stochastic pulsing method (SPM) versus deterministic pulsing (DPM) in which the data acquisition is synchronized to start when the accelerator pulses. The SPM randomization shifts the time base of the data and

produces a neutron source that now is a doubly stochastic Poisson or Cox process with a statistically constant average but a variance that is over-Poisson[149].

Several authors have extended the stationary Feynman-alpha formula to account for the statistics of a periodically-pulsed neutron source[150-155]. The Stochastic Feynman-Alpha equation was originally derived assuming Dirac-delta pulses but this was later extended to square and Gaussian shaped pulses[156, 157]. The equation for a finite width (3-5 μsec) square pulse was used here (Equation 5.9) because the energy spread of the linac pulse with time was unknown in RACE experiments but was expected to be non-Gaussian from RF pulsed linear accelerator characteristics.

$$\frac{\sigma_Z^2(T)}{\langle Z(T)\rangle} = 1 + \frac{2\lambda_d S T_0^5 \alpha}{T\pi^4 W}\sum_{n=1}^{\infty}\frac{1}{(4n^6\pi^2 + n^4\alpha^2 T_0^2)} \times \left(\sin\frac{n\pi T}{T_0}\right)^2\left(\sin\frac{n\pi W}{T_0}\right)^2 + \frac{\lambda_d\lambda_f}{\alpha^2}\langle\nu(\nu-1)\rangle\left(1-\frac{1-e^{-\alpha T}}{\alpha T}\right) \tag{5.9}$$

Where:

λ_d, λ_f are probability of a neutron detection or a neutron causing fission respectively

T is the time gate width or interval of detection

T_0 is the linac pulse repetition rate

W is the width of the linac pulse

α is the prompt neutron decay constant (fitting parameter)

$\langle\nu(\nu-1)\rangle$ second moment of the neutron multiplicity (Diven parameter)

S is the external source strength

Degweker developed a similar formula for the Stochastic Feynman-alpha under the assumption of instantaneous (delta) pulses[158]

$$Y(T) = \frac{r_1\lambda_d}{\alpha}\left\{\frac{u(T_0-u)}{T_0T} + \frac{e^{-\alpha(u-T_0)} + e^{-\alpha u} - e^{-\alpha T_0} - 1}{\alpha T(1-e^{-\alpha T_0})}\right\} + \frac{\lambda_d\lambda_f\langle\nu(\nu-1)\rangle}{\alpha^2}[1+\delta^*]\left(1-\frac{1-e^{-\alpha T}}{\alpha T}\right) \quad (5.10)$$

where

r_1 is the expectation value for the number of neutron produced in each pulse,

$u = T-[T/T_0]T_0$,

δ^* is the source enhancement factor.

Several interesting aspects of Equation 5.9 and 5.10 are relevant to the data analysis. First, the equations consist of two separate parts, the continuous Feynman equation (second part of equation 5.9) and an oscillating part that is a function of the linac periodicity. Secondly, the continuous source portion of the equation is multiplied by the fission multiplication term, the Diven factor, but the oscillating portion has no relationship to the core multiplicity giving a clear separation from a source-dominated and a fission-dominated subcritical system. A plot of the stochastic Y-parameter will therefore have an oscillatory shape or humps with a minimum oscillation at the linac repetition rate and the lower bound of the function determined by the assembly subcriticality level and fission multiplicity. This behavior is shown in Figure 5.8.

Fig. 5.8. Typical stochastic Feynman-alpha curve.

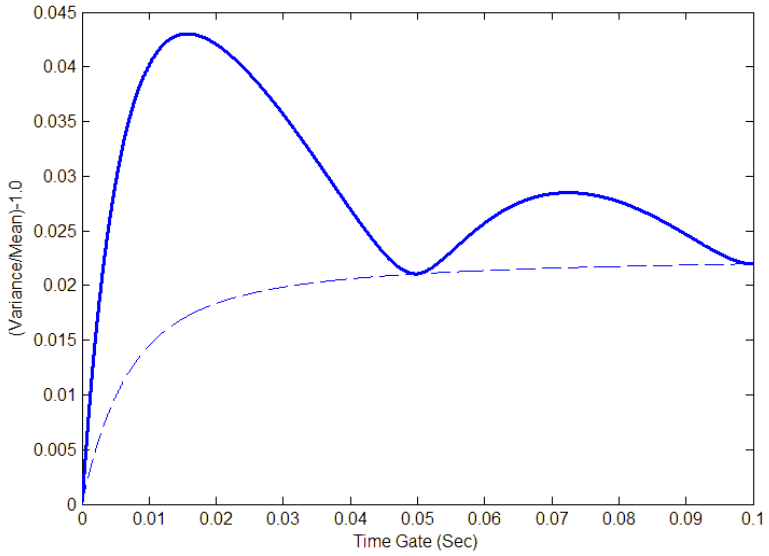

The oscillating portion of the function is directly proportional to the source strength and has an approximate inverse response to α. The fact that the source strength does not cancel out in the stochastic variance-to-mean ratio is significant and caused by the correlations between different counting gates due to the stochastic pulsing method introducing a non-zero covariance**.** The traditional (continuous-source) Y-function behaves as $1/\alpha^2$ and this indicates the weight of the oscillating portion of the stochastic Feynman-Alpha function will decrease more as the assembly gets closer to critical (the system alpha gets smaller) which makes qualitative sense as the source importance of the ADS becomes dominated by the internal fission source at low subcriticalities. However, a strong pulsed neutron source may still overshadow the internal fission multiplicity. Future transmutation ADSS will have very strong spallation neutron sources so it is likely that these sources will also dominate the low multiplicity of the fuel. Figure 5.9 compares a simulated stationary Feynman-alpha measurement (α = 150) to simulated Stochastic Feynman Method measurements with strong and weak pulsing neutron sources to show how a strong source dominates the measurements even with low subcriticality (an α of 150 is approximately a multiplication factor of 0.999).

Fig. 5.9. Stochastic Feynman-Alpha as a function of source strength.

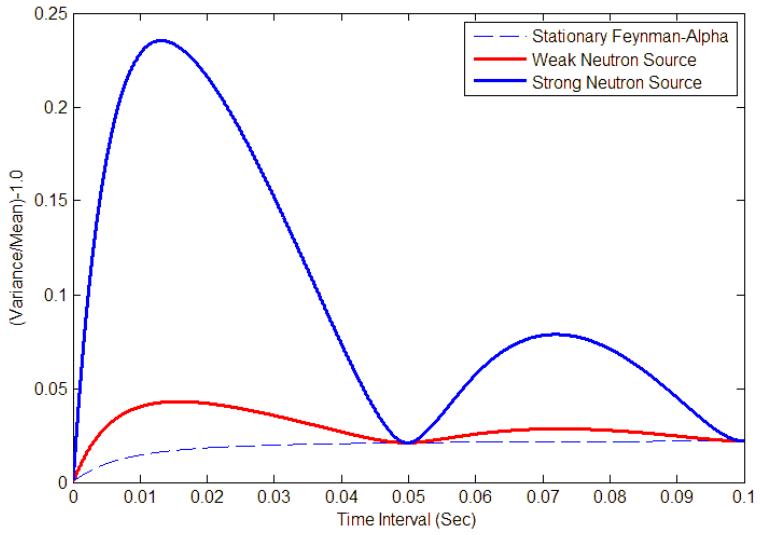

5.8 Statistics of Neutron Counting in Current Mode of Operation

Detector and amplifier dead time issues were eliminated in the neutron counting system by operating the fission chambers (FC) in current mode, but this mode of operation requires an evaluation of the current mode and of the inherent system time constants upon the system statistics for error analysis and any bias introduced into the Feynman-alpha results.

The detector, cabling and picoammeter formed a single RC circuit with the detector storing an electrical charge and discharging through the input resistance of the K6485 at a time constant, τ. All detected particles at an average rate, R, within the FC during a time period (0 to t_0) accumulate an average total charge, $Q_{m,}$

$$Q_m(t_0) = \int_0^{t_0} qR\,\mathrm{e}^{-(t_0-t)/\tau}\,dt = qR\tau(1-e^{-(t_0/\tau)}) \tag{5.11}$$

with a circuit time constant, τ, and a detector total charge, qR. The variance or second moment of the measured charge over a time interval Δt is

$$\sigma^2(\Delta Q) = \left(\frac{\delta\Delta Q}{\delta(R\Delta t)}\right) R\Delta t = \left(qe^{-\frac{t}{\tau}}\right)^2 R\Delta t = q^2 R\Delta t e^{-\frac{2t}{\tau}}. \tag{5.12}$$

All pulses contribute to the total charge accumulated over the measurement interval but taking a measurement at the end of an integration time, t_0 gives

$$\sigma^2(Q_m) = \int_0^{t_0} q^2 R e^{-2(t_0-t)/\tau} dt = \frac{1}{2} q^2 R\tau(1-e^{-2t_0/\tau}). \tag{5.13}$$

For long intervals, $t_0 >> \tau$, the variance of the signal from a detector operating in the current mode is half that measured in pulse mode but with emphasis weighted towards those events at the end of the integration period. Time bin lengths established with the DAQLab for UT-RACE determined the time integration period of 20 μs which is shorter than the system effective RC time constant of 227.3 μs determined by the specification bandwidth of the K6485. The short integration times reduced the smoothing and improved the time response to rapid changes in the detector signal. The ratio of the variance of the current to the average current is now

$$\frac{\sigma^2(Q_m)}{(Q_m)} = \frac{q^2 aRC(1-e^{-2t_0/RC})}{2qaRC(1-e^{-t_0/RC})} = 0.9538q. \qquad (5.14)$$

As noted before in Chapter 3, the average charge, q, deposited by a fission fragment in a gas-filled fission chamber is approximately $2x10^{-13}$ Coulombs (C) yielding a value for the ratio in Equation 5.14 of $1.908x10^{-13}$ C. Thus, the relatively slow time response of the data acquisition system reduced the value of the variance to mean ratio to much less than unity when the detectors were operating in current mode. This small value does not eliminate using the current from neutron detectors to perform neutron noise experiments because it only represents a correction factor to the traditional Feynman-alpha method. For example, Bennett developed an alternative to the Feynman-alpha method using the ratio of the mean square value of the difference between time gates to their mean using neutron detectors operating in the current mode[159]. The magnitude of the variance to mean ratio in current mode could be increased if desired by using a data acquisition system with shorter governing time constants, and by using higher gas pressure fission chambers or solid-state detectors such as scintillation neutron detectors.

For the Stochastic Feynman Method, this under-Poisson behavior reduces the weighting of the continuous Feynman portion of Equation 5.9 to essentially zero with respect to the over-Poisson oscillating term. This resulted in an almost undetectable system multiplicity as the statistics of the periodic source dominated the detector response. A more representative version of the Stochastic Feynman Method in current mode is

$$\frac{\sigma_Z^2(T)}{\langle Z(T)\rangle} = \frac{2\lambda_d S T_0^5 \alpha}{T\pi^4 W} \sum_{n=1}^{\infty} \frac{1}{(4n^6\pi^2 + n^4\alpha^2 T_0^2)} \times \left(\sin\frac{n\pi T}{T_0}\right)^2 \left(\sin\frac{n\pi W}{T_0}\right)^2. \qquad (5.15)$$

The system prompt neutron decay constant may still be obtained by fitting the above equation to the ratio of the variance to the mean as a function of gate length. Figure 5.10 contains several plots of Equation 5.15 with several simulated subcriticalities and a constant strength neutron source.

Fig. 5.10. Current mode stochastic Feynman-alpha at different subcriticalities.

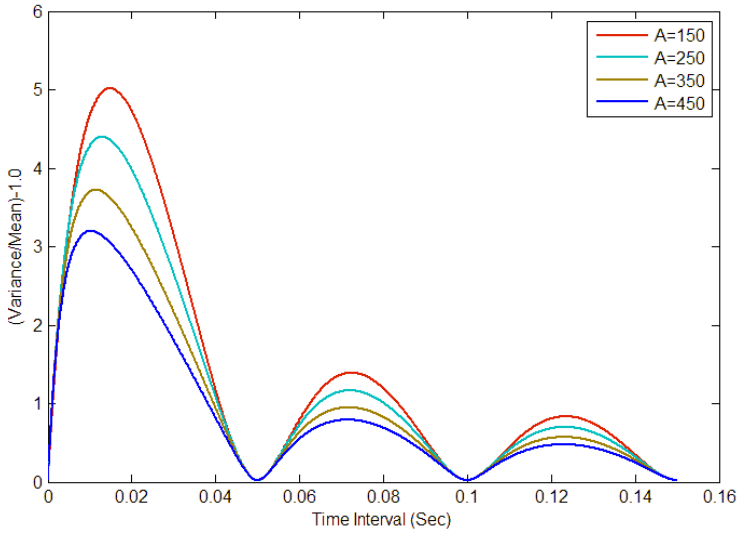

Chapter 6
Measurements and Results

6.1 Introduction

The Stochastic Feynman Alpha Method (SFM) was used extensively to evaluate the subcriticality of the TRIGA reactor under the UT-RACE project during steady-state and transient conditions. This method has advantages over previously applied noise and pulsed neutron techniques because the data may be taken in a relatively short period of time, the data has the potential to be automatically processed in near real-time and the results may be obtained at accelerator repetition rates closer to the system Alpha. The significant differences between the use of SFM for UT-RACE and the few previous experimental applications is the higher neutron source strength of the electron linac-based bremsstrahlung source, the operation of the neutron detection system in current mode and the performance of the experiments on a relatively high power critical assembly operating in a subcritical configuration with significant fission product and MA poisoning. This research project has evaluated this relatively new method of subcritical reactivity determination in an experimental system that is closer in size and parameters to full scale ADSS transmutation systems than any previous experiment.

The decision to use SFM for analysis was made after the UT-RACE project began to acquire data with detectors in current mode and prevented a full review of the SFM results before the project ended so the data was not optimized for this particular method. However, many experiments were completed during UT-RACE that provided sufficient data to evaluate the strength of the method.

1. SFM spatial dependence
2. SFM using small data sets for potential real-time reactivity determination
3. SFM evaluation at different linac frequencies
4. SFM dependency on source strength stability
5. SFM during reactor transients
6. SFM comparisons at different core reactivities using central fuel element
7. SFM comparisons at different control rod heights

As previously determined, the 78 element TRIGA reactor was negative $ 0.181 subcritical with all control rods withdrawn and with a corrected multiplication value of 0.99873± 0.00069. Fixing the values of the parameters Λ and β as 53 μs and 0.00700 respectively for an operational TRIGA reactor yields a benchmark alpha of 155.993 ± 12.968 s^{-1}.

The UT-RACE subcritical TRIGA reactor configuration had several empty core grid locations around the core edge to permit insertion of 3.175 cm diameter aluminum, watertight neutron detector tubes that were long enough to reach the top of the pool and maintain the cables dry. Only two fission chamber neutron detectors of equal volumes were available (but with different masses of uranium) and these were moved to different locations (shown in Figure 6.1) to evaluate the neutron pulse moderation and subcritical reactivity monitoring methods.

Fig. 6.1. UT-RACE core and available detector locations.

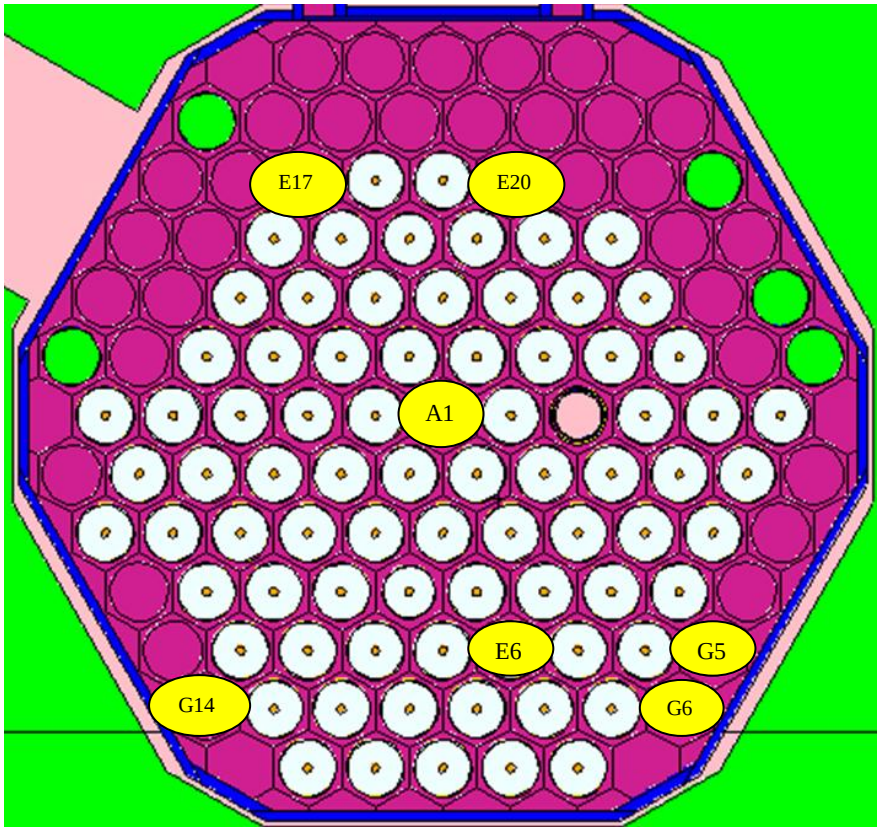

6.2 List Form Acquisition and MATLAB Processing of Data

The raw data acquired during each experimental run was stored in binary list form on a PC with each data point time-stamped with the magnitude of the measured voltage at the analog output of the K6485 picoammeter. To simplify viewing the data in real time and comparison of individual data sets, the picoammeters were operated on the 2 or 20 μAmp range with auto-scaling disabled so the analog voltage output would scale for a 1:1 or 1:10 VDC to μA conversion. The DAQView acquisition control program could be manually started, automatically triggered with an external signal or triggered by the detection of a magnitude change in the input signals. Storing the acquired data in list form proved very flexible for data analysis and later experiment review but created very

large data files from experiments. For example, a ten-minute experimental run monitoring two input signals created a single ASCII file exceeding 1 GB. These file sizes limited the length of data acquisition times because the conversion of the binary files was PC memory and processor intensive and would often prevent the conversion of larger data files. In several cases the limited acquisition time was a problem because the ADSS had not fully stabilized following a transient but one of the goals of the UT-RACE project was reliable subcriticality monitoring in near real-time and hardware limited data acquisition times encouraged new evaluation methods. Most of the subcriticality results obtained during the UT-RACE project were obtained using data acquisition times of less than five minutes.

The detail available in the list format provided information on the linac performance over time that was not accessible using standard multi-scaling time analyzers that reset after every pulse. Figure 6.2 is a response plot of a neutron detector located in G5 while the linac was operating at 50 Hz.

Fig. 6.2. Linac intensity variation with time at 50 Hz.

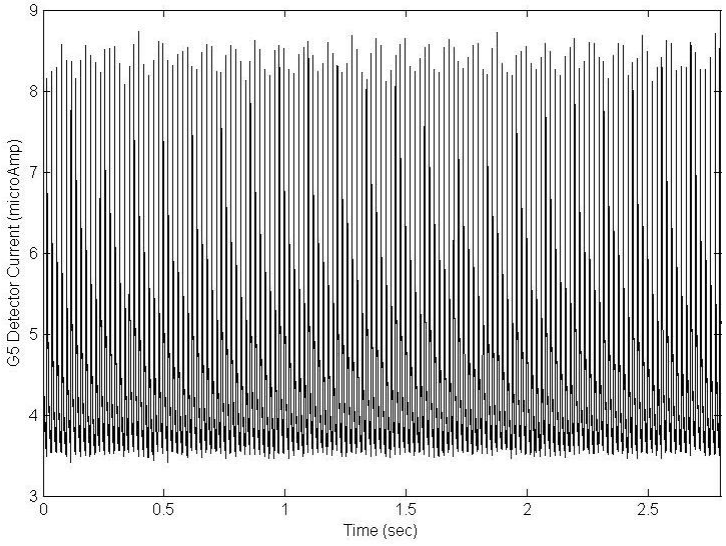

The above figure shows there is a lower frequency pulse intensity change within the 50 Hz primary linac frequency. Some authors have attempted to model a pulsed ADS as a series of delta functions with constant-source Poisson statistics under the assumption that the high neutron multiplicity within the neutron source was itself a random variable from a Poisson distribution and each pulse interval was "periodic stationary". This assumption cannot be made for a pulsed RF linac as the neutron source has a non-random variability within the periodic structure of the neutron source strength. The lower frequency variation in the magnitude of each linac pulse is evidenced by the variation of the peak neutron current around 8.5 μA at an approximate 10 Hz frequency. Additional lower frequency electron pulse spreading is seen near a frequency of 0.6 Hz with features of an exponential decay occurring at an 8.3 Hz frequency. As was discussed in Chapter 3, during the UT-RACE experiments there was also a non-periodic variability in beam intensity from unknown causes resulting in varying neutron source strength with identical linac control settings. These cyclic features in the linac beam are examples that even when the linac is thought to be operating at a constant frequency and injection current there will be an unavoidable variation of the beam and, hence, the neutron source intensity over time.

For the data to be processed and analyzed using the Feynman method (either continuous or stochastic forms) the small time bins needed to be summed to create sequential and larger time blocks as would be created when a time analyzer or multichannel scaler acquires time-dependent data[160]. This processing technique has been called a "data synthesis" method by Yamane[161, 162]**;** however, the original technique was developed by Turkcan and Dragt[163]. A script routine was written for MATLAB (FAlpha.m) that would process a data file and create larger time bins by adding the data in consecutive bins. The processing of the large data files created very large matrices which often exceeded the available memory (3GB) on a 32-bit Windows XP computer running a 32-bit version of MATLAB and the maximum number of matrix elements ($2x10^8$) allowed in 32-bit versions of MATLAB[164]**.** A maximum number of data bins had to be used to provide sufficient precision for later mean and variance calculations so the

data analysis was transferred to a 64-bit version of MATLAB (v.2006b and v.2007b) operating on a 64-bit machine running Windows XP64 permitting larger matrices with up to 2.8×10^{14} elements which required approximately 30 GB of PC memory to process.

The processed and binned data was then operated upon by another MATLAB script that calculated the ratio of the variance and the mean for each synthesized time gate and created another, final data file. A plot of a final data set from an example 50Hz data run with the fission chamber located in G5 is given in Figure 6.3 to show the unique characteristics of the Stochastic Feynman Alpha plot for the UT-RACE project.

Fig. 6.3. 50 Hz variance to mean plot for UT-RACE.

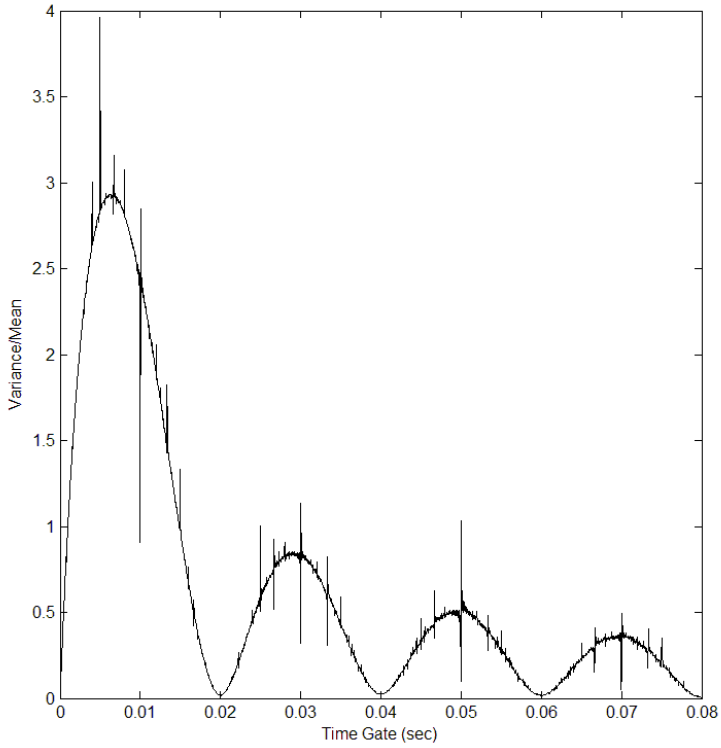

The expected oscillating form displayed has minimum values at the pulsing rate of the linac corresponding to the very small variance of the neutron density (high source multiplicity) following a linac pulse. There is no lower bound formed by the continuous

form of the Feynman-alpha equation as previously shown in Figure 5.8. This is the combined result of the strong linac neutron source making the source statistics over-Poisson and the under-Poisson core response due to the detectors operating in current mode as noted before. The variance to mean plots also indicate a unique feature of neutron production using an RF linac and that is the addition of harmonics that are multiples of the primary accelerator frequency. The detector current versus time plots (Figure 6.2 above) did not indicate harmonic contamination but it is visible in a spectral plot of the detector data with the linac operating at 50 Hz as shown in Figure 6.4.

Fig. 6.4. Spectral plot of G5 detector data at 50 Hz.

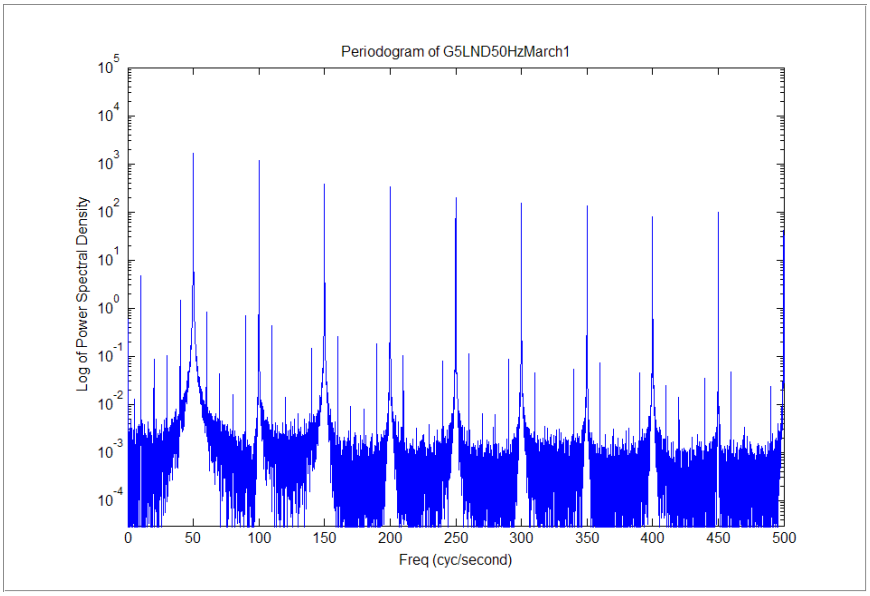

6.3 MATLAB Curve Fitting

To complete the processing of the raw detector data, the variance to mean data versus gate length was fit to Equation 5.15 using the MATLAB curve fitting tool with an improved fit by treating the harmonic "spikes" on the primary waveform as outliers and excluding them from the fitted data set.

The fitting equation had three parameters, the alpha-value (α or A), a source strength term, Y_0, and a constant term added to the equation to accommodate baseline

shift, Xi. The source strength term ($Y_0 = \lambda_d S$) was not intended to be directly correlated to the number of neutrons produced by the linac but was a variable used to account for the linac source strength and the efficiency of neutron detection both of which were unknown values. The curve in Figure 6.3 above was from a detector located in G5 and the curve fit determined an Alpha (α) of 240.6±2.0. The curve fit parameter results for Figure 6.5 are summarized in Table 6.1.

Fig. 6.5. Variance to mean curve: G5 detector location.

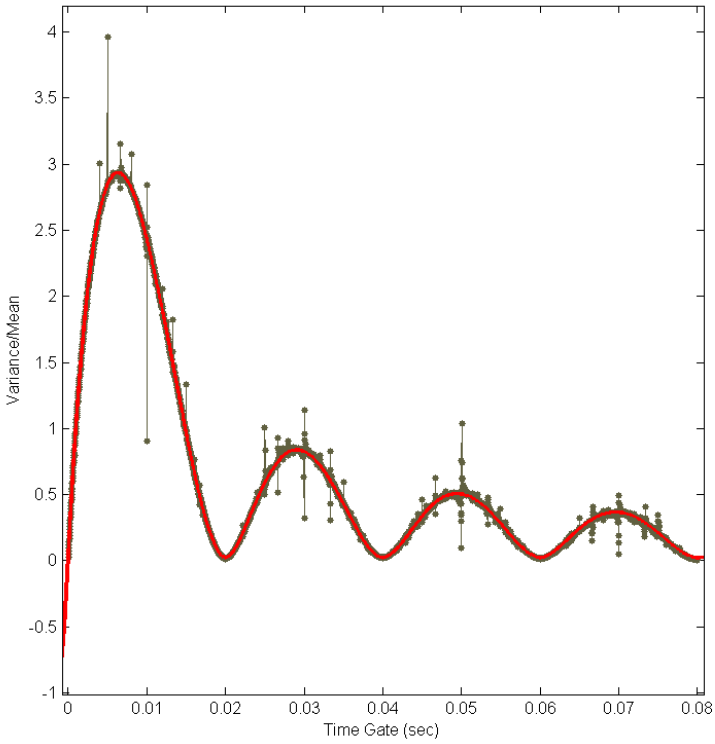

Table 6.1. Fitting parameters using SFM for detector in G5.

Alpha	Source Term, Y_0	Xi	Curve R^2	Calculated Multiplication Factor
240.6 ± 2.0	1.534E8 ± 4E5	0.02127 ± 0.00055	0.9997	0.99428±0.0001

The R^2 value or the "coefficient of determination" is a statistical parameter from the least mean square fitting that determines how good a fit was achieved[165]. If the R^2 is equal to 1.0, the equation is a perfect fit to the data (but it does not take the standard deviation into account).

6.4 Detector Location Effects

Previous research has shown that pulsed reactivity measurement techniques are influenced by the location of the neutron detector in and around the nuclear assembly[166-168]. The major spatial effects are caused by neutron flux harmonics within the reactor from the same time dependency (prompt decay constant) that is used to determine the subcriticality level but there may be additional significant spatial errors caused by the reflected and moderated neutrons that slowly diffuse back into and through the core over several tens of milliseconds from the initial neutron pulse. The initial neutron pulse from the linac will also influence the detectors near the linac source due to localized source harmonics as the neutron pulse wave slows down from the pulsed linac source with a neutron density decay time that is influenced by local moderator materials and the subsequent fission production in the fuel.

There were few options to evaluate spatial effects on the accuracy and repeatability of the SFM within the TRIGA core while maintaining the core in a known reactivity condition because of the limited potential neutron detector locations, the large size of the available neutron detectors, and the limited number of available detector systems. The central location, A1, of the TRIGA core was designed to insert experiments that benefit from the highest available reactor neutron flux but it also provides a location to install a fission chamber detector tube without significantly perturbing the core reactivity. Other locations around the core that were external to the fuel region and within the water reflector were selected to place fuel between the source and the detector

so the fission chambers were measuring neutrons resulting from prompt fission and not the linac neutron source.

Figure 6.6 is a plot of two fission detectors located on opposite sides of the UT-RACE core in E17 and G14. G14 was the closest neutron detector to the linac target with a higher base current but the data was shifted and scaled so the detector currents overlaid at the same point for time comparison purposes.

Fig. 6.6. 50 Hz detector response in G14 and E17.

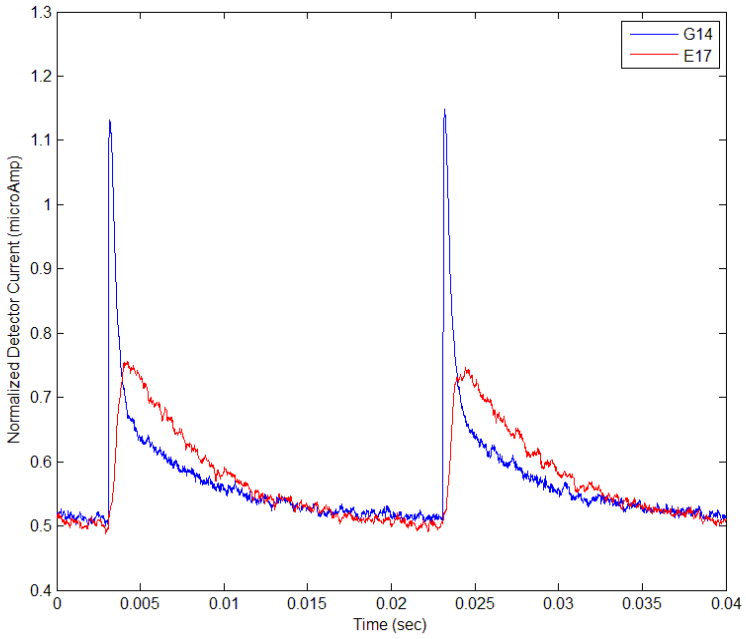

The detector in G14 exhibits a fast pulse rise time with the expected exponential decay but the detector in E17 has a slower pulse rise time due to the thermalization and diffusion of the original linac neutron pulse through the reactor core and the additional neutrons produced by fission. Figure 6.7 is the same plot of the detector response in E17 and G14 following a single linac pulse with the time axis narrowed to show the detail of the two pulses.

Fig. 6.7. Individual pulse extracted from 50 Hz data in G14 and E17.

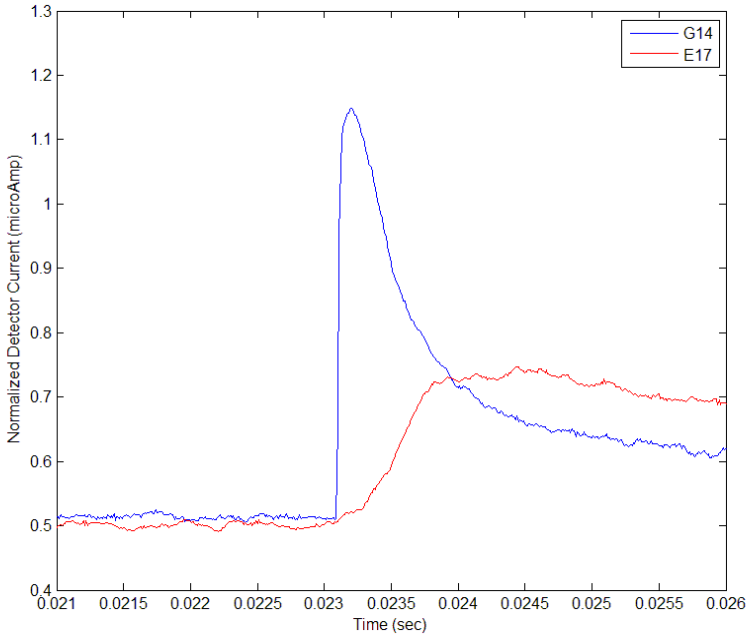

The detector current in location E17 begins to rise immediately with the leading edge of the G14 detector pulse indicating no apparent time delay that could be attributed to the time of flight of the neutrons produced in the linac target and production of neutrons directly from the created fission chains. The detector response and time delay was evaluated by modeling the UT-RACE core and several detector locations using MCNPX. A single, square linac pulse was simulated by a 5 μs wide neutron pulse produced in the center of the linac target and the resulting neutron population was tracked with time in the subcritical core model. The results of the time simulation are shown in Figure 6.8 where it can be seen that neutron flux in all detector locations begins to increase immediately after the initial linac pulse measured in location G15 (indicated as a thin, vertical linac pulse line at t=0). The simulation also shows that the subcritical core neutron flux peaked approximately one msec after the initial pulse and then decreased across the core and edges at the same rate.

Fig. 6.8. MCNPX time simulation of neutron flux in detectors.

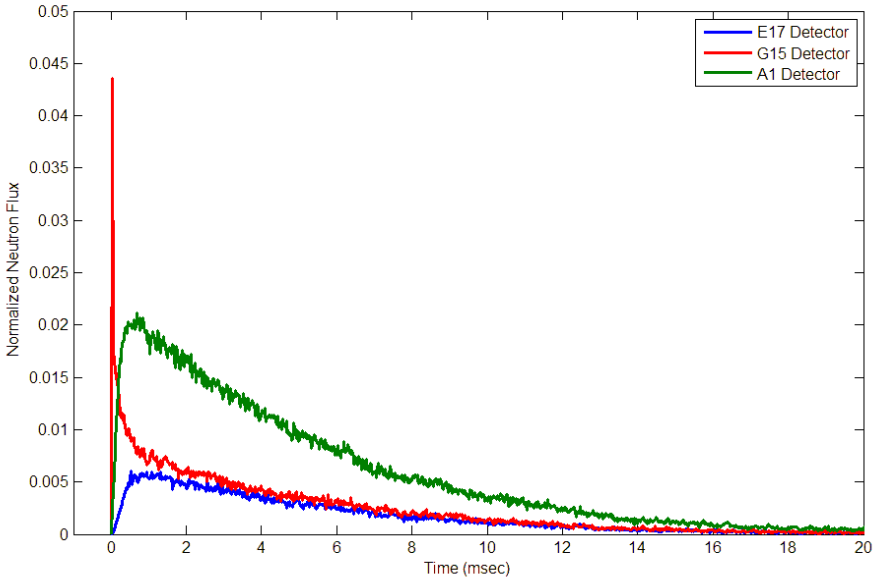

The MCNPX simulations and detector measurements appear to indicate there is no time delay between the beginning of neutron pulse detection at G15 and the E17 location on the opposite side of the core. However, closer examination of the MCNPX output with small time bins immediately following the start of the initial pulse shows the neutron transport begins during the initial 5 μs square pulse and there is a slight time delay (~70 ns) before the initial pulse of neutrons is registered in the E17 detector due to the neutron time of flight from the linac source (Figure 6.9). The finite neutron time of flight is much shorter than the linac pulse width so the neutron detectors in all locations have begun to respond to the increase in neutron population before the linac pulse ends. This results in an initial appearance of instantaneous response as shown in the plot of the simulated single pulse in Figure 6.10.

Fig. 6.9. MCNPX time simulation, t =0 to t = 90 ns.

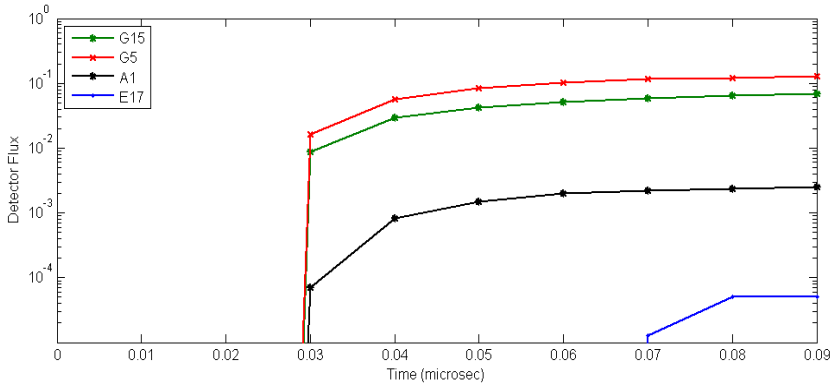

Fig. 6.10. MCNPX time simulation showing response to 5 μs pulse.

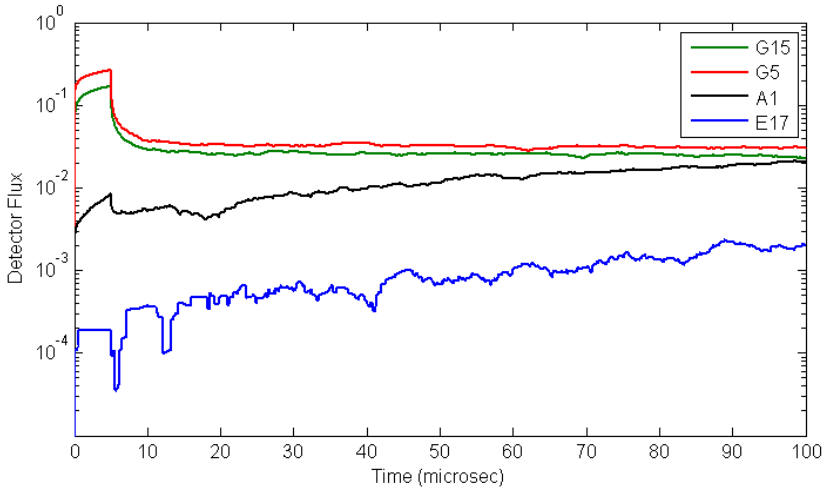

The MCNPX simulated detector fluxes provided the means to evaluate the prompt neutron decay simulated in several core locations. Viewing the plots with a logarithmically scaled Y-axis shows the equality of the prompt decay slopes (Figure 6.11). Performing a simple curve fit to the data gives the MCNPX simulated Alpha for three neutron detector locations for the time interval 2 to 10 ms (Table 6.2).

Fig. 6.11. MCNPX time simulation of ADSS response to single pulse.

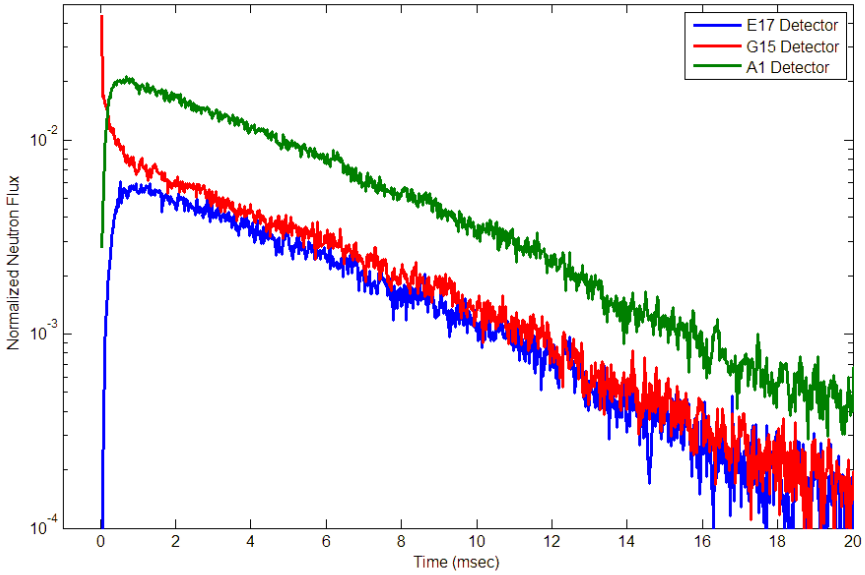

Table 6.2. MCNPX alpha from curve fits.

MCNPX Detector Location	**Curve Fit α**
E17	181.5 ± 3.9
G15	182.1 ± 3.6
A1	188.5 ± 2.4

The average value of α of 184.03 ± 5.82 represents a multiplication factor of 0.99725 but also indicates the subcritical core was in spatial equilibrium 2 ms after the pulse because the neutron flux in the center (A1) and the core edge (E17 and G15) all decrease at essentially the same rate. Unfortunately, this MCNPX simulation does not represent the reality of the UT-RACE project because MCNPX will only simulate a single pulse and not a pulse train as was produced by the operating linac and target. The simulation could also not successfully model the buildup of delayed neutrons resulting

from an average driven subcritical multiplication level or the neutron reflection back into the detectors and core from the surrounding water and graphite but was adequate to represent the time response of the system to a single, square neutron pulse.

6.5 SFM Stability over Short Time Periods and Small Data Sets

Ten consecutive one-second data runs ($1x10^5$ points collected with 10 μsec bins) were performed with all rods out and the linac operating at 50Hz but only three sets were selected and analyzed (Set 1, 4, and 7) to evaluate consistency of the subcriticality determination assuming minor linac beam drift between short data runs. The linac was operated at 50 Hz for seven minutes until the neutron level as indicated on the TRIGA console had stabilized at 9 W. All data was obtained from a fission detector located in E17 which is on the opposite side of the core from the neutron source. The neutron detector data was not plotted here for clarity and it can be easily seen that the fitted curves lie very close to one another (it is unlikely the curve fit routine would converge to identical equations from different data sets). The plot and table (Figure 6.12 and Table 6.3) below presents three methods of SFM data analysis in order to evaluate the sensitivity to a variable or fixed Source Term in the MATLAB fitting routine:

a. Source term with little constraint and a wide search range;
b. Source term with small, realistic search range;
c. Fixed source term.

Table 6.3. Curve fit α results with varying initial parameters.

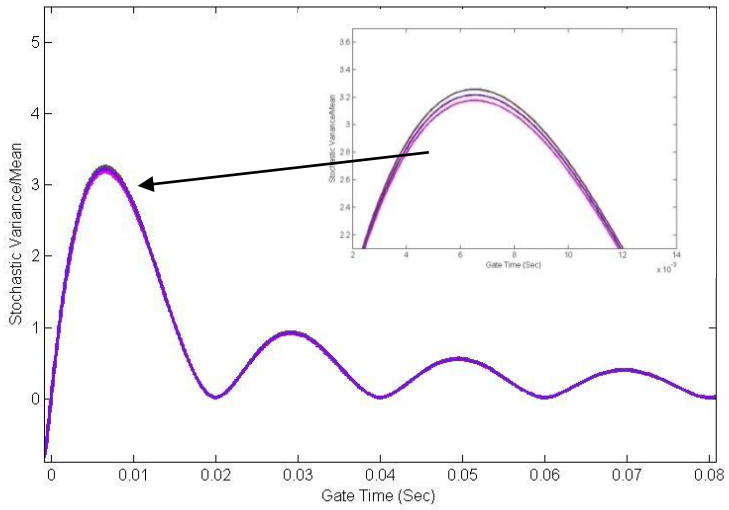

Table 6.3. Curve fit α results with varying initial parameters.

Curve	**α**	**Xi**	**Source**	**R^2 Value**	**Multiplication Factor**
Case 1a	148.3±13.9	0.021±.003	$2.166x10^8$ ± $0.134\ x10^8$	0.9844	0.99914 ±0.00072
Case 2a	148.7±13.9	0.018±.003	$2.11\ x10^8$ ± $0.134x10^8$	0.9842	0.99912 ±0.00073
Case 3a	142.0±15.2	0.016±.003	$2.205E^8$ ± 0.162 $x10^8$	0.9823	0.99947 ±0.00081
Case 1b	156.2±13.1	0.021±.003	$2.094\ x10^8$± $0.112\ x10^8$	0.9844	0.99872 ±0.00071
Case 2b	150.7±13.7	0.018±.003	$2.092\ x10^8$ ± $0.124\ x10^8$	0.9842	0.99901 ±0.00072
Case 3b	151.8±14.4	0.015±.003	$2.11\ x10^8$ ± $0.131\ x10^8$	0.9823	0.99896 ±0.00076
Case1c	144.9±0.6	0.022±.003	$2.2\ x10^8$	0.9844	0.99932 ±0.00076
Case2c	139.8±0.6	0.018±.003	$2.2\ x10^8$	0.9842	0.99959 ±0.00003
Case3c	142.6±0.6	0.016±.003	$2.2\ x10^8$	0.9823	0.99944 ±0.00003

The first case used the values in TABLE 6.4 below as the range of allowed values for all parameters. The MATLAB curve fitting routine would usually not converge to physically realistic values if approximate ranges were not provided as initial values.

Table 6.4. General fitting parameters for SFM fits.

α	**Source**	**Xi (offset term)**
100 to 400	$1x10^{4}$ to $1x10^{12}$	-1 to 1

The next three curve fitting cases (1b, 2b, 3b) were evaluated the same way but assumed a Source Term with small variation between $2.09x10^{8}$ and $2.11\ x10^{8}$. The final three cases (1c, 2c, 3c) were fitted by assuming the Source term was constant but based on previous fitted values. Fixing Y_0 without a good, prior estimate occasionally resulted in the curve fitting routine not converging to a solution but in this particular case the resulting average Alpha ($142.433 \pm 1.04\ s^{-1}$) had a smaller confidence interval and was 8.6% from the benchmark value of $155.9\ s^{-1}$. The process of providing a relatively small interval for the source term (to account for the drift in the accelerator source output) yielded the best results as given by Case 1b, 2b, and 3b in which their average (152.9 ± 23.8) is within 2.0% of the benchmark. It will be shown that the value of Y_0 must be allowed to change as it is sensitive to linac frequency, detector location and reactivity in the reactor core.

6.6 SFM at Various Linac Frequencies

The electron linac was able to operate continuously at frequencies of 1 to 200 Hz, but for data consistency the majority of the operations were performed at 20, 50 and 100 Hz. The fitted curves below (Figure 6.13) indicate how the Variance to Mean ratio is dependent on the linac frequency through the source term, Y_0, and that the change in magnitude of this ratio is a non-linear function of linac frequency.

Fig. 6.13. Variance to mean plot with all rods withdrawn and three frequencies.

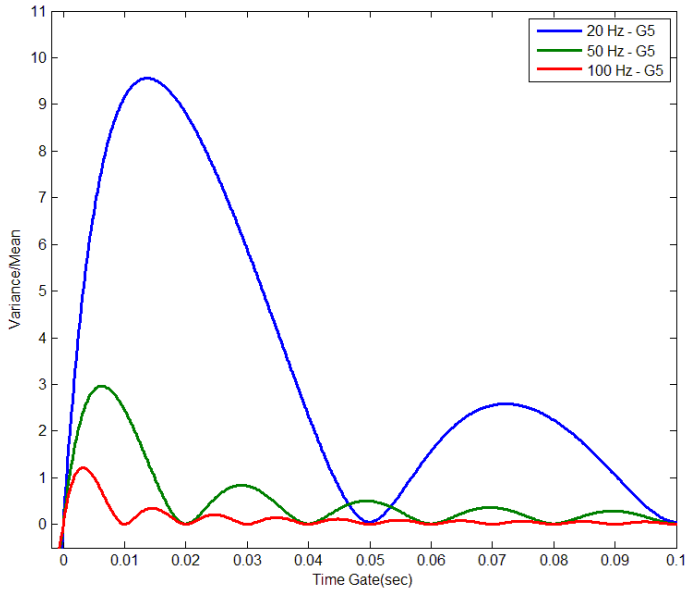

Table 6.5. SFM results at different linac frequencies.

Frequency (Hz)	**α**	**Source Term**	**Multiplication Factor**
20	205.4 ± 1.4	$2.019 \times 10^{8} \pm 5.0 \times 10^{5}$	0.99613 ± 0.00007
50	246.7 ± 5.3	$1.543 \times 10^{8} \pm 1.0 \times 10^{7}$	0.99396 ± 0.00028
100	383.1 ± 9.2	$1.397 \times 10^{8} \pm 1.7 \times 10^{6}$	0.98687 ± 0.00047

The initial fits were performed by setting wide initial parameter ranges as shown in TABLE 6.5 above. The Alpha parameter was found to consistently overestimate the subcriticality level as a function of linac frequency due to harmonics. Equation 5.9 indicated the value of Alpha found by curve fitting of the data is dependent on the source strength as detected by the neutron detectors but also to the frequency of the linac source due to the reduction in overall measured signal variance with the higher frequencies.

Figures 6.14 and 6.15 below compare the overall improved smoothness of the data at 100 Hz versus 50 Hz.

Fig. 6.14. Detector in E17 (50 Hz, α is150, k=0.9990509).

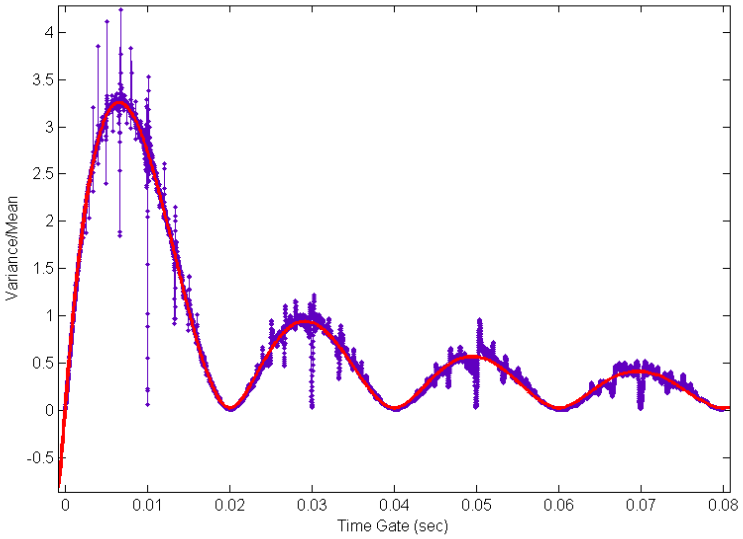

Fig. 6.15. Detector in A1 (is 307.5, k= 0.99079).

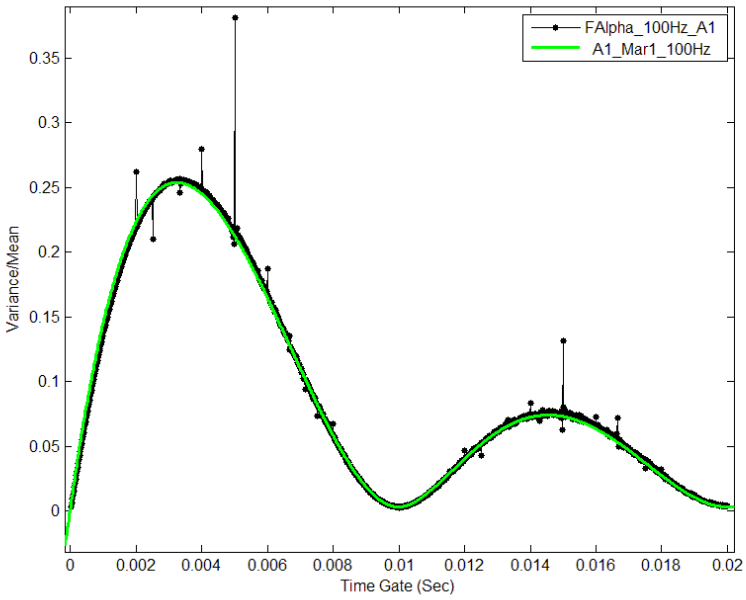

6.7 SFM at Various Subcriticalities

The insertion of neutron detector tubes around the edge of the reactor fuel introduced air voids but only minor reactivity effects. A large change in core reactivity occurred when a central element from location E6 was removed to install a neutron detector tube and monitor the neutron flux internal to the core. This location was selected to place a neutron detector in a core region more central to the offset configuration and away from the Transient Rod.

The removal of the element was modeled using MCNPX which calculated the multiplication factor of the 77 element (no E6) core to be 0.98756 ± 0.00053. This was then compared to the 78 element core reactivity to arrive at the single fuel element (E6) differential reactivity worth of \$0.863 ± 0.104. This value of reactivity was subtracted from the benchmark UT-RACE core multiplication factor of 0.99873 to determine the core multiplication factor with an element removed from E6 of 0.99269 ± 0.00100. Figure 6.16 below compares the shape of the variance to mean curve for the 77 and 78

element cores at the same linac frequency and detector location to show the most significant change in the curves occur in the short time gates where the width is less than $1/\alpha$.

Fig. 6.16. Comparison of variance to mean plots for 78 and 77 element core.

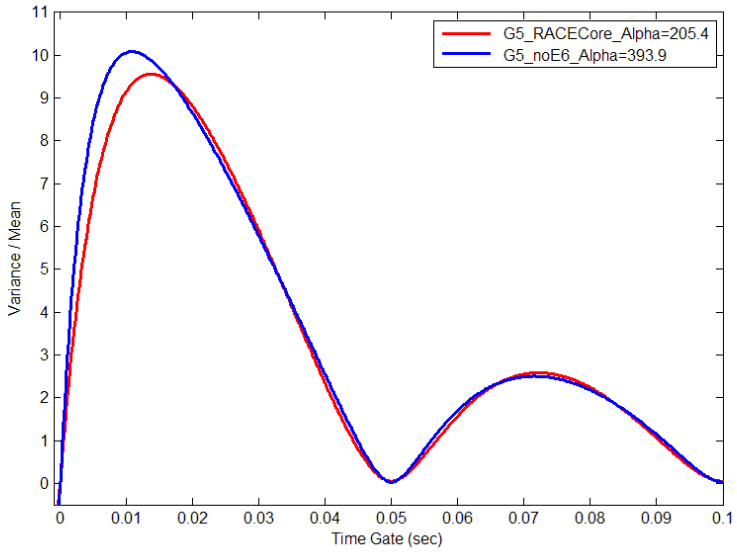

The α determined by SFM from three detector locations is given in Table 6.6. In all three cases, the SFM method overestimated the subcritical level from the calculated benchmark Alpha value of 271.02. A confirmatory single pulse of the linac was performed to determine α by the PNS method and the α of 242.8 ± 3.6 was found by curve fitting the pulse decay. This value of α provided confidence that the calculated subcritical level with E6 removed was closer to the true reactivity of the core.

Table 6.6. SFM applied to detector data from three locations with E6 removed.

Detector Location	Alpha	K_{eff}
G5	393.9 ± 2.3	0.98631
E6	360.5 ± 1.7	0.98804
A1	338.6 ± 2.3	0.98917

6.8 ADSS Linac Transients

One concern for an operational ADSS is how the system will respond to rapid changes in accelerator frequency or during accelerator startup. To evaluate the UT-RACE subcritical core in the most severe transient possible with the given system, the linac was switched on operating at 200 Hz with the UT-TRIGA configured with 78 elements and all control rods withdrawn. A plot of the response of a neutron detector in G5 is given in Figure 6.17 and Figure 6.18. The appearance of a partial pulse at the beginning is due to the linac klystron switching on at the same time as the linac power and there is a finite time required to create sufficient RF energy to accelerate an electron pulse in the cavities. The ADS response was similar to a rapid insertion of positive reactivity into a near-critical reactor because the reactor neutron level immediately increased in a step-jump when the linac switched on and then a much slower increase in the neutron level occurred over the next five to ten minutes as delayed neutrons from fission products reached equilibrium with the accelerator driven neutron level.

Fig. 6.17. ADSS transient for instant-on linac to 200 Hz.

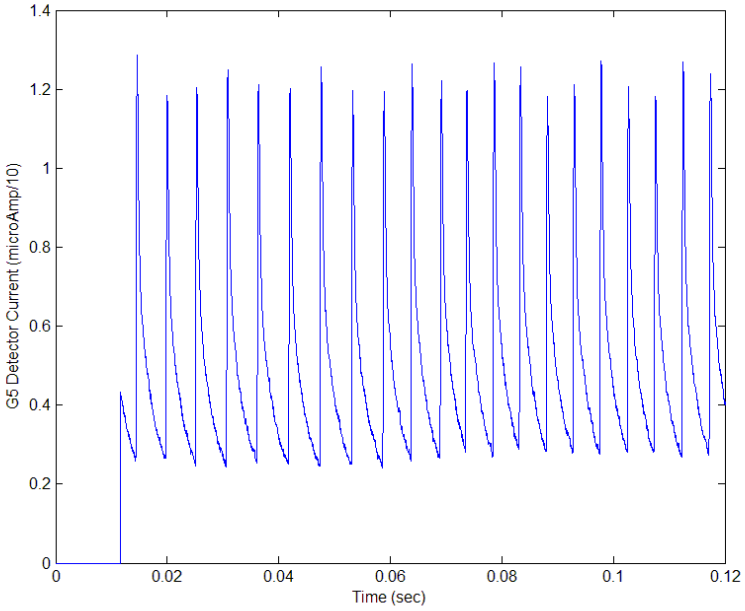

Fig. 6.18. ADSS response to linac power transient.

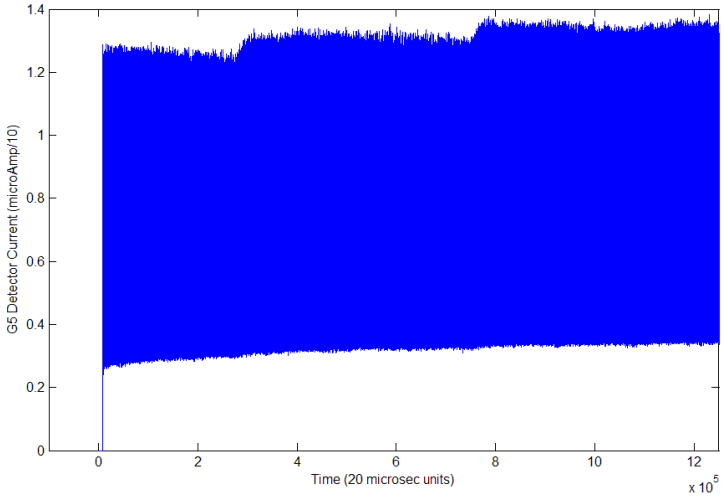

The SFM was applied to the data to determine how quickly and how well the reactivity level of the core could be determined once the accelerator had been turned on. As seen in Figure 6.19, the plot of the Variance to Mean for the data has an increasing trend over time due to the delayed neutrons adding to the average neutron population and creating correlations between time gates. The result is a variance plot with an increasing trend which is a function of the buildup of delayed neutrons (Figure 6.20).

Fig. 6.19. Variance to mean plot for 200 Hz linac transient.

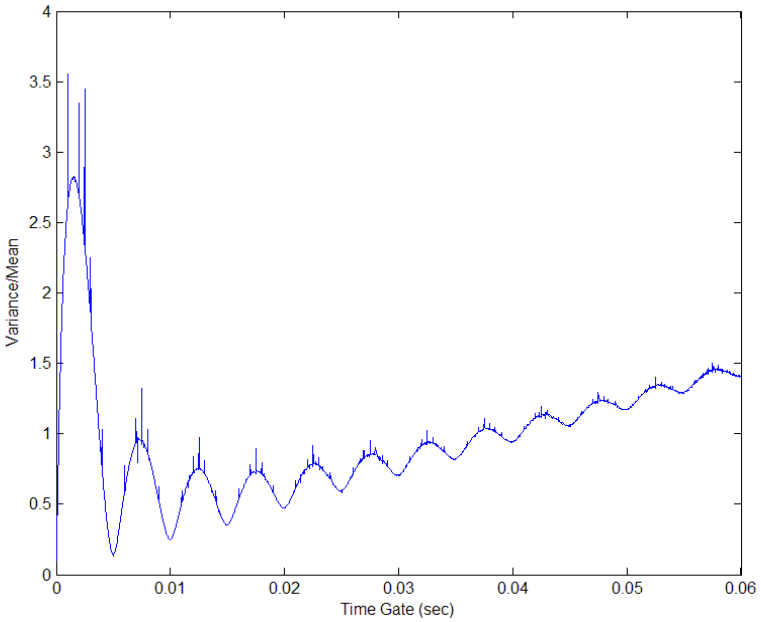

Fig. 6.20. Plot of variance to time gate width following linac transient.

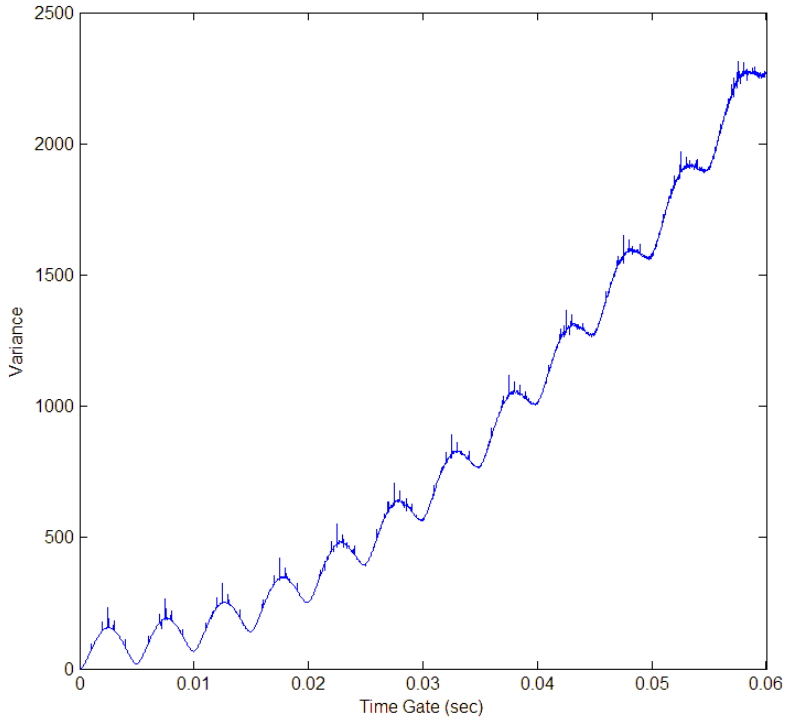

The SFM fitting equation for the variance to mean data was modified to include a linear polynomial term in an attempt to adjust the equation to accommodate the non-stationary data condition. The results of using SFM with and without an additional linear term are given in Figure 6.21 and Table 6.7.

Fig. 6.21. Curve fitting to variance to mean data for linac 200 Hz transient.

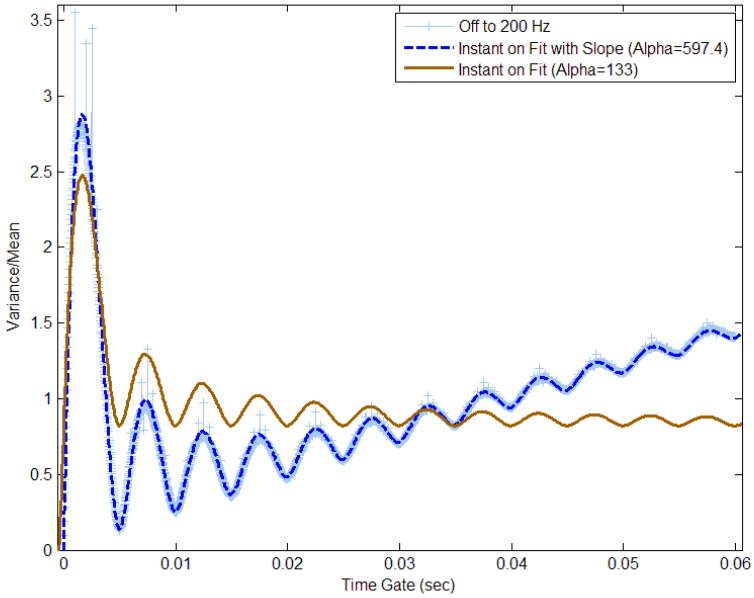

Table 6.7. SFM fits to 200 Hz transient with and without linear polynomial term.

Curve Fit	α	Slope Constant	R^2 Value
No Slope	133 ±3736	0.0	0.4375
Slope Added	597.4 ±69.1	22.92	0.9910

The addition of a linear polynomial term to the fitting equation significantly improved the fit but the α value obtained did not represent the true subcritical conditions. The large value of α does; however, follow the trend demonstrated in Table 6.5 of an increasing overestimation of α values with increasing accelerator frequency.

A less severe transient was initiated when the linac was turned on with a step power increase from beam-off to 50Hz with two neutron detectors (E17 and E20) on the

opposite side of the reactor core from the neutron source. The delayed neutrons caused detector current to continue increasing following the initial prompt jump to power resulting in a measurable increase in the average detector current over the data acquisition period of 7.4 seconds but the rise was lower than seen at 200 Hz because the lower average source driven power produced a proportionally lower delayed neutron density. The addition of a linear polynomial relation to the SFM curve fit equation improved the curve fit and yielded the results given in Figure 6.22 and Table 6.8.

Fig. 6.22. Variance to mean and SFM fit plots for 50 Hz linac transient.

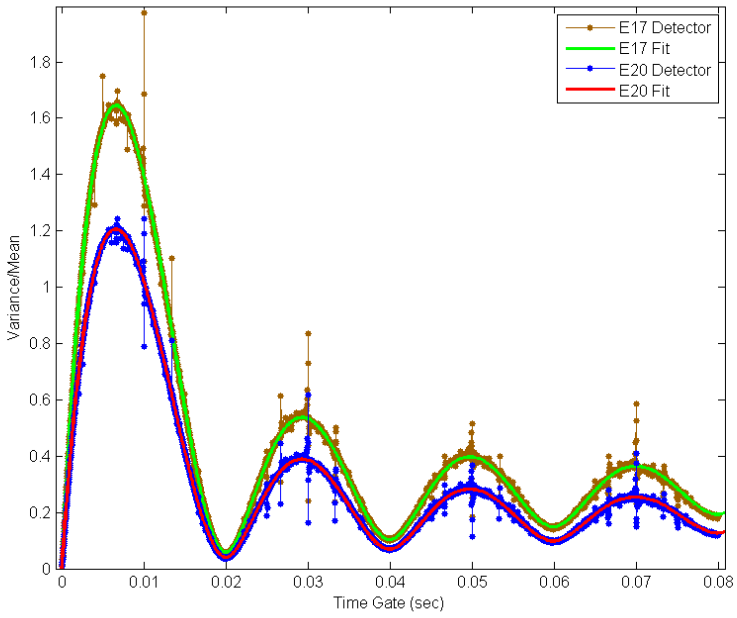

Table 6.8. SFM applied to 0-50 Hz ADSS transient.

Detector	Alpha	Source Term	Slope Value	Multiplication Factor
E17	145.0 ± 7.4	1.099E8 ± 3.7E6	2.241 ± 0.037	0.99932 ± 0.0004
E20	150.8 ± 6.5	7.849E7 ± 2.2E6	1.446 ± 0.024	0.99900 ± 0.0003

The two curve fitted with an additional linear term are very good fits and the resulting Alphas are within 7% of the benchmark value. These results indicate improved measurements may be taken on the other side of the fueled assembly from the pulsed linac source to allow source harmonics to decay and only measure the prompt response of the reactor fission chains.

6.9 Operation with Linac Frequency Above System α

With the linac operating at the maximum sustained frequency of 240 Hz the pulse repetition rate is less than 1/α (0.00417 s versus 0.00641 s) and the neutron pulses begin to show poor exponential decay features as shown in Figure 6.23. Only limited operation time was available at this frequency (< 2 minutes) because the linac klystron would overheat and trip off the accelerator due to limited cooling so the system never achieved steady-state conditions. Short data runs were performed while the reactor power continued to increase due to delayed neutrons. This data was also fit with a modification to the SPM curve fitting equation to include a linear term for a better fit to the increasing trend of the data although it did not change the calculated α appreciably and the result had very large confidence intervals (Figure 6.24 and Table 6.9) indicating very unreliable results.

Fig. 6.23. G5 detector location response to 240 Hz linac.

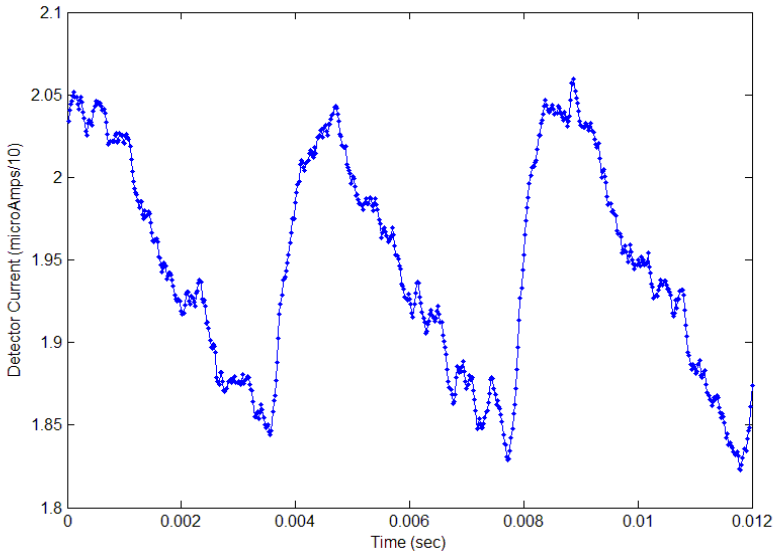

Fig. 6.24. Variance to mean plots and curve fits for G5 and G6 with linac at 240 Hz.

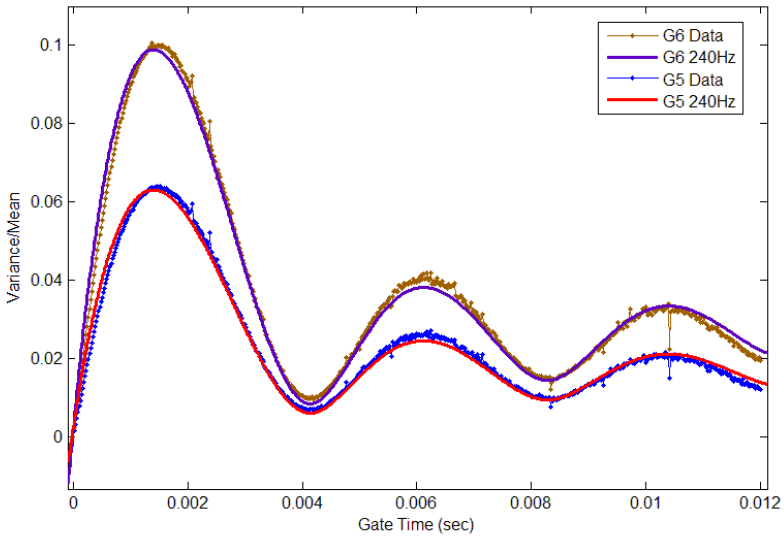

Table 6.9. SFM applied to ADSS operating at 240 Hz.

Detector Location	**α**	**Source Term**	**R^2 Value**
G5 240Hz	102.9 (-980.8, 1187)	1.092×10^8 (-1.03×10^9, 1.25×10^9)	0.9903
G6 240Hz	106.1(-877.1, 1089)	1.690×10^8 (-1.382×10^9, 1.72×10^9)	0.9913

6.10 ADSS Reactivity Transients

During another series of short experiments, the Transient Rod (TR) was dropped while the linac was operating at 50 Hz and, after the system was again steady state, pneumatically ejected to perform a rod drop and rod ejection reactivity measurement. This data was subsequently analyzed using SPM to determine the response time of the method or the time it would take for a reliable reactivity measurement to be obtained following a large reactivity transient. The data was analyzed in order to consider the reactivity measured by the SFM prior to and just after the transient (either dropping or ejecting the TR). The data acquisition time was relatively short (~45 s) but sufficient to capture the system response immediately before and after the transients (Figure 6.25 and Figure 6.26). The data analysis was performed after allowing 30 s for the power level to stabilize following the transient. Figure 6.27 compares the prompt neutron decay for the two TR conditions.

Fig. 6.25. ADSS transient for TR drop at 50Hz.

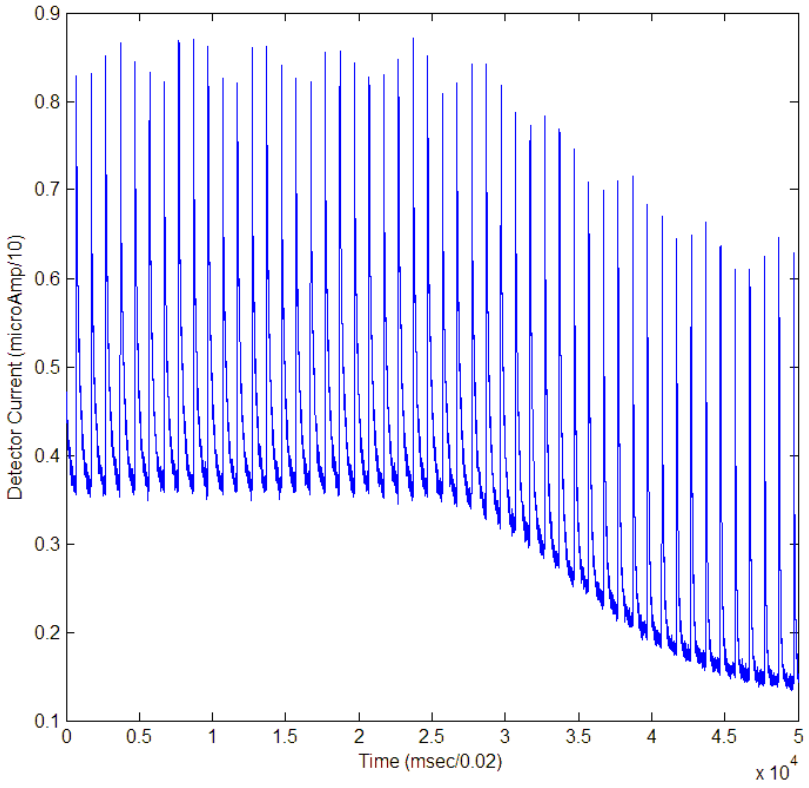

Fig. 6.26. ADSS transient for TR ejection at 50 Hz.

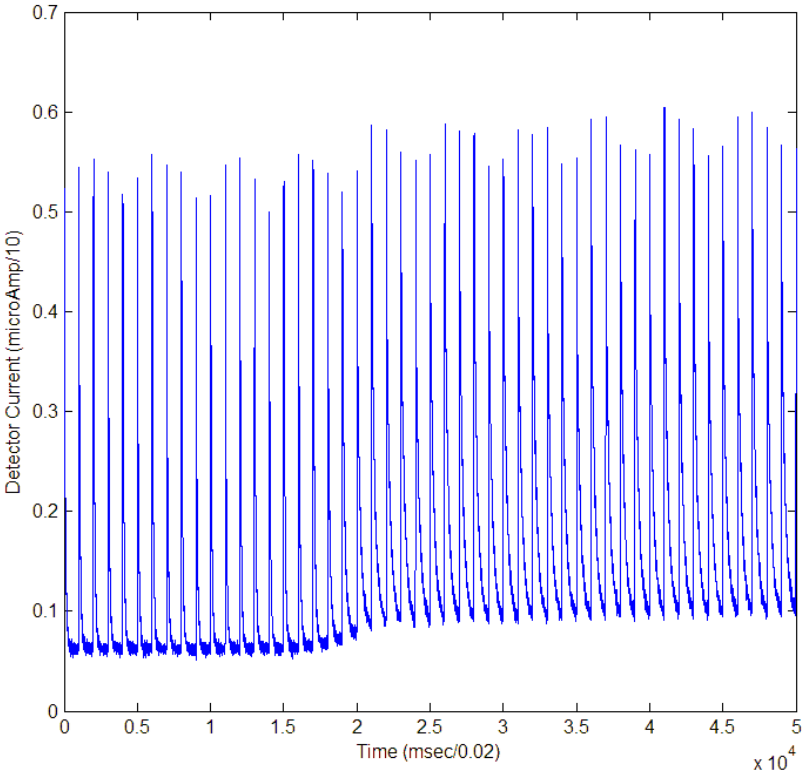

Fig. 6.27. ADSS decay for TR UP (Blue) and DOWN (Red) at 50 Hz.

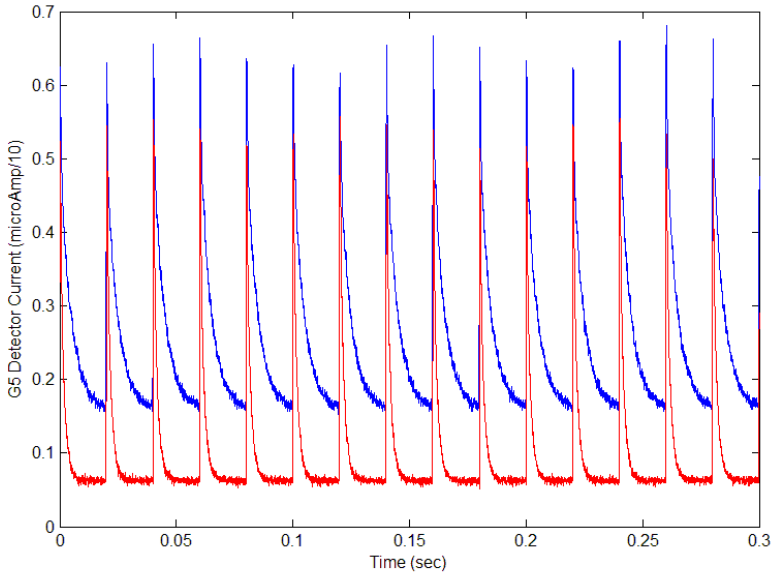

Figure 6.28 shows the variance to mean data and the SFM fits to compare the true variability of the raw data that is somewhat obscured by the smooth curve fits. The data for the time period before the TR dropped has more noise because there was only two seconds of data recorded prior to the TR dropping as seen in Figure 6.25 above. Even with sparse data, the curve fit to the SFM equation provides an accurate good value for the system α with an error of 9.7%.

Fig. 6.28. SFM measurements before and after Transient Rod drop.

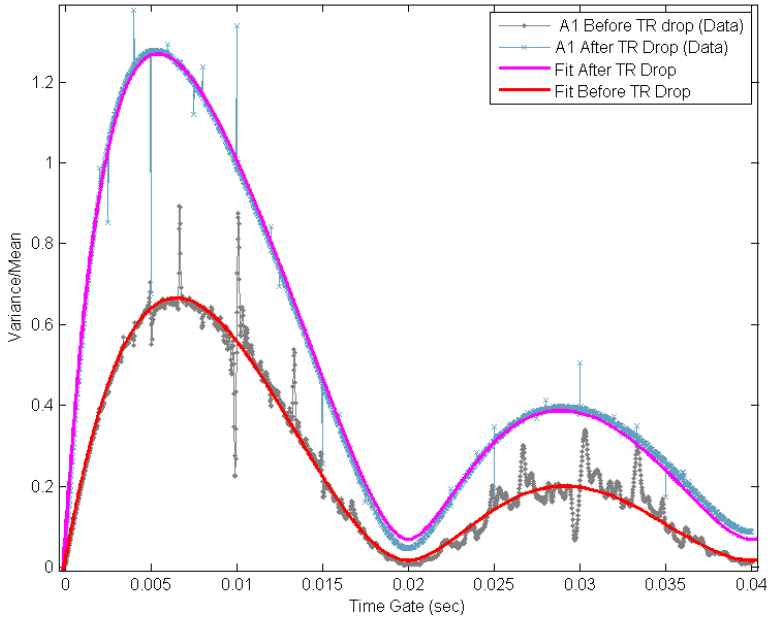

Table 6.10 and Figure 6.29 compare reactivity estimates for TR up and down for each transient (drop and ejection). Although the SFM curve fits do not lie near one other for essentially the same core reactivity conditions this is expected because the data was acquired immediately following a large and rapid reactivity transient and the detector currents had not stabilized to a constant average. However, there is a clear separation of the curve sets indicating the SFM method will respond to rapid reactivity transients and provide good data as seen in Table 6.10.

Table 6.10. SFM for TR drop and ejection transients.

Detector-Condition	α	Source Term	R^2 Value	Multiplication Factor
A1 Before Drop	171.2 ± 16.2	$1.962 \times 10^8 \pm 1.08 \times 10^7$	0.9914	0.99793 ±0.00086
A1 After Drop	538.7 ±7.6	$3.196 \times 10^8 \pm 1.8 \times 10^6$	0.9965	0.97890 ±0.00039
A1 Before Ejection	537.2 ±15.6	$4.242 \times 10^8 \pm 4.7 \times 10^6$	0.9869	0.97898 ±0.00079
A1 After Ejection	185.1 ± 13.9	$5.22 \times 10^7 \pm 2.05 \times 10^7$	0.9926	0.99720 ±0.00074

Fig. 6.29. SFM curve fits before and after Transient Rod drop and ejection.

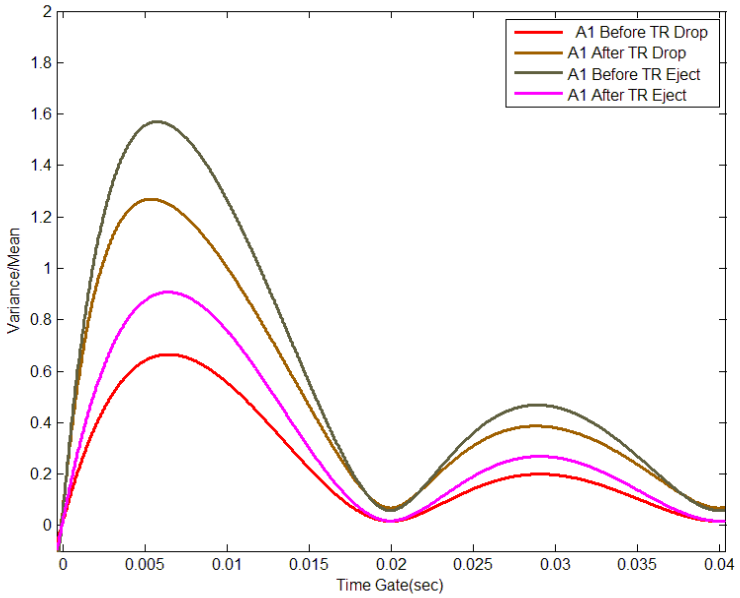

The SFM Alpha estimates with the TR withdrawn agreed with the benchmark α for UT-RACE with an error of less than 20%. The measured α with the TR down had an error of 6.5% from the value of 505.45 s^{-1} that was derived using measured TR worth.

The TR post-drop data was in very good agreement with the steady-state pre-ejection α but the post-ejection SFM Alpha had a larger error (17.5%) due to the buildup of delayed neutrons and spatial harmonics immediately following the TR ejection.

6.11 Shim Safety #2 Reactivity Calibrations

To evaluate the sensitivity of the SFM and other ADS reactivity measurement techniques, Shim Safety 2 (SS2) was repositioned by the reactor operator inward by 100 unit increments while the linac was operated at a frequency of 50 Hz. After waiting for the delayed neutrons to reach equilibrium at each holding position, a one to ten s data set was acquired with 20 μs time bins. Additional data sets were taken at each rod position that included individual low frequency or single neutron pulse data acquisition to evaluate whether a neutron detector operating in current mode could provide sufficient data for accurate reactivity determination. As discussed in Chapter 4, the control rod was calibrated in a critical configuration to find the total measured rod worth of $1.27 after loading an additional nine elements. The variance to mean plots for all control rod data sets is shown in Figure 6.30.

Fig. 6.30. SFM curve fits for SS #2 at various rod heights.

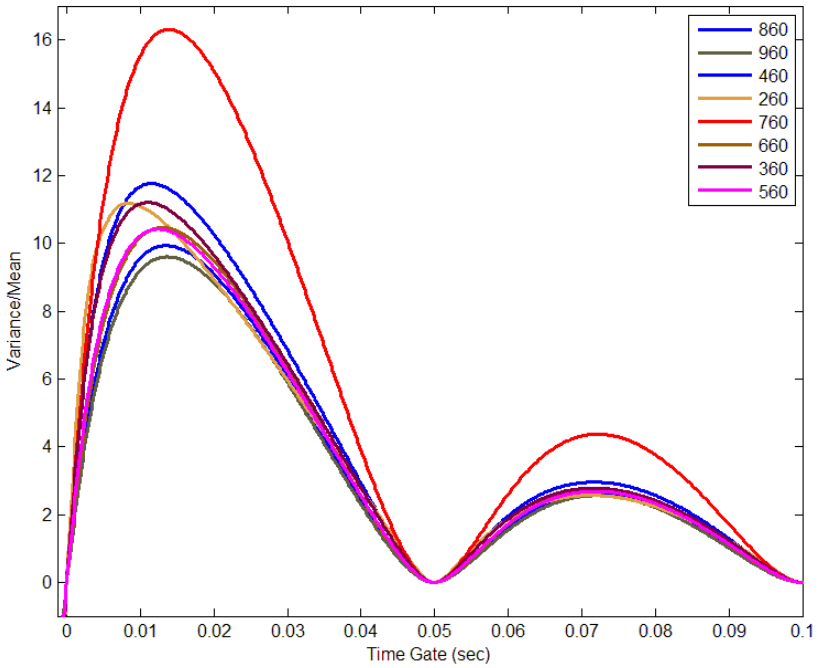

The variance to mean curve for SS2 at 760 units in Figure 6.30 stands out unexpectedly with a significantly higher magnitude peak value than the curve fits for other SS2 positions. The reason for this anomalous curve was investigated by comparing the similar sized data set for SS2 at 760 and 560 units in Figure 6.31. The data for both curves have noticeably more variability as the time gates get larger but this is due to the total data acquisition time of 1.35 s limiting the number of populated time gates.

Fig. 6.31. Raw variance to mean data from SS2 at 760 and 560 units.

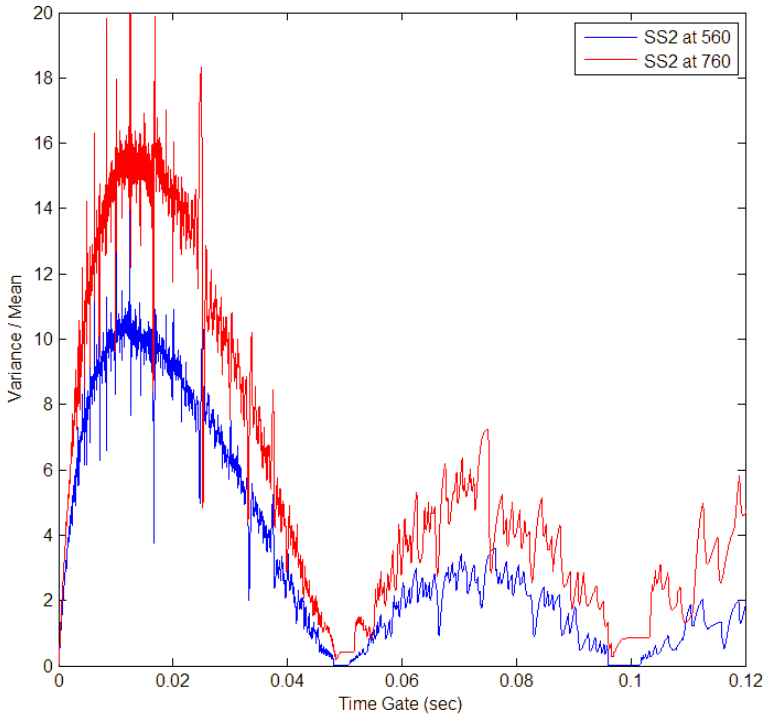

The cause of the large variance in this particular case was a change in the linac beam intensity during the time interval that the data was acquired. Figure 6.32 and Figure 6.33 compare the two data sets processed in Figure 6.31 above. The intensity of the linac pulses for the data taken with the SS2 at 760 changes from approximately 0.05 to 0.07 μA over the eighteen individual pulses in the data set. This intensity variation may have been caused by the linac operator or from systemic periodic beam intensity changes but demonstrates the sensitivity of the SFM to minor source fluctuations. The results of the SFM reactivity measurements for various SS2 heights are given in Table 6.11.

Fig. 6.32. Linac 20 Hz SS2 at 760 units with change in beam intensity.

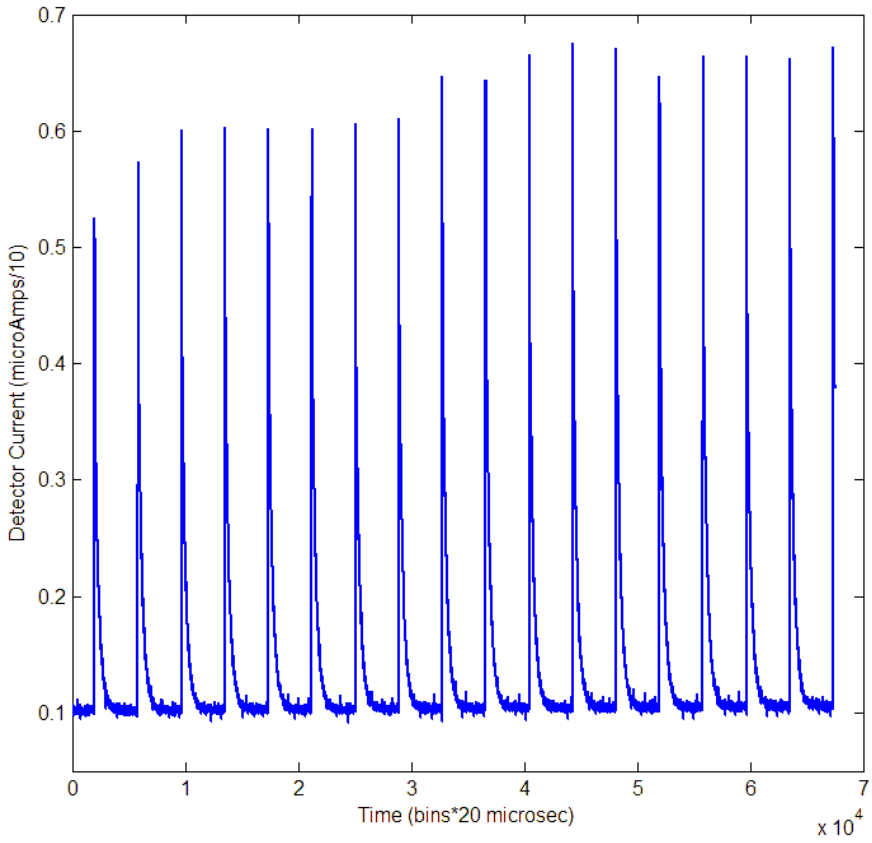

Fig. 6.33. SS2 at 560 units and linac operating at 20 Hz.

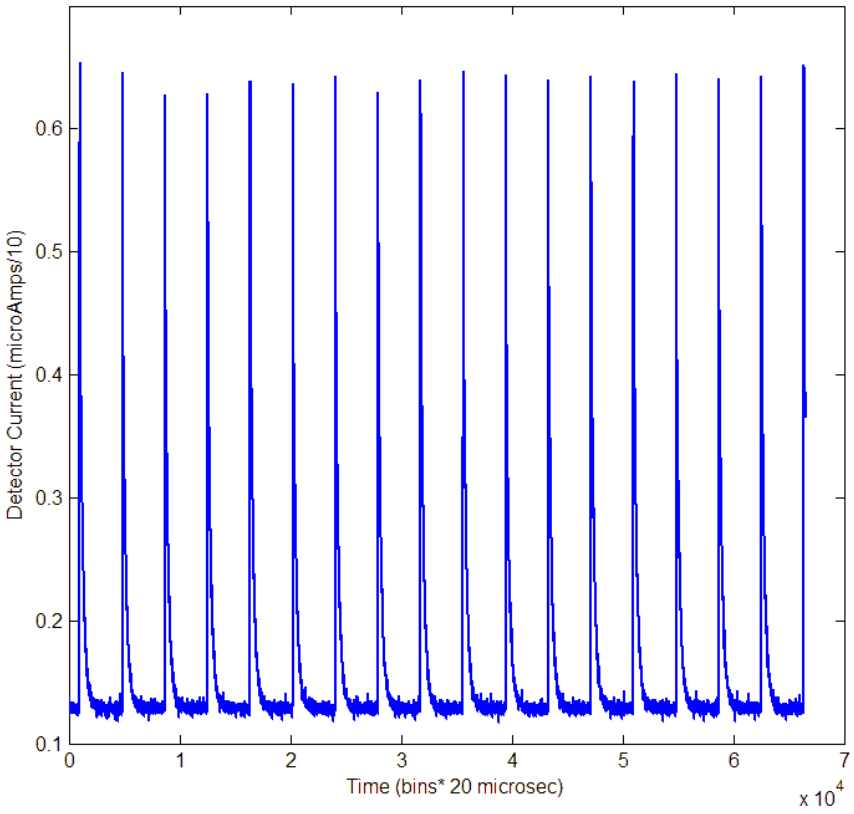

Table 6.11. SFM subcritical measurements for changes in SS2 height.

Shim Safety 2 Height	α	Source Term	R^2 Value
960	204.8 ± 2.6	$1.005x10^9 \pm 4x10^6$	0.9886
860	215.1 ± 1.6	$1.056\ x10^9 \pm 3x10^6$	0.9959
760	194.5 ± 5.4	$1.683\ x10^9 \pm 1.3\ x10^7$	0.9369
660	242.4 ± 2.9	$1.16\ x10^9 \pm 6x10^6$	0.9878
560	275.5 ± 3.1	$1.225\ x10^9 \pm 7x10^6$	0.9890
460	338.7 ± 2.5	$1.538x10^9 \pm$ 7x106	0.9947
360	376.0 ± 4.3	$1.556\ x10^9 \pm 1.2x10^7$	0.9866
260	404.7 ± 2.9	$1.589\ x10^9 \pm 8x10^6$	0.9951

Single linac pulses were also used to evaluate the subcritical level and control rod worth as another method of acquiring operational reactivity data. The operation of the fission chambers in current mode were not subject to dead-time and other counting issues and could potentially enable an ADSS operator to determine the core subcriticality with good precision with a single linac pulse rather than data acquisition over many minutes or hours using pulse counting electronics.

The G5 detector data from all single pulse evaluations for different SS2 heights are overlaid and plotted in Figure 6.34 to show that the minor difference in the logarithmically transformed slopes for SS2 heights between 660 and 960 units. This area correlates to the portion of the SS2 integral worth curve where the worth only changes by $0.10 over this range. Single pulse α-decay measurements are compared to SS2 calibrated critical rod worths in Table 6.12. Differential and Integral rod worth curves for the SFM and PNS methods are compared to the calibrated SS2 rod curves in Figures 6.35 and 6.36. Data from measurements taken at 760 unit height were treated as outliers and not used in SFM rod worth determination.

Fig. 6.34. Detail of single linac pulse detector response (G5) used for curve fits.

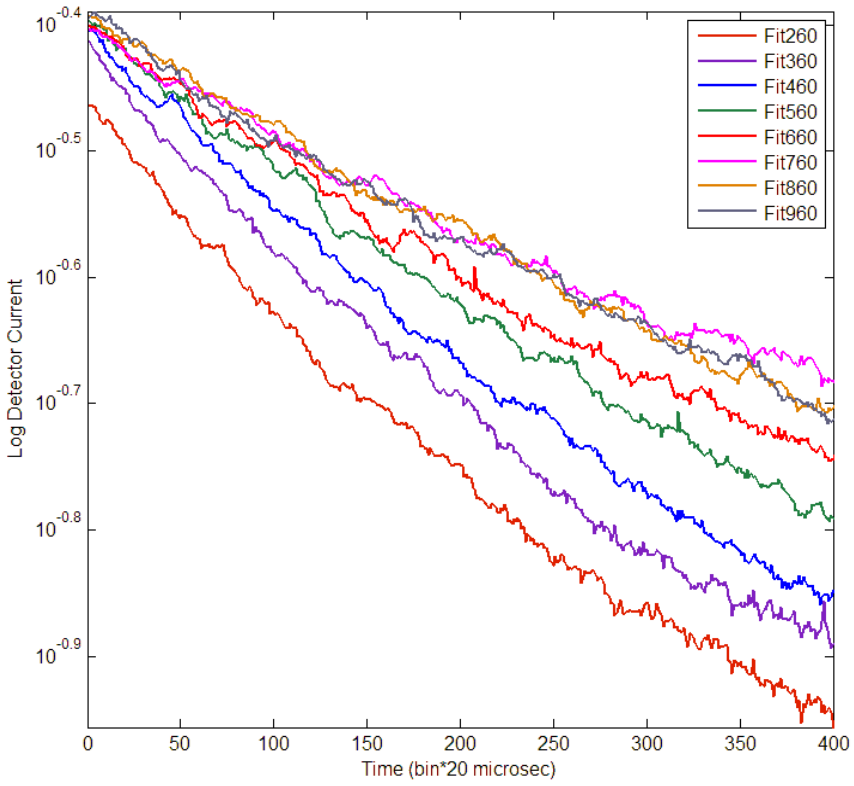

Table 6.12. α from single pulse fits compared to calibrated values for SS2.

Shim Safety 2 Height	**α from Single Pulse**	**α from Calibrated Rod**
960	174.1 ± 3.5	155.99
860	164.3 ± 2.5	158.03
760	149.3 ± 2.9	165.77
660	178.1 ± 3.0	179.90
560	204.3 ± 3.9	200.94
460	237.6 ± 3.1	226.50
360	265.3 ±3.7	253.86
260	289.9 ± 3.4	279.46

Using the SFM and single pulse exponential fits, a differential rod worth curve was derived (Figure 6.35) and compared to the calibrated rod worth curve obtained by loading the UT-RACE core with an additional nine elements and performing a standard critical rod calibration.

Fig. 6.35. SS2 differential rod worth curve by three methods.

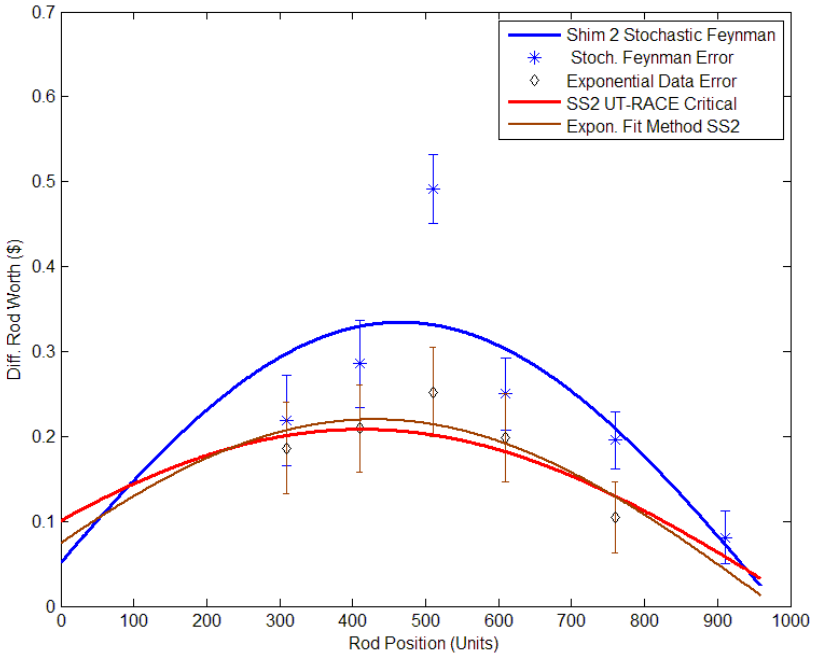

The differential rod worth curve was then used to generate an integral rod worth curve with MATLAB to arrive at total measured rod worth (Figure 6.36).

Fig. 6.36. SS2 integral rod worth by three methods.

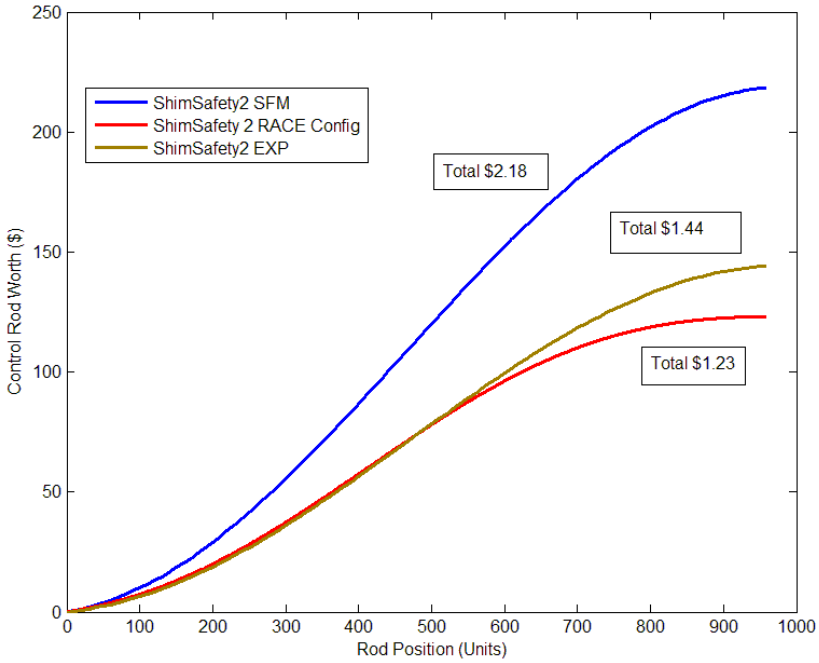

The differential rod worth (DRW) curve using SFM overestimates the core reactivity but this was expected as the only useful fission chamber data was obtained from the detector in G5 which was influenced by the linac produced neutrons and diffusion of thermal neutrons from the graphite reflector from previous linac pulses. However, an examination of the DRW curve (Figure 6.35) shows the strong influence the rod worth measurement from 560 to 460 units had on the overall differential rod worth curve. The SFM curves for SS2 height 560 and 660 are very similar (Figure 6.37), resulting in nearly equivalent α values (Table 6.11) so it is probable that the α parameter

found at 560 units could be an outlier value due to linac intensity drift but it was left in the data set for comparison and discussion purposes.

Fig. 6.37. SS2 variance to mean SFM curve fits showing detail and curve separation.

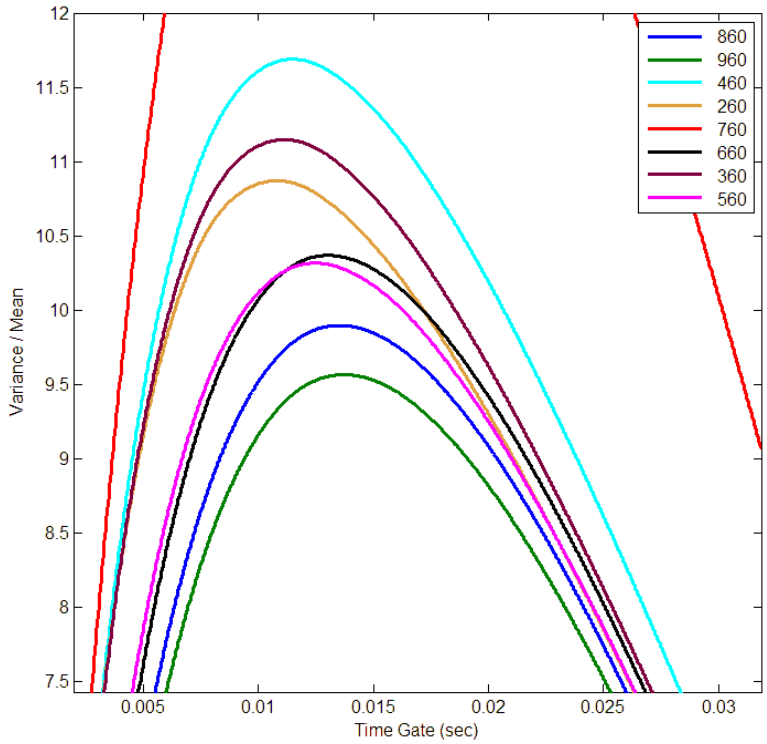

The results of the SS2 rod calibration show that the exponential fitting method was more accurate but that SFM has potential to provide good accuracy with stable linac intensity, optimum detector locations and larger data sets.

Chapter 7
Summary and Conclusion

Previous ADSS projects were performed on critical assemblies with little or no fuel depletion or on small research reactors utilizing a low output neutron generator. This project was intended (within a limited experimental budget) to push the limits of available intense neutron sources and drive a high-burn fuel assembly in order to demonstrate the feasibility of such a prototype ADSS. The UT-RACE experiments demonstrated the operational characteristics of thermal reactor systems but, unfortunately due to the relatively low linac power and inefficiencies of the neutron source, the TRIGA reactor never reached the temperature reactivity feedback regime[169]. The project did serve to help bridge the knowledge gap between low and high power ADSS and provide preliminary information to support a future repeat of the project with a higher power linac or a new target design.

One of the original goals of the UT-RACE project was to install and operate an electron linear accelerator adjacent to the TRIGA reactor as a demonstration ADSS but overall the successful project provided much more. Many of the operational problems found and corrected during the project are likely to be encountered in larger proton-driven ADSS but also in any project utilizing an electron linac to produce neutrons (*e.g.* for cross-section measurements)[170,171]. The gamma-flash instrumentation issues and the saturation of the pulse counting electronics which had previously prevented the acquisition of useful data was resolved by discarding previous techniques and operating the neutron detectors in current mode. Coupling low-cost picoammeters and off-the-shelf data acquisition systems provided imperfect but quite adequate experiment monitoring and data logging that revealed linac operational characteristics which had a significant effect on later data analysis.

The asymmetric injection of the neutrons from the tangential linac beam resulted in a high neutron leakage and low subcritical multiplication of the TRIGA core but an internal source installation and operation was cost prohibitative. Asymmetric neutron

sources may reduce the engineering complexity of installing a high power accelerator target within the middle of a future ADSS core assembly but the neutron losses may prove to be unacceptable. The fixed design of the UT-RACE core and reflector assembly increased the neutron losses because the linac target was effectively surrounded with the graphite reflector material but it was unlikely the overall linac system inefficiencies would have resulted in the ADSS reaching the point of adding heat even if the source had been placed in the central core region.

Electron beam characterization and beam optics within limited space and long drift distances requires further research. The four meter distance from the exit of the accelerator to the target without refocusing was essential to the success of the project but resulted in an unexpected loss of 50% of the beam current. Operation of the linac without information on average beam energy and an unknown current versus energy relationship contributed to the lower than expected neutron production within the target. The stability of the linac and changes in neutron production from day to day for identical linac settings was a problem identified early in the UT-RACE experiments but was never resolved. Several possible solutions, such as retuning the accelerator, were proposed late in the project but there was insufficient available experiment time remaining to make the corrections and evaluate the results.

Traditional reactivity monitoring methods on subcritical systems utilized low pulse rate neutron sources or noise methods with long acquisition times. These methods work well in a laboratory environment but cannot be reasonably applied to an operational ADSS because the ADSS safety and burn efficiency both require the system to operate in a limited subcriticality band and thus continuous reactivity monitoring must be achieved. A relatively new method of reactivity monitoring, the Stochastic Feynman Method (SFM), combining the techniques of statistical noise analysis and pulsed neutron interrogation was investigated and shows promise as a near real-time reactivity monitor for an ADSS. It was shown that the SFM will provide good subcritical reactivity measurement results but it is sensitive to detector location and linac beam stability. SFM results were improved by using neutron detectors on the opposite side of the reactor fuel

from the linac target to eliminate interference from the neutrons produced directly from the target and thermalized neutrons leaking into the reactor from the graphite reflector. Reactivity measurements could be obtained using the SFM technique in less than five minutes which represents a substantial improvement in previous techniques for subcriticality monitoring. It was also shown in this dissertation that very good reactivity measurements may be obtained using neutron detectors in current mode from a single pulse of neutrons. This method still requires the user perform a curve fit to extract the prompt decay constant from the data but substantially improves the time normally required to obtain the curve from pulse counting electronics and multiscaling systems.

The small size of the TRIGA core in the UT-RACE configuration enabled all detectors to respond within the initial pulse width permitting direct time correlation and separation of linac and fission sources but there were insufficient neutron detector systems to exploit this and evaluate several locations simultaneously. With a central accelerator target as proposed for future ADSS there may be insufficient fissile material between the neutron detectors and the source to avoid detection of neutrons directly from the target and this will cause the overestimation of subcritical level as was seen from neutron detectors in G5 and E6.

Any sensor or detector monitoring a parameter requires a determination of how close the measurement is to the true value, but if this error is constant (systemic) the instrument or indication may be manually corrected to represent the actual value of the parameter. The SFM technique could be calibrated to correct for spatial errors in the reactivity measurements but the stability of the accelerator source was shown to have a large effect on the SFM results and this would require an additional real-time correction. The SFM accuracy went down considerably as the linac frequency approached the system Alpha but these frequencies (~200Hz) still provided data from which a variance-to-mean curve and SFM fit produced a value for the system Alpha. The limited amount of data available at higher frequencies and from various detector locations prevented an evaluation of the ADSS response and SFM monitoring at high frequencies but additional

research could determine if the SFM technique were a viable real-time subcriticality monitor.

As was discussed previously, the goal of the UT-RACE project was to support international HLW transmutation research by installing an electron linac configured to produce neutrons via bremsstrahlung induced reactions in a tungsten-copper target and drive a subcritical TRIGA to relatively high power as an intermediate step to develop larger and higher power ADSS. At full power operation the IAC linac raised the neutron level of the core to approximately 100 W equivalent power or an increase of five orders of magnitude from a shutdown TRIGA reactor making the UT-RACE system the highest power ADSS facility to date. The overall project was limited by the available instrumentation and the amount of time allowed for exclusive use of the TRIGA reactor but sufficient time was available to develop and use several novel instrumentation and subcritical monitoring techniques that move the ADSS experimental prototype closer to a full-scale operational accelerator driven transmutation system for burning high level radioactive waste.

Appendices

A.1 MATLAB Scripts

FAlpha.m

```
%FAlpha.m:  a MATLAB script that sequentially processes large list-form
%  data sets from the UT-RACE experiment.  Creates large matrix
"TimeGate"
%  that is then processed by MATLAB script "AVERAGE.m" called from
within
%  FAlpha.
q=1;
n=1;
k=1;

[d,z]=size(G5TR_Up_afterdrop);
TimeGate=zeros(92500,4000);
d=92500;
z=4000;

    %if q==1  ;  %This populates first column
        for p=1:d;
            TimeGate(p,q)=G5TR_Up_afterdrop((p),1);

        end
    p=1;
   q=q+1;
    while (q>1)&&(q<=z); %This sequentially fills matrix

        %for p=1:(15000); %Counts down the rows to fill new line

            for n=1:q:(d-1) %Skips the groups by column number
                B=0;
                %k=n;
                 for k=n:(n+(q-1)); %Loops through the gate to sum
                    if k<=d
                    B= TimeGate(k,1)+ B;
                    end
                 end

                TimeGate(p,q)= B;
                p=p+1;
            end

            q=q+1 ;
            p=1;
    end

AVERAGE;
```

AVERAGE.m

```
%script to find Stochastic Feynman-Alpha.  May be used for stationary
%Feynman-Alpha processing but Variance/Mean must have 1.0 subtracted
%
k=1;
V=0;
M=0;
n=1;
[d,z]=size(TimeGate);

for q=1:z
    for p=1:d/q;

        Hold(p,1)=TimeGate(p,q);

    end
        M(n,1)=mean(Hold);
        V(n,1)=var(Hold);
        n=n+1;
        clear Hold;
end

 q=1;
 p=1;
 for p=1:z
    TR_up_afterdrop_Fey(p,1)=(V(p,1)/M(p,1));
 end
   for v=1:z;
        Time4K(v,1)=v*.00002;  %sets time base of interval based on
data
                               % time bins
   end
```

A.2 MONTEBURNS Input Deck

```
NETL TRIGA Core Burn Using MCNP5 and ORIGEN22
PC        ! Type of Operating System
12        ! Number of MCNP materials to burn
20        !
21        !
22        !
23         !
24        !
25       !
26        !
27        !
28        !
29        !
30         !
31        ! MCNP material number #31 (will burn all cells with this mat)
1184.208   !
1184.208    !
1973.680    !
1973.680    !
3157.888    !Material #1 volume (cc), input 0 to use mcnp value (if exists)
3157.888    !
4736.832    !
4736.832    !
5921.04     !
5921.04     !
592.104     !
592.104     ! Material #1 volume (cc), input 0 to use mcnp value (if exists)
1.0       ! Power in MWt (for the entire system modeled in mcnp deck)
-222.     ! Recov. energy/fis (MeV);  times 1.11 for gamma and delayed neutrons
260       ! Total number of days burned (used if no feed)
4         ! Number of outer burn steps
40        ! Number of internal burn steps (multiple of 10)
1         ! Number of predictor steps (+1 on first step), 1 usually sufficient
0         ! Step number to restart after (0=beginning)
PWRU     ! number of default origen2 lib - next line is origen2 lib location
G:\ORIGEN22\LIBS
0.000000       !fractional importance (track isos with abs,fis,atom,mass fraction)
0         ! Intermediate keff calc. 0) No 1) Yes
13         ! Number of automatic tally isotopes, followed by list.
45103.00c
54135.00c
54131.00c
60143.00c
61147.00c
62149.00c
62151.00c
92235.00c
92238.00c
94239.00c
94240.00c
94241.00c
94242.00c
13
```

45103.00c
54135.00c
54131.00c
60143.00c
61147.00c
62149.00c
62151.00c
92235.00c
92238.00c
94239.00c
94240.00c
94241.00c
94242.00c
13
45103.00c
54135.00c
54131.00c
60143.00c
61147.00c
62149.00c
62151.00c
92235.00c
92238.00c
94239.00c
94240.00c
94241.00c
94242.00c
13
45103.00c
54135.00c
54131.00c
60143.00c
61147.00c
62149.00c
62151.00c
92235.00c
92238.00c
94239.00c
94240.00c
94241.00c
94242.00c
13
45103.00c
54135.00c
54131.00c
60143.00c
61147.00c
62149.00c
62151.00c
92235.00c
92238.00c
94239.00c
94240.00c

94241.00c
94242.00c
13
45103.00c
54135.00c
54131.00c
60143.00c
61147.00c
62149.00c
62151.00c
92235.00c
92238.00c
94239.00c
94240.00c
94241.00c
94242.00c
13
45103.00c
54135.00c
54131.00c
60143.00c
61147.00c
62149.00c
62151.00c
92235.00c
92238.00c
94239.00c
94240.00c
94241.00c
94242.00c
13
45103.00c
54135.00c
54131.00c
60143.00c
61147.00c
62149.00c
62151.00c
92235.00c
92238.00c
94239.00c
94240.00c
94241.00c
94242.00c
13
45103.00c
54135.00c
54131.00c
60143.00c
61147.00c
62149.00c
62151.00c
92235.00c

92238.00c
94239.00c
94240.00c
94241.00c
94242.00c
13
45103.00c
54135.00c
54131.00c
60143.00c
61147.00c
62149.00c
62151.00c
92235.00c
92238.00c
94239.00c
94240.00c
94241.00c
94242.00c
13
45103.00c
54135.00c
54131.00c
60143.00c
61147.00c
62149.00c
62151.00c
92235.00c
92238.00c
94239.00c
94240.00c
94241.00c
94242.00c
13
45103.00c
54135.00c
54131.00c
60143.00c
61147.00c
62149.00c
62151.00c
92235.00c
92238.00c
94239.00c
94240.00c
94241.00c
94242.00c

A.3 MCNPX Input Deck

```
***** UT RACE -January 2006 *** Case: RACE Core all rods out
c   Monteburns 2.0 and Origen 2.2 created burn concentrations
c  ENDF/B-VII and new photonuclear xs
c    Coordinate origin on core axis at core midplane
c    Experiment tubes, empty beam ports, empty RSR
c
c
c    678901234567890123456789012345678901234567890123456789012345
c    ****0*********0*********0*********0*********0*********0*****
c    Problem geometry cells.
c    ****0*********0*********0*********0*********0*********0*****
c    0         -100  -110  +120                  $Problem region
c              +150  +155                       $Hex core region
c    ****0*********0*********0*********0*********0*********0*****
c    Cells   0 - 199 Basic TRIGA reactor core components
c    ****0*********0*********0*********0*********0*********0*****
c    Reactor core configuration
c    Cells 0 - 9 core grid, plates and holes
  9999  1  -1.0   -202  +206                          $Core region
              -231  +232  -233  +234  -235  +236
              -241  +242  -243  +244  -245  +246  FILL=1  IMP:N=1
  1  2  -2.7   -206  +207                          $Lower gridplate
              -211  +212  -213  +214  -215  +216
              -221  +222  -223  +224  -225  +226   FILL=3   IMP:N=1
c                           $+150  +155
  2  2  -2.7   -203  -201  +202       FILL=5     IMP:N=1       $Upper
gridplate
c
c    ****0*********0*********0*********0*********0*********0*****
c    Define configuration U = 1 to 5
  3  1  -1.0   -101  +102  -103                   $Core lattice
              +104  -105  +106        U=1  LAT=2 IMP:N=1
         FILL=-7:7 -7:7 0:0
       1 1 1 1 1 1 1 1 1 1 1 1 1 1 1                     $D17 E23
       1 1 1 1 1 1 1   1  34  30  30 30  34   1   1       $Row 1 G20-G16
       1 1 1 1 1 1  51 34 34  33  32  32  34  11  1
       1 1 1 1 1  13 33   33  33  33  33  33  34  12 1  $Row 3
       1 1 1 1  51  32 33  32 19(9) 32  32  33  33  51   1  $D5
       1 1 1  32  32  33 32  31   31   31   32  33  32  51    1
       1 1  51  32  33  32   31  30  30  31  32  33  33 51   1
       1   1  34  33 32 19(9) 30  10  30 7(9)  32 33  34   1   1
         1 06  51  33  32   31  30  30   31  32  33  51  6   1 1
           1  51  51  33  32  31   31  31  32  33  51 6 1 1 1
             1  51  51  33 32 19(9) 32  32 33  51  51    1 1 1 1
               1  51  51  14  33  33  15  51 51  06  1 1 1 1 1
                 1  6  51  51  51  51  51  51 51   1 1 1 1 1 1
                   1   1  51  51  51  51  51  1  1 1 1 1 1 1 1
                              1 1 1 1 1 1 1 1 1 1 1 1 1 1
c
c    ****0*********0*********0*********0*********0*********0*****
  4  1  -1.0   -205     IMP:N=1                 U=2
  5  2  -2.7    #4      IMP:N=1                 U=2
c    ****0*********0*********0*********0*********0*********0*****
  6  2  -2.7   -101  +102  -103                   $Cell lattice
```

```
              +104  -105  +106        U=3  LAT=2 IMP:N=1
         FILL=-7:7 -7:7 0:0
       3 3 3 3 3 3 3 3 3 3 3 3 3 3 3
       3 3 3 3 3 3 3   3  02  02  02  02  02   3   3
       3 3 3 3 3 3  02   2   2   2   2   2   2  02   3
       3 3 3 3 3  02   2   2   2   2   2   2   2  02   3
       3 3 3 3  02   2   2  2 19(9) 2  2   2   2  02   3
       3 3 3  02   2   2   2   2   2   2   2   2   2    2    3
       3 3  02   2   2   2   2   2   2   2   2   2   2  02   3
       3   3   2   2   2 19(9)   2  10  2  7(9) 2  2  2   3  3
         3  02   2   2   2   2   2   2   2   2   2   2  02   3 3
           3  02   2   2   2   2   2   2   2   2   2  02   3 3 3
             3  02   2   2 02 19(9) 02  02  2  2   2  02 3 3 3
               3  02   2   2   2   2   2   2   2  02   3 3 3 3 3$
                 3  02   2   2   2   2   2   2  02   3 3 3 3 3 3$
                   3   3  02  02  02  02  02   3   3 3 3 3 3 3 3$
                                 3 3 3 3 3 3 3 3 3 3 3 3 3 3 3$
c
c    ****0*********0*********0*********0*********0*********0*****
  7  1  -1.0   -200    IMP:N=1                  U=4
  8  2  -2.7    #7      IMP:N=1                  U=4
c    ****0*********0*********0*********0*********0*********0*****
  9  2  -2.7   -101  +102  -103                   $Cell lattice
              +104  -105  +106        U=5  LAT=2  IMP:N=1
         FILL=-7:7 -7:7 0:0
       5 5 5 5 5 5 5 5 5 5 5 5 5 5 5
       5 5 5 5 5 5 5   5  04  04  04  04  04   5   5
       5 5 5 5 5 5  04   4   4   4   4   4   4  04   5
       5 5 5 5 5  04   4   4   4   4   4   4   4  04   5
       5 5 5 5  04   4   4  4 19(9) 4  4   4   4   4  04
       5 5 5  04   4   4   4   4   4   4   4   4   4  04   5
       5 5  04   4   4   4   4   4   4   4   4   4   4  04   5
       5   5   4   4   4 19(9)  4  10  4  7(9)  4   4   4   5   5
         5  04   4   4   4   4   4   4   4   4   4   4  04   5 5
           5  04   4   4   4   4   4   4   4   4   4   4  04   5 5 5
             5  04   4   4  4 19(9)  4  4   4   4  04   5 5 5 5
               5  04   4   4   4   4   4   4   4  04   5 5 5 5 5$
                 5  04   4   4   4   4   4   4  04   5 5 5 5 5 5$
                   5   5  04  04  04  04  04   5   5 5 5 5 5 5 5$
                                 5 5 5 5 5 5 5 5 5 5 5 5 5 5 5$
c
c    ****0*********0*********0*********0*********0*********0*****
c
c    Reactor core structure
c    Cells 10 - 29 reflector inner core shroud
 10  2  -2.7   -300  +302  -303  +202  IMP:N=1            $Alignment
ring
 11  2  -2.7   -300  -202  +352                   $Alignment ring
              (+231: -232: +241: -242:
               +233: -234: +243: -244:
               +235: -236: +245: -246) IMP:N=1
 12  2  -2.7   +305  -306  +307                   $Shroud loadring
              (-311  +312  -321  +322
               -313  +314  -323  +324
```

```
               -315  +316  -325  +326) IMP:N=1
 13  2  -2.7   -301  -352  +304                  $Alignment ring
              (+331: -332: +341: -342:
               +333: -334: +343: -344:
               +335: -336: +345: -346) IMP:N=1
 14  2  -2.7   +231  -331  -233  +236            $Reflector plate
               -352  +306                IMP:N=1
 15  2  -2.7   -232  +332  +234  -235            $Reflector plate
               -352  +306                IMP:N=1
 16  2  -2.7    241  -341  -343  -345            $Reflector, bp3
               -352  +306  +363         IMP:N=1
 17  2  -2.7   -242  +342  +344  +346            $Reflector plate
               -352  +306                IMP:N=1
 18  2  -2.7   +233  -333  -331  -343            $Reflector plate
               -352  +306                IMP:N=1
 19  2  -2.7   -234  +334  +332  +344            $Reflector plate
               -352  +306                IMP:N=1
 20  2  -2.7   +235  -335  +332  -345            $Reflector plate
               -352  +306                IMP:N=1
 21  2  -2.7   -236  +336  -331  +346            $Reflector plate
               -352  +306              IMP:N=1
 22  2  -2.7   +243  -343  -241  -233            $Reflector plate
               -352  +306         IMP:N=1
 23  2  -2.7   -244  +344  +242  +234            $Reflector plate
               -352  +306              IMP:N=1
 24  2  -2.7   +245  -345  -241  -235            $Reflector plate
               -352  +306             IMP:N=1
 25  2  -2.7   -246  +346  +242  +236            $Reflector plate
               -352  +306                IMP:N=1
 26  2  -2.7   +241  -363 364 -360  IMP:N=1            $Reflector BP3
 27  2  -2.7   -361  +362  -100         IMP:N=1            $Reflector
BP1&5
c
c    ****0*********0*********0*********0*********0*********0*****
c    Cells 30 - 39 reflector outer shroud structure
 30  2  -2.7   -355  +361                        $Reflector cylin
               -350  +351  -352  +353 IMP:N=1
 31  2  -2.7   +355  +363                        $Reflector cylin
               -350  +351  -352  +353  IMP:N=1
 32  2  -2.7   -370  +371  -372  +373  IMP:N=1           $Cylinder,
top
 33  2  -2.7   -374  -375  +376                  $Cylinder, bot
              (+331: -332: +341: -342:
               +333: -334: +343: -344:
               +335: -336: +345: -346)  IMP:N=1
 34  2  -2.7   -370  +374  -375  +377   IMP:N=1          $Rflctr edge
rng
 35  2  -2.7   -352  -371  +380  +381   IMP:N=1          $Rflctor
rsrunit
 36  2  -2.7   -380  +300  +381  -382   IMP:N=1          $Rflctor
rsrunit
 37  2  -2.7   -352  +301  -300  +381   IMP:N=1          $Rflctor
rsrunit
```

```
 38  1  -1.0   +370  -351  -377  +120   IMP:N=1           $Edge ring
error
c    ****0*********0*********0*********0*********0*********0*****
c    Cells 40 - 49 reflector graphite moderator
 40  4  -1.60    -400  +401  -402  +403  IMP:N=1          $Rflctr
graphite
 41  4  -1.60    -400  -403  +375  -404  +361
                (+411: -412: +421: -422:
                 +413: -414: +423: -424:
                 +415: -416: +425: -426)
               #(-361  +405)              IMP:N=1         $Graphite,
bp1&5
 42  4  -1.60   (-400  -403  +375  +404  +363
                (+411: -412: +421: -422:
                 +413: -414: +423: -424:
                 +415: -416: +425: -426))
               #(-406 +408) #(-407 +409)  IMP:N=1         $Graphite,
bp3
 43  8 -1.15e-3 (+371 -351 -373 +403) #40   IMP:N=1  $graphite void
 44  8 -1.15e-3 (-351  -403  +375  -404  +361
                (+331: -332: +341: -342:
                 +333: -334: +343: -344:
                 +335: -336: +345: -346)) #41 IMP:N=1     $graphite
void
 45  8 -1.15e-3 (-351  -403  +375  +404  +363
                (+331: -332: +341: -342:
                 +333: -334: +343: -344:
                 +335: -336: +345: -346)) #42 IMP:N=1      $graphite
void
 46  8 -1.15e-3  -304  +403  -301
                (+331: -332: +341: -342:
                 +333: -334: +343: -344:
                 +335: -336: +345: -346) IMP:N=1          $graphite
void
 47  8 -1.15e-3  +301  -371  +403  -381  IMP:N=1          $graphite
void
c    ****0*********0*********0*********0*********0*********0*****
c    Cells 50 - 59 pool coolant water
c    exterior core water, above and below grid plates
 50  1  -1.0   -203  +201  -110        IMP:N=1           $Upper
gridplate
 51  1  -1.0   +203  -302  +202  -110  IMP:N=1           $Upper
gridplate
 52  1  -1.0   +302  -300  +303  -110  IMP:N=1           $Upper
gridplate
 53  1  -1.0   -305  -306  +307        IMP:N=1           $Lower
gridplate
 54  1  -1.0   -307  +120                                $Lower gridplate
              (-311  +312  -321  +322
               -313  +314  -323  +324
               -315  +316  -325  +326)   IMP:N=1
 55  1  -1.0   -207  +306                        $Lower gridplate
              (-231  +232  -241  +242
               -233  +234  -243  +244
```

```
               -235  +236  -245  +246)   IMP:N=1
 56  1  -1.0   -206  +207                      $Lower gridplate
              (+211: -212: +221: -222:
               +213: -214: +223: -224:
               +215: -216: +225: -226)
              (-231  +232  -241  +242
               -233  +234  -243  +244
               -235  +236  -245  +246)   IMP:N=1
 57  1  -1.0   -351  +371  +372  -110    IMP:N=1          $Upper
reflector
 58  1  -1.0   -374  -376  +120              $Lower reflector
              (+311: -312: +321: -322:
               +313: -314: +323: -324:
               +315: -316: +325: -326)    IMP:N=1
 59  1  -1.0   +306  -376                      $Lower reflector
              (+331: -332: +341: -342:
               +333: -334: +343: -344:
               +335: -336: +345: -346)
              (-311  +312  -321  +322
               -313  +314  -323  +324
               -315  +316  -325  +326)     IMP:N=1
c    ****0*********0*********0*********0*********0*********0*********0*****
C    CELLS 60 - 69 POOL COOLANT WATER
C    EXTERIOR CORE WATER, AROUND REACTOR CORE ASSEMBLY
c
 60  1  -1.0   +350  -355  +361
              (-100  -110  +120) $#1770 #1771 #1772 #1773 #1774 #1775
                IMP:N=1                $ #950 #951     $Beam ports 1&5
 61  1  -1.0   +350  +355  +363
              (-100  -110  +120) $#1770 #1771 #1772 #1773 #1774 #1775 $
            #(-406 +408) #(-407 +409)    IMP:N=1           $Beam ports
2&4
 62  1  -1.0   -363  +364  +360  -350     IMP:N=1         $rflctr BP3
 63  1  -1.0   -350  +351  +352  -110     IMP:N=1         $rflctr
cylinder
 64  1  -1.0   -350  +351  -353  +120     IMP:N=1         $rflctr
cylinder
 65  1  -1.0   -370  +374  -377  +120     IMP:N=1         $rflctr
edgering
 66  1  -1.0   +300  -371  +303  -110     IMP:N=1        $RSR removal
 67  2  -2.7   +370  -351  -375  +377     IMP:N=1        $edge ring
error
 68  2  -2.7   -351  +370  -372  +373     IMP:N=1        $edge ring
error
c    ****0*********0*********0*********0*********0*********0*********0*****
c    Cells 70 - 79  beam port structure
c    bp 2 & 4 structure
c 70   2  -2.7    +241 +364 -363 -360   IMP:N=1          $Al Reflect
around BP3
 71  2  -2.7    (-406  +430)
                +350  +355  -100  IMP:N=1         $Reflector BP2
 72  2  -2.7    (-407  +440)
                +350  +355  -100  IMP:N=1        $Reflector BP4
c    beam port 3 structure
```

```
 73  2  -2.7     +461 -462 -464 +463 +241    IMP:N=1         $Reflector
BP3
 74  2  -2.7     -463  +464  +461  -100  IMP:N=1          $Reflector
BP3
 75  2  -2.7     +241  -364  -461        IMP:N=1          $Reflector
BP3
 76  1  -1.0     +463  -364  +461  -100  IMP:N=1         $Reflector BP3
 77  1  -1.0    360 364 -363 -100        IMP:N=1         $water outside
BP3
c    beam port 1, 3, 5 cavity
c 78
 79  2 -2.7  (-462 -464 461)         IMP:N=1          $Reflector BP3
 80  8 -1.15e-3    -100 -362  #1771 #1772 #1773 #1774 #1775 #1776
                             IMP:N=1          $Reflector BP5
c    Cells 81 - 89 beam port cavity
c    beam ports 1, 2, 3, 4 & 5
c 81  8 -1.15e-3  +451  -362  -100        IMP:N=1          $Reflector
BP1
 82  8 -1.15e-3 (-430  +408) +350  -100  IMP:N=1        $Reflector BP2
 83  8 -1.15e-3    +462 -464  -100        IMP:N=1       $Reflector BP3
 84  8 -1.15e-3 (-440  +409) +350  -100  IMP:N=1       $Reflector BP4
c 85  8 -1.15e-3  -455  -362  -100        IMP:N=1       $Reflector BP5
C    CELLS 90 - 94  RSR UNIT
C     ROTARY SPECIMEN RACK
 90  8 -1.15e-3  +300  -303  +352  -371   IMP:N=1       $RSR unit
 91  8 -1.15e-3  +300  +304  -352  -380   IMP:N=1      $RSR unit
 92  8 -1.15e-3  +300  -304  -380  +382   IMP:N=1      $RSR unit
c    ****0*********0*********0*********0*********0*********0*********0*****
c    Cells 100 - 199 Fill universe for reactor core grid
c                    Basic core components U = 6 to 9
c    ****0*********0*********0*********0*********0*********0*********0*****
c    Cells 100 - 104 graphite reflector elements
c
100  1 -1.0  #101 #102 #103 #104        U=6  IMP:N=1      $coolant
101  4  -1.60  -610                     U=6  IMP:N=1      $graphite
102  2  -2.7   -611 +610                U=6  IMP:N=1      $Al Clad
103  2  -2.7   -612                     U=6  IMP:N=1      $Bottom
Fitting
104  2  -2.7   -613                     U=6  IMP:N=1      $Top Fitting
C    CELLS 110 - 119 REACTOR PULSE CONTROL
C      TRANSIENT CONTROL ROD
 110  1 -1.0  #111 #112 #113 #114
          #115 #116 #117 #118 #119   U=7 IMP:N=1       $coolant
 111  2 -2.7  -520 -521 -523 -524
                -525 -527 +526 +522  U=7 IMP:N=1       $Al Clad
 112  6 -2.52      -522              U=7 IMP:N=1       $poison element
 113  2 -2.7       +522 -523         U=7  IMP:N=1      $clad around
poison
 114  2 -2.7       -525 +526         U=7  IMP:N=1      $Air Void Clad
 115  8  -1.15e-3  -526              U=7  IMP:N=1      $Air Void
 116  2 -2.7       -524              U=7  IMP:N=1      $plug separator
 117  2 -2.7       -520              U=7  IMP:N=1      $Top
 118  2 -2.7       -521              U=7  IMP:N=1      $Plug Top
 119  2 -2.7       -527              U=7  IMP:N=1      $Bottom Plug
```

```
c
c    ****0*********0*********0*********0*********0*********0*********0*****
C    CELLS 120 - 127 STANDARD TRIGA FUEL ELEMENT
120  1   -1.0  #121 #122 #123 #124 #125 #126 #127 #128 U=8  IMP:N=1
$Coolant
121  3   -7.9    -605 +600 +601 +603 +604 U=8  IMP:N=1     $SS Clad
122  4   -1.60   -603               U=8  IMP:N=1     $Graphite,low
123  4   -1.60   -604               U=8  IMP:N=1     $Graphite,up
124  3   -7.9    -606               U=8  IMP:N=1     $Lower Fitting
125  3   -7.9    -607               U=8  IMP:N=1     $Upper Fitting
126  5   -6.05   -600 +602          U=8  IMP:N=1     $Upper Fuel
127  5   -6.05   -601 +602          U=8  IMP:N=1     $Lower Fuel
128  7   -6.49   -602               U=8  IMP:N=1     $Zr Rod
c    ****0*********0*********0*********0*********0*********0*********0*****
C     RING B STANDARD TRIGA FUEL ELEMENT
 1200  1   -1.0  #1210 #1220 #1230 #1240 #1250 #1260 #1270 #1280 U=30
IMP:N=1 $Coolant
 1210  3   -7.9    -605 +600 +601 +603 +604 U=30  IMP:N=1     $SS Clad
 1220  4   -1.60   -603               U=30  IMP:N=1     $Graphite,low
 1230  4   -1.60   -604               U=30  IMP:N=1     $Graphite,up
 1240  3   -7.9    -606               U=30  IMP:N=1     $Lower Fitting
 1250  3   -7.9    -607               U=30  IMP:N=1     $Upper Fitting
 1260  20   -6.05   -600 +602          U=30  IMP:N=1     $Upper Fuel
 1270  21   -6.05   -601 +602          U=30  IMP:N=1     $Lower Fuel
 1280  7   -6.49   -602               U=30  IMP:N=1     $Zr Rod
c    ****0*********0*********0*********0*********0*********0*********0*****
C     RING C STANDARD TRIGA FUEL ELEMENT
 1201  1   -1.0  #1211 #1221 #1231 #1241 #1251 #1261 #1271 #1281 U=31
IMP:N=1 $Coolant
 1211  3   -7.9    -605 +600 +601 +603 +604 U=31  IMP:N=1     $SS Clad
 1221  4   -1.60   -603               U=31  IMP:N=1     $Graphite,low
 1231  4   -1.60   -604               U=31  IMP:N=1     $Graphite,up
 1241  3   -7.9    -606               U=31  IMP:N=1     $Lower Fitting
 1251  3   -7.9    -607               U=31  IMP:N=1     $Upper Fitting
 1261  22   -6.05   -600 +602          U=31  IMP:N=1     $Upper Fuel
 1271  23   -6.05   -601 +602          U=31  IMP:N=1     $Lower Fuel
 1281  7   -6.49   -602               U=31  IMP:N=1     $Zr Rod
c    ****0*********0*********0*********0*********0*********0*********0*****
C     RING D STANDARD TRIGA FUEL ELEMENT
 1202  1   -1.0  #1212 #1222 #1232 #1242 #1252 #1262 #1272 #1282 U=32
IMP:N=1 $Coolant
 1212  3   -7.9    -605 +600 +601 +603 +604 U=32  IMP:N=1     $SS Clad
 1222  4   -1.60   -603               U=32  IMP:N=1     $Graphite,low
 1232  4   -1.60   -604               U=32  IMP:N=1     $Graphite,up
 1242  3   -7.9    -606               U=32  IMP:N=1     $Lower Fitting
 1252  3   -7.9    -607               U=32  IMP:N=1     $Upper Fitting
 1262  24   -6.05   -600 +602          U=32  IMP:N=1     $Upper Fuel
 1272  25   -6.05   -601 +602          U=32  IMP:N=1     $Lower Fuel
 1282  7   -6.49   -602               U=32  IMP:N=1     $Zr Rod
c    ****0*********0*********0*********0*********0*********0*********0*****
C     RING E STANDARD TRIGA FUEL ELEMENT
 1203  1   -1.0  #1213 #1223 #1233 #1243 #1253 #1263 #1273 #1283 U=33
IMP:N=1 $Coolant
 1213  3   -7.9    -605 +600 +601 +603 +604 U=33  IMP:N=1     $SS Clad
```

```
 1223  4   -1.60   -603              U=33  IMP:N=1     $Graphite,low
 1233  4   -1.60   -604              U=33  IMP:N=1     $Graphite,up
 1243  3   -7.9    -606              U=33  IMP:N=1     $Lower Fitting
 1253  3   -7.9    -607              U=33  IMP:N=1     $Upper Fitting
 1263  26   -6.05   -600 +602         U=33  IMP:N=1     $Upper Fuel
 1273  27   -6.05   -601 +602         U=33  IMP:N=1     $Lower Fuel
 1283  7   -6.49   -602              U=33  IMP:N=1     $Zr Rod
c    ****0*********0*********0*********0*********0*********0*****
c    ****0*********0*********0*********0*********0*********0*****
C     RING F STANDARD TRIGA FUEL ELEMENT  0.5 MWD Burn
 1204  1   -1.0  #1214 #1224 #1234 #1244 #1254 #1264 #1274 #1284 U=34
IMP:N=1 $Coolant
 1214  3   -7.9    -605 +600 +601 +603 +604 U=34  IMP:N=1     $SS Clad
 1224  4   -1.60   -603              U=34  IMP:N=1     $Graphite,low
 1234  4   -1.60   -604              U=34  IMP:N=1     $Graphite,up
 1244  3   -7.9    -606              U=34  IMP:N=1     $Lower Fitting
 1254  3   -7.9    -607              U=34  IMP:N=1     $Upper Fitting
 1264  28   -6.05   -600 +602         U=34  IMP:N=1     $Upper Fuel
 1274  29   -6.05   -601 +602         U=34  IMP:N=1     $Lower Fuel
 1284  7   -6.49   -602              U=34  IMP:N=1     $Zr Rod
c    ****0*********0*********0*********0*********0*********0*****
c
c    Cells 130 - 149 fuel follower control rods
c      control rods: reg, shim1 & shim2
c 130  1 -1.0  #131 #132 #133 #134 #135 #136 #139   $138 &137 removed
for testing
c               #140 #141 #142 #143 #144 #145   U=9 IMP:N=1
$element clad
c 131  3 -7.9    -500          U=9 IMP:N=1             $upper end plug
c 132  8 -1.15e-3 -501         U=9 IMP:N=1             $void above
poison
c 133  2 -2.7     -502         U=9 IMP:N=1              $plug/spacer
c 134  3 -7.9     -503         U=9 IMP:N=1             $magneform upper
c 135  6 -2.52   -504          U=9 IMP:N=1               $poison B4C
c 136  3 -7.9    -514 +504      U=9 IMP:N=1               $gap around
poison
c c 137  2 -2.7      -505        U=9 IMP:N=1              $spacer
under poison
c  c 138  8 -1.15e-3   -506       U=9 IMP:N=1        $void top of fuel
c 139  5 -6.05     -507 +509   U=9 IMP:N=1            $upper fuel
follower
c 140  5 -6.05     -508 +509   U=9 IMP:N=1           $lower fuel
follower
c 141  7 -6.49     -509        U=9 IMP:N=1               $Zr rod
c 142  3 -7.9     +507 +508 -513   U=9 IMP:N=1           $gap around
fuel
c 143  2 -2.7      -510        U=9 IMP:N=1           $spacer under fuel
c 144  8 -1.15e-3  -511        U=9 IMP:N=1           $void
c 145  3 -7.9      -512        U=9 IMP:N=1           $stainless end
plug
c
*********************************************************************
*******
c    BURNUP fuel follower control rods
```

```
c      control rods: reg, shim1 & shim2
1300  1 -1.0  #1310 #1320 #1330 #1340 #1350 #1360 #1390   $138 &137
removed for testing
              #1400 #1410 #1420 #1430 #1440 #1450   U=19 IMP:N=1
$element clad
1310  3 -7.9    -500          U=19 IMP:N=1             $upper end plug
1320  8 -1.15e-3 -501         U=19 IMP:N=1             $void above
poison
1330  2 -2.7     -502         U=19 IMP:N=1              $plug/spacer
1340  3 -7.9     -503         U=19 IMP:N=1             $magneform upper
1350  6 -2.52   -504          U=19 IMP:N=1               $poison B4C
1360  3 -7.9   -514 +504      U=19 IMP:N=1                $gap around
poison
c 137  2 -2.7     -505        U=19 IMP:N=1               $spacer under
poison
c 138  8 -1.15e-3  -506       U=19 IMP:N=1        $void top of fuel
1390  30 -6.05     -507 +509   U=19 IMP:N=1            $upper fuel
follower
1400  31 -6.05     -508 +509   U=19 IMP:N=1           $lower fuel
follower
1410  7 -6.49     -509         U=19 IMP:N=1              $Zr rod
1420  3 -7.9  +507 +508 -513   U=19 IMP:N=1           $gap around fuel
1430  2 -2.7      -510         U=19 IMP:N=1          $spacer under fuel
1440  8 -1.15e-3  -511         U=19 IMP:N=1          $void
1450  3 -7.9      -512         U=19 IMP:N=1          $stainless end
plug
c
**********************************************************************
**********
C    CELLS 200 - 499 CORE EXPERIMENTS
C     CT TUBE
200  1 -1.0     +900               U=10  IMP:N=1   $CT cell water
201  2 -2.7     -900  +901         U=10  IMP:N=1   $Center tube
202  1 -1      -901  +902         U=10  IMP:N=1   $CT fill water
203  1 -1      -902  +903         U=10  IMP:N=1   $Sample Volume 1by8"
205  1 -1      -903               U=10  IMP:N=1   $CT sample and
detector
c
C     CT TUBE
6200  1 -1.0     +900                    U=11  IMP:N=1   $CT cell water
6201  2 -2.7     -900  +901              U=11  IMP:N=1   $Center tube
6202  1 -1      -901  +902         U=11  IMP:N=1   $CT fill water
6203  1 -1      -902  +903         U=11  IMP:N=1   $Sample Volume 1by8"
6205  1 -1     -903               U=11  IMP:N=1   $CT sample and
detector
c
C     CT TUBE
2200  1 -1.0     +900                    U=12  IMP:N=1   $CT cell water
2201  2 -2.7     -900  +901              U=12  IMP:N=1   $Center tube
2202  1 -1      -901  +902         U=12  IMP:N=1   $CT fill water
2203  1 -1     -902  +903         U=12  IMP:N=1   $Sample Volume 1by8"
2205  1 -1      -903               U=12  IMP:N=1   $CT sample and
detector
c
```

```
C     CT TUBE
3200  1 -1.0     +900                    U=13  IMP:N=1   $CT cell water
3201  2 -2.7     -900  +901               U=13  IMP:N=1   $Center tube
3202  1 -1      -901  +902          U=13  IMP:N=1   $CT fill water
3203  1 -1      -902  +903          U=13  IMP:N=1   $Sample Volume 1by8"
3205  1 -1      -903                U=13  IMP:N=1   $CT sample and
detector
c     CT TUBE
4200  1 -1.0     +900                    U=14  IMP:N=1   $CT cell water
4201  2 -2.7     -900  +901               U=14  IMP:N=1   $Center tube
4202  1 -1     -901  +902          U=14  IMP:N=1   $CT fill water
4203  1 -1      -902  +903          U=14  IMP:N=1   $Sample Volume 1by8"
4205  1 -1      -903                U=14  IMP:N=1   $CT sample and
detector
c
C     CT TUBE
5200  1 -1.0     +900                    U=15  IMP:N=1   $CT cell water
5201  2 -2.7     -900  +901               U=15  IMP:N=1   $Center tube
5202  1 -1     -901  +902          U=15  IMP:N=1   $CT fill water
5203  1 -1     -902  +903          U=15  IMP:N=1   $Sample Volume 1by8"
5205  1 -1      -903                U=15  IMP:N=1   $CT sample and
detector
c ***************************************************
c   WATER HOLES
490  1  -1.0    #491    U=51  IMP:N=1
491  1  -1.0    -490    U=51  IMP:N=1
c   Spots for tally 492 to 499  ####
c
c    Cells 500 - 799 beam port experiments
c 500  2  -2.7 +1010 -1011 -100   IMP:N=1        $target Al tube
c
c    Cells 800 - 999 other modifications
c    Core experiment modifications U = 60 to 90
C  ********** ACCELERATOR TARGET FOR LOW POWER PHASE **************
c  1770
 1771    17   -18.5     -249          IMP:N=1 $ target in flange
 1772    17   -18.5     -248         IMP:N=1 $ target main body
 1773    18   -1.29e-11 -250         IMP:N=1  $ vacuum port
 1774     3    -7.9     -251 249 247    IMP:N=1 $ flange
 1775     2    -2.7     -247 250    IMP:N=1 $ beam tube
 1776    17   -18.5     -252           IMP:N=1 $ target conical part
c    ****0*********0*********0*********0*********0*********0*****
c 900  1  -1.0    -150  +160 -165   U=99  IMP:N=1   $Detector
c 901  1  -1.0 -150 +160 -165  fill=99 (+0.0  +64.0  +0.0) $Detector
c
c 950  8 -1.15e-3 -150    IMP:N=1
c     *TRCL (-60.00  00.00   00.00   00  90  90   90  00  90) $Det
c 951  8 -1.15e-3 -150    IMP:N=1
c      *TRCL ( 57.96   -15.53   00.00   00  90  90   90  00  90) $Det
c 952  8 -1.15e-3 -150     IMP:N=1
c     *TRCL ( 42.43    42.43   00.00   00  90  90   90  00  90) $Det
C
999     0           +100: +110: -120  IMP:N=0     $Non Problem region
c                    :(-100  -150)
```

```
c                    :(-100  -155)
c    ****0*********0*********0*********0*********0*********0*****

c    ****0*********0*********0*********0*********0*********0*****
C    *  PROBLEM GEOMETRY SURFACES.
c    ****0*********0*********0*********0*********0*********0*****
C    DEFINE PROBLEM RADIAL DOMAIN:
 100     CZ     +75                    $Cylinder around problem
C    HEXAGONAL CELL LATTICE SURFACES
 101     PX      +2.17678              $Fuel lattice hex-prism
 102     PX      -2.17678              $Fuel lattice hex-prism
 103     P   +1   1.73205  0  +4.35356 $Fuel lattice hex-prism
 104     P   +1   1.73205  0  -4.35356 $Fuel lattice hex-prism
 105     P   -1   1.73205  0  +4.35356 $Fuel lattice hex-prism
 106     P   -1   1.73205  0  -4.35356 $Fuel lattice hex-prism
c    Define PROBLEM axial domain:
 110     PZ     +75                    $UPPER BOUND
 120     PZ     -75                    $LOWER BOUND
C 150     CZ     +5.08                  $N-Detector Cylinder
C 160     PZ     +10                    $Detector Lower
C 165     PZ     +30                    $Detector Upper
 150     RCC 0.0  0.0 +10.0  0.0  0.0 +20.0 5.08  $N-Detector
c
c    ****0*********0*********0*********0*********0*********0*****
c
C    REACTOR CORE GRID PLATE SURFACES
 200     CZ       1.91135    $Grid plate element holes
 201     PZ     +32.3850     $Upper grid plate region
 202     PZ     +30.7975     $Upper grid plate region
 203     CZ      27.6225     $Upper grid plate diameter
 205     CZ       1.5875     $Grid plate coolant holes
 206     PZ     -33.17875    $Lower grid plate region
 207     PZ     -36.35375    $Lower grid plate region
c 208     CZ     +27.6225    $Effective core radius
 211     PX     +26.1216               $Lower grid plate edge
 212     PX     -26.1216               $Lower grid plate edge
 213     P   +1   0.57735  0  +29.0240 $Lower grid plate edge
 214     P   +1   0.57735  0  -29.0240 $Lower grid plate edge
 215     P   -1   0.57735  0  +29.0240 $Lower grid plate edge
 216     P   -1   0.57735  0  -29.0240 $Lower grid plate edge
 221     PY     +25.1360              $Lower grid plate edge
 222     PY     -25.1360              $Lower grid plate edge
 223     P   +1   1.73205  0  +52.2432 $Lower grid plate edge
 224     P   +1   1.73205  0  -52.2432 $Lower grid plate edge
 225     P   -1   1.73205  0  +52.2432 $Lower grid plate edge
 226     P   -1   1.73205  0  -52.2432 $Lower grid plate edge
 231     PX      +26.6700              $Core shroud inside surface
 232     PX      -26.6700              $Core shroud inside surface
 233     P   +1   0.57735  0  +29.2100 $Core shroud inside surface
 234     P   +1   0.57735  0  -29.2100 $Core shroud inside surface
 235     P   -1   0.57735  0  +29.2100 $Core shroud inside surface
 236     P   -1   0.57735  0  -29.2100 $Core shroud inside surface
 241     PY     +25.4000              $Core shroud inside surface
 242     PY     -25.4000              $Core shroud inside surface
```

```
 243     P   +1   1.73205  0  +54.9275 $Core shroud inside surface
 244     P   +1   1.73205  0  -54.9275 $Core shroud inside surface
 245     P   -1   1.73205  0  +54.9275 $Core shroud inside surface
 246     P   -1   1.73205  0  -54.9275 $Core shroud inside surface
C    ****0*********0*********0*********0*********0*********0*****
C    CORE STRUCTURE SURFACES
C    REFLECTOR INNER SHROUD
 300     CZ      30.083125             $Grid plate alignment ring
 301     CZ      29.765625             $Grid plate alignment ring
 302     CZ      27.9400               $Grid plate alignment ring
 303     PZ     +33.9725               $Grid plate alignment ring
 304     PZ     +26.3525               $Grid plate alignment ring
C    SHROUD LOAD RING
 305     CZ      24.7650               $Reflector shroud load ring
 306     PZ     -37.30625              $Reflector shroud load ring
 307     PZ     -39.52875              $Reflector shroud load ring
C
 311     PX     +29.2100               $Reflector shroud support
 312     PX     -29.2100               $Reflector shroud support
 313     P   +1   0.57735  0  +32.385  $Reflector shroud support
 314     P   +1   0.57735  0  -32.385  $Reflector shroud support
 315     P   -1   0.57735  0  +32.385  $Reflector shroud support
 316     P   -1   0.57735  0  -32.385  $Reflector shroud support
 321     PY     +27.9400               $Reflector shroud support
 322     PY  -27.9400                  $Reflector shroud support
 323     P   +1   1.73205  0  +59.3725 $Reflector shroud support
 324     P   +1   1.73205  0  -59.3725 $Reflector shroud support
 325     P   -1   1.73205  0  +59.3725 $Reflector shroud support
 326     P   -1   1.73205  0  -59.3725 $Reflector shroud support
C
 331     PX     +27.3050               $Core shroud plate exterior
 332     PX     -27.3050               $Core shroud plate exterior
 333     P   +1   0.57735  0  +29.8450 $Core shroud plate exterior
 334     P   +1   0.57735  0  -29.8450 $Core shroud plate exterior
 335     P   -1   0.57735  0  +29.8450 $Core shroud plate exterior
 336     P   -1   0.57735  0  -29.8450 $Core shroud plate exterior
 341     PY     +26.0350               $Core shroud plate exterior
 342     PY     -26.0350               $Core shroud plate exterior
 343     P   +1   1.73205  0  +56.5150 $Core shroud plate exterior
 344     P   +1   1.73205  0  -56.5150 $Core shroud plate exterior
 345     P   -1   1.73205  0  +56.5150 $Core shroud plate exterior
 346     P   -1   1.73205  0  -56.5150 $Core shroud plate exterior
C    REFLECTOR OUTER SHROUD
 350     CZ      54.76875    $Reflector outer shroud
 351     CZ      53.49875    $Reflector outer shroud
 352     PZ     +28.8925     $Outer shroud upper edge
 353     PZ     -32.0675     $Outer shroud lower edge
 355     PY      +0.0        $Core shroud section plane
C    REFLECTOR BEAM PORTS
 360     PY     +55.5625                 $Radial penetrating beam port
BP3
 361     C/X    -35.2552  -6.985   7.62   $Tangential thru beam port
BP5
```

```
 362     C/X    -35.2552  -6.985   6.9088 $Tangential thru beam port
BP5
 363     C/Y      0.0     -6.985  10.160  $Radial penetrating beam port
 364     C/Y      0.0     -6.985   9.525  $Radial penetrating beam port
c 1008       c/x -35.2552 -6.985 -5         $Target pipe  RACE
c 1009       c/x -35.2552 -6.985 -5.5        $Target Pipe
c 1010       c/x -35.2552 -6.985 -5.9        $Target Pipe
c 1011       c/x -35.2552 -6.985 -6.4        $Target Pipe
c
 370     CZ      53.3400     $Reflector top shroud
 371     CZ      37.4650     $Reflector top shroud
 372     PZ     +29.5275     $Reflector top shroud
 373     PZ     +28.2575     $Reflector top shroud
 374     CZ      52.0700     $Reflector inner shroud base
 375     PZ     -27.9400     $Reflector inner shroud base
 376     PZ     -29.5275     $Reflector inner shroud base
 377     PZ     -36.8300     $Reflector shroud edge ring
C    RSR EXPERIMENT SYSTEM
 380     CZ      37.1475     $RSR cavity outer ring
 381     PZ      +6.9850     $RSR cavity base
 382     PZ      +7.3025     $RSR cavity base
C    ****0*********0*********0*********0*********0*********0*****
C    GRAPHITE REFLECTOR SURFACES
 400     CZ      53.0225     $Graphite reflector outer radius
 401     CZ      37.7825     $Graphite reflector inner radius
 402     PZ      27.6225     $Graphite reflector upper section
 403     PZ       6.3500     $Graphite reflector section plane
 404     PY     -20.32       $Graphite reflector section plane
 405     PY     -35.2552     $Beam port penetration
c        C/Y      0.0     -6.985  10.160         $Radial penetrating
beam port, bp3
 406  2  CY      7.62        $Tangential beam port, bp2
 407  4  CY      7.62        $Radial beam port, bp4
 408  2  PY      0.0         $Tangential beam port, bp2
 409  4  PY      0.0         $Radial beam port, bp4
 411     PX    +27.78125               $Graphite inner surface
 412     PX    -27.78125               $Graphite inner surface
 413     P   +1  0.57735  0  +31.00875  $Graphite inner surface +1
 414     P   +1  0.57735  0  -31.00875  $Graphite inner surface +1
 415     P   -1  0.57735  0  +31.00875  $Graphite inner surface +1
 416     P   -1  0.57735  0  -31.00875  $Graphite inner surface +1
 421     PY    +26.431875              $Graphite inner surface
 422     PY    -26.431875              $Graphite inner surface
 423     P   +1  1.73205  0  +57.30875 $Graphite inner surface +1
 424     P   +1  1.73205  0  -57.30875  $Graphite inner surface +1
 425     P   -1  1.73205  0  +57.30875  $Graphite inner surface +1
 426     P   -1  1.73205  0  -57.30875  $Graphite inner surface +1
c
 430  2  CY      6.9088      $Tangential beam port, bp2
 440  4  CY      6.9088      $Radial beam port, bp4
c 450        C/X    -35.2552  -6.985   7.62          $Tangential thru
beam port,  bp1&5
c 450     PX      0.0         $BP1&5 origin
C    BEAM PORT TALLY SURFACES BP1&5 AND BP3
```

```
c 451     PX     +10.16       $BP1
c 453     PY     +40.90       $BP3
c 455     PX    -10.16        $BP5
c    pool structure pipe, bp3
 461     PY     +25.600               $Radial penetrating beam port,
bp3
 462     PY     +26.235               $Radial penetrating beam port,
bp3
 463     C/Y      0.0  -6.985  7.62    $Radial penetrating beam port,
bp3
 464     C/Y      0.0  -6.985  6.9088  $Radial penetrating beam port,
bp3
c
c    WATER HOLE
490  RCC 0.000 0.000 -31.5877 0.00 0.00 59.3245 1.90  $just water for
flux tally
c
c    ****0*********0*********0*********0*********0*********0*****
C    CONTROL ELEMENT SURFACES
c
c  FUEL FOLLOWED CONTROL RODS
c
 500  RCC 0.000 0.000 31.115  0.00 0.00 3.81  1.7145 $element end plug
 501  RCC 0.000 0.000 20.6375 0.00 0.00 10.4775 1.7145 $upper void
 502  RCC 0.000 0.000 19.3675 0.00 0.00 1.27 1.7145  $magneform plug
 503  RCC 0.000 0.000 +19.05  0.00 0.00 .3175 1.7145 $Magneform upper
 504  RCC 0.000 0.000 -19.05  0.00 0.00 38.1 1.6637 $B4C Absorber
c 505  RCC 0.000 0.000 -20.32  0.00 0.00 1.27  1.7145  $magneform
separator
c 506  RCC 0.000 0.000 -20.955 0.00 0.00 0.635 1.7145 $void
 507  RCC 0.000 0.000 -38.1 0.00 0.00 19.05 1.6637 $Upper Fuel Follower
 508  RCC 0.000 0.000 -57.15 0.00 0.00 19.05 1.6637 $Lower fuel
follower
 509  RCC 0.000 0.000 -57.15 0.00 0.00 38.1  0.28575 $Zr Rod
 510  RCC 0.000 0.000 -59.69 0.00 0.00 2.54  1.7145 $magneform plug
 511  RCC 0.000 0.000 -73.025 0.00 0.00 13.335 1.7145 $void
 512  RCC 0.000 0.000 -74.295 0.00 0.00 1.27 1.7145 $plug end
 513  RCC 0.000 0.000 -57.15 0.00 0.00 38.1 1.7145 $Fuel Clad
 514  RCC 0.000 0.000 -19.05 0.00 0.00 38.1  1.7145 $B4C clad
 515  RCC 0.00 0.000 -74.295 0.00 0.00 107.315 1.7145 $full SS clad
c
c    PULSING ROD
 520   RCC  0.00 0.00 +24.13   0.00 0.00 0.635 1.5875 $TR top plug
 521   RCC  0.00 0.00 +19.05   0.00 0.00 5.08 1.5875  $magneform plug,
upper
 522   RCC  0.00 0.00 -19.05   0.00 0.00 38.1  1.5113  $b4c poison
 523   RCC  0.00 0.00 -19.05   0.00 0.00 38.1  1.5875  $clad on poison
 524   RCC  0.00 0.00 -21.59   0.00 0.00  2.54 1.5875  $magneform
plug,lower
 525   RCC  0.00 0.00 -70.8025 0.00 0.00 49.2125 1.5875  $Air
Follower,clad
 526   RCC  0.00 0.00 -70.8025 0.00 0.00 49.2125 1.5113  $Air Follower
 527   RCC  0.00 0.00 -72.7075 0.00 0.00  1.905  1.5875    $TR bottom
plug
```

```
c    ****0*********0*********0*********0*********0*********0*****
C    FUEL AND MODERATOR ELEMENT SURFACES
c
c  MACROBODY FUEL ELEMENT SURFACES
 600  RCC 0.000 0.000   0.05  0.000 0.000 +19.0  1.816    $Fuel Up Half
 601  RCC 0.000 0.000   0.05  0.000 0.000 -19.1  1.816    $Fuel Lower
Half
 602  RCC 0.000 0.000 -19.05   0.000 0.000 +38.1   0.28575  $Zr Rod
 603  RCC 0.000 0.000 -19.05   0.000 0.000 -8.6868 1.816    $Graphite
Lower
 604  RCC 0.000 0.000 +19.05   0.000 0.000 +8.6868 1.816    $Graphite
Upper
 605  RCC 0.000 0.000 -27.7368 0.000 0.000 +55.4736 1.867   $SS Clad
 606  RCC 0.000 0.000 -31.5877 0.000 0.000 +3.8509 1.5306  $Bottom
Fitting
 607  RCC 0.000 0.000 +27.7368 0.000 0.000 +3.8509 1.5306  $Top Fitting
c
c   MACROBODY GRAPHITE ELEMENT SURFACES
610  RCC 0.000 0.000 -27.7368 0.000 0.000 +55.4736 1.816    $Graphite
611  RCC 0.000 0.000 -27.7368 0.000 0.000 +55.4736 1.867   $Al Clad
612  RCC 0.000 0.000 -31.5877 0.000 0.000 +3.8509 1.5306  $Bottom
Fitting
613  RCC 0.000 0.000 +27.7368 0.000 0.000 +3.8509 1.5306  $Top Fitting
c
c    ****0*********0*********0*********0*********0*********0*****
C   REACTOR CORE MODIFICATIONS, SURFACES
C    CENTER TUBE IRRADIATIONS
900     RCC  0.000 0.000 -35.0  0.000 0.000 +105 1.5875  $Experiment
Tube
901     RCC  0.000 0.000 -35.0  0.000 0.000 +105 1.54686 $Experiment
Tube
902     RCC  0.000 0.000 -10.16 0.000 0.000 +20.32 1.27  $N-Fission
Chamber
903     RCC  0.000 0.000 -10.0  0.000 0.000 +20.0  1.20  $FC inner wall
c
C    TARGET SURFACES
 247     rcc -65 -35.2552  -10. 64  0 0 2       $ outside wall of beam
tub
 248     rcc  +3.0203 -35.2552 -10. 4.234 0 0 3.4925        $ target
main body
 249     rcc  -1.0 -35.2552  -10.   1.239 0 0 1.905        $ target in
flange
 250     rcc -65 -35.2552 -10. 64 0 0 1.365            $ vacuum port
 251     rcc -3.04 -35.2552 -10. 2.54 0 0 3.4925         $ flange
 252     trc  +.239 -35.2552 -10. 2.7813 0 0 1.905 3.4925 $cone of
target
c    ****0*********0*********0*********0*********0*********0*****

c    Transformations for beam tube locations:
c
c Thru port, small
  *TR1  0.0      -35.255  -6.985  00  90  90   90  00  90  $BP1
c Tang port, small
  *TR2  +35.255  -06.222  -6.985  30 120  90   60  30  90  $BP2
```

```
c Radial port, large
  *TR3  0.0      +25.600  -6.985  00  90  90   90  00  90  $BP3
c Radial port, small
  *TR4  -22.871  +13.216  -6.985  60  30  90  150  60  90  $BP4
c Thru port, large
  *TR5  0.0      -35.255  -6.985  00  90  90   90  00  90  $BP5
c
c    Transformations for control rod positions:
c
c  TR6  0  0  00.00     1 0 0  0 1 0    $(000 u) shutdown condition
c  TR7  0  0  12.6352    1 0 0  0 1 0    $(325 u) low 50 w power
critical
c  TR8  0  0  27.78125  1 0 0  0 1 0    $(700 u) design high power
  TR9  0  0  38.1     1 0 0  0 1 0    $(960 u) full-out condition
c
c    ****0*********0*********0*********0*********0*********0*****
c    Materials for reactor components
c
c    H2O, coolant & moderator
M1   1001.00c  0.666567
     1002.00c  0.0001
     8016.00c  0.3332063
     8017.00c  0.000127
MT1  HH2O.00t   $S(alpha,beta) at 294K
MX1:P  model
       1002
       8016
       8017      $ mix and match hydrogen
c
c
c     Aluminum Alloy 6061 ********************
M2   13027.00c   -0.9670               $Al 0.9670
     26054.00c   -0.000316              $iron: 0.0056
     26056.00c   -0.005147  26057.00c  -0.000121
     26058.00c   -0.000016
     14028.00c   -0.007350               $silicon: 0.008
     14029.00c   -0.000387  14030.00c  -0.000263
     12024.00c   -0.0110             $magnesium: 0.8-1.2
     24050.00c   -0.000084              $chromium: 0.02
     24052.00c   -0.001674  24053.00c  -0.000193  24054.00c -0.000049
     25055.00c   -0.00130               $manganese: 0.13
     22048.00c   -0.0007              $titanium: 0.07
     28058.00c   -0.000269  28060.00c  -0.000107  28061.00c  -0.000005
     28062.00c   -0.000015  28064.00c  -0.000004  $ nickel
     29063.00c   -.002055   29065.00c  -0.000945  $ copper
     30000.00c   -.0010              $zinc: 0.25  Assume all Zn64
MT2     Al.00t
c    Stainless Steel type 304L ******************
M3   26054.00c   -0.038390              $iron: 0.0056
     26056.00c   -0.624930  26057.00c  -0.014691
     26058.00c   -0.001989
     14028.00c   -0.009187               $silicon: 0.01
     14029.00c   -0.000483  14030.00c  -0.000329
     24050.00c   -0.007930               $chromium: 0.19
```

```
     24052.00c   -0.159029  24053.00c  -0.018380  24054.00c -0.004661
     28058.00c   -0.067198  28060.00c  -0.026776  28061.00c  -0.001183
     28062.00c   -0.003834  28064.00c  -0.001009  $ nickel
     25055.00c   -0.020              $manganese: 2.0
c
c     Graphite *********************************
M4    6012.50c    -1.0                 $C graphite
MT4   GRAPH.00t
c grph.60t                         $ S(alpha, beta) 300K
c    Zr-H Fuel Fresh 19.75% enriched 8.5 w/o 1.6 Hydride
c
M5     40090.00c  -0.462589
       40091.00c -0.100879
       40092.00c  -0.154196
       40094.00c -0.15626
       40096.00c -0.025175
      1001.00c   -0.015895           $91.5% ZrH1.6
     92238.00c   -0.068213            $U  0.8025 * 8.5%
     92235.00c   -0.016788            $U  0.1975 * 8.5%
c
c
MT5  ZrZrH.00t
      HZrH.00t
c
c
c     B4C poison (2.48 g/cc)
M6    5010.00c     0.159936             $B4C
      5011.00c     0.64096             $B4C
      6012.50c     0.200                $carbon
MT6  GRAPH.00t
M7     40090.00c  -0.5145
       40091.00c -0.1122
       40092.00c  -0.1715
       40094.00c  -0.1738
       40096.00c  -0.0280    $Zr Rod
c    Air (density 1.205e-3 g/cc at STP)
M8    8016.00c   -0.23                $air
      7014.00c   -0.77
c
m17   74182.00c    -0.198735  $ W-Cu Target
      74183.00c    -0.1074
      74184.00c    -0.23
      74186.00c    -0.2132
      29063.00c    -0.173
      29065.00c    -0.0771
c    VACUUM (density 1.205e-11 g/cc )
M18    8016.00c   -0.23e-9               $vacuum
      7014.00c    -0.77e-9
c  PHOTONUCLEAR
c
mx2:p
     13027              $Al 0.9670
     26054                $iron: 0.0056
     26056
```

```
     26057
     26058
     14028               $silicon: 0.008
     14029
     14030
     12024             $magnesium: 0.8-1.2
     24050             $chromium: 0.02
     24052
     24053
     24054
     25055                $manganese: 0.13
     22048                $titanium: 0.07
     28000
     28060
     28061
     28062
     28064    $ nickel
     29063
     29065    $ copper
     30064                 $zinc: 0.25
MX3:P
     26054                $iron: 0.0056
     26056
     26057
     26058
     14028                   $silicon: 0.01
     14029
     14030
     24050                   $chromium: 0.19
     24052
     24053
     24054
     28058
     28060
     28061
     28062
     28064          $ nickel
     25055                   $manganese: 2.0
c
 mx4:p    6012
MX5:P
       40090
       40091
       40092
       40094
       40096
      model              $91.5% ZrH1.6
     92238              $U  0.8025 * 8.5%
     92235               $U  0.1975 * 8.5%
c
MX6:P
       model           $B4C
       model            $B4C
       6012            $carbon
```

```
MX7:P     40090
          40091
          40092
          40094
          40096     $Zr Rod
mx8:p  8016
       7014
c
MX17:P 74182   $ W-Cu Target
      74183
      74184
      74186
      29063
      29065
c
MX18:p  8016 7014
c ********************** Fuel Pins with Burn
c   RING B UPPER Fuel
c M20  40090.00c  -0.462589
c     40091.00c -0.100879
c     40092.00c  -0.154196
c     40094.00c -0.15626
c     40096.00c -0.025175           $ Burn of 2.5 MWD
c      1001.00c   -0.015895            $91.5% ZrH1.6
c    92238.00c   -0.068213            $U  0.8025 * 8.5%
c     92235.00c   -0.016788             $U  0.1975 * 8.5%
M20     1001.    -1.59E-02       $MAT 1  MCNP20  1.008 MWD
        1002.    -9.01E-07
       40090.    -4.63E-01
       40091.    -1.01E-01
       40092.    -1.54E-01
       40093.    -4.16E-06
       40094.    -1.56E-01
       40095.    -6.91E-07
       40096.    -2.52E-02
       41095.    -2.74E-07
       92235.    -1.59E-02
       92236.    -1.47E-04
       92237.    -4.89E-08
       92238.    -6.81E-02
       93237.    -3.45E-07
       93239.    -2.19E-06
       94239.    -7.39E-05
       94240.    -1.45E-06
       94241.    -4.88E-08
       94242.    -4.32E-10
       45103.    -6.54E-06
       54131.    -1.14E-05
       60143.    -2.32E-05
       61147.    -9.23E-06
       62149.    -7.51E-07
       62151.    -1.41E-06
c
c
```

```
       NLIB=00
MT20  ZrZrH.00t
       HZrH.00t
c      RING B LOWER FUEL
c    M21   40090.00c  -0.462589
c          40091.00c -0.100879
c          40092.00c  -0.154196
c         40094.00c -0.15626
c         40096.00c -0.025175
c         1001.00c   -0.015895            $91.5% ZrH1.6
c         92238.00c   -0.068213             $U  0.8025 * 8.5%
c         92235.00c   -0.016788             $U  0.1975 * 8.5%
M21        1001.    -1.59E-02        $ MAT 2  MCNP 21  1.254 MWD
           1002.    -1.18E-06
          40090.    -4.63E-01
          40091.    -1.01E-01
          40092.    -1.54E-01
          40093.    -5.47E-06
          40094.    -1.56E-01
          40095.    -8.85E-07
          40096.    -2.52E-02
          41095.    -3.55E-07
          92234.    -2.83E-08
          92235.    -1.56E-02
          92236.    -1.90E-04
          92237.    -7.24E-08
          92238.    -6.81E-02
          93237.    -5.14E-07
          93239.    -2.63E-06
          94239.    -9.33E-05
          94240.    -2.40E-06
          94241.    -1.04E-07
          94242.    -1.22E-09
          45103.    -8.58E-06
          54131.    -1.48E-05
          60143.    -3.02E-05
          61147.    -1.20E-05
          62149.    -7.52E-07
          62151.    -1.63E-06
c
c
c
     NLIB=00
MT21  ZrZrH.00t
      HZrH.00t
c   RING C UPPER FUEL
c M22   40090.00c  -0.462589
c      40091.00c -0.100879
c      40092.00c  -0.154196
c      40094.00c -0.15626
c      40096.00c -0.025175
c       1001.00c   -0.015895           $91.5% ZrH1.6
c      92238.00c   -0.068213            $U  0.8025 * 8.5%
c      92235.00c   -0.016788            $U  0.1975 * 8.5%
```

```
M22     1001.    -1.59E-02
        1002.    -7.53E-07
       40090.    -4.63E-01
       40091.    -1.01E-01
       40092.    -1.54E-01
       40093.    -3.63E-06          $MAT 3 MCNP 22 0.852 MWD
       40094.    -1.56E-01
       40095.    -6.17E-07
       40096.    -2.52E-02
       41095.    -2.44E-07
       92235.    -1.60E-02
       92236.    -1.25E-04
       92237.    -3.82E-08
       92238.    -6.81E-02
       93237.    -2.85E-07
       93239.    -1.94E-06
       94239.    -6.91E-05
       94240.    -1.19E-06
       94241.    -3.78E-08
       94242.    -2.82E-10
       45103.    -5.48E-06
       54131.    -9.54E-06
       60143.    -1.95E-05
       61147.    -7.76E-06
       62149.    -7.62E-07
      62151.    -1.26E-06
c
c
     NLIB=00
MT22   ZrZrH.00t
       HZrH.00t
C RING C LOWER FUEL
c
c M23   40090.00c  -0.462589
c      40091.00c -0.100879
c      40092.00c  -0.154196
c      40094.00c  -0.15626
c      40096.00c -0.025175
c      1001.00c   -0.015895            $91.5% ZrH1.6
c     92238.00c   -0.068213             $U  0.8025 * 8.5%
c     92235.00c   -0.016788             $U  0.1975 * 8.5%
M23    1001.  -1.59E-02
       1002.  -1.03E-06
      40090.  -4.63E-01          $MaT 4 MCNP 23  1.106 MWD
      40091.  -1.01E-01
      40092.  -1.54E-01
      40093.  -4.88E-06
      40094.  -1.56E-01
      40095.  -8.10E-07
      40096.  -2.52E-02
      41095.  -3.27E-07
      92234.  -2.70E-08
      92235.  -1.57E-02
      92236.  -1.69E-04
```

```
       92237.  -6.31E-08
       92238.  -6.81E-02
       93237.  -4.58E-07
       93239.  -2.61E-06
       94239.  -8.99E-05
       94240.  -2.04E-06
       94241.  -8.53E-08
       94242.  -8.72E-10
       45103.  -7.52E-06
       54131.  -1.30E-05
       60143.  -2.65E-05
       61147.  -1.05E-05
       62149.  -7.55E-07
       62151.  -1.53E-06
c
     NLIB=00
c
MT23   ZrZrH.00t
       HZrH.00t
c  RING D UPPER FUEL
c M24   40090.00c  -0.462589
c       40091.00c -0.100879
c       40092.00c  -0.154196
c       40094.00c -0.15626
c       40096.00c -0.025175
c       1001.00c   -0.015895            $91.5% ZrH1.6
c       92238.00c   -0.068213             $U  0.8025 * 8.5%
c       92235.00c   -0.016788             $U  0.1975 * 8.5%
M24     1001.   -1.59E-02
        1002.   -6.63E-07
       40090.   -4.63E-01
       40091.   -1.01E-01
       40092.   -1.54E-01
       40093.   -3.19E-06                      $MAT 5 MCNP 24 0.7424
MWD
       40094.   -1.56E-01
       40095.   -5.35E-07
       40096.   -2.52E-02
       41095.   -2.12E-07
       92235.   -1.61E-02
       92236.   -1.10E-04
       92237.   -3.12E-08
       92238.   -6.81E-02
       93237.   -2.33E-07
       93239.   -1.73E-06
       94239.   -6.09E-05
       94240.   -9.09E-07
       94241.   -2.57E-08
       94242.   -1.66E-10
       45103.   -4.85E-06
       54131.   -8.43E-06
       60143.   -1.72E-05
       61147.   -6.87E-06
       62149.   -7.60E-07
```

```
       62151.   -1.15E-06
c
c
c
     NLIB=00
c
MT24   ZrZrH.00t
       HZrH.00t
c   RING D LOWER FUEL
c M25   40090.00c  -0.46258
c      40091.00c -0.10087
c      40092.00c  -0.15419
c      40094.00c  -0.15626
c      40096.00c -0.02517
c      1001.00c   -0.01589               $91.5% ZrH1.6
c      92238.00c   -0.06821             $U  0.8025 * 8.5%
c      92235.00c   -0.01678             $U  0.1975 * 8.5%
M25     1001.   -1.59E-02
        1002.   -8.87E-07
       40090.   -4.63E-01
       40091.   -1.01E-01     $   MAT 6 MCNP 25 0.9588 MWD
       40092.   -1.54E-01
       40093.   -4.22E-06
       40094.   -1.56E-01
       40095.   -6.96E-07
       40096.   -2.52E-02
       41095.   -2.80E-07
       92235.   -1.59E-02
       92236.   -1.46E-04
       92237.   -4.87E-08
       92238.   -6.81E-02
       93237.   -3.52E-07
       93239.   -2.21E-06
       94239.   -7.72E-05
       94240.   -1.52E-06
       94241.   -5.42E-08
       94242.   -4.78E-10
       45103.   -6.48E-06
       54131.   -1.12E-05
       60143.   -2.29E-05
       61147.   -9.12E-06
       62149.   -7.58E-07
       62151.   -1.40E-06
c
c
     NLIB=00
c
MT25   ZrZrH.00t
      HZrH.00t
c   RING E UPPER FUEL
c M26   40090.00c  -0.46258
c      40091.00c -0.10087
c      40092.00c  -0.15419
c      40094.00c -0.15626
```

```
c      40096.00c -0.02517
c       1001.00c   -0.01589        $91.5% ZrH1.6
c      92238.00c   -0.06821             $U  0.8025 * 8.5%
c      92235.00c   -0.01678             $U  0.1975 * 8.5%
c
M26    1001.   -1.59E-02
       1002.   -5.53E-07
      40090.   -4.63E-01
      40091.   -1.01E-01   $ MAT 7 MCNP 26 0.6229 MWD
      40092.   -1.54E-01
      40093.   -2.65E-06
      40094.   -1.56E-01
      40095.   -4.48E-07
      40096.   -2.52E-02
      41095.   -1.78E-07
      92235.   -1.62E-02
      92236.   -9.21E-05
      92237.   -2.15E-08
      92238.   -6.82E-02
      93237.   -1.72E-07
      93239.   -1.45E-06
      94239.   -4.99E-05
      94240.   -6.20E-07
      94241.   -1.41E-08
      94242.   -7.77E-11
      45103.   -4.06E-06
      54131.   -7.05E-06
      60143.   -1.44E-05
      61147.   -5.76E-06
      62149.   -7.57E-07
      62151.   -1.01E-06
c
c
c
      NLIB=00
c
MT26   ZrZrH.00t
       HZrH.00t
c   RING E LOWER FUEL
c M27   40090.00c  -0.46258
c       40091.00c -0.10087
c      40092.00c  -0.15419
c      40094.00c -0.1562
c      40096.00c -0.02517
c      1001.00c   -0.01589            $91.5% ZrH1.6
c      92238.00c   -0.06821             $U  0.8025 * 8.5%
c      92235.00c   -0.01678             $U  0.1975 * 8.5%
M27      1001.    -1.59E-02
         1002.    -6.94E-07
        40090.    -4.63E-01
        40091.    -1.01E-01
        40092.    -1.54E-01
        40093.    -3.32E-06
        40094.    -1.56E-01      $MAT 8 MCNP 27  0.7529 MWD
```

```
        40095.    -5.52E-07
        40096.    -2.52E-02
        41095.    -2.21E-07
        92235.    -1.61E-02
        92236.    -1.15E-04
        92237.    -3.14E-08
        92238.    -6.81E-02
        93237.    -2.45E-07
        93239.    -1.73E-06
        94239.    -6.19E-05
        94240.    -9.61E-07
        94241.    -2.74E-08
        94242.    -1.87E-10
        45103.    -5.11E-06
        54131.    -8.83E-06
        60143.    -1.81E-05
        61147.    -7.20E-06
        62149.    -7.61E-07
        62151.    -1.19E-06
c
c
        NLIB=00
MT27   ZrZrH.00t
       HZrH.00t
c   RING F UPPER FUEL            Ring F 0.5 MWD Burn for Universe
c M28   40090.00c  -0.462589
c      40091.00c -0.100879
c      40092.00c  -0.154196
c      40094.00c -0.15626
c      40096.00c -0.025175
c       1001.00c   -0.015895            $91.5% ZrH1.6
c      92238.00c   -0.068213             $U  0.8025 * 8.5%
c      92235.00c   -0.016788             $U  0.1975 * 8.5%
M28     1001.    -1.59E-02
        1002.    -4.37E-07
       40090.    -4.63E-01
       40091.    -1.01E-01     $   MAT 9  MCNP 28  0.4897 MWD
       40092.    -1.54E-01
       40093.    -2.02E-06
       40094.    -1.56E-01
       40096.    -2.52E-02
       41095.    -1.31E-07
       92235.    -1.63E-02
       92236.    -7.20E-05
       92237.    -1.37E-08
       92238.    -6.82E-02
       93237.    -1.08E-07
       93239.    -1.03E-06
       94239.    -3.63E-05
       94240.    -3.45E-07
       94241.    -5.78E-09
       94242.    -2.43E-11
       45103.    -3.22E-06
       54131.    -5.59E-06
```

```
       60143.    -1.14E-05
       61147.    -4.57E-06
       62149.    -7.46E-07
       62151.    -8.39E-07
c
c
       NLIB=00
MT28  ZrZrH.00t
       HZrH.00t
c  RING F LOWER FUEL
c M29   40090.00c  -0.462589
c      40091.00c -0.100879
c      40092.00c  -0.154196
c       40094.00c -0.15626
c       40096.00c -0.025175
c       1001.00c   -0.015895    $91.5% ZrH1.6
c       92238.00c   -0.068213             $U  0.8025 * 8.5%
c       92235.00c   -0.016788             $U  0.1975 * 8.5%
M29      1001.    -1.59E-02
         1002.    -5.33E-07
        40090.    -4.63E-01
        40091.    -1.01E-01  $MAT 10  MCNP 29  0.585 MWD
        40092.    -1.54E-01
        40093.    -2.44E-06
        40094.    -1.56E-01
        40096.    -2.52E-02
        41095.    -1.62E-07
        92235.    -1.62E-02
        92236.    -8.76E-05
        92237.    -1.77E-08
        92238.    -6.82E-02
        93237.    -1.43E-07
        93239.    -1.17E-06
        94239.    -4.32E-05
        94240.    -5.06E-07
        94241.    -1.04E-08
        94242.    -5.38E-11
        45103.    -3.93E-06
        54131.    -6.81E-06
        60143.    -1.39E-05
        61147.    -5.57E-06
        62149.    -7.57E-07
        62151.    -9.78E-07
c
c
        NLIB=00
MT29   ZrZrH.00t
      HZrH.00t
c   FUEL FOLLOWED RODS UPPER FUEL
c M30   40090.00c  -0.462589
c       40091.00c -0.100879
c      40092.00c  -0.154196
c      40094.00c -0.15626
c      40096.00c -0.025175
```

```
c      1001.00c   -0.015895            $91.5% ZrH1.6
c      92238.00c   -0.068213             $U  0.8025 * 8.5%
c      92235.00c   -0.016788             $U  0.1975 * 8.5%
M30   1001.    -1.59E-02
      1002.    -8.85E-07
     40090.    -4.63E-01
     40091.    -1.01E-01              $MAT 11  MCNP 30  0.9793 MWD
     40092.    -1.54E-01
     40093.    -4.19E-06
     40094.    -1.56E-01
     40095.    -6.98E-07
     40096.    -2.52E-02
     41095.    -2.77E-07
     92235.    -1.59E-02
     92236.    -1.46E-04
     92237.    -4.89E-08
     92238.    -6.81E-02
     93237.    -3.62E-07
     93239.    -2.24E-06
     94239.    -7.76E-05
     94240.    -1.52E-06
     94241.    -5.29E-08
     94242.    -4.58E-10
     45103.    -6.45E-06
     54131.    -1.12E-05
     60143.    -2.28E-05
     61147.    -9.10E-06
     62149.    -7.72E-07
     62151.     -1.39E-06
c
c
c
c
      NLIB=00
MT30   ZrZrH.00t
      HZrH.00t
c    FUEL FOLLOWED RODS LOWER FUEL
c M31   40090.00c  -0.462589
c      40091.00c -0.100879
c      40092.00c  -0.154196
c      40094.00c -0.15626
c      40096.00c -0.025175
c      1001.00c   -0.015895            $91.5% ZrH1.6
c      92238.00c   -0.068213             $U  0.8025 * 8.5%
c      92235.00c   -0.016788             $U  0.1975 * 8.5%
M31     1001.    -1.59E-02
        1002.    -4.76E-07
        40090.    -4.63E-01  $Bottom FFCR is low burn
        40091.    -1.01E-01
        40092.    -1.54E-01   $ MAT 12 MCNP 31  0.52 MWD
        40093.    -2.17E-06
        40094.    -1.56E-01
        40096.    -2.52E-02
        41095.    -1.40E-07
```

```
       92235.    -1.63E-02
       92236.    -7.86E-05
       92237.    -1.28E-08
       92238.    -6.82E-02
       93237.    -1.16E-07
       93239.    -1.06E-06
       94239.    -3.89E-05
       94240.    -3.99E-07
       94241.    -6.91E-09
       94242.    -3.17E-11
       45103.    -3.53E-06
       54131.    -6.11E-06
       60143.    -1.25E-05
       61147.    -5.00E-06
       62149.    -7.60E-07
       62151.    -8.97E-07
c
c
       NLIB=00
c
c
MT31  ZrZrH.00t
      HZrH.00t
c *****************  Photonuclear
*******************************************
MX20:P
     40090     40091   40092
     40094    40096
      model              $91.5% ZrH1.6
     92238                $U  0.8025 * 8.5%
     92235                $U  0.1975 * 8.5%
MX21:P
     40090     40091   40092
     40094    40096
      model              $91.5% ZrH1.6
     92238                $U  0.8025 * 8.5%
     92235                $U  0.1975 * 8.5%
MX22:P  40090     40091   40092
     40094    40096
      model              $91.5% ZrH1.6
     92238                $U  0.8025 * 8.5%
     92235                $U  0.1975 * 8.5%
MX23:P 40090
     40091
     40092
     40094
     40096
      model              $91.5% ZrH1.6
     92238                $U  0.8025 * 8.5%
     92235                $U  0.1975 * 8.5%
MX24:P 40090
     40091
     40092
     40094
```

```
     40096
      model              $91.5% ZrH1.6
     92238                $U  0.8025 * 8.5%
     92235                $U  0.1975 * 8.5%
MX25:P 40090
       40091
       40092
     40094
     40096
      model              $91.5% ZrH1.6
     92238                $U  0.8025 * 8.5%
     92235                $U  0.1975 * 8.5%
MX26:P   40090     40091   40092
     40094    40096
      model              $91.5% ZrH1.6
     92238                $U  0.8025 * 8.5%
     92235                $U  0.1975 * 8.5%
MX27:P     40090     40091   40092
     40094    40096
      model              $91.5% ZrH1.6
     92238                $U  0.8025 * 8.5%
     92235                $U  0.1975 * 8.5%
MX28:P  40090     40091   40092
     40094    40096
      model              $91.5% ZrH1.6
     92238                $U  0.8025 * 8.5%
     92235                $U  0.1975 * 8.5%
MX29:P  40090     40091   40092
     40094    40096
      model              $91.5% ZrH1.6
     92238                $U  0.8025 * 8.5%
     92235                $U  0.1975 * 8.5%
MX30:P 40090     40091   40092
     40094    40096
      model              $91.5% ZrH1.6
     92238                $U  0.8025 * 8.5%
     92235                $U  0.1975 * 8.5%
MX31:P   40090     40091   40092
     40094    40096
      model              $91.5% ZrH1.6
     92238                $U  0.8025 * 8.5%
     92235                $U  0.1975 * 8.5%
c    ****0*********0*********0*********0*********0*********0*****
c
c    CRITICALITY CALCULATION
 kcode   20000     1         200       300
c ksrc    3.5       0         0
 ksrc      -8.7 -23.5  0  -4.4 -23.5  0   0   -23.5  0    4.4 -23.5  0
$bottom row
            8.7 -23.5  0
c
           -11   -19.6  0  -6.5 -19.6  0  -2.2 -19.6  0    2.2 -19.6  0
$2nd r
         6.5 -19.6  0  11   -19.6  0
```

```
c
          -13   -16    0  -8.8 -16    0  -4.3 -16    0    0   -16    0
$3rd row
          4.3 -16    0   8.8 -16    0  13   -16    0
          -15.3 -12    0                                    $only used
with a full 3L
c
          -11   -12    0  -6.6 -12    0  -2.2 -12    0    2.2 -12    0
$4th row
          6.6 -12    0  11   -12    0 -15.3 -12    0
          -17.3  -8.5  0 -13    -8.5  0     $only used with a full 3L
c
         -21.8 -8.5 0   -18.7 -8.5 0   -14.3 -8.5  0  -8.5 -8.5 0  -4.5
-8.5 0 $5th row
         0 -8.5 0
          4.3  -8.5  0   8.7  -8.5  0   13 -8.5  0   17.3  -8.5   0
c
         -19.6  -4.5  0 -15.3  -4.5  0 -11    -4.5  0  -6.6  -4.5   0
$6th row
          -2.2  -4.5  0   2.2  -4.5  0   6.6  -4.5  0  11    -4.5
c
         -21.0 0 0  -18.0 0 0  -13.2 0 0  -9.5 0 0  -4.3 0 0  4.5 0 0
13.0 0 0  $CenterRow
c
            -15.0 3.0 0   -11 2.7 0   -6.0 3.0 0   -2.6 2.7 0   $8th
Row
         2.3 2.7 0     6.0 3.0 0   11.0 3.0 0   14.0 3.0 0
c
         -13.5 7.0 0    -8.5 8.5 -1.0   -5.0 8.5 1.0   0 7.0 0   5.0
7.9 -2  $9th Row
         10 7.5 0    13.0 8.3  -4.0
c
         -12.0 12.0 -3.0    -7  12.0  0  -1.0 11.5  3.0   3.0  12.0 -6
$10th Row
            6.0 11.0 0.0   10.0 10.5 0
c
            -4.2  16.0  -3  -4.2 15.5 2.0  -4.0 14.5 0   0.5 15.0 -4.0
$Top row
            0.2 16.0 5.0
c
c
c
c    EXECUTION CONTROLS
MODE N P
phys:n 20
phys:p 20 0 0 1 1
c phys:e 30 0 0 0 0 1 1 0
  cut:n  1e+33
c  cut:p  1e+33 4.
c  cut:e  1e+33
c
c nps       20000
c
print  40 50 55 110 10
```

```
prdmp   5000  -60  1  4 0         $ print and dump cycle
c
c
c    ****0*********0*********0*********0*********0*********0*****
TMESH1
    CMESH1:n flux
c  ERGSH1: 1e-2 15
    CORA1   0 98i 70
    CORB1  -35 -30 -25 -20 -15 -10 -5 0 5 10 15 20 25 30 35
    CORC1    358i 360
c
c     CMESH11:n traks
c      CORA11   0 98i 40
c      CORB11    1 0 1 5 10 20
c      CORC11    358i 360
c
c  CORA2 0.1 25i
c    ERGSH1 1e-4 20
 ENDMD
c
c    ****0*********0*********0*********0*********0*********0*****
c SDEF erg=3 pos= 0.0 0.0 0.0
c
c SDEF  par=3 erg=18 POS= -9.525 -35.2552 -10.42  vec= 1 0 0
c      dir = 1 axs = 1 0 0 rad = d1 ccc=99
c si1 0 0.25
c sp1 -21
c
c SDEF PAR=N ERG=D1 X= -0.5 Y=-35.2552 Z=-10.0 WGT=5E6 $Neutron Pulse
Watt spectrum at target
c SP1 -3  $Watt Spectrum built in for simulation
c
c    ****0*********0*********0*********0*********0*********0*****
c
c    ****0*********0*********0*********0*********0*********0*****
c     Define instrument detector tallies:
E0 0  1E-8 1E-6 1e-4 1E-2 0.1 0.5 1 2 3 4 5 6 10 12 15 20
c T0 -1 1 501 1001 1E4 5e4 1e5 5E5 7E5 1E6 2E6 3E6 4E6 5E6 6E6 7E6 8E6
9E6 1E7 1E8
 f4:n     205
c T4
 E4
c FT4 TMC  1 500
 FC4     Neutron Flux in Central Thimble Detector
 f14:N   2205
c T14
 E14
c FT14 TMC  1 500
 FC14   G5 Detector Flux
 F24:N   3205
c T24
 E24
c FT24 TMC  1 500
 FC24    G15 Detector Flux
```

```
 F34:N   4205
c T34
 E34
c  FT34 TMC  1 500
 FC34    E17 Detector Flux
 F44:N   5205
c  T44
 E44
c  FT44 TMC  1 500
 FC44    E20 Detector Flux
 F54:N   6205
c T54
 E54
c  FT54 TMC  1 500
 FC54    G6 Detector Flux
c
c
c     Define experiment facility tallies:
c f24:n   205 90 91 92
c f16:n   205 90 91 92
c     Define beam port tallies (neutron):
c f101:n  81 82 83 84 85 T
c f104:n  81 82 83 84 85 T
c f104:n     82    84    T
```

A.4 Example MONTEBURNS Output Files

OUTPUT FILE "BURN14.chk"

NETL TRIGA Core Burn Using MCNP5 and ORIGEN22

Total Power (MW) = 1.00E+00 Days = 2.60E+02
outer steps = 8, # inner steps = 50, # predictor steps = 1
Importance Fraction = 0.0000

Monteburns Spectrum for Each Predictor Step

Monteburns Spectrum for Each Predictor Step for material 1

	<.1eV	<1eV	<100eV	<100keV	<1MeV	<20MeV
0	20.85	9.67	10.37	19.24	18.47	21.39
1	20.17	9.52	10.55	19.43	18.82	21.51
1	20.31	9.61	10.55	19.33	18.83	21.37
2	20.45	9.52	10.43	19.28	18.84	21.48
3	20.57	9.65	10.53	19.34	18.78	21.13
4	20.70	9.62	10.55	19.43	18.61	21.09
5	20.59	9.66	10.49	19.36	18.71	21.19
6	20.90	9.57	10.42	19.14	18.90	21.07
7	20.95	9.66	10.45	19.14	18.55	21.25
8	21.31	9.47	10.40	19.07	18.63	21.13

Monteburns Spectrum for Each Predictor Step for material 2

	<.1eV	<1eV	<100eV	<100keV	<1MeV	<20MeV
0	20.91	9.68	10.49	19.05	18.65	21.23
1	20.74	9.55	10.39	19.07	18.65	21.60
1	20.59	9.65	10.32	19.25	18.82	21.37
2	20.61	9.75	10.48	19.17	18.69	21.30
3	20.99	9.56	10.39	18.94	18.79	21.33
4	21.07	9.69	10.56	19.24	18.42	21.02
5	21.31	9.77	10.49	19.01	18.44	20.99
6	21.38	9.76	10.47	18.98	18.41	21.01
7	21.37	9.84	10.30	19.11	18.35	21.03
8	21.65	9.65	10.37	19.04	18.41	20.87

Monteburns Spectrum for Each Predictor Step for material 3

	<.1eV	<1eV	<100eV	<100keV	<1MeV	<20MeV
0	18.73	9.46	10.88	20.10	19.36	21.47
1	18.31	9.50	10.92	20.19	19.36	21.73
1	18.14	9.53	10.93	20.47	19.44	21.49
2	18.33	9.43	10.88	20.30	19.39	21.68
3	18.44	9.44	10.83	20.19	19.38	21.72
4	18.63	9.46	10.91	20.10	19.46	21.45
5	18.75	9.41	10.90	20.20	19.32	21.41
6	18.74	9.47	10.93	20.31	19.26	21.29
7	18.99	9.60	10.93	20.23	19.14	21.12
8	18.81	9.51	10.88	20.13	19.23	21.43

Monteburns Spectrum for Each Predictor Step for material 4

	<.1eV	<1eV	<100eV	<100keV	<1MeV	<20MeV
0	19.34	9.55	10.73	19.90	19.14	21.33
1	19.05	9.61	10.87	19.94	19.12	21.40
1	19.12	9.60	10.89	19.99	19.17	21.24
2	19.16	9.57	10.87	19.85	19.11	21.45
3	19.16	9.60	10.84	19.90	19.08	21.42
4	19.31	9.67	10.80	19.94	19.07	21.21
5	19.57	9.53	10.62	19.75	19.21	21.33
6	19.77	9.64	10.77	19.69	18.91	21.22
7	19.80	9.73	10.77	19.75	18.77	21.18
8	19.83	9.64	10.70	19.70	18.90	21.23

Monteburns Spectrum for Each Predictor Step for material 5

	<.1eV	<1eV	<100eV	<100keV	<1MeV	<20MeV
0	18.71	9.57	10.90	20.13	19.18	21.51
1	18.44	9.47	10.90	20.33	19.30	21.57
1	18.49	9.61	10.92	20.27	19.25	21.46

2	18.33	9.55	10.89	20.33	19.33	21.57
3	18.51	9.42	10.98	20.19	19.45	21.47
4	18.54	9.43	11.06	20.25	19.33	21.39
5	18.66	9.58	10.89	19.99	19.37	21.52
6	18.73	9.58	10.93	20.09	19.18	21.49
7	18.80	9.49	10.92	20.12	19.25	21.42
8	18.86	9.56	10.76	20.09	19.47	21.26

Monteburns Spectrum for Each Predictor Step for material 6

	<.1eV	<1eV	<100eV	<100keV	<1MeV	<20MeV
0	19.30	9.64	10.80	19.84	19.10	21.31
1	18.93	9.61	10.99	19.98	19.20	21.29
1	19.06	9.58	10.90	19.89	19.21	21.36
2	19.13	9.61	10.76	19.94	19.18	21.38
3	19.05	9.58	10.87	19.98	19.20	21.32
4	19.30	9.59	10.79	19.92	19.08	21.31
5	19.45	9.68	10.87	19.72	19.04	21.25
6	19.41	9.63	10.72	19.82	18.96	21.46
7	19.59	9.63	10.78	19.74	19.02	21.25
8	19.61	9.68	10.77	19.76	19.07	21.12

Monteburns Spectrum for Each Predictor Step for material 7

	<.1eV	<1eV	<100eV	<100keV	<1MeV	<20MeV
0	18.81	9.64	10.84	19.99	19.23	21.48
1	18.72	9.56	10.84	20.05	19.38	21.43
1	18.66	9.57	10.87	20.08	19.32	21.50
2	18.83	9.49	10.86	20.08	19.24	21.50
3	18.55	9.58	10.90	20.16	19.23	21.57
4	18.77	9.52	10.82	20.03	19.32	21.54
5	18.78	9.52	10.88	20.19	19.17	21.46
6	18.72	9.58	10.86	20.10	19.27	21.47
7	18.94	9.51	10.85	20.01	19.24	21.46
8	19.07	9.50	10.83	19.95	19.33	21.32

Monteburns Spectrum for Each Predictor Step for material 8

	<.1eV	<1eV	<100eV	<100keV	<1MeV	<20MeV
0	19.14	9.53	10.80	19.98	19.19	21.36
1	18.93	9.58	10.85	20.04	19.24	21.36
1	18.95	9.62	10.89	19.97	19.23	21.35
2	18.76	9.52	10.84	20.12	19.25	21.50
3	18.84	9.58	10.92	19.90	19.30	21.46
4	18.94	9.54	10.81	19.98	19.35	21.38
5	19.17	9.54	10.86	19.98	19.10	21.34
6	19.21	9.59	10.86	19.88	19.14	21.33
7	19.23	9.58	10.83	19.95	19.08	21.32
8	19.39	9.60	10.79	19.96	19.02	21.24

Monteburns Spectrum for Each Predictor Step for material 9

	<.1eV	<1eV	<100eV	<100keV	<1MeV	<20MeV
0	21.04	9.70	10.48	19.27	18.60	20.90
1	20.74	9.69	10.51	19.33	18.69	21.04
1	20.79	9.70	10.56	19.29	18.56	21.09
2	20.86	9.62	10.46	19.20	18.65	21.21
3	20.73	9.74	10.53	19.26	18.71	21.03
4	20.73	9.68	10.43	19.34	18.80	21.03
5	20.83	9.64	10.53	19.35	18.64	21.01
6	21.00	9.72	10.45	19.07	18.67	21.09
7	20.97	9.67	10.43	19.22	18.72	20.99
8	21.08	9.61	10.45	19.26	18.71	20.89

Monteburns Spectrum for Each Predictor Step for material 10

	<.1eV	<1eV	<100eV	<100keV	<1MeV	<20MeV
0	21.42	9.67	10.45	19.05	18.54	20.87
1	20.86	9.77	10.50	19.25	18.62	20.98
1	20.87	9.66	10.48	19.27	18.73	21.00
2	20.78	9.72	10.53	19.19	18.82	20.96
3	20.81	9.66	10.47	19.25	18.72	21.09

4	20.97	9.71	10.45	19.25	18.67	20.95
5	21.07	9.72	10.45	19.18	18.59	20.99
6	21.11	9.64	10.46	19.25	18.62	20.91
7	21.16	9.68	10.42	19.14	18.80	20.81
8	21.15	9.73	10.43	19.24	18.51	20.94

Monteburns Spectrum for Each Predictor Step for material 11

	<.1eV	<1eV	<100eV	<100keV	<1MeV	<20MeV
0	19.70	9.48	10.88	19.87	19.00	21.07
1	19.10	9.40	10.91	20.22	19.20	21.17
1	18.84	9.65	10.98	20.17	19.10	21.27
2	19.48	9.42	10.67	20.13	18.86	21.43
3	19.42	9.39	11.00	19.64	19.40	21.15
4	19.70	9.47	10.91	19.87	18.64	21.41
5	19.91	9.40	10.77	19.78	18.78	21.35
6	19.86	9.47	10.95	19.52	18.91	21.29
7	19.74	9.46	10.57	19.94	18.89	21.40
8	20.23	9.60	10.81	19.51	18.77	21.08

Monteburns Spectrum for Each Predictor Step for material 12

	<.1eV	<1eV	<100eV	<100keV	<1MeV	<20MeV
0	22.16	10.03	10.50	19.02	17.94	20.35
1	21.50	10.02	10.51	18.65	18.68	20.64
1	21.28	9.97	10.43	18.99	18.34	20.99
2	21.56	9.64	10.69	18.95	18.46	20.69
3	21.57	9.74	10.42	19.31	18.20	20.76
4	21.85	9.98	10.70	18.61	18.04	20.80
5	21.69	9.95	10.27	19.04	18.26	20.80
6	21.73	9.89	10.35	19.03	18.56	20.44
7	21.55	9.96	10.47	19.16	18.34	20.53
8	22.27	9.86	10.57	18.76	18.16	20.38

NOTE: Only steps initial and final steps for Material 1 (Material 20 in MCNPX, Ring B-upper) are given here as an example because the full printout was approximately 400 pages.

Fractional Importance of Radionuclides Sent From ORIGEN2 to MCNP

Fractional Importance of Radionuclides Sent From ORIGEN2
to MCNP for material 1

step#		isotope	grams	mass fra	atom fra	capture	fission
0	14	10010	1.14E+02	1.59E-02	6.09E-01	2.55E-01	0.00E+00
0	15	400900	3.31E+03	4.63E-01	1.97E-01	5.96E-02	0.00E+00
0	16	400910	7.23E+02	1.01E-01	4.25E-02	1.41E-01	0.00E+00
0	17	400920	1.10E+03	1.54E-01	6.42E-02	4.21E-02	0.00E+00
0	18	400940	1.12E+03	1.56E-01	6.37E-02	1.49E-02	0.00E+00
0	19	400960	1.80E+02	2.52E-02	1.00E-02	2.14E-02	0.00E+00
0	1	451030	7.16E-33	1.00E-36	3.72E-37	1.65E-34	0.00E+00automatic
0	2	541310	7.16E-33	1.00E-36	2.92E-37	1.08E-34	0.00E+00automatic
0	4	601430	7.16E-33	1.00E-36	2.68E-37	9.27E-35	0.00E+00automatic
0	5	611470	7.16E-33	1.00E-36	2.61E-37	1.95E-34	0.00E+00automatic
0	6	621490	7.16E-33	1.00E-36	2.57E-37	2.26E-32	0.00E+00automatic
0	7	621510	7.16E-33	1.00E-36	2.54E-37	2.22E-33	0.00E+00automatic
0	8	922350	1.20E+02	1.68E-02	2.74E-03	3.46E-01	9.91E-01
0	9	922380	4.89E+02	6.82E-02	1.10E-02	1.20E-01	8.55E-03
0	11	942400	7.16E-33	1.00E-36	1.60E-37	2.00E-34	7.23E-37automatic
0	12	942410	7.16E-33	1.00E-36	1.59E-37	7.42E-35	1.46E-34automatic

```
  1  14     10010  1.14E+02  1.59E-02  6.09E-01  2.54E-01  0.00E+00
  1  15     10020  7.93E-04  1.11E-07  2.12E-06  6.17E-10  0.00E+00
  1  16    400900  3.31E+03  4.63E-01  1.97E-01  2.57E-02  0.00E+00
  1  17    400910  7.23E+02  1.01E-01  4.25E-02  6.47E-02  0.00E+00
  1  18    400920  1.10E+03  1.54E-01  6.42E-02  2.46E-02  0.00E+00
  1  19    400930  3.61E-03  5.04E-07  2.08E-07  1.27E-06  0.00E+00
  1  20    400940  1.12E+03  1.56E-01  6.37E-02  7.18E-03  0.00E+00
  1  21    400960  1.80E+02  2.52E-02  1.00E-02  5.70E-03  0.00E+00
  1   8    922350  1.19E+02  1.67E-02  2.72E-03  3.58E-01  9.96E-01
  1  22    922360  1.32E-01  1.84E-05  2.99E-06  1.35E-04  1.85E-06
  1   9    922380  4.89E+02  6.82E-02  1.10E-02  1.82E-01  3.09E-03
  1  23    932390  1.40E-02  1.96E-06  3.14E-07  2.12E-05  4.18E-07
  1  10    942390  5.34E-02  7.46E-06  1.20E-06  7.02E-04  7.73E-04
  1  11    942400  1.19E-04  1.66E-08  2.64E-09  4.15E-06  4.37E-09
  1  12    942410  4.64E-07  6.48E-11  1.03E-11  5.31E-09  7.97E-09automatic
  1  13    942420  4.58E-10  6.39E-14  1.01E-14  1.91E-12  1.19E-14automatic
  1  24    360830  1.32E-03  1.84E-07  8.49E-08  1.08E-05  0.00E+00
  1  25    360860  5.18E-03  7.23E-07  3.22E-07  1.94E-08  0.00E+00
***** MB WARNING: mcnp xs not found        360870
  1  26    370870  6.67E-03  9.31E-07  4.10E-07  1.88E-07  0.00E+00
  1  27    380880  9.78E-03  1.36E-06  5.94E-07  4.41E-09  0.00E+00
***** MB WARNING: mcnp xs not found        380890
  1  28    380900  1.54E-02  2.15E-06  9.15E-07  4.77E-07  0.00E+00
  1  16    400900  3.31E+03  3.86E-09  1.64E-09  2.15E-10  0.00E+00repeat
  1  29    390910  1.43E-02  1.99E-06  8.39E-07  8.26E-07  0.00E+00
  1  17    400910  7.23E+02  1.91E-07  8.06E-08  1.23E-07  0.00E+00repeat
  1  18    400920  1.10E+03  2.25E-06  9.38E-07  3.59E-07  0.00E+00repeat
  1  19    400930  2.09E-02  2.42E-06  9.95E-07  6.11E-06  0.00E+00repeat
  1  20    400940  1.12E+03  2.44E-06  9.96E-07  1.12E-07  0.00E+00repeat
  1  30    400950  1.67E-02  2.33E-06  9.40E-07  1.30E-06  0.00E+00
  1  21    400960  1.80E+02  2.52E-06  1.01E-06  5.72E-07  0.00E+00repeat
  1  31    430990  1.32E-02  1.84E-06  7.11E-07  3.88E-05  0.00E+00
  1  32    441010  1.53E-02  2.14E-06  8.13E-07  1.43E-05  0.00E+00
***** MB WARNING: mcnp xs not found        441020
  1  33    441030  8.47E-03  1.18E-06  4.40E-07  6.99E-06  0.00E+00
  1   1    451030  1.27E-03  1.77E-07  6.59E-08  2.05E-05  0.00E+00
***** MB WARNING: mcnp xs not found        441040
  1  34    451050  4.26E-04  5.95E-08  2.17E-08  1.32E-04  0.00E+00
  1  35    461050  2.79E-03  3.89E-07  1.42E-07  3.25E-06  0.00E+00
***** MB WARNING: mcnp xs not found        461070
  1  36    461080  3.07E-04  4.29E-08  1.52E-08  6.43E-07  0.00E+00
  1  37    471090  1.46E-04  2.04E-08  7.19E-09  1.67E-06  0.00E+00
***** MB WARNING: mcnp xs not found        481130
***** MB WARNING: mcnp xs not found        491150
  1  38    531290  2.57E-03  3.59E-07  1.06E-07  2.05E-06  0.00E+00
***** MB WARNING: mcnp xs not found        521300
***** MB WARNING: mcnp xs not found        531310
  1   2    541310  5.07E-03  7.07E-07  2.07E-07  4.75E-05  0.00E+00
***** MB WARNING: mcnp xs not found        521320
***** MB WARNING: mcnp xs not found        541320
***** MB WARNING: mcnp xs not found        541330
  1  39    551330  1.39E-02  1.94E-06  5.60E-07  3.58E-05  0.00E+00
  1  40    541340  3.06E-02  4.28E-06  1.22E-06  3.22E-07  0.00E+00
  1   3    541350  4.20E-04  5.86E-08  1.66E-08  6.58E-02  0.00E+00
  1  41    551350  1.21E-02  1.69E-06  4.79E-07  6.83E-06  0.00E+00
***** MB WARNING: mcnp xs not found        541360
  1  42    551370  2.51E-02  3.50E-06  9.78E-07  1.49E-07  0.00E+00
  1  43    561380  2.80E-02  3.91E-06  1.09E-06  2.31E-07  0.00E+00
***** MB WARNING: mcnp xs not found        571390
***** MB WARNING: mcnp xs not found        561400
***** MB WARNING: mcnp xs not found        571400
***** MB WARNING: mcnp xs not found        581400
***** MB WARNING: mcnp xs not found        581410
  1  44    591410  3.76E-03  5.24E-07  1.42E-07  1.28E-06  0.00E+00
***** MB WARNING: mcnp xs not found        581420
***** MB WARNING: mcnp xs not found        581430
***** MB WARNING: mcnp xs not found        591430
```

```
  1   4    601430  6.52E-03  9.10E-07  2.44E-07  9.80E-05  0.00E+00
***** MB WARNING: mcnp xs not found        581440
  1  45    601450  1.66E-02  2.31E-06  6.12E-07  3.41E-05  0.00E+00
***** MB WARNING: mcnp xs not found        601460
  1  46    601470  6.29E-03  8.77E-07  2.29E-07  2.74E-05  0.00E+00
  1   5    611470  3.72E-03  5.19E-07  1.35E-07  4.58E-05  0.00E+00
  1  47    601480  7.50E-03  1.05E-06  2.71E-07  1.40E-06  0.00E+00
  1  48    611480  2.37E-06  3.30E-10  8.55E-11  5.97E-07  0.00E+00
***** MB WARNING: mcnp xs not found        611481
  1  49    611490  9.45E-04  1.32E-07  3.39E-08  2.68E-05  0.00E+00
  1   6    621490  2.75E-03  3.84E-07  9.88E-08  1.03E-02  0.00E+00
  1  50    621500  1.14E-03  1.59E-07  4.06E-08  3.70E-06  0.00E+00
***** MB WARNING: mcnp xs not found        611510
  1   7    621510  1.63E-03  2.27E-07  5.76E-08  7.65E-04  0.00E+00
  1  51    621520  1.33E-03  1.86E-07  4.69E-08  2.11E-05  0.00E+00
***** MB WARNING: mcnp xs not found        621530
  1  52    631530  6.35E-04  8.86E-08  2.22E-08  9.50E-06  0.00E+00
  1  53    631550  1.67E-04  2.34E-08  5.77E-09  1.26E-05  0.00E+00
***** MB WARNING: mcnp xs not found        631560
  1  54    641570  2.71E-05  3.78E-09  9.21E-10  6.44E-05  0.00E+00

  1  14     10010  1.14E+02  1.59E-02  6.09E-01  2.50E-01  0.00E+00
  1  15     10020  7.84E-04  1.09E-07  2.10E-06  1.34E-09  0.00E+00
  1  16    400900  3.31E+03  4.63E-01  1.97E-01  2.55E-02  0.00E+00
  1  17    400910  7.23E+02  1.01E-01  4.25E-02  6.43E-02  0.00E+00
  1  18    400920  1.10E+03  1.54E-01  6.42E-02  2.50E-02  0.00E+00
  1  19    400930  3.69E-03  5.16E-07  2.12E-07  7.82E-07  0.00E+00
  1  20    400940  1.12E+03  1.56E-01  6.37E-02  7.44E-03  0.00E+00
  1  21    400960  1.80E+02  2.52E-02  1.00E-02  5.74E-03  0.00E+00
  1   8    922350  1.19E+02  1.67E-02  2.72E-03  3.53E-01  9.96E-01
  1  22    922360  1.31E-01  1.83E-05  2.97E-06  1.58E-04  2.78E-06
  1   9    922380  4.89E+02  6.82E-02  1.10E-02  1.92E-01  3.19E-03
  1  23    932390  1.49E-02  2.07E-06  3.33E-07  4.12E-05  5.49E-07
  1  10    942390  5.66E-02  7.90E-06  1.27E-06  7.43E-04  8.26E-04
  1  11    942400  1.33E-04  1.86E-08  2.97E-09  4.74E-06  5.09E-09
  1  12    942410  5.45E-07  7.60E-11  1.21E-11  6.17E-09  9.38E-09automatic
  1  13    942420  5.45E-10  7.61E-14  1.20E-14  2.29E-12  1.46E-14automatic
  1  24    360830  1.30E-03  1.82E-07  8.40E-08  2.22E-05  0.00E+00
  1  25    360860  5.13E-03  7.15E-07  3.19E-07  2.95E-08  0.00E+00
***** MB WARNING: mcnp xs not found        360870
  1  26    370870  6.61E-03  9.22E-07  4.06E-07  1.95E-07  0.00E+00
  1  27    380880  9.68E-03  1.35E-06  5.88E-07  1.31E-08  0.00E+00
***** MB WARNING: mcnp xs not found        380890
  1  28    380900  1.52E-02  2.13E-06  9.06E-07  3.80E-08  0.00E+00
  1  16    400900  3.31E+03  3.83E-09  1.63E-09  2.11E-10  0.00E+00repeat
  1  29    390910  1.41E-02  1.97E-06  8.30E-07  1.76E-06  0.00E+00
  1  17    400910  7.23E+02  1.89E-07  7.98E-08  1.21E-07  0.00E+00repeat
  1  18    400920  1.10E+03  2.23E-06  9.29E-07  3.62E-07  0.00E+00repeat
  1  19    400930  2.08E-02  2.39E-06  9.85E-07  3.63E-06  0.00E+00repeat
  1  20    400940  1.12E+03  2.42E-06  9.86E-07  1.15E-07  0.00E+00repeat
  1  30    400950  1.65E-02  2.31E-06  9.31E-07  2.56E-06  0.00E+00
  1  21    400960  1.80E+02  2.50E-06  9.97E-07  5.70E-07  0.00E+00repeat
  1  31    430990  1.30E-02  1.82E-06  7.04E-07  5.48E-05  0.00E+00
  1  32    441010  1.52E-02  2.12E-06  8.05E-07  1.82E-05  0.00E+00
***** MB WARNING: mcnp xs not found        441020
  1  33    441030  8.38E-03  1.17E-06  4.35E-07  8.53E-06  0.00E+00
  1   1    451030  1.26E-03  1.75E-07  6.52E-08  1.99E-05  0.00E+00
***** MB WARNING: mcnp xs not found        441040
  1  34    451050  4.17E-04  5.82E-08  2.12E-08  2.97E-04  0.00E+00
  1  35    461050  2.73E-03  3.81E-07  1.39E-07  5.43E-06  0.00E+00
***** MB WARNING: mcnp xs not found        461070
  1  36    461080  3.04E-04  4.25E-08  1.51E-08  6.09E-07  0.00E+00
  1  37    471090  1.45E-04  2.03E-08  7.13E-09  2.13E-06  0.00E+00
***** MB WARNING: mcnp xs not found        481130
***** MB WARNING: mcnp xs not found        491150
  1  38    531290  2.54E-03  3.55E-07  1.05E-07  2.57E-06  0.00E+00
***** MB WARNING: mcnp xs not found        521300
```

```
***** MB WARNING: mcnp xs not found        531310
  1   2    541310  5.02E-03  7.00E-07  2.05E-07  4.76E-05  0.00E+00
***** MB WARNING: mcnp xs not found        521320
***** MB WARNING: mcnp xs not found        541320
***** MB WARNING: mcnp xs not found        541330
  1  39    551330  1.38E-02  1.92E-06  5.54E-07  4.60E-05  0.00E+00
  1  40    541340  3.03E-02  4.23E-06  1.21E-06  9.75E-07  0.00E+00
  1   3    541350  4.19E-04  5.85E-08  1.66E-08  6.43E-02  0.00E+00
  1  41    551350  1.21E-02  1.68E-06  4.77E-07  9.04E-06  0.00E+00
***** MB WARNING: mcnp xs not found        541360
  1  42    551370  2.48E-02  3.46E-06  9.69E-07  3.47E-07  0.00E+00
  1  43    561380  2.77E-02  3.87E-06  1.07E-06  5.59E-07  0.00E+00
***** MB WARNING: mcnp xs not found        571390
***** MB WARNING: mcnp xs not found        561400
***** MB WARNING: mcnp xs not found        571400
***** MB WARNING: mcnp xs not found        581400
***** MB WARNING: mcnp xs not found        581410
  1  44    591410  3.72E-03  5.19E-07  1.41E-07  1.80E-06  0.00E+00
***** MB WARNING: mcnp xs not found        581420
***** MB WARNING: mcnp xs not found        581430
***** MB WARNING: mcnp xs not found        591430
  1   4    601430  6.45E-03  9.00E-07  2.41E-07  9.57E-05  0.00E+00
***** MB WARNING: mcnp xs not found        581440
  1  45    601450  1.64E-02  2.29E-06  6.05E-07  4.94E-05  0.00E+00
***** MB WARNING: mcnp xs not found        601460
  1  46    601470  6.22E-03  8.69E-07  2.26E-07  3.32E-05  0.00E+00
  1   5    611470  3.68E-03  5.14E-07  1.34E-07  4.79E-05  0.00E+00
  1  47    601480  7.42E-03  1.04E-06  2.68E-07  1.66E-06  0.00E+00
***** MB WARNING: mcnp xs not found        611481
  1  48    611490  9.34E-04  1.30E-07  3.35E-08  6.30E-05  0.00E+00
  1   6    621490  2.74E-03  3.82E-07  9.82E-08  1.00E-02  0.00E+00
  1  49    621500  1.12E-03  1.56E-07  3.99E-08  6.61E-06  0.00E+00
***** MB WARNING: mcnp xs not found        611510
  1   7    621510  1.61E-03  2.25E-07  5.71E-08  7.45E-04  0.00E+00
  1  50    621520  1.32E-03  1.84E-07  4.63E-08  3.01E-05  0.00E+00
***** MB WARNING: mcnp xs not found        621530
  1  51    631530  6.29E-04  8.78E-08  2.20E-08  1.21E-05  0.00E+00
  1  52    631550  1.62E-04  2.26E-08  5.60E-09  4.08E-05  0.00E+00
***** MB WARNING: mcnp xs not found        631560
  1  53    641570  1.65E-05  2.30E-09  5.60E-10  1.24E-04  0.00E+00

  1  14     10010  1.14E+02  1.59E-02  6.09E-01  2.51E-01  0.00E+00
  1  15     10020  1.58E-03  2.20E-07  4.22E-06  2.71E-09  0.00E+00
  1  16    400900  3.31E+03  4.63E-01  1.97E-01  2.48E-02  0.00E+00
  1  17    400910  7.23E+02  1.01E-01  4.25E-02  6.31E-02  0.00E+00
  1  18    400920  1.10E+03  1.54E-01  6.42E-02  2.45E-02  0.00E+00
  1  19    400930  7.26E-03  1.01E-06  4.17E-07  1.52E-06  0.00E+00
  1  20    400940  1.12E+03  1.56E-01  6.37E-02  7.45E-03  0.00E+00
  1  21    400960  1.80E+02  2.52E-02  1.00E-02  6.75E-03  0.00E+00
  1   8    922350  1.19E+02  1.66E-02  2.70E-03  3.52E-01  9.95E-01
  1  22    922360  2.63E-01  3.68E-05  5.97E-06  3.00E-04  5.39E-06
  1  23    922370  1.11E-04  1.55E-08  2.50E-09  6.64E-07  1.85E-09
  1   9    922380  4.89E+02  6.82E-02  1.10E-02  1.85E-01  3.14E-03
  1  24    932370  2.20E-04  3.07E-08  4.96E-09  9.55E-07  8.30E-09
  1  25    932390  1.45E-02  2.02E-06  3.24E-07  3.99E-05  5.32E-07
  1  10    942390  1.23E-01  1.71E-05  2.74E-06  1.61E-03  1.80E-03
  1  11    942400  5.85E-04  8.17E-08  1.30E-08  1.97E-05  2.21E-08
  1  12    942410  4.67E-06  6.52E-10  1.04E-10  5.29E-08  8.08E-08automatic
  1  13    942420  9.60E-09  1.34E-12  2.12E-13  4.30E-11  2.55E-13automatic
  1  26    350810  1.03E-03  1.43E-07  6.79E-08  7.28E-07  0.00E+00
  1  27    360830  2.64E-03  3.68E-07  1.70E-07  4.55E-05  0.00E+00
  1  28    360840  5.15E-03  7.19E-07  3.28E-07  2.46E-07  0.00E+00
  1  29    370850  5.03E-03  7.02E-07  3.17E-07  4.78E-07  0.00E+00
  1  30    360860  1.03E-02  1.44E-06  6.39E-07  5.98E-08  0.00E+00
***** MB WARNING: mcnp xs not found        360870
  1  31    370870  1.33E-02  1.85E-06  8.17E-07  3.41E-07  0.00E+00
  1  32    380880  1.95E-02  2.73E-06  1.19E-06  2.63E-08  0.00E+00
```

```
***** MB WARNING: mcnp xs not found        380890
  1  33    390890  4.90E-03  6.84E-07  2.94E-07  2.35E-07  0.00E+00
  1  34    380900  3.06E-02  4.27E-06  1.82E-06  7.57E-08  0.00E+00
  1  16    400900  3.31E+03  9.84E-09  4.19E-09  5.28E-10  0.00E+00repeat
  1  35    390910  2.63E-02  3.68E-06  1.55E-06  3.25E-06  0.00E+00
  1  17    400910  7.23E+02  7.42E-07  3.12E-07  4.64E-07  0.00E+00repeat
  1  18    400920  1.10E+03  4.53E-06  1.89E-06  7.18E-07  0.00E+00repeat
  1  19    400930  4.23E-02  4.89E-06  2.02E-06  7.33E-06  0.00E+00repeat
  1  20    400940  1.12E+03  4.86E-06  1.98E-06  2.32E-07  0.00E+00repeat
  1  36    400950  3.05E-02  4.26E-06  1.72E-06  4.45E-06  0.00E+00
  1  37    410950  4.62E-03  6.45E-07  2.60E-07  1.33E-06  0.00E+00
  1  21    400960  1.80E+02  5.02E-06  2.00E-06  1.35E-06  0.00E+00repeat
  1  38    430990  3.07E-02  4.28E-06  1.66E-06  1.26E-04  0.00E+00
  1  39    441010  3.05E-02  4.26E-06  1.62E-06  3.73E-05  0.00E+00
***** MB WARNING: mcnp xs not found        441020
  1  40    441030  1.47E-02  2.06E-06  7.65E-07  1.50E-05  0.00E+00
  1   1    451030  4.62E-03  6.45E-07  2.40E-07  7.34E-05  0.00E+00
***** MB WARNING: mcnp xs not found        441040
  1  41    451050  4.19E-04  5.85E-08  2.13E-08  2.99E-04  0.00E+00
  1  42    461050  5.96E-03  8.31E-07  3.03E-07  1.17E-05  0.00E+00
***** MB WARNING: mcnp xs not found        461070
  1  43    461080  6.17E-04  8.61E-08  3.06E-08  1.32E-06  0.00E+00
  1  44    471090  3.03E-04  4.23E-08  1.49E-08  4.35E-06  0.00E+00
***** MB WARNING: mcnp xs not found        481130
***** MB WARNING: mcnp xs not found        491150
  1  45    531270  8.66E-04  1.21E-07  3.65E-08  1.06E-06  0.00E+00
  1  46    531290  5.25E-03  7.33E-07  2.18E-07  5.30E-06  0.00E+00
***** MB WARNING: mcnp xs not found        521300
***** MB WARNING: mcnp xs not found        531310
  1   2    541310  1.47E-02  2.05E-06  6.00E-07  1.38E-04  0.00E+00
***** MB WARNING: mcnp xs not found        521320
***** MB WARNING: mcnp xs not found        541320
***** MB WARNING: mcnp xs not found        541330
  1  47    551330  3.90E-02  5.44E-06  1.57E-06  1.24E-04  0.00E+00
  1  48    541340  6.11E-02  8.52E-06  2.44E-06  1.94E-06  0.00E+00
  1   3    541350  4.18E-04  5.84E-08  1.66E-08  6.43E-02  0.00E+00
  1  49    551350  2.46E-02  3.44E-06  9.75E-07  1.84E-05  0.00E+00
***** MB WARNING: mcnp xs not found        541360
  1  50    551370  4.98E-02  6.95E-06  1.94E-06  7.00E-07  0.00E+00
  1  51    561380  5.57E-02  7.78E-06  2.16E-06  1.13E-06  0.00E+00
***** MB WARNING: mcnp xs not found        571390
***** MB WARNING: mcnp xs not found        561400
***** MB WARNING: mcnp xs not found        571400
***** MB WARNING: mcnp xs not found        581400
***** MB WARNING: mcnp xs not found        581410
  1  52    591410  1.36E-02  1.90E-06  5.17E-07  6.57E-06  0.00E+00
***** MB WARNING: mcnp xs not found        581420
***** MB WARNING: mcnp xs not found        581430
***** MB WARNING: mcnp xs not found        591430
  1   4    601430  2.33E-02  3.25E-06  8.72E-07  3.46E-04  0.00E+00
***** MB WARNING: mcnp xs not found        581440
  1  53    601450  3.33E-02  4.65E-06  1.23E-06  1.00E-04  0.00E+00
***** MB WARNING: mcnp xs not found        601460
  1  54    601470  8.49E-03  1.18E-06  3.09E-07  4.51E-05  0.00E+00
  1   5    611470  1.13E-02  1.58E-06  4.11E-07  1.37E-04  0.00E+00
  1  55    621470  1.02E-04  1.42E-08  3.70E-09  5.31E-07  0.00E+00
  1  56    601480  1.49E-02  2.08E-06  5.39E-07  3.25E-06  0.00E+00
  1  57    611480  1.04E-05  1.45E-09  3.76E-10  1.03E-06  0.00E+00
***** MB WARNING: mcnp xs not found        611481
  1  58    611490  9.41E-04  1.31E-07  3.38E-08  6.32E-05  0.00E+00
  1   6    621490  4.38E-03  6.12E-07  1.57E-07  1.61E-02  0.00E+00
***** MB WARNING: mcnp xs not found        601500
  1  59    621500  4.33E-03  6.05E-07  1.55E-07  2.50E-05  0.00E+00
***** MB WARNING: mcnp xs not found        611510
  1   7    621510  3.25E-03  4.53E-07  1.15E-07  1.51E-03  0.00E+00
  1  60    621520  2.83E-03  3.95E-07  9.95E-08  6.66E-05  0.00E+00
***** MB WARNING: mcnp xs not found        621530
```

```
   1  61    631530  1.40E-03  1.95E-07  4.89E-08  2.65E-05  0.00E+00
   1  62    631550  3.16E-04  4.41E-08  1.09E-08  7.99E-05  0.00E+00
   1  63    641550  1.83E-06  2.56E-10  6.32E-11  1.05E-06  0.00E+00
 ***** MB WARNING: mcnp xs not found        631560
   1  64    641570  1.95E-05  2.72E-09  6.65E-10  1.48E-04  0.00E+00



8  14     10010  1.14E+02  1.59E-02  6.09E-01  2.51E-01  0.00E+00
   8  15     10020  1.23E-02  1.72E-06  3.30E-05  2.12E-08  0.00E+00
   8  16    400900  3.31E+03  4.63E-01  1.97E-01  2.51E-02  0.00E+00
   8  17    400910  7.23E+02  1.01E-01  4.25E-02  6.28E-02  0.00E+00
   8  18    400920  1.10E+03  1.54E-01  6.42E-02  2.45E-02  0.00E+00
   8  19    400930  5.69E-02  7.94E-06  3.27E-06  1.03E-05  0.00E+00
   8  20    400940  1.12E+03  1.56E-01  6.37E-02  7.33E-03  0.00E+00
   8  21    400950  6.22E-03  8.69E-07  3.50E-07  8.81E-07  0.00E+00
   8  22    400960  1.80E+02  2.52E-02  1.00E-02  5.61E-03  0.00E+00
   8  23    410950  3.11E-03  4.35E-07  1.75E-07  2.49E-06  0.00E+00
   8  24    922340  2.93E-04  4.09E-08  6.69E-09  1.32E-06  9.63E-09
   8   8    922350  1.08E+02  1.51E-02  2.46E-03  3.19E-01  9.81E-01
   8  25    922360  1.96E+00  2.73E-04  4.43E-05  2.13E-03  4.20E-05
   8  26    922370  5.59E-04  7.80E-08  1.26E-08  7.36E-06  1.96E-08
   8   9    922380  4.88E+02  6.81E-02  1.10E-02  1.84E-01  3.29E-03
   8  27    932370  7.59E-03  1.06E-06  1.71E-07  5.23E-05  2.68E-07
   8  28    932390  1.55E-02  2.16E-06  3.46E-07  4.21E-05  5.93E-07
   8  10    942390  9.65E-01  1.35E-04  2.16E-05  1.26E-02  1.53E-02
   8  11    942400  3.60E-02  5.02E-06  8.01E-07  1.24E-03  1.43E-06
   8  12    942410  2.33E-03  3.25E-07  5.16E-08  2.64E-05  4.36E-05
   8  13    942420  3.99E-05  5.57E-09  8.82E-10  1.71E-07  1.11E-09automatic
   8  29    340770  3.48E-04  4.85E-08  2.41E-08  1.30E-06  0.00E+00
   8  30    340800  4.49E-03  6.27E-07  3.00E-07  2.35E-07  0.00E+00
   8  31    350810  7.71E-03  1.08E-06  5.09E-07  2.99E-06  0.00E+00
   8  32    340820  1.22E-02  1.70E-06  7.92E-07  7.85E-08  0.00E+00
   8  33    360830  1.96E-02  2.73E-06  1.26E-06  3.37E-04  0.00E+00
   8  34    360840  3.89E-02  5.43E-06  2.47E-06  1.02E-06  0.00E+00
 ***** MB WARNING: mcnp xs not found        360850
   8  35    370850  3.81E-02  5.32E-06  2.40E-06  3.90E-06  0.00E+00
   8  36    360860  7.69E-02  1.07E-05  4.78E-06  4.37E-07  0.00E+00
 ***** MB WARNING: mcnp xs not found        360870
   8  37    370870  9.96E-02  1.39E-05  6.12E-06  2.75E-06  0.00E+00
   8  38    380880  1.47E-01  2.05E-05  8.92E-06  1.95E-07  0.00E+00
 ***** MB WARNING: mcnp xs not found        380890
   8  39    390890  1.35E-01  1.88E-05  8.11E-06  2.67E-05  0.00E+00
   8  40    380900  2.27E-01  3.17E-05  1.35E-05  5.51E-07  0.00E+00
   8  16    400900  3.31E+03  2.95E-07  1.26E-07  1.60E-08  0.00E+00repeat
   8  41    390910  7.85E-02  1.10E-05  4.61E-06  9.75E-06  0.00E+00
   8  17    400910  7.23E+02  2.26E-05  9.52E-06  1.41E-05  0.00E+00repeat
   8  18    400920  1.10E+03  3.42E-05  1.42E-05  5.45E-06  0.00E+00repeat
   8  19    400930  3.24E-01  3.72E-05  1.53E-05  4.85E-05  0.00E+00repeat
   8  20    400940  1.12E+03  3.64E-05  1.49E-05  1.71E-06  0.00E+00repeat
   8  21    400950  1.01E-01  1.33E-05  5.36E-06  1.35E-05  0.00E+00repeat
   8  23    410950  5.13E-02  6.72E-06  2.71E-06  3.85E-05  0.00E+00repeat
   8  22    400960  1.81E+02  3.76E-05  1.50E-05  8.38E-06  0.00E+00repeat
   8  42    430990  2.59E-01  3.62E-05  1.40E-05  1.04E-03  0.00E+00
   8  43    441010  2.29E-01  3.20E-05  1.21E-05  2.71E-04  0.00E+00
 ***** MB WARNING: mcnp xs not found        441020
   8  44    441030  3.37E-02  4.70E-06  1.75E-06  3.35E-05  0.00E+00
   8   1    451030  1.11E-01  1.55E-05  5.76E-06  1.74E-03  0.00E+00
 ***** MB WARNING: mcnp xs not found        441040
   8  45    451050  4.37E-04  6.10E-08  2.23E-08  3.10E-04  0.00E+00
   8  46    461050  4.89E-02  6.83E-06  2.49E-06  9.58E-05  0.00E+00
 ***** MB WARNING: mcnp xs not found        441060
   8  47    461060  5.47E-03  7.64E-07  2.76E-07  4.31E-07  0.00E+00
 ***** MB WARNING: mcnp xs not found        461070
   8  48    461080  5.33E-03  7.43E-07  2.64E-07  1.06E-05  0.00E+00
   8  49    471090  2.75E-03  3.83E-07  1.35E-07  3.85E-05  0.00E+00
```

```
***** MB WARNING: mcnp xs not found        481110
***** MB WARNING: mcnp xs not found        481130
***** MB WARNING: mcnp xs not found        491150
***** MB WARNING: mcnp xs not found        511210
***** MB WARNING: mcnp xs not found        511230
  8  50    531270  8.43E-03  1.18E-06  3.55E-07  1.12E-05  0.00E+00
***** MB WARNING: mcnp xs not found        521280
  8  51    531290  4.31E-02  6.02E-06  1.79E-06  4.35E-05  0.00E+00
***** MB WARNING: mcnp xs not found        521300
***** MB WARNING: mcnp xs not found        531310
  8   2    541310  1.59E-01  2.22E-05  6.48E-06  1.48E-03  0.00E+00
***** MB WARNING: mcnp xs not found        521320
***** MB WARNING: mcnp xs not found        541320
***** MB WARNING: mcnp xs not found        541330
  8  52    551330  3.85E-01  5.37E-05  1.55E-05  1.20E-03  0.00E+00
  8  53    541340  4.59E-01  6.41E-05  1.83E-05  1.44E-05  0.00E+00
  8  54    551340  1.96E-03  2.73E-07  7.81E-08  1.02E-05  0.00E+00
  8   3    541350  3.99E-04  5.56E-08  1.58E-08  6.15E-02  0.00E+00
  8  55    551350  1.84E-01  2.57E-05  7.28E-06  1.36E-04  0.00E+00
***** MB WARNING: mcnp xs not found        541360
  8  56    551370  3.72E-01  5.19E-05  1.45E-05  5.21E-06  0.00E+00
  8  57    561380  4.19E-01  5.84E-05  1.62E-05  8.45E-06  0.00E+00
***** MB WARNING: mcnp xs not found        571390
***** MB WARNING: mcnp xs not found        561400
***** MB WARNING: mcnp xs not found        571400
***** MB WARNING: mcnp xs not found        581400
***** MB WARNING: mcnp xs not found        581410
  8  58    591410  3.00E-01  4.19E-05  1.14E-05  1.44E-04  0.00E+00
***** MB WARNING: mcnp xs not found        581420
***** MB WARNING: mcnp xs not found        581430
***** MB WARNING: mcnp xs not found        591430
  8   4    601430  3.36E-01  4.68E-05  1.25E-05  4.98E-03  0.00E+00
***** MB WARNING: mcnp xs not found        581440
***** MB WARNING: mcnp xs not found        601440
  8  59    601450  2.51E-01  3.50E-05  9.25E-06  7.44E-04  0.00E+00
***** MB WARNING: mcnp xs not found        601460
  8  60    601470  9.67E-03  1.35E-06  3.52E-07  5.05E-05  0.00E+00
  8   5    611470  1.25E-01  1.75E-05  4.55E-06  1.48E-03  0.00E+00
  8  61    621470  1.07E-02  1.49E-06  3.88E-07  6.56E-05  0.00E+00
  8  62    601480  1.12E-01  1.56E-05  4.05E-06  2.43E-05  0.00E+00
  8  63    611480  1.72E-04  2.40E-08  6.22E-09  1.72E-05  0.00E+00
***** MB WARNING: mcnp xs not found        611481
***** MB WARNING: mcnp xs not found        621480
  8  64    611490  9.47E-04  1.32E-07  3.40E-08  6.34E-05  0.00E+00
  8   6    621490  5.24E-03  7.31E-07  1.88E-07  1.93E-02  0.00E+00
***** MB WARNING: mcnp xs not found        601500
  8  65    621500  6.67E-02  9.30E-06  2.38E-06  3.78E-04  0.00E+00
***** MB WARNING: mcnp xs not found        611510
  8   7    621510  1.38E-02  1.93E-06  4.89E-07  6.47E-03  0.00E+00
  8  66    631510  3.01E-05  4.21E-09  1.07E-09  7.87E-06  0.00E+00
  8  67    621520  3.30E-02  4.60E-06  1.16E-06  7.32E-04  0.00E+00
***** MB WARNING: mcnp xs not found        621530
  8  68    631530  1.22E-02  1.70E-06  4.26E-07  2.32E-04  0.00E+00
***** MB WARNING: mcnp xs not found        621540
  8  69    631540  3.77E-04  5.27E-08  1.31E-08  3.48E-05  0.00E+00
  8  70    631550  1.64E-03  2.29E-07  5.67E-08  4.11E-04  0.00E+00
  8  71    641550  1.95E-05  2.73E-09  6.74E-10  3.52E-05  0.00E+00
***** MB WARNING: mcnp xs not found        631560
  8  72    641560  1.87E-03  2.61E-07  6.41E-08  1.07E-06  0.00E+00
  8  73    641570  2.11E-05  2.95E-09  7.19E-10  1.60E-04  0.00E+00

  8  14     10010  1.14E+02  1.59E-02  6.09E-01  2.53E-01  0.00E+00
  8  15     10020  1.32E-02  1.85E-06  3.53E-05  2.29E-08  0.00E+00
  8  16    400900  3.31E+03  4.63E-01  1.97E-01  2.53E-02  0.00E+00
  8  17    400910  7.23E+02  1.01E-01  4.25E-02  6.42E-02  0.00E+00
  8  18    400920  1.10E+03  1.54E-01  6.42E-02  2.44E-02  0.00E+00
  8  19    400930  6.08E-02  8.49E-06  3.50E-06  1.19E-05  0.00E+00
```

```
  8  20    400940  1.12E+03  1.56E-01  6.37E-02  7.35E-03  0.00E+00
  8  21    400950  6.34E-03  8.85E-07  3.57E-07  9.55E-07  0.00E+00
  8  22    400960  1.80E+02  2.52E-02  1.00E-02  5.87E-03  0.00E+00
  8  23    410950  3.21E-03  4.48E-07  1.81E-07  2.52E-06  0.00E+00
  8  24    922340  3.14E-04  4.39E-08  7.18E-09  1.46E-06  1.03E-08
  8   8    922350  1.07E+02  1.50E-02  2.44E-03  3.19E-01  9.81E-01
  8  25    922360  2.09E+00  2.91E-04  4.72E-05  2.07E-03  4.30E-05
  8  26    922370  5.55E-04  7.74E-08  1.25E-08  7.36E-06  1.92E-08
  8   9    922380  4.88E+02  6.80E-02  1.10E-02  1.77E-01  3.27E-03
  8  27    932370  8.44E-03  1.18E-06  1.90E-07  5.84E-05  2.96E-07
  8  28    932390  1.51E-02  2.11E-06  3.37E-07  4.11E-05  5.75E-07
  8  29    942380  1.30E-04  1.81E-08  2.91E-09  5.89E-07  2.41E-08
  8  10    942390  1.02E+00  1.42E-04  2.28E-05  1.31E-02  1.60E-02
  8  11    942400  4.06E-02  5.67E-06  9.05E-07  1.46E-03  1.61E-06
  8  12    942410  2.86E-03  4.00E-07  6.35E-08  3.25E-05  5.36E-05
  8  13    942420  5.23E-05  7.30E-09  1.15E-09  2.20E-07  1.44E-09automatic
  8  30    340770  3.72E-04  5.19E-08  2.58E-08  1.41E-06  0.00E+00
  8  31    340800  4.80E-03  6.70E-07  3.21E-07  2.52E-07  0.00E+00
  8  32    350810  8.23E-03  1.15E-06  5.43E-07  3.24E-06  0.00E+00
  8  33    340820  1.30E-02  1.81E-06  8.46E-07  8.80E-08  0.00E+00
  8  34    360830  2.09E-02  2.91E-06  1.34E-06  3.62E-04  0.00E+00
  8  35    360840  4.16E-02  5.80E-06  2.64E-06  1.09E-06  0.00E+00
***** MB WARNING: mcnp xs not found        360850
  8  36    370850  4.07E-02  5.68E-06  2.56E-06  4.21E-06  0.00E+00
  8  37    360860  8.21E-02  1.15E-05  5.11E-06  4.68E-07  0.00E+00
***** MB WARNING: mcnp xs not found        360870
  8  38    370870  1.06E-01  1.48E-05  6.53E-06  2.99E-06  0.00E+00
  8  39    380880  1.57E-01  2.19E-05  9.52E-06  2.00E-07  0.00E+00
***** MB WARNING: mcnp xs not found        380890
  8  40    390890  1.47E-01  2.05E-05  8.84E-06  2.93E-05  0.00E+00
  8  41    380900  2.42E-01  3.38E-05  1.44E-05  5.81E-07  0.00E+00
  8  16    400900  3.31E+03  3.33E-07  1.42E-07  1.82E-08  0.00E+00repeat
  8  42    390910  7.96E-02  1.11E-05  4.67E-06  9.84E-06  0.00E+00
  8  17    400910  7.23E+02  2.48E-05  1.04E-05  1.58E-05  0.00E+00repeat
  8  18    400920  1.10E+03  3.66E-05  1.52E-05  5.78E-06  0.00E+00repeat
  8  19    400930  3.46E-01  3.98E-05  1.64E-05  5.56E-05  0.00E+00repeat
  8  20    400940  1.12E+03  3.89E-05  1.59E-05  1.83E-06  0.00E+00repeat
  8  21    400950  1.03E-01  1.35E-05  5.44E-06  1.46E-05  0.00E+00repeat
  8  23    410950  5.27E-02  6.90E-06  2.78E-06  3.88E-05  0.00E+00repeat
  8  22    400960  1.81E+02  4.02E-05  1.60E-05  9.36E-06  0.00E+00repeat
  8  43    430990  2.77E-01  3.87E-05  1.50E-05  1.10E-03  0.00E+00
  8  44    441010  2.45E-01  3.42E-05  1.30E-05  2.77E-04  0.00E+00
***** MB WARNING: mcnp xs not found        441020
  8  45    441030  3.40E-02  4.74E-06  1.76E-06  3.39E-05  0.00E+00
  8   1    451030  1.20E-01  1.68E-05  6.25E-06  1.91E-03  0.00E+00
***** MB WARNING: mcnp xs not found        441040
  8  46    451050  4.45E-04  6.22E-08  2.27E-08  3.18E-04  0.00E+00
  8  47    461050  5.24E-02  7.31E-06  2.67E-06  1.03E-04  0.00E+00
***** MB WARNING: mcnp xs not found        441060
  8  48    461060  6.12E-03  8.55E-07  3.09E-07  5.22E-07  0.00E+00
***** MB WARNING: mcnp xs not found        461070
  8  49    461080  5.74E-03  8.02E-07  2.84E-07  1.19E-05  0.00E+00
  8  50    471090  2.97E-03  4.14E-07  1.46E-07  4.16E-05  0.00E+00
***** MB WARNING: mcnp xs not found        481110
***** MB WARNING: mcnp xs not found        481130
***** MB WARNING: mcnp xs not found        491150
***** MB WARNING: mcnp xs not found        511210
***** MB WARNING: mcnp xs not found        511230
  8  51    531270  9.05E-03  1.26E-06  3.81E-07  1.23E-05  0.00E+00
***** MB WARNING: mcnp xs not found        521280
  8  52    531290  4.61E-02  6.44E-06  1.91E-06  4.69E-05  0.00E+00
***** MB WARNING: mcnp xs not found        521300
***** MB WARNING: mcnp xs not found        531310
  8   2    541310  1.70E-01  2.37E-05  6.93E-06  1.53E-03  0.00E+00
***** MB WARNING: mcnp xs not found        521320
***** MB WARNING: mcnp xs not found        541320
***** MB WARNING: mcnp xs not found        541330
```

```
  8  53    551330  4.12E-01  5.74E-05  1.65E-05  1.28E-03  0.00E+00
  8  54    541340  4.91E-01  6.85E-05  1.96E-05  1.55E-05  0.00E+00
  8  55    551340  2.24E-03  3.13E-07  8.94E-08  1.17E-05  0.00E+00
  8   3    541350  4.00E-04  5.59E-08  1.59E-08  6.24E-02  0.00E+00
  8  56    551350  1.96E-01  2.73E-05  7.76E-06  1.44E-04  0.00E+00
***** MB WARNING: mcnp xs not found        541360
  8  57    551370  3.97E-01  5.54E-05  1.55E-05  5.59E-06  0.00E+00
  8  58    561380  4.47E-01  6.24E-05  1.73E-05  9.05E-06  0.00E+00
***** MB WARNING: mcnp xs not found        571390
***** MB WARNING: mcnp xs not found        561400
***** MB WARNING: mcnp xs not found        571400
***** MB WARNING: mcnp xs not found        581400
***** MB WARNING: mcnp xs not found        581410
  8  59    591410  3.25E-01  4.54E-05  1.23E-05  1.58E-04  0.00E+00
***** MB WARNING: mcnp xs not found        581420
***** MB WARNING: mcnp xs not found        581430
***** MB WARNING: mcnp xs not found        591430
  8   4    601430  3.60E-01  5.02E-05  1.34E-05  5.39E-03  0.00E+00
***** MB WARNING: mcnp xs not found        581440
***** MB WARNING: mcnp xs not found        601440
  8  60    601450  2.68E-01  3.74E-05  9.88E-06  8.00E-04  0.00E+00
***** MB WARNING: mcnp xs not found        601460
  8  61    601470  9.80E-03  1.37E-06  3.56E-07  5.07E-05  0.00E+00
  8   5    611470  1.33E-01  1.86E-05  4.84E-06  1.57E-03  0.00E+00
  8  62    621470  1.22E-02  1.70E-06  4.42E-07  7.64E-05  0.00E+00
  8  63    601480  1.20E-01  1.67E-05  4.32E-06  2.52E-05  0.00E+00
  8  64    611480  1.84E-04  2.57E-08  6.65E-09  1.85E-05  0.00E+00
***** MB WARNING: mcnp xs not found        611481
***** MB WARNING: mcnp xs not found        621480
  8  65    611490  9.63E-04  1.34E-07  3.45E-08  6.51E-05  0.00E+00
  8   6    621490  5.25E-03  7.33E-07  1.88E-07  1.93E-02  0.00E+00
***** MB WARNING: mcnp xs not found        601500
  8  66    621500  7.16E-02  9.99E-06  2.55E-06  4.15E-04  0.00E+00
***** MB WARNING: mcnp xs not found        611510
  8   7    621510  1.41E-02  1.97E-06  5.00E-07  6.72E-03  0.00E+00
  8  67    631510  3.21E-05  4.49E-09  1.14E-09  8.46E-06  0.00E+00
  8  68    621520  3.58E-02  5.00E-06  1.26E-06  8.03E-04  0.00E+00
  8  69    631520  1.43E-05  1.99E-09  5.02E-10  5.60E-07  0.00E+00
***** MB WARNING: mcnp xs not found        621530
  8  70    631530  1.31E-02  1.83E-06  4.59E-07  2.50E-04  0.00E+00
***** MB WARNING: mcnp xs not found        621540
  8  71    631540  4.31E-04  6.01E-08  1.49E-08  3.97E-05  0.00E+00
  8  72    631550  1.71E-03  2.39E-07  5.90E-08  4.31E-04  0.00E+00
  8  73    641550  2.02E-05  2.81E-09  6.95E-10  3.70E-05  0.00E+00
***** MB WARNING: mcnp xs not found        631560
  8  74    641560  2.07E-03  2.88E-07  7.08E-08  1.27E-06  0.00E+00
  8  75    641570  2.10E-05  2.93E-09  7.15E-10  1.62E-04  0.00E+00
```

END MATERIAL 1 PRINTOUT

A.5 UT-RACE Experiment Review Package

RACE Project Linear Electron Accelerator-Reactor Coupling

The radiation producing machine is a Varian Clinac 20 (serial number 133-435-01) reconfigured to produce 10^{11} to 10^{13} neutrons per second via bremsstrahlung radiation and subsequent photofission or photoneutron production in a high-Z target located adjacent to the 1 MW NETL research reactor. The Clinac is not to be used for human or animal irradiations but will provide a large neutron source for the NETL TRIGA research reactor in a subcritical or near critical configuration. The experimental project is to simulate the operation of an accelerator driven subcritical system for computational benchmarking and transient or feedback response of the system.

The overall research project is titled Reactor-Accelerator Coupling Experiments (RACE) and is directed and funded by the Idaho Accelerator Center of the Idaho State University (ISU) located in Pocatello, Idaho. The project is a multi-university collaboration involving ISU, the University of Nevada-Las Vegas, Texas A&M University, The University of Texas at Austin and the University of Michigan. The project has recently been endorsed by EUROTRANS, the European Union transmutation research consortium. An official Memorandum of Understanding was signed in June 2005 between the European Union representatives, the Department of Energy, Idaho State University, Texas A&M University and The University of Texas at Austin forming an international research partnership involving 10 countries and 14 nuclear research laboratories.

Scope of Safety Review

Current proposals are that the RACE Program will have two main phases; a low power phase (< 1 kW beam) and a high power phase (20-30 kW beam). This experiment review only covers the low power phase of operation utilizing the NETL Beam Port 5. This low power phase is expected to be performed over a one year period with smaller projects occurring into 2007. So-called RACE-ECATS, the high power phase (unfunded at this time), will require significantly greater engineering design and safety analysis.

RACE-ECATS would be performed with much greater participation of the European partners and the Department of Energy.

Purpose of RACE Experiments:

1. Support international efforts in high level radioactive waste transmutation
2. Design, model and conduct electron accelerator-reactor coupling experiments as a first-of-its-kind experiment
3. Predict and measure subcriticality and subcritical multiplication with and without thermal feedback
4. Predict and analyze unique subcritical source-driven transients and reactivity control methods
5. Evaluate neutron instrumentation in high gamma flash background
6. Evaluate asymmetric injection ADSS design concepts
7. Investigate power/current/source importance relationships
8. Determine optimum methods of operating ADSS

Accelerator Configuration and Location

The linear electron accelerator (Linac) is to be used in a horizontal configuration in the shielded area of neutron beam port number 5 (BP5) in Room 1.104 of the NETL. The operation of the linac at the NETL for the BP5 experiment has been authorized by the Texas Department of Health Services. Any changes to the machine (increase in power, etc) require a new application to the State of Texas. The physical location of the accelerator (BP5) is shown below. This experimental area has been configured for approximately 10 years for neutron radiography utilizing a collimated thermal neutron beam from the reactor. Recently the shielding walls were rebuilt in a new configuration with more efficient use of space and reduced scattered radiation out of the "cave" area. The BP5 is considered a tangential neutron beam and the beam pipe passes along side the TRIGA nuclear reactor core.

The Linac beam will be focused on a high atomic weight target (tungsten-copper) located directly adjacent to the reactor core. Bremsstrahlung radiation from the interaction of the electrons with the target material will cause photoneutron production within the target. Therefore, the primary radiation source will be located within the reactor tank and thus heavily shielded. Gamma ray flash and neutrons from the source traveling backward into the accelerator will be shielded within the concrete block structure surrounding the linac. Because the NETL has an active neutron radiography and reactor research program, the intention is to install the linac such that the beam pipe and target may be removed routinely for normal reactor experiments. The linac is mobile (although heavy) and may be rolled out of the way within the BP5 cave when necessary. The 12 foot long beam pipe may then be extracted from the beam port tube.

The actual neutron production will occur near the reactor within the linac target. The reactor will not be "on" or critical during the experiments. Calculations using MCNP, a Monte Carlo code, indicate the designed system will bring the NETL TRIGA to an equivalent reactor power of approximately 1 to 2 kW[1]. The design configuration will have no bends in the beam pipe and therefore no expected synchrotron radiation production. BP5/BP1 is a single beam pipe (a through-port) that allows simultaneous use of both experiment areas. BP1 will be plugged with neutron and gamma radiation shield plugs preventing any radiation streaming from BP1. Backscatter of neutron radiation from the target and reactor will produce some activation of accelerator components but this is not expected to be a radiation hazard based on experiences in Idaho.

Bremsstrahlung neutron production

The rate at which electromagnetic energy is radiated from a slowing down (or speeding up) electron is proportional to the square of the acceleration. The force on the electron is greater with high atomic mass (high Z) elements. The photons produced by the slowing down electrons (de-accelerated) are called *Bremsstrahlung* (German for "braking radiation"). For a thick target, the following graph indicates the relative photon yield for different energy electrons[2]. Note that the highest photon energy created is also

the highest energy electrons. Several photons may be produced by a single electron slowing down.

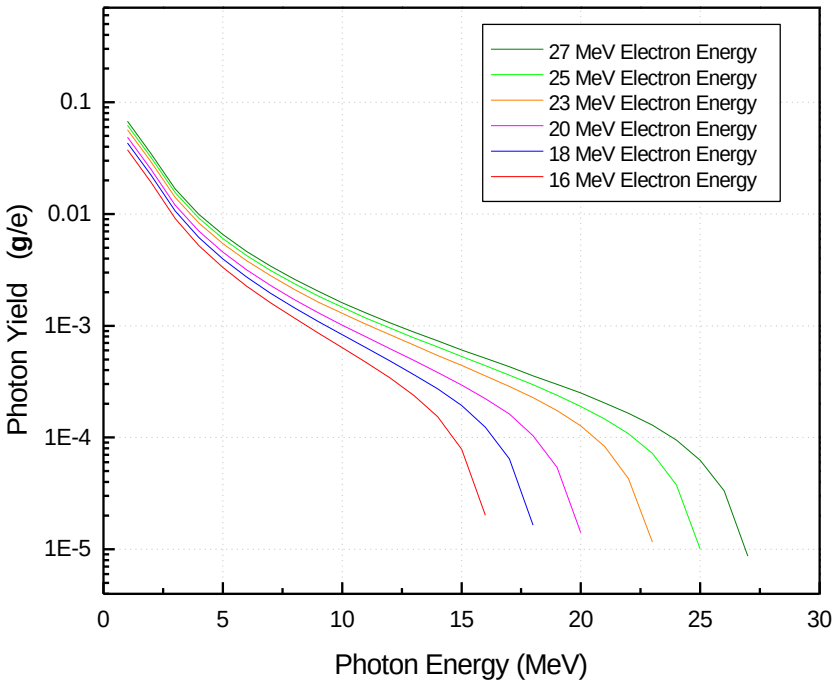

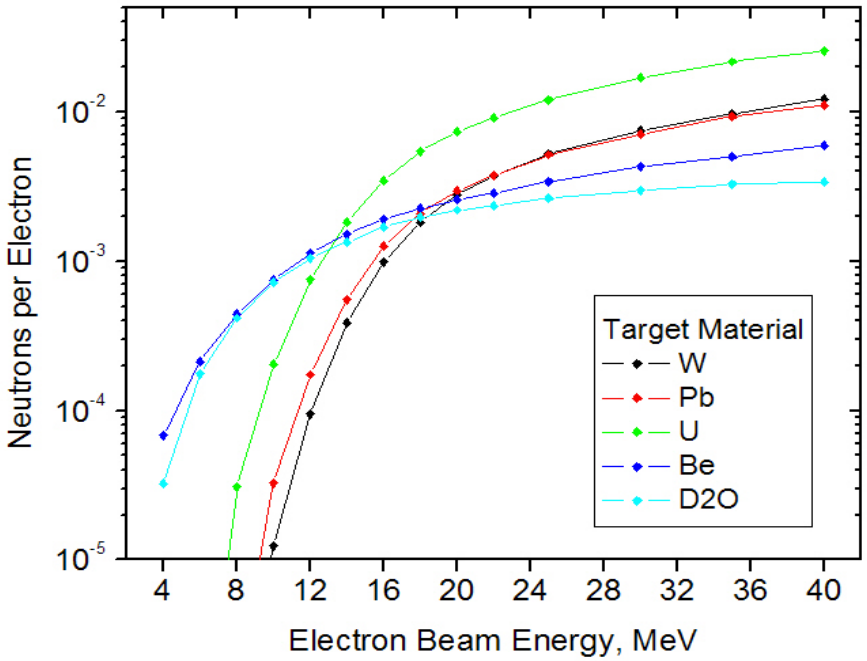

The high energy photons produce neutrons in non-fissile materials via the giant dipole resonance (GDR) cross section which occurs in the range of 10 to 30 MeV. These evaporation neutrons are born at high energies essentially equivalent to fission energy neutrons with an average neutron energy of approximately 1 MeV with the highest energy around 10 MeV. These neutrons may be absorbed in the target, target coolant or the surrounding materials. As the neutrons are moderated and slow down to thermal energies they may cause fissioning of the nearby TRIGA fuel.

Bremsstrahlung Target Cooling

The linac target is a 2.75 inch diameter by 3.5 inch machined W-Cu piece cooled by a dedicated water chiller. The ratio of W to Cu is 80 to 20 weight percent where the copper was required in the piece for machining and brazing of the unit. The cooling line loops through the target parallel with beam direction to avoid absorbing the neutrons from the target.

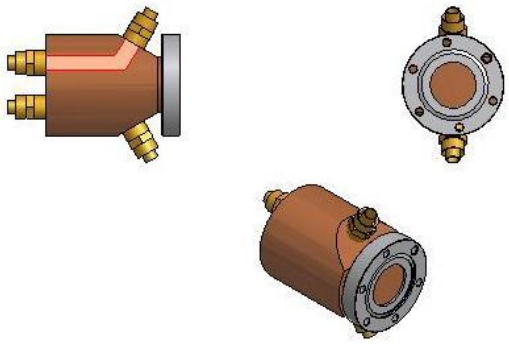

The Linac will operate as a pulsing accelerator. Expected beam current is 80-100 mA of current per pulse. Pulse width can be from 100 nanoseconds to 4 microseconds. The power klystron modulator for this machine will operate at least at 200 Hz. Heat production in the target is a function of the location where the most electrons are stopped and produce neutrons via photoreactions . The graphs below show the peak location of the heat and neutron production is very much concentrated in the first few centimeters of target.

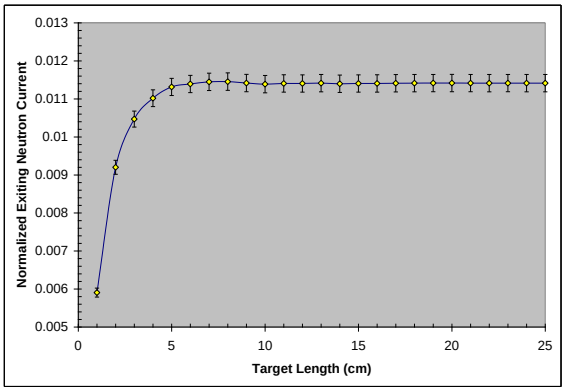

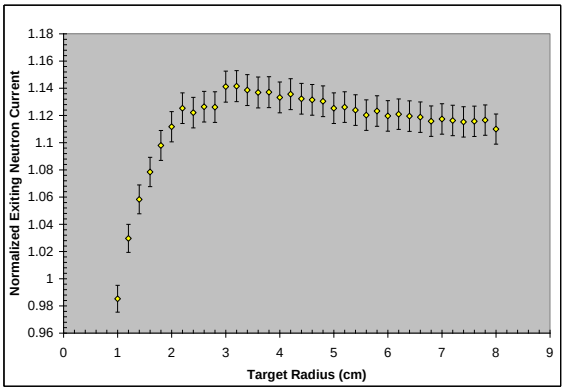

The peak power produced within the target has been calculated by MCNP modeling to be 1.3 kW within the target. The target will be cooled by dedicated Remcor-brand cooling system. The Remcor CH951 chiller has a cooling capacity of 3.5 kW and

will maintain coolant temperature between ambient and 39 degrees Celsius with a flow rate of 4 gpm. The chiller will be placed within the shielded area of BP#4 to protect personnel from the decay of N-16 from the linac target area but still allow remote observations during operations. An interlock pressure switch on the chiller will shutdown the linac if cooling flow to the target is lost. An additional thermocouple will be installed on the target to monitor target temperature during operations.

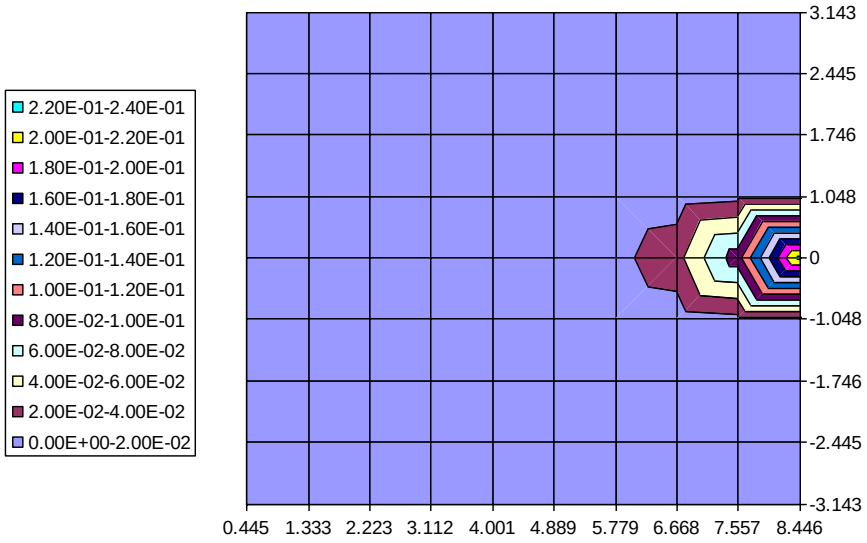

Energy deposition (MeV/gram/incident e) (Electron Beam at "0" spot)

The target will be isolated from the actual beam port aluminum walls by an inner 4 inch ID aluminum pipe sleeve approximately 12 feet long that will protect the beam port bellows assembly, minimize impact of water leaks and provide an easier method to insert and remove the linac target and beam pipe. The high heat conductivity of the aluminum will remove radiated heat from the target area but the target temperature will be monitored and kept below 200C which is a recommended upper limit when preheating aluminum for welding. Initial testing of the linac will consist of plotting heatup of the target as function of beam current and energy to determine operational limits.

Beam Port 5 Cave Safety

The BP5 cave area will be ventilated during linac operation by a portable fan. This ventilation is a precaution to minimize ozone buildup and quickly remove SF6 insulating gas from within the area in the event of a gas leak. The quantity of both these gases is very low at all times. An SF6 leak would be indicated by arcing within the accelerator and detected by fluctuations in the linac power supplies. The gas is heavier than air and will sink to the floor if a leak were to occur.

Access to the BP5 cave is through a locked chain-link gate. An interlock in the gate will trip the linac off if the gate is opened during linac operation. The BP5 cave has always been a controlled high radiation area during reactor operations and requires a Radiation Work Permit for access. A radiation survey will be required within the BP5 shield area following linac operation or as necessary by the Health Physicist.

Target Activation During Operation

The W-Cu target is brazed onto a stainless-steel vacuum flange which is in-turn fastened to a stainless-steel beam pipe 140 inches long. Copper cooling lines are attached directly to the target. The target is supported within a 4 inch diameter aluminum pipe (Alloy 6061-T6). During operation, expected peak neutron strength has been calculated to be approximately 1.3E12 neutrons/sec. Euroatom, who has had previous experience with non-linac based experiments in Rome, Italy had suggested that a ten hour experimental day would be useful. However, based on personnel resources and unknown equipment operations, the NETL expects to average less than 6 hours of operation per day. The following values are the results of activation of the components at the end of a 6 hour day of linac operations. Assumptions were a point source and only the primary isotopes (> several mCi) were listed.

Isotope	Activity at T=6 hrs	Activity after 5 days	Activity after 10 days
W-187 (24 h)	15.2 Ci	463.4 mCi	14.12 mCi
Cu-64 (13 h)	7.33 Ci	10.5 mCi	15.05 microCi
Al-28 (2 m)	3.6 Ci	0	0
W-185 (75 d)	10.5 mCi	10.5 mCi	9.61 mCi
Cr-51 (28 d)	6.63 mCi	5.85 mCi	5.16 mCi

It is clear from this table that a full week of daily operations of not more than 6 hours a day will result in high activities primarily due to W-187 and Cu-64 (half-life of 23.8 and 12.7 hours respectively) but increasing cumulative activities from isotopes such as W-185 and Cr-51. A log of linac operation time on target will be required to be kept and monitor the cumulative activation and decay of the target. A computer program (most likely ORIGEN or MCNP) will be developed and maintained up-to-date to account for all radioisotopes produced in the target. Tungsten is a very good radiation shield, having a density greater than lead, but it is assumed the material is evenly activated and a homogeneous source with little self-shielding.

In order to remove the target from the beam tube for other reactor experiments it will be necessary to allow approximately 7 to 10 days of no linac or fission neutrons on the target. A potential scenario would be to stop experiments on a Thursday and allow the experiment to decay for the following work week to handle and change the target or beam port 5 collimator the following Monday. A central hoist and I-beam will be installed in the BP5 cave so either experiment may be removed without direct physical contact in the high activity area. The activated target (or BP5) collimator will drop into a shielded area at the front of the BP5 cave. This shielded area is 24 inches long with a cylindrical area 6 inches in diameter to receive the end of the 4.5 OD target pipe. The linac target will be surrounded with 6 to 8 inches of lead. A shielding calculation using MicroShield 5 and assuming 1 Ci of W-187, 0.5 Ci of Cr-51, 0.1 Ci of Cu-64 and 0.5 Ci of W-185 results in a total dose (including buildup in the shield) of 0.00015 microRem/hr on the outside of the 8-inch shield. Using the values from the table for 6 hours of activation results in a dose rate of 0.11 microRem/hr. The radiography collimator will

also be stored in the same area but its activation is less due to it location and construction so less shielding will be necessary. Flexible leaded bags may be used as necessary to shield other areas on the beam pipe or the BP5 collimator.

Experiment Design and Schedule

The RACE experiment is designed to drive a subcritical facility to a significant neutron level and resulting higher fission rate. The NETL reactor core will be unloaded such that the fuel remaining in the core grid plate is a non-critical loading. Verification of subcriticality will be performed by withdrawing a neutron-absorbing control rods and monitoring for reactor criticality. Although the license and NRC regulations no longer requires strict controls on a subcritical configuration, the reactor controls will be monitored continuously by a licensed reactor operator while the control rods are withdrawn or the accelerator is in operation.

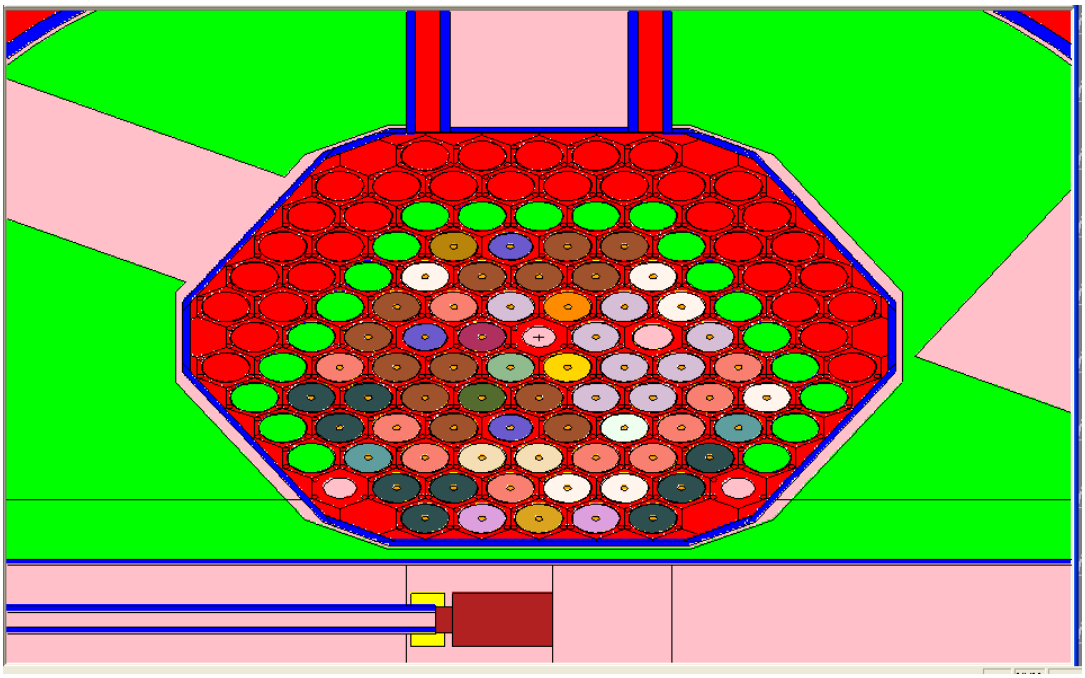

Proposed NETL TRIGA core configuration for RACE experiment

Neutron detectors will be installed directly into the reactor core to closely monitor neutron levels while moving fuel and during linac operations (indicated by small pink circles above). A Californium-252 neutron source capsule will be loaded into the TRIGA RSR and moved into the approximate linac target location for calibration of neutron detectors prior to operation of the linac. This source will be removed during linac operations. A self-powered neutron detector will be installed within the core adjacent to the linac neutron source to monitor source dynamics and provide additional subcriticality information. A thermocouple instrumented fuel element may be used at a later date to evaluate temperature of the fuel during linac operations. The TRIGA reactor fuel will not be damaged by the operation of the accelerator due to its inherent ruggedness. The TRIGA reactor fuel is designed to be pulsed to almost 2000 MW in less than a second. The overall RACE experiment plan has been developed with input from the EuroTrans and DOE partners. Several experimentalists from France, Spain, Italy, Germany and Belgium who have participated in similar experiments in Europe will be traveling for short periods to Austin to assist in the experiments. Changes to the experiment plan that go beyond the scope of this approval must be reviewed separately by the Reactor Oversight Committee.

The following is the expected order of RACE experiments and operations for the month of August. Some minor variations are to be expected as the program develops and new equipment becomes available.

> Week 1: Unload TRIGA core for initial linac testing and calibrations. Linac operator training will occur at this time and instrumentation system performance will be evaluated.
>
> Week 2: Partial loading of fuel near source (approximately 20 elements) and measurements of subcriticality by pulsed neutron source methods and source multiplication methods. These will be compared to similar measurements taken previously in European ADSS experiments.

Week 3: Loading of additional fuel (appr. 40 total) and repeat of experiments for comparison. Linac frequency may be adjusted to determine Transfer Function of TRIGA core in this configuration. Typical "break" frequency of TRIGA is 20 Hz although linac may operate up to 200 Hz.

Week 4: Full loading to operational but subcritical core for repeat of previous experiments in a near critical configuration. Measurements of subcriticality level will confirm previous calculations and benchmark several core models.

The initial RACE experiments will be stopped by August 20 to allow radioactive decay and reconfiguration of the TRIGA core for critical experiments to occur in September. An evaluation of the experiments will be prepared and submitted to the Reactor Oversight Committee for review in September. A more detailed experimental plan will be submitted at that time during a scheduled ROC meeting based on the August results and input from experimenters. The month of September will be used to evaluate the initial RACE experiments and plan for further experiments to occur in October. The tentative experimental schedule must allow for sufficient operation in critical and subcritical modes to satisfy all experimenters. Current proposals for decay and conversion of the core are to alternate operations approximately every 2 weeks starting in October 2005. A week of decay for targets will be required between each conversion.

References

1. T. W.V. Krishna, *Reactor Accelerator Coupling Experiments: A Feasibility Study*, MS Thesis, Nuclear Engineering, Texas A&M University (2005).

2. F. Harmon, *ISU-IAC Accelerators for ADSS Experiments*, First Annual Workshop on Accelerator-Driven Subcritical Systems (ADSS) Experiments, Pocatello, Idaho August 21-22 (2003).

A.6 Initial RACE Review for UT Reactor Oversight Committee

Reactor Oversight Committee
RACE Experiment and Safety Review
(Minutes from September 2005 Meeting)

In the July 22 meeting of the UT Reactor Oversight Committee (ROC), the NETL proposed a review of the initial RACE the experiments following the initial testing and commissioning of the LINAC and present the planned full experimental program in a September meeting. The following is a review of the RACE project immediately after the July meeting until the reactor was returned to normal operations in late August.

1. Week of July 25

LINAC target arrived with cooling line fittings sealed with plumber's (Teflon) tape. This tape is commonly used to seal pipe connections but will fail quickly under ionizing radiation. NETL required the tape be removed and the copper cooling lines brazed in place. Additionally, the total diameter of the target system had to fit inside the 4 inch aluminum pipe that served as a thermal barrier to the reactor beam pipe. This pipe would contain and control any unexpected leakage from the target cooling system. The UT welding shop at PRC attempted to braze the cooling connections but found it difficult to apply sufficient heat to melt the solder. Although this caused fabrication problems, it gave the NETL confidence that the solder would not melt under even extreme operating conditions. The welding shop used larger welding torches in an attempt to preheat the W-Cu mass for soldering but caused such damage to the vacuum sealing surfaces that the target was ruined. The fabrication of two new targets was begun on Friday (7/29) in Idaho in an attempt to stay on schedule. These were to be shipped early the following week.

An independent, self-contained chiller unit shipped from Idaho with a flow rate of approximately 25 gpm cools the LINAC machine (on the cart). The LINAC klystron

power amplifier and beam cavities must be cooled to prevent detuning (and damage) from thermal expansion. The RF power supplies and pulse forming network in the cabinet were to be cooled from a separate, smaller chiller in series with the target cooling. The NETL requested a different cooling power supply cooling method due to the length of copper lines and the potential for Nitrogen-16 flowing outside of the shielded area. The NETL instrumentation cooling system was modified to provide a separate cooling flow to these power supplies.

Neutron detector systems for monitoring the experiment were prepared during this week. Several neutron detection fission chambers had been on order for months but had not yet arrived. Therefore, two fission chambers were borrowed from TAMU. Both chambers had been previously irradiated and had been tested but one did not work when put into use at UT. With only one fission detector available, NETL chose to use a neutron sensitive ion chamber which produces a very small current that is proportional to both gamma and neutron interactions. Electronics to support the project were limited so some equipment was shipped to Texas from Idaho.

The reactor core was unloaded to a point with only 45 elements in the center of the grid-plate. This loading was selected because the reactor was very subcritical and the control rods did not have to be removed (which would have significantly increased the maintenance period). The accelerator target would still be highly decoupled from the fuel for the initial experiment plan.

2. Week of August 1

The first replacement target arrived on Wednesday. The target was immediately machined to accept temperature monitoring thermocouples and leak checked with water. On Thursday, a cooling line braze was found to be leaking and Idaho was notified. The cause of the leak was likely from damage during shipping as it had not leaked in Idaho

and the shipping box appeared damaged on receipt. The staff chose to use the remaining target rather than attempt another repair using local UT welders because Idaho had more experience brazing the large targets. The second target was completed in Idaho and was shipped on Friday (8/5) to Texas.

During this week the LINAC was placed onto short, high-loading rollers so that it could be manipulated in the BP5 cave without a crane. This also permitted the shimming and leveling of the LINAC relative to the beam port pipe. At this point, the roof of the cave could be installed. The BP5 cave roof was installed over several days with the equipment of any length pre-installed in the room.

Further testing of the neutron monitors was completed and the detectors were installed in two one-inch aluminum tubes designed to go into the reactor grid plate.

3. Week of August 8

The LINAC target arrived in Austin on Monday morning but due to an addressing problem it arrived at NETL in the afternoon. The target was leak checked and installed on the end of the vacuum pipe. Thermocouples were installed on the target and routed to a monitoring system external to the cave. One thermocouple was near the beam end and the other was on the far end of the target away to measure temperature gradients.

Wiring verification by ISU this week found that the bending magnet wiring was incorrect. This would have cause a diagonal adjustment rather than right to left or up and down. This was of concern because the beam had been tuned at ISU with the magnets wired incorrectly. However the beam spot produced during this tuning was small and nearly centered on the end of the pipe indicating a good focus and beam tuning in Idaho. The magnetic field could not be mapped because NETL guassmeter for magnetic field measurements was out for repair and calibration at this time. The target was installed into

the BP5 port and coupled to the LINAC and a separate beam pipe vacuum system on August 8.

3.1 Accelerator Operations and Radiation Shielding

On August 9, the vacuum system to the target was verified leak tight and the main gate valves from the LINAC were opened. Interlocks to the LINAC and from the control room were verified. In the afternoon, the LINAC was powered up and operated at low frequency (low power). As the frequency was increased, the temperature of the target began to rise slightly as indicated on the two thermocouples. Radiation levels external to the cave rose linearly with LINAC power and the system was shutdown at 60 Hz (1/3 maximum) due to high radiation levels (500 mR/hr) directly on the roof of the cave. Dose rates in the control console area were less than 5 mrem/hr. Sufficient surveys were performed to locate radiation streaming from the shielded cave.

Additional layers of brick were added to the cave roof on August 10. The ISU accelerator engineer suspected there was some scatter from the bending and quadrapole magnet areas so lead blankets and bricks were placed alongside or over these areas. The bending magnets had to remain cooled by ambient air flow because of the current flow in the magnets (I^2R losses). The sequence of shielding adjustments over the remainder of the week is described in a separate attachment. Essentially, higher than expected dose rates were found on the cave exterior in the vicinity of the final LINAC focusing magnets (approximately 3 to 5 feet from the wall). NETL was able to provide enough additional shielding to reduce dose rates in uncontrolled areas to values in the range of previous neutron radiography operations (2-20 mrem/hr, see attached map).

The LINAC was brought to full power of 180 Hz on August 11th. Doses rates on the BP5 cave exterior were controlled with additional shielding and found to be acceptable. The temperature of the W-Cu target reached approximately 40C at the LINAC end (beam

dump) with 3-5 degree delta-T across the target. The target cooled quickly when the beam was turned off. Neutron ion chamber current and thermocouple readings were used to monitor and adjust the LINAC for maximum beam on target. Thermocouple data was graphed and captured but a computer reboot caused the curves to be lost. NETL staff have modified the thermocouple instrument to plot and record future target operations.

A final shielding adjustment was made on August 13 to reduce dose rates on the stairway (measured at 6 mrem/hr) such that the personnel would not have to pass through a radiation area. The planned experiments for the week of August 15 were cancelled due to a cooling system failure in a power supply over the weekend. The cooling system developed a leak on a cracked (possibly from overtorquing) fitting that sprayed low pressure water onto the deenergized power supplies. The power supplies were returned to Idaho for testing and found to have no damage. The TRIGA core was converted to critical operations by reloading all fuel into the core. The LINAC and target were removed from the beam port the following week and the neutron radiography system collimator was installed in the beamport.

3.2 Instrumentation

Not all the photons interact to produce neutrons when the LINAC pulses. These extra photons produce a gamma "flash" which is significantly higher than the neutron field. This high gamma ray background has made it difficult to monitor neutron pulses or counts directly due to instrumentation saturation. LINAC output was monitored using the neutron sensitive (Boron-10 lined) ion chamber. Although the neutron current could not be separated from the gamma-ray current it provided a reliable means to adjust the LINAC for maximum beam on target. Monitoring of the neutron production is highly important for future accelerator driven systems (to determine subcritical levels) thus the RACE experiment will provide a test bed for testing of various detector designs and instrumentation configurations. It should be noted that that installed TRIGA fission

chamber did detect the LINAC operation and indicated approximately 500 milliwatts with the LINAC at full power. This indicated power is not calibrated to the subcritical system nor reliably compensated for gamma flash but it did serve as a backup to the indications on the ion chamber.

3.3 Target Dose Rates

The LINAC was only operated for approximately 2 hours total during the testing phase of the RACE project but only 1 hour at full power. As approved by the ROC, the target and beam system was not handled until at least 5 days of radioactive decay but NETL waited 13 days due to operational issues. The target was easily removed on August 25 from the BP5 using remote tools and a pulley system installed in the BP5 cave. Calculations performed prior to handling using conservative assumptions gave an expected radiation dose rate of 73 mrem/hr at one foot from the target. Actual radiation measurements made at 3 inches from the target were background (2 mrem/hr in the BP5 cave) levels.

3.4 Target Inspection

The ROC requested a visual inspection of the target following irradiation. The NETL reactor has operated nearly everyday in September for 8 hours a day. The limited space in BP5 cave requires the target sleeve go into the BP5 beam tube to remove the target or a boroscope (which NETL does not currently have) be used during reactor shutdown. As this has not been possible in September due to the reactor operations, the target will be inspected in October prior to the next set of experiments.

4. Conclusions

The RACE experiments were a first-of-a-kind project and unanticipated problems occurred. But the experiment performed essentially as expected and all safety parameters

and radiation fields were monitored when the LINAC was in operation. The beam port cave had been reconfigured therefore shielding effectiveness had to be determined during LINAC operation. The original assumptions for the LINAC shielding were based on Idaho Accelerator Center experience with electron LINACs. Recent computational thermal simulation of the LINAC target with 1.6 kW of heating shows that peak temperature should be closer to 120C (still less than 200C as permitted in the original experiment approval). Further, the higher than expected radiation levels (mixed neutron and gamma) may indicate that some of the electron beam is being absorbed or deflected prior to entering the biological reactor shield. It appears the beam optics may have been slightly misaligned during shipping to Texas or the rewiring of the bending magnet had more of a detrimental effect than expected. Backscatter from the target is less likely a source of the radiation because the dose rates did not change even when significant lead shielding was added around the beam pipe and the fact the radiation source appeared to be between the LINAC and the wall. If the collimated radiation were coming from the beam port we would expect the radiation to scatter towards the rear of the LINAC but the measured dose rates are clearly in the electron beam direction.

A.7 Linac Texas Registration Application

RACE Project Electron Linear Accelerator Registration

This document is presented to demonstrate compliance with the Texas Department of State Health Services requirements for the registration of a radiation producing machine. Specifically, this document addresses the registration requirements described by 25 Texas Administrative Code (TAC) §289. The established policies and procedures govern the utilization of an electron linac (20 MeV, Varian Clinac 20) in room 1.104 of the Nuclear Engineering Teaching Laboratory (NETL). The NETL is located on the J. J. Pickle Research Campus (PRC) of The University of Texas at Austin. The physical address of the NETL is Building 159 on the PRC, 10100 North Burnet Road, Austin. This location appears as Site 001 in the existing Certificate of X-ray Registration, R00183. Figure 1 in the Appendix shows the location of the NETL on the PRC.

The radiation producing machine is a Varian Clinac 20 (serial number 133-435-01) reconfigured to produce 10^{11} to 10^{13} neutrons per second via bremsstrahlung radiation and subsequent photofission or photoneutron production in a high-Z target located adjacent to a 1 MW research reactor. The Clinac is not to be used for human or animal irradiations but will provide a large neutron source for the NETL TRIGA research reactor in a subcritical or near critical configuration. The experimental project is to simulate the operation of an accelerator driven subcritical system for computational benchmarking and transient or feedback response of the system.

The overall research project is titled Reactor-Accelerator Coupled Experiment (RACE) and is directed and funded by the Idaho Accelerator Center of the Idaho State University (ISU) located in Pocatello, Idaho. The project is a multi-university collaboration involving ISU, the University of Nevada-Las Vegas, Texas A&M University and The University of Texas at Austin. The project has recently been endorsed by EUROTRANS European Union transmutation research consortium.

Accelerator Configuration and Location

The linear electron accelerator (Linac) is to be used in a horizontal configuration in the shielded area of neutron beam port number 5 (BP5) in Room 1.104 of the NETL. The physical location of the accelerator (BP5) is shown in Figures 2 and 3. This experimental area has been configured for approximately 10 years for neutron radiography utilizing a collimated thermal neutron beam from the reactor. The BP5 is considered a tangential neutron beam and the beam pipe passes along side the TRIGA nuclear reactor core.

The Linac beam will be focused on a high atomic weight target (tungsten, lead, or encapsulated depleted or natural uranium) located directly adjacent to the reactor core. Bremsstrahlung radiation from the interaction of the electrons with the target material will cause photofission neutron production within the target. Therefore, the primary radiation source will be located within the reactor tank and thus heavily shielded. Neutron production is avoided in typical Linac facilities but neutron production will be optimized in the designed configuration. The Linac neutron production and equipment operation has been initially tested and verified at the Idaho Accelerator Center in Pocatello, Idaho.

The actual neutron production will occur near the reactor within the Linac target. The reactor will not be "on" or critical during the experiments. The project will simulate the operation of an accelerator driven subcritical system or ADSS for potential future high level radioactive waste transmutation facilities. Calculations using MCNP, a Monte Carlo code, indicate the designed system will bring the NETL TRIGA to an equivalent reactor power of 10 to 20 kW[1]. The design configuration will have no bends in the beam pipe and therefore no expected synchrotron radiation production. BP5/BP1 is a single beam pipe (a through-port) that allows simultaneous use of both experiment areas. BP1 will be plugged with neutron and gamma radiation shield plugs preventing any radiation streaming from BP1. Backscatter of neutron radiation from the target and reactor will

produce some activation of accelerator components. From experience, the activation of experiments in the neutron beam is generally low and most of the half-lives of accelerator materials (aluminum and copper) are relatively short.

The NETL TRIGA reactor generally operates between 250 and 1000 kW while using the neutron radiography system. Thus, the expected neutron and gamma flux during Linac operation is significantly lower than normal reactor-based experiments using BP5.

The Linac will operate as a pulsing accelerator. Expected beam current is 80-100 mA of current per pulse. Pulse width can be from 100 nanoseconds to 4 microseconds. The power klystron modulator for this machine will operate at least 200 Hz.

General Registration Requirements (25TAC§289.226(e))

Dr. Donna J. O'Kelly, NETL Laboratory Manager will be the designated Linac Supervisor. As Lab Manager, Dr. O'Kelly also manages the NETL Health Physics program. This program includes radiological controls for the Reactor Facility License (USNRC R-129), Special Nuclear Material License (USNRC SNM-180), and The University of Texas at Austin broad scope materials license (TDSHS L00485). Dr. O'Kelly is a member of the Radiation Safety Committee for the broad scope materials license.

Dr. O'Kelly has extensive experience in the operation and maintenance of particle accelerators for academic research having built, tested and operated a 2 MV tandem at Texas A&M University. Dr. O'Kelly will be receiving job specific training from the Idaho Accelerator Center staff during installation and acceptance testing of the Linac at the NETL. Dr. O'Kelly will train and direct several additional Linac operators as necessary. Dr. O'Kelly's resume is given in Appendix D.

Oversight and compliance verification will be provided by the University's Radiation Safety Office, Environmental Health and Safety. The Radiation Safety Officer, Scott Pennington, is directly responsible for the University's radiation safety programs and the radiological safety and registration of all radiation producing machines on campus.

Shielding Design Requirements (25TAC§289.229(f)(2))

Primary Barrier

The primary barrier will be the reactor tank. The top view of the tank is shown in Figure 2. The NETL reactor tank is 8 meters deep and is designed to shield the radiations produced from the reactor operating at 1 MW. The section of the NETL TRIGA Reactor Safety Analysis Report discussing the reactor biological shield is attached to this submittal as Appendix 2.

Accelerator Shielding and Secondary Barrier

The primary radiation barrier around the accelerator and primary support components will be a previously constructed concrete block shielded area at BP5. The shielded interior area is 5 feet wide by 15 feet long and 6.5 feet high and was designed and used for neutron radiography and large area neutron irradiations. The walls are 16 inches thick and composed of unmortared concrete blocks. The roof of the area is composed of stacked concrete blocks approximately 12 inches thick. This area is shown in Figures 1 and 2. The areas to the left and right of the BP5 area are also locked and controlled. One adjacent shielded area is the Beam Port 4 experiment area. BP4 is currently used as a storage area for radioactive materials controlled with a locked gate. The other side of the BP5 area is the (gated and locked) NETL radioactive material (RAM) storage area. RAM stored in this location include low level contaminated trash from various experiments, radioactive calibration sources and irradiated experiments that are expected

to be used again in the reactor. The exterior of the "Radiography Cave" is routinely surveyed during BP5 use and the exterior radiation levels (gamma and neutron) are generally less than 5 mR/hr during full (1 MW) reactor operation. A recent survey is attached as Appendix ?. The NETL Health Physics Staff will perform a new survey at new power levels or during new experiments and post radiation areas with signs and barriers as appropriate.

Additional Access Controls

Room 1.104 of the NETL is a strictly controlled access area due to the TRIGA reactor and use of radioactive materials in the room. All persons with unescorted access to the room are required to have completed the University and NETL occupational radiation worker training programs. Members of the general public are not permitted in room 1.104 without a qualified escort and are not permitted in radiation areas. All access doors into room 1.104 are locked. Coded key-cards with interface to the University's Department of Locks and Keys computer system open the doors for staff and students granted access by NETL management.

Radiation Monitoring

Radiation monitoring of room 1.104 is required by the NRC reactor license. Gamma area monitors are in place at various locations in the room with local readout and alarms. One such area monitor is located near the BP5 area. Remote monitoring is available to the reactor operators in the Reactor Control Room. Portable gamma and neutron detectors are calibrated and used by the NETL radiation protection staff for detailed radiation surveys.

NETL staff and experimenters are issued personnel dosimetry provided by the current University vendor, Landauer. These dosimeters are replaced monthly and an individual

dose report is provided to the University. In addition to the NVLAP dosimeters, full time staff, part-time students, visitors and occasional experimenters are issued calibrated, self-reading pocket dockets which are read daily.

Linac Controls and Interlock Systems

The control console will be located in room 1.104 in the vicinity of the BP5 shielded area. The final location will be determined after the equipment is fully installed. Photographs of the typical control console are included in the operational procedures in the Appendices. A rotating amber warning light will be energized while the Linac systems are in operation to warn personnel of the radiation hazard.

The interlock system for the Varian Clinac machines is a proven design and this system has been maintained for the RACE project. Additional interlocks and shutdowns will be used for the RACE experimental program. The BP5 area is controlled by a locked gate at all times, an additional system interlock will added to cause a Linac trip if the gate is opened. Remote shutdown by the TRIGA reactor operators will be available from the reactor control room in the event of a facility emergency. All interlocks or Linac trips must be manually reset before restarting the Linac. All interlocks are fail-safe and operate independently from each other.

Byproduct Material Produced from RACE Project

Production of neutrons in the Linac target will cause activation of some components in and around the target. However, the neutrons produced by the reactor subcritical multiplication induced by the bremsstrahlung target will also produce significant radioactivation and byproduct materials. The USNRC considers all byproduct materials produced from radiations directly from the TRIGA reactor to be licensed under the Facility License R-129. Thus, all fission products and byproduct materials produced

within the Linac target will be licensed under the NETL facility license while the target is within BP5. There will be no operation of the Linac and target systems except when the system is installed in BP5.

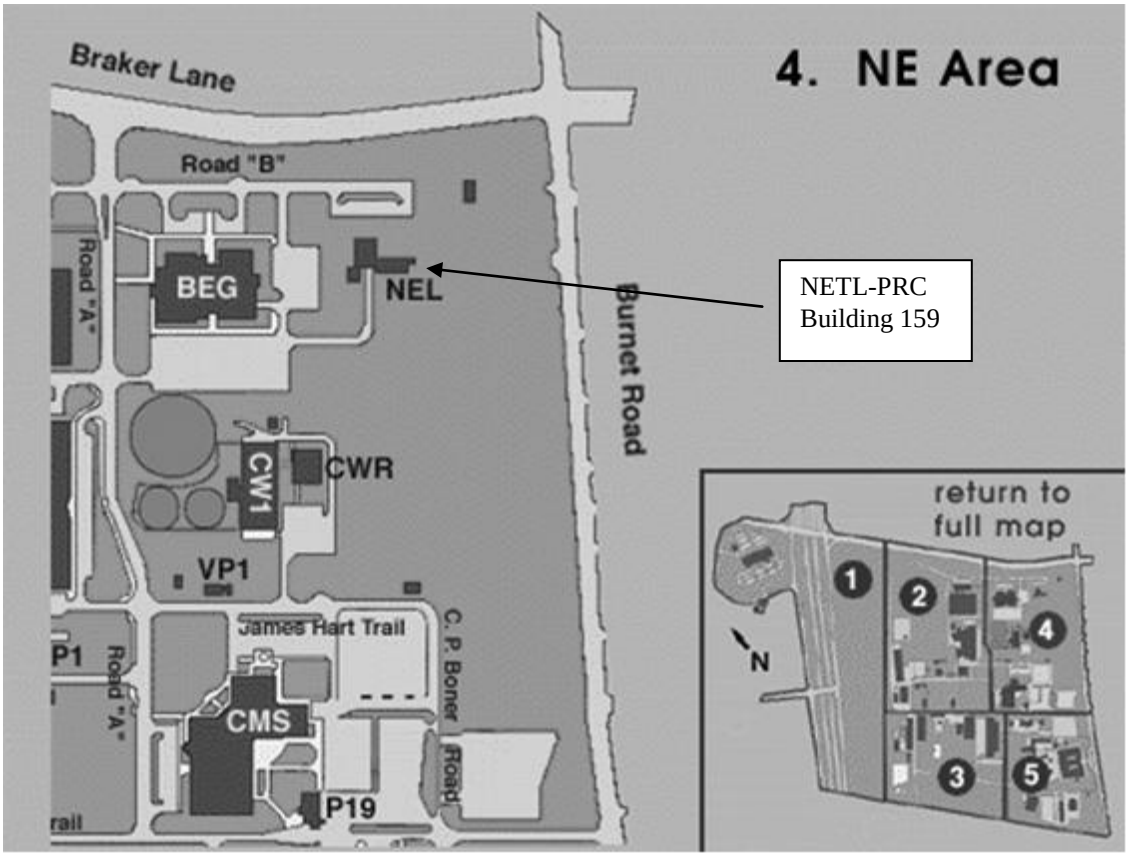

Figure 1. Physical Location of NETL

References

1. T. W.V. Krishna, *Reactor Accelerator Coupling Experiments: A Feasibility Study*, MS Thesis, Nuclear Engineering, Texas A&M University (2005).

Bibliography

1. D.S. O'Kelly, J.D. Braisted, B.J. Hurst, M.G. Krause, and L.S. Welch, "University of Texas Accelerator Driven Subcritical Experiments," *Proc. 8th Intern. Topical Mtg on Nucl. App. and Util. of Accel. (ACCAPP'07)*, pp 843-847, Pocatello, ID, July 29-August 2, 2007.

2. D.S. O'Kelly, T. Green, W. Charlton, "Reactor Accelerator Coupling Experiments (RACE) at The University of Texas at Austin," *Trans. Am. Nucl. Soc.*, **91**, pp. 445-446 (2004).

3. I. Pázsit, M. Ceder, and Z. Kuang, "Theory and Analysis of the Feynman-Alpha Method for Deterministically and Randomly Pulsed Neutron Sources," *Nucl. Sci. Eng*., **148**, pp. 67-78 (2004).

4. *Global Nuclear Energy Partnership (GNEP): Statement of Principles*, GNEP Ministerial Meeting, U.S. Dept. of Energy, Sept. (2007).

5. Committee on Separations Technology and Transmutation Systems, National Research Council, *Nuclear Wastes: Technologies for Separations and Transmutation*, National Academies Press, Washington DC, (1996).

6. "A Roadmap for Developing Accelerator Transmutation of Waste (ATW) Technology," DOE/RW-0519, U.S. Dept. of Energy (1999).

7. *Report to Congress: Spent Nuclear Fuel Recycling Program Plan*, U.S. Dept. of Energy, May (2006).

8. *Report to Congress on Advanced Fuel Cycle Initiative: The Future Path for Advanced Spent Fuel Treatment and Transmutation Research,"* U.S. DOE Office Nucl. Energy, Science and Technology, Jan (2003).

9. J.U. Knebel, et al. "Overview on Integrated Project EUROTRANS: EURopean Research Programme for the TRANSmutation of High Level Nuclear Waste in an Accelerator Driven System," 3rd Annual Idaho ADSS Experiments Workshop, Pocatello, ID, June 15-17 (2005).

10. *Accelerator-Driven Systems (ADS) and Fast Reactors (FR) in Advanced Nuclear Fuel Cycles-A Comparative Study*, Nucl. Energy Agency/Org. Econ.Coop Devel (NEA/OECD) Report (2002).

11. F. Venneri, N. Li, M. Williamson, M. Houts, and G. Lawrence, "Disposition of Nuclear Waste Using Subcritical Accelerator-Driven Systems: Technology Choices and One Implementation Scenario," Los Alamos National Lab. Report LA-UR-98-985, Inter. Conf. on Nucl. Eng. ICONE-6 (1998).

12. W.M. Stacey, *Nuclear Reactor Physics*, John Wiley & Sons, New York, NY (2001).

13. *Lawrence and the Cyclotron*, American Institute of Physics, Center for History of Physics, College Park, MD (2008).

14. F. Goldner, "Advanced Fuel Cycle Initiative (AFCI)," Idaho Workshop on Accelerator-Driven Subcritical System (ADSS) Experiments, Pocatello, ID August (2003).

15. Oak Ridge National Laboratory Spallation Neutron Source, http://neutrons.ornl.gov.

16. D. De Bruyn et al., "On-going activities in Belgium in the field of ADS: from MYRRHA to XT-ADS, perspectives for implementation," 39th Annual Meeting of the IAEA TWG on FR and ADS, Bejing, China (2006).

17. A. Billebaud, et al., "Neutronic Studies in Support of ADS: The MUSE Experiments in the MASURCA Facility," *Nucl. Sci. Eng*., **148**, pp. 124-152 (2004).

18. C. Rubbia et al., "Neutronic Analysis of the TRADE Demonstration Facility," *Nucl. Sci. Eng.,* **148**, pp. 103-123 (2004).

19. C. Ronsivalle, et al., "Design of the Proton Beamline for the TRADE Experiment," Proc. EPAC (Europe. Physics. Acc. Conf.) 2004, Lucerene, Switzerland (2004).

20. Y. Kitamura, H. Yamauchi, Y. Yamane, T. Misawa, C. Ichihara and H. Nakamura, "Experimental investigation of variance-to-mean formula for periodic and pulsed neutron source," Ann. Nucl. Energy, Vol. 31, pp. 163-172 (2004).

21. M. Tanigaki, et al., "Construction of FFAG Accelerators in Kurri for ADS Study," Proc. Particle Accel. Conf. (PAC) 2005, pp. 350-352 May (2006).

22. K. Mishima, "Present Status of FFAG Project and Neutron Utilization in KURRI," FFAG Workshop, Research Reactor Institute, Kyoto University, Kyoto, Japan Nov. (2007).

23. Domanska G., Taczanowski S., Janczyszyn J., Pohorecki W., Shvetsov V.S., "Investigations of the SAD design parameters for optimum experimental performance," *Annals of Nucl. Ener.*, **31,** pp. 2127-2138, (2004),

24. P. Baeten, "The 'GUINEVERE' Project at the VENUS Facility," *5th Workshop Util. and Reliability of High Power Proton Accelerators (HPPA5)*, Mol, Belgium, May (2007).

25. M. Baylac, et al., "The GENEPI-3C Accelerator for the GUINEVERE Project," *Proc. 8th Intern. Topical Mtg on Nucl. App. and Util. of Accel. (ACCAPP'07)*, Pocatello, ID, July 29-August 2, 2007.

26. F. Harmon, K. Folkman and C. O'Neil, "IAC Accelerators for ADSS," Third Annual Workshop on ADSS Experiments, Pocatello, ID, June (2005).

27. L. Price, "SNS-Key Lessons Learned," OECM Workshop, 2006 DOE Project Management Workshop, ORNL, Nov. (2006).

28. M. Carta, et al., "Electron versus proton accelerator driven sub-critical system performance using TRIGA reactors at power," *PHYSOR-2006, ANS Topical Meeting on Reactor Physics*, Vancouver, BC September (2006).

29. G.I. Bell and S. Glasstone, *Nuclear Reactor Theory*, Robert E. Krieger Pub. Co., Huntington, NY (1979).

30. D. L. Hetrick, *Dynamics of Nuclear Reactors*, Amer. Nuclear Society, Inc., La Grange Park, IL (1993).

31. J.J. Duderstadt, *Nuclear Reactor Analysis*, John Wiley & Sons, Inc., New York, NY (1976).

32. A. Gandini and M. Salvatores, "The Physics of Subcritical Multiplying Systems," J. *Nucl. Sci. Eng*., **39**, pp. 673-686 (2002).

33. V. V. Kulik and J. C. Lee, "Space-Time Correction for Reactivity Determination in Source-Driven Subcritical Systems," *Nucl. Sci. Eng*., **153**, pp. 69-89 (2006).

34. V. V. Kulik, "Space-Time Analysis for Reactivity Determination in Source-Driven Subcritical Systems," PhD dissertation, Uni. Michigan (2004).

35. H. Nifenecker, O. Meplan, S. David, *Accelerator Driven Subcritical Reactors*, Institute of Physics, Series in Fund. and Applied Nucl. Phys., IOP Publishing Ltd., Philadelphia (2003).

36. K. Behringer and P. Wydler, "On the problem of monitoring the neutron parameters of the fast energy amplifier," Ann. Nucl. Energy, Vol 26, pp. 1131-1157 (1999).

37. M. Eriksson, J.E. Cahalan and W.S. Yang, "On the Performance of Point Kinetics for the Analysis of Accelerator Driven Systems," Nucl. Sci. Eng., 149, pp. 298-311 (2005).

38. J. Blázquez and M. Embid, "The Core-Source Dominated Regime in ADS, Application to the TRADE Project," Proc. AccApp'05, 5th Topical Meeting on Nuclear Applications and Utilization of Accelerators, San Diego, CA (2003).

39. J. Lewins, "Renaming the generation time the reproduction time," *Ann. of Nucl. Energy*, **33**, p 1071 (2006).

40. J.R. Lamarsh, *Introduction to Nuclear Reactor Theory*, Addison-Wesley Publishing Co., Inc. Reading, Mass. (1972).

41. G. D. Spriggs and J. M. Campbell, "A Summary of Measured Delayed Neutron Group Parameters," *Prog. Nucl. Ener.*, **41**, pp 145-201 (2002).

42. A.E. Profio, *Experimental Reactor Physics*, J. Wiley & Sons, Inc., New York (1976).

43. P. Baeten, et al., "Analytical investigation and experimental application of the source modulation technique to measure ρ/β_{eff}," Prog. Nucl. Energy, 48, pp. 550-558 (2006).

44. C. Jammes, B. Geslot, P. Fougeras, R. Rosa, and G. Imel, "A Neutron-Noise-Based Experiment in a TRIGA Reactor," *29th IMORN-International Meeting on Reactor Noise*, Budapest, Hungary, May (2004).

45. UT TRIGA Safety Analysis Report, Rev. 1.01 (1991).

46. B. Bärs, "The Delayed-Neutron Fraction-Neutron Lifetime Ratio in a TRIGA Reactor from Noise Analysis,", *Nucl. Sci. Eng.*, **30**, pp. 104-108 (1967).

47. P. Seltborg, *Source Efficiency and High-Energy Neutronics in Accelerator-Driven Systems*, PhD thesis, Royal Institute of Technology, Stockholm (2005).

48. N. Burgio, C. Ciavola, and A. Santagata, "Monte Carlo simulation of a TRIGA source-driven core configuration: Preliminary results," *Proc. 1st Annual TRIGA Meeting*, Pavia, Italy, June 16-20 (2002).

49. International Atomic Energy Agency, "Accelerator Driven Systems: Energy Generation and Transmutation of Nuclear Waste, Status Report," *IAEA-TECDOC-985*, Nov. 1997.

50. A. Herrera-Martínez, Y. Kadi, and G. Parks, "Transmutation of nuclear waste in accelerator-driven systems: Thermal spectrum," *Ann. Nucl. Energy*, **34**, pp. 550-563 (2007).

51. K. Folkman, "IAC Accelerator Guide," Idaho Acc. Center, Pocatello, Idaho (2003).

52. J. Braisted, K. Folkman, B. Hurst, D. Tillman, D.J. O'Kelly and S. O'Kelly, "Performance of the Electron Linac for RACE at UT Austin," *Proc. 8th Intern. Topical Mtg on Nucl. App. and Util. of Accel. (ACCAPP'07)*, pp 843-847, Pocatello, ID, July 29-August 2, 2007.

53. G.E. Dale and J.M. Gahl, "Analysis of the Photoneutron Yield and Thermal Neutron Flux in an Unreflected Electron Accelerator-Driven Neutron Source," *Nucl. Sci. and Eng*., **149**, pp. 288-297 (2005).

54. C. Ongrao, J. Rodenas, A. Leon, J. Perez, A. Zanini, and K. Burn, "Monte Carlo Simulation and Experimental Evaluation of Photoneutron Spectra Produced in Medical Linear Accelerators, " *Proc. IEEE Part. Accel. Conf.*, pp. 2531-2533 (1999).

55. W.C. Barber and W.D. George, "Neutron Yields from Targets Bombarded by Electrons," *Phys. Rev*, **116**, pp. 1551-1559 (1959).

56. M. J. Berger and S.M. Seltzer, "Bremsstrahlung and Photoneutrons from Thick Tungsten and Tantalum Targets," *Phys. Rev. C*, **2**, pp. 621-631 (1970).

57. I. Akkurt, J-O Adler, et al, "Photoneutron Yields from Tungsten in the Energy Range of the Giant Dipole Resonance," *Phys. Med. Biol*., **48**, pp. 3345-3352 (2003).

58. H. Hirayama and T. Nakamura, "Measurement of Bremsstrahlung Spectra Produced in Iron and Tungsten Targets by 15-MeV Electrons with Activation Detectors," *Nucl. Sci. Eng.*, **50**, pp. 248-256 (1973).

59. *Neutron Contamination from Medical Electron Accelerators*, NCRP Report No. 79 (National Council on Radiation Protection and Measurements), Bethesda, MD (1984).

60. M.C. White, R.C. Little , and M.B. Chadwick, "Photonuclear Physics in MCNP(X)," LA-UR-99-4827, Los Alamos National Laboratory, *Proc. Topical Accel Appl. Conf.(ACCAPP99)*, Long Beach, CA (1999).

61. C.O. Maidana, A. W. Hunt, D. Beller, and K. Folkman, "Design, modeling and simulations in the RACE project: First study for the development of a transport line," *Nucl. Instr. Methods A*, **562**, pp. 892-895 (2006).

62. *Radiation Protection for Particle Accelerator Facilities*, NCRP Rep. 114, National Council on Radiation Protection and Measurements, Bethesda, MD (2003).

63. Federal Code of Regulations Chapter 10: Energy, Section 20.

64. D. Beller, "RACE Experimental Program," UT Reactor Oversight Committee Minutes September 2005.

65. S. O'Kelly, B. Hurst, K. Folkman and F. Harmon, "Beam Monitoring Techniques Used During the UT/RACE Experiment," ," *Proc. 8th Intern. Topical Mtg on Nucl. App. and Util. of Accel. (ACCAPP'07)*, Pocatello, ID, July 29-August 2, 2007.

66. B. Hurst and K. Folkman, "Position Indicating Split Toroid for the RACE Experiment," *Nucl. Inst. Meth. B*, **261**, pp. 31-33 (2007).

67. S. Falabella, Y-J Chen, T. Houch, J. McCarrick, S. Sampayan and J. Weir, *Effect of Backscattered Electrons on Electron Beam Focus* LLNL Report UCRL-JC-138342, Proc. 20th Inter. Linear Accel. Conf. (2000).

68. K. Sabourov, "IAC RACE: Instrumentation," *3rd Workshop on ADSS Experiments*, Pocatello, ID, June (2005).

69. G.F. Knoll, *Radiation Detection and Measurement*, 3rd Ed., J. Wiley & Sons, New York (2000).

70. W.J. Price, *Nuclear Radiation Detection*, McGraw-Hill Book Co., New York, (1964).

71. P.E. Koehler, J.A. Harvey, and N.W. Hill, "Two detectors for (n,p) and (n,α) measurements at white neutron sources," *Nucl. Inst. Meth. A*, **361**, pp. 270-276 (1995).

72. M. Petit, et al., "A compensated fission detector based on photovoltaic cells," *Nucl. Inst. Meth. A*, **554**, pp. 340-346 (2005).

73. Keithley Instruments, Inc., *Model 6485 Picoammeter*, *Model 6487 Picoammeter/Voltage Source User's Manual*, Doc. No. 6487-903-01 Rev. A, Cleveland, Ohio (2003).

74. J. S. Bendat and A. G. Piersol, *Random Data: Analysis and Measurement Procedure*, J. Wiley & Sons, Inc. New York 3rd Ed. (2000).

75. LND 30772 Specification sheets, LND, Inc. Oceanside, New York.

76. J. Millman and H. Taub, *Pulse, Digital, and Switching Waveform*, McGraw-Hill Book Co. New York (1965).

77. DAQLab-2005 Technical Manual, IOTech, Cleveland, Ohio.

78. K.R. Prasad, S.P. Chaganty, V. Balagi, E. Unnikrishnan, and K. Venkateswara Rao, "Development and applications of LPRM detectors," *Nucl. Instr. Methods A*, **418**, pp. 420-428 (1998).

79. S. Chabod, G. Fioni, A. Letourneau, and F. Marie, "Modeling of fission chambers in current mode-Analytical approach," *Nucl. Inst. Meth. A*, **566**, pp. 633-653 (2006).

80. O. Poujade and A. Lebrun, "Modeling of the saturation current of a fission chamber taking into account the distortion of the electric field due to space charge effects," *Nucl. Inst. Methods A*, **433**, pp. 673-682 (1999).

81. S.V. Chuklyaev, Yu. N. Pepyolyshev, A.S. Koshelev, and Yu. M. Odinstov, "A Method of Determining the Average Charge inside a Fission Chamber," *Instruments and Experimental Techniques*, **44**, pp. 153-159 (2001).

82. Kahn, S. Harman, " " Nucl. Sci. Ener., **23**, pp. 8-14 (1965).

83. K. Hashimoto, H. Shirai, T. Horiguchi and S. Shiroya, "Experimental Investigation on Secondary-Count Effect in Feynman-α Measurement by Fission Counter," *Ann. Nucl. Energy*, **24**, pp. 907-915 (1997).

84. K. Hashimoto, K. Ohya and Y. Yamane, "Experimental Investigations of Dead-Time Effect on Feynman-α Method," *Ann. Nucl. Energy*, **23**, pp. 1099-1104 (1996).

85. D. C. Giancoli, *Physics for Scientists and Engineers*, 2nd Ed., Prentice Hall, New Jersey (1988).

86. T. C. Green IV, "*Simulation and Measurement of Total Flux and Neutron Energy Spectra During RACE Experiments,"* MSc Thesis, The University of Texas at Austin (2006).

87. J.R. Lamarsh and A.J. Baratta, *Introduction to Nuclear Engineering*, 3rd Ed., Prentice Hall, New Jersey (2001).

88. T. Wang and J. Pier, "An iterative approach for TRIGA fuel burn-up determination using nondestructive gamma-ray spectrometry," *Applied Rad. Isotopes*, **52**, pp. 105-118 (2000).

89. J.J. King and G.N. Hoggard, "The Detection of Enrichment of Uranium System: A Portable System for Nondestructive Assay of TRIGA Spent Nuclear Fuel*," J. Nucl. Mat. Management*, **33,** pp. 34-48 (2005).

90. Nuclear Engineering Teaching Laboratory Fuel Log.

91. A.G. Croff, "A User's Manual for the ORIGEN2 Computer Code," ORNL/TM-7175, July (1980).

92. A. G. Croff, "ORIGEN2: A Versatile Computer Code for Calculating the Nuclide Compositions and Characteristics of Nuclear Materials," Nucl. Tech., 62, pp. 335-353 (1983).

93. A. Grisell, *Validation of Monte-Carlo Continuous Energy Burnup Code (MCB) on Light Water Reactor Fuel*, MS Thesis, Dept of Nucl. Reactor Phys., Stockholm, Sweden (2004).

94. A. Talamo, W. Ji, J. Cetnar, and W. Gudowski, "Comparison of MCB and MONTEBURNS Monte Carlo burnup codes on a one-pass deep burn, " *Ann. Nucl. Ener.*, **33**, pp 1176-1188 (2006).

95. T.H. Newton, M.S. Kazimi, and E.E. Pilat, "Development of a Low-Enriched-Uranium Core for the MIT Reactor," *Nucl. Sci. Eng.*, **157**, pp. 264-279 (2007).

96. E.P. Loewen, K.D. Weaver, and J.K. Hohorst, "Reactivity, Isotopic and Thermal Steady-State Analysis of Homogeneous Thoria-Urania Fuel," *Nucl. Sci. Eng*, **137**, pp. 97-110 (2002).

97. K.S. Allen, and E.P. Naessens, "Monte Carlo-Based Analysis for the Transmutation of Transuranic Waste Recycled in Light Water Reactors," *Nucl. Sci. Eng*, **152**, pp. 354-366 (2005).

98. D.I. Poston and H.R. Trellue, "User's Manual, Version 2.0 for Monteburns," *Monteburns 2.0: An Automated, Multi-Step Monte Carlo Burnup Code System*, PSR-455 RSICC, ORNL (2003).

99. W.B. Wilson et. al., *Recent Development of the CINDER'90 Transmutation Code and Data Library for Actinide Transmutation Studies*, presented at GLOBAL'95, LA-UR-2181, LANL (1995).

100. J.S. Hendricks, et. al., *MCNPX, Version 26D*, LA-UR-06-4137, LANL June 20, 2007.

101. J.S. Hendricks, et. al., *MCNPX, Version 26C*, LA-UR-06-7991, LANL December 7, 2006.

102. T. Goorley, "Large Voxel Models with MCNP5 & stack overflow & speedup" MCNP5 e-notebook forum, (RSICC.ORNL.GOV/rsic-cgi-bin/enote.pl?nb= c730&action=vie&page=443) August 26, 2007.

103. X-5 Monte Carlo Team, *MCNP--A General Monte Carlo N-Particle Transport Code, Version 5*, LA-UR-03-1987, LANL, Revised Oct. 3, 2005.

104. R. Jeraj, T. Zagar, and M. Ravnik, "Monte Carlo Simulation of the TRIGA Mark II Benchmark Experiment with Burned Fuel," *J. Nucl. Tech*., **137**, pp. 169-180 (2002).

105. A.L. Hanson and D.J. Diamond, *Determination of Inventories and Power Distributions for the NBSR*, BNL-76769-2006-CP, presented at 2005 TRTR/IGORR meeting, Gaithersburg, MD, Sept. 12-16, 2005.

106. M.Q. Huda, S. I. Bhuiyan, T. Obara, "Burnup Analysis and In-Core Fuel Management Study of the 3 MW TRIGA Mark II Research Reactor," *Ann. Nucl. Energy*, **35**, pp. 141-147 (2008).

107. J.W. Sterbentz, *Radionuclide Mass Inventory, Activity, Decay Heat, and Dose Rate Parametric Data For TRIGA Spent Nuclear Fuels*, INEL-96/0482 (1997).

108. NEA Nuclear Science Committee, *International Handbook of Evaluated Criticality Safety Benchmark Experiments,"* Nuclear Energy Agency, September 2007.

109. M.Q. Huda, M. Rahman, M.M. Sarker, and S.I. Bhuiyan, "Benchmark analysis of the TRIGA Mark II research reactor using Monte Carlo techniques," *Ann. Nucl. Energy*, **31**, pp. 1299-1313 (2004).

110. B. Nacir, A. Htet, L. Erradi and E. Chakir, "Results of MCNP Analysis for Moroccan TRIGA Mark-II Reactor," *Proc. World TRIGA Users Conference*, Pavia, Italy June 6-12 (2002).

111. B. Nacir, Personal Communication, August 2007.

112. A.M. Weinberg and E.P. Wigner, *The Physical Theory of Neutron Chain Reactors*, Univ. Chicago Press, (1959).

113. A. Gandini, "On the Evaluation of ADS Subcriticality," Ann. Nucl. Energy, Vol. 29, pp. 623-630 (2002).

114. J. Wright, *Development and Investigation of Reactivity Measurement Methods in Subcritical Cores*, Thesis for Degree of Licentitate of Eng., CTH-RF-190, Chalmers University of Technology, Göteborg, Sweden (2005).

115. D.D. Glower, *Experimental Reactor Analysis and Radiation Measurements*, McGraw-Hill, New York (1965).

116. K.O. Ott and R.J. Neuhold, *Introductory Nuclear Reactor Dynamics*, Am. Nucl. Society, La Grange Park, IL (1985).

117. C. James, B. Geslot, R. Rosa, G. Imel, and P. Fourgeras, "Comparison of Reactivity Estimations Obtained from Rod-Drop and Pulsed Neutron Source Experiments," *Ann. Nucl. Energy*, **32**, pp. 1131-1145 (2005).

118. E.F. Bennett, "Methods and Errors in Subcriticality Measurements by Rod-Drop-Flux Profile Analysis," ZPR-TM-139, ANL-7966, Argonne National Laboratory (1972).

119. A. Billebaud, R. Brissot, C. Le Brun, E. Liatard and J. Vollair, "Prompt multiplication factor measurements in subcritical systems: From MUSE experiment to demonstration ADS," *Prog. Nucl. Energy*, **49**, pp. 142-160 (2007).

120. P. Baeten and H. A. Abdrrahim, "Reactivity Monitoring in ADS, Application to the MYRRHA ADS Project," *Prog. Nucl. Energy*, **43**, pp. 413-419 (2003).

121. Y. Rugama, J.L.Munoz-Cobo, and T.E. Valentine, "Modal influence of the detector location for the noise calculation of the ADS," *Ann. Nucl. Energy*, **29**, pp. 215-234 (2002).

122. J. Wright and I. Pázsit, "Neutron kinetics in subcritical cores with application to the source modulation method," *Ann. Nucl. Energy*, **33**, pp. 149-158, (2005).

123. C. Jammes, B. Geslot and G. Imel, "On the Area Pulsed Neutron Source Technique Reactivity Estimator," *AccApp'05-Proc. Int. Conf. on Accel. Applications*, Venice, Italy (2005).

124. F. Perdu, et al., "Prompt reactivity determination in a subcritical assembly through the response to a Dirac pulse," *Prog. Nucl. Energy*, **42**, pp. 107-118 (2003).

125. A. Billebaud, et al., "Reactivity Measurements and Neutron Spectroscopy in the MUSE-4 Experiment," Am. Nucl. Soc. *Proc. PHYSOR 2004-Physics of Fuel Cycles and Advanced Nuclear Systems*, Chicago, IL (2004).

126. J.B. Dragt, "On the Applicability of Sjöstrand's Area Method for Reactivity Measurement by the Pulsed-Neutron Technique," *Nucl. Sci. Eng*, **50**, pp. 216-219 (1973).

127. F.D. Judge and P.B. Daitch, "Time-Dependent Neutron Flux in Pulsed Multiplying Assemblies," *Nucl. Sci. Eng*., **26**, pp. 472-486 (1966).

128. R.E. Uhrig, Ed., *Neutron Noise, Waves, and Pulse Propagation*, Symp. Proc. Uni. Florida, Feb. 14-16, (1966).

129. R. Uhrig, *Random Noise Techniques in Nuclear Reactor Systems,* The Ronald Press Company, New York (1970).

130. J. A. Thie, *Power Reactor Noise,* Amer. Nuclear Society, Inc., La Grange Park, IL (1981).

131. M.M.R. Williams, *Random Processes in Nuclear Reactors*, Pergamon Press, New York (1974).

132. N. Pacilio, *Reactor-Noise Analysis in the Time Domain*, U.S. Atomic Energy Commission, Division of Tech. Infor., Oak Ridge, TN (1969).

133. I. Pázsit, "Neutron Fluctuations in Traditional and Accelerator Driven Reactors," *Fluctuation and Noise Letters*, **1**. pp. 101-118 (2001).

134. Z.F. Kuang and I. Pázsit, "The generalized theory of neutron noise in a random medium," *Proc. R. Soc. London A*, **458**, pp. 233-253 (2001).

135. L. Pál, "Neutron Noise and Random Trees Links Between Past and Present," *Prog. Nucl. Energy*, **43**, pp. 5-25 (2003).

136. Y. Rugama, J.L. Kloosterman and A. Winkelman, "Experimental Results from Noise Measurements in a Source Driven Subcritical Fast Reactor," *Prog. Nucl. Energy*, **44**, pp. 1-12 (2004).

137. J. D. Orndoff, "Prompt Neutron Periods of Metal Critical Assemblies," *Nucl. Sci. Eng.*, **2**, pp. 450-460 (1956).

138. R.P. Feynman, F. De Hoffmann, R. Serber, "Dispersion of the Neutron Emission in U-235 Fission," *J. Nuclear Energy*, **3**, pp. 64-69 (1956).

139. R.D. Evans, *The Atomic Nucleus*, McGraw-Hill, New York (1995).

140. *Reactor Physics Constants*, 2nd Ed. Argonne National Laboratory, ANL-5800 (1963).

141. B.C. Diven, H.C. Martin, R.F. Taschek, and J. Terrell, "Multiplicities of Fission Neutrons," *Phys. Rev*., Vol. 101, pp. 1012-1017 (1956).

142. T. Hazama, "Practical Correction of Dead Time Effect in Variance-to-Mean Ratio Measurement," *Ann. Nucl. Energy*, **30**, pp. 615-631 (2003).

143. I. Pázsit and V. Arzhanov, "Theory of Neutron Noise Induced by Source Fluctuations in Accelerator-Driven Subcritical Reactors," *Ann. Nucl. Energy*, **26**, pp. 1371-1393 (1999).

144. M. Ceder, *Reactivity Determination in Accelerator Driven Nuclear Reactors by Statistics from Neutron Detectors (Feynman-Alpha Method),* MSc Thesis, Report CTH-RF-163, Chalmers University of Technology, Göteborg, Sweden (2002).

145. I. Pázsit and Y. Yamane, "The Backward Theory of Feynman- and Rossi-Alpha Methods with Multiple Emission Sources," Nucl. Sci. Eng., Vol. 133, pp. 269-281 (1999).

146. Y. Yamane, Y. Kitamura, H. Kataoka, and K. Ishitani, "Application of Variance-to-Mean Method to Accelerator-Driven Subcritical System," *PHYSOR 2002,* Seoul, Oct (2002).

147. H. Yamauchi, Y. Kitamura, Y. Yamane, T. Misawa, and H. Unesaki, "Study on Variance-to-Mean Method as Subcriticality Monitor for Accelerator Driven System Operated with Pulse-Mode," *Proc. ICNC2003-7th Conf. Nucl. Criticality. Safety*, pp. 147-152 ((2003).

148. M. Ceder and I. Pázsit, "Analytical Solution for the Feynman-Alpha Formula for ADS with Pulsed Neutron Sources," *Prog. Nucl. Energy*, **43**, pp. 429-436 (2003).

149. J. Grandell, *Doubly Stochastic Poisson Processes,* Lecture Notes in Mathematics, Springer-Verlag, New York (1976).

150. S.B. Degweker, "Some variants of the Feynman alpha method in critical and accelerator driven subcritical systems," *Ann. Nucl. Energy*, **27**, pp. 1245-1257 (2000).

151. I. Pázsit and L. Pál, *Neutron Fluctuations: A Treatise on the Physics of Branching Processes,* Elsevier Ltd., Boston (2008).

152. Z.F. Kuang and I. Pázsit, "The general backward theory of neutron fluctuations in subcritical systems with multiple emission sources," *Il Nuovo Cimento, Societá Italinana di Fisica,* **112**, pp. 1067-1092 (1999).

153. Y. Kitamura, I. Pázsit, J. Wright, A. Yamamota, and Y. Yamane, "Calculation of the pulsed Feynman- and Rossi-alpha formula with delayed neutrons," *Ann. Nucl. Energy*, **32**, pp. 671-692 (2005).

154. I. Pázsit, Z.F. Kuang, and A.K. Prinja, "A Unified Theory of Zero Power and Power Reactor Noise Via Backward Master Equations," Ann. Nucl. Energy, Vol. 29. pp. 169-192 (2002).

155. D. Ballester, J.L Munoz-Cobo, and J.L. Kloosterman, "On the applicability of the pulsing Feynman-α method: Validation with MUSE experiments," Ann. Nucl. Energy, Vol. 32, pp. 1476-1494 (2005).

156. D. Ballester, and J.L Munoz-Cobo, "Feynman-Y function for a subcritical assembly with intrinsic spontaneous fissions driven by external pulsed sources," Ann. Nucl. Energy, 32, pp. 493-519 (2005).

157. I. Pázit and Y. Yamane, "The Variance-to-Mean Ratio in Subcritical Systems Driven by a Spallation Source," Ann. Nucl. Energy, 25, pp. 667-676 (1998).

158. S.B. Degweker, "Reactor Noise in Accelerator Driven Systems," *Ann. Nucl. Energy*, **30**, pp. 223-243 (2003).

159. E.F. Bennett, "The Rice Formulation of Pile Noise," *Nucl. Sci. Eng.*, **8**, pp. 53-61 (1960).

160. J.L. Kloosterman and Y. Rugama, "Feynman-α Measurements on the Fast Critical Zero-Power Reactor MASURCA," Prog. in Nucl. Energy, Vol. 46, pp. 111-125 (2005).

161. Y. Yamane, T. Misawa, S. Shiroya and H. Unesaki, "Formulation of Data Synthesis Technique for Feynman-α Method," Ann. Nucl. Energy, Vol. 25, pp. 141-148 (1998).

162. Y. Kitamura, T. Misawa, H. Unesaki, and S. Shiroya, "General formula for the Feynman-α with the bunching technique," Ann. Nucl. Energy, 27, pp. 1199-1216 (2000).

163. E. Turkcan and J.B. Dragtt, *Experimental Study of Different Techniques for Analyzing Reactor Noise Measured by a Neutron Counter*, Dutch Report RCN-INT-75 (1967).

164. http://www.mathworks.com/support/tech-notes/1100/1110.html.

165. J. Neter, M.H. Kutner, C.J. Nachtsheim, and W. Wasserman, *Applied Linear Regression Models*, 3rd Ed., Richard D. Irwin, Inc., Chicago, IL (1996).

166. Y. Yamane and D-I Ito, "Feynman-α Formula with Dead Time Effect for a Symmetric Coupled-Core System," Ann. Nucl. Energy, Vol. 23, pp. 981-987 (1996).

167. F. Hiraga, "Effects of Spatial Harmonics on Power Distribution in Accelerator Driven Subcritical Cores," J. Nucl. Sci. Tech., Vol. 36, pp. 888-901 (1999).

168. C. E. Cohn, "Reflected Reactor Kinetics," *Nucl. Sci. Eng.*, 13, pp. 12-17 (1962).

169. T. W.V. Krishna, *Reactor Accelerator Coupling Experiments: A Feasibility Study*, MS Thesis, Nuclear Engineering, Texas A&M University (2005).

170. D. Ridikas, H. Safa, and M.L. Giacri, "Conceptual Study of Neutron Irradiator Driven by Electron Accelerator," *7th Information Exchange Meeting on Actinide and Fission Product P&T*, JeJu, Korea, Oct (2002).

171. B. Bernardin, D. Ridikas, H. Safa, "A Prototype Sub-Critical Reactor Driven by Electron Accelerators," *Proc. Int. Conf. on Accel. Applications AccApp'01*, Reno, Nevada November (2001).

Vita

David Sean O'Kelly was born in Kingsville, Texas on May 1, 1961 to James Robert O'Kelly and Beverly Whipple O'Kelly. He enlisted in the U.S. Navy immediately after graduating Raleigh-Egypt High School in Memphis, Tennessee in 1979 and served aboard the U.S.S. Benjamin Franklin (SSBN-640B) and as an instructor at the Naval Reactor Facility located at the Idaho Nuclear Engineering Laboratory. He married Donna Ann Johnson on July 21, 1983 while stationed in Charleston, South Carolina. After receiving an honorable discharge in 1988, he attended Texas A&M University and received the degree of Bachelor of Science (cum laude) in Physics in 1992. He was employed at the Texas A&M University Nuclear Science Center from 1988 to 1999 as the Reactor Supervisor and Assistant Director. His daughter, Erin Alexandra was born in 1990 and his son, Devin Sean, was born in 1993. He attended graduate school at Texas A&M University beginning in 1994 and received the degree of Master of Science in Industrial Engineering in 2000. He has been employed as the Associate Director at the University of Texas at Austin's Nuclear Engineering Teaching Laboratory since 1999.

Permanent Address: 15508 Gustine Cove, Austin, Texas 78717

This dissertation was typed by the author.